Extrusion of Polymers and Polymer Blends with Supercritical Carbon Dioxide

By

Minhee Lee

A Thesis
presented to the University of Waterloo
in fulfillment of the
thesis requirement for the degree of
Doctor of Philosophy
in
Chemical Engineering

Waterloo, Ontario, Canada, 1999

The University of Waterloo requires the signatures of all persons using or photocopying this thesis. Please sign below, and give address and date.

ABSTRACT

Extrusion of various polymers and polymer blends was carried out in the presence of supercritical carbon dioxide and the effects of the supercritical CO_2 on the viscosity and morphology of polymers and polymer blends were investigated. Various extrusion systems such as single-screw, twin-screw, and twin / single tandem extruders were utilized. In order to ensure a single-phase polymer / CO_2 solution, generating high pressure in extruders is essential, and special extruder setups equipped with an CO_2 injection device and a secondary die were designed. The solubility of CO_2 in polymers and the density prediction of polymer / CO_2 solutions were also studied.

Effects of supercritical CO_2 on the polymer viscosity was mainly studied in polystyrene / carbon dioxide solution system. The viscosity of PS/CO_2 solutions was measured on-line using a linear capillary tube die mounted on a single-screw foaming extruder and a wedge die mounted on a twin-screw extruder. The measured solution viscosity was described as a sensitive function of shear rate, temperature, pressure, and CO_2 content. In order to mathematically describe the decrease of the shear viscosity due to the dissolved CO_2 in the PS melts, several theoretical models were considered. Cross, Carreau, and generalized Cross-Carreau models were employed to describe the shear-thinning behavior of PS/CO_2 solutions at various shear rates. The zero-shear viscosity in these models was derived in terms of the temperature, pressure and CO_2 content based on the free volume change due to these variables. Various forms of the zero-shear viscosity, including a generalized Arrhenius equation and a WLF equation, were used. The modeling procedure and comparison of the models are presented in detail.

The effects of dissolved supercritical CO_2 on the viscosity and morphological properties of polyethylene / polystyrene blending systems were also investigated using a twin-screw extruder equipped with a wedge die. A considerable reduction of viscosity was found when CO_2 was dissolved in the blend. It was observed that the dissolution of CO_2 into PE/PS blends, regardless of the CO_2 content used, led to decreased shear thinning behavior. The cell structure of foamed PE/PS blends showed a typical dependence on pressure and CO_2 concentration, with higher operating pressures and CO_2 content leading to a smaller cell size. Also, it was noted that the size of the dispersed PS phase in the PE/PS blends decreased by increasing the CO_2 concentration, and that the dispersed PS phase domains were highly elongated in the direction normal to the cell radius.

A twin / single tandem extrusion system was designed for investigating the effects of dissolved supercritical CO_2 on the morphological properties of the PE/PS blends. This tandem extrusion system allowed for preferential dissolution of the CO_2 into the matrix and/or dispersed polymer phase. By introducing devolatilization to the tandem system, the morphological behaviors of PE/PS blends were investigated on unfoamed filaments. In general, the mixing between two polymers was improved by the dissolution of CO_2. The size reduction of the dispersed phase was qualitatively explained using the viscosity ratio of the two polymers and possible effects of the interfacial tension.

Reactive extrusion of a polyethylene / polyamide-6 / polyethylene-g-maleic anhydride system was performed in the presence of supercritical CO_2. Effects of the dissolved CO_2 and the polyethylene-g-maleic anhydride (PE-g-MAH) on the viscosity and the blending morphology were investigated in the tandem extrusion system. It was

found that the addition of a small amount of polyethylene-g-maleic anhydride to polyethylene / polyamide-6 (PE/PA6) blends causes an increase of blend viscosity, which results from the reaction between PA6 and PE-g-MAH. The reaction was verified by observing an imide peak at 1701 cm^{-1} using FTIR. The size of the dispersed PA6 phase decreased by increasing the concentration of PE-g-MAH concentration. It was found that the injected CO_2 affects the size of the dispersed phase when the concentration of PE-g-MAH was low (5 wt%).

ACKNOWLEDGEMENTS

I would like to express my sincere thanks to my supervisors, Dr. Costas Tzoganakis and Dr. Chul B. Park. Their consistent encouragement and advice cannot be properly described in any word. I appreciate their support.

I would like to thank Dr. J. K. Yeo, the director of LG Chemical Research Park, Korea. His supports are greatly appreciated.

I would like to thank the students of the polymer processing group at the University of Waterloo. I wish to thank Gifford Shearer and Karen Xiao. I wish Anle Xue good luck in his Ph.D. study. Don't worry about the interfacial tension measurements.

With respect to donated materials, thanks goes to Nova Chemicals, Allied Signals. I would like to specifically thank Dr. Petra Poetschke at Institut fur Polymerforschung Dresden e.V., Germany for SEM analysis, and Mr. Jungmin Kim at LG Chemical Research Park for TEM analysis. The financial support of Materials and Manufacturing Ontario (MMO) is greatly acknowledged.

I wish to thank my parents in Korea. I am so sorry for being away from them for such a long time.

Finally, I want to thank my wife and son. I dedicate this thesis to them.

I have been crucified with Christ
and I no longer live,
but Christ lives in me.
The life I live in the body,
I live by faith in the Son of God,
who loved me and gave Himself for me.

- Galatians 2:20 -

To Misun and Jai

TABLE OF CONTENTS

LIST OF TABLES

LIST OF FIGURES

NOMENCLATURE

Abbreviations

ABS	Acrylonitrile-butadiene-styrene terpolymer
CFC	Chlorofluorocarbon
EOS	Equation-of-state
EPDM	Ethylene propylene diene monomer
F-H	Flory-Huggins
FTIR	Fourier transform infrared spectroscopy
GPC	Gel permeation chromatography
HCFC	Hydrochlorofluorocarbon
HDPE	High density polyethylene
HFC	Hydrofluorocarbon
HIPS	High impact polystyrene
IGC	Inverse gas chromatography
LDPE	Low density polyethylene
PBMA	Poly(butyl methacrylate)
PC	Polycarbonate
PDMS	Poly(dimethylsiloxane)
PE	Polyethylene
PE-g-MAH	Polyethylene-grafted-maleic anhydride
PIB	Polyisobutylene
PMMA	Poly(methyl methacrylate)
PO	Polyolefin
PP	Polypropylene
PS	Polystyrene
P-V EOS	Panayiotou-Vera equation-of-state
PVAc	Poly(vinyl acetate)
RESS	Rapid expansion of supercritical fluids
RMS	Rheometrics mechanical spectrometer
RSS	Sum of square
SAS	Supercritical anti-solvent process
SCF	Supercritical fluid
SEM	Scanning electron microscopy
S-L EOS	Sanchez-Lacombe equation-of-state
TEM	Transmission electron microscopy
VRF	Viscosity reduction factor

Symbols

γ_{app}	Apparent shear rate, s^{-1}
$\tilde{\rho}$	Reduced density
$\tilde{P}$	Reduced pressure
$\tilde{T}$	Reduced temperature
$\dot{\gamma}$	True shear rate, s^{-1}
a	Parameter in the generalized Cross-Carreau model
A, A', A''	Constants, Pa-s
B, B', B''	Constants
C	Concentration of gas, g/g
c	Weight fraction of the dissolved gas in Henry's law
C_0	Gas concentration
C_1, C_2	Constants in WLF equation
c_p	Specific heat of polymer
C_r	Reference concentration of gas, g/g
E_d	Activation energy for diffusion, cal/mol
E_s	Heat of solution, cal/mol
f	Fractional free volume
f_0	Frequency factor for foam nucleation
f_g	Fractional free volume at glass transition temperature
H	Henry's law constant, cm^3(PTP)/g-atm
h	Height of a wedge die, cm
h_0	Height of the wedge die at the entrance
H_0	Henry's law constant at reference temperature
h_1	Height of the wedge die at the exit
H_1	Henry's law constant at T_1
k	Boltzmann's constant, 1.38×10^{-23} J/K
K	Consistency index of power-law model
K	Consistency index, Pa-s^n
L	Length of the capillary die
L/D	Length to diameter ratio of capillary die
l/d	Length to diameter ratio of the nozzle
M	Molecular weight
M_c	Critical entanglement molecular weight
M_n	Number average molecular weight, g/mol
M_w	Weight average molecular weight, g/mol
n	Parameter in the generalized Cross-Carreau model
N	Total number of molecules of solution
N_1	First normal stress difference
N_{HOM}	Rate of nucleation site
N_i	Number of molecules of component i
P	Pressure, Pa
p	Viscosity ratio of the matrix and particle

P^*	Characteristic pressure
P_0	Pressure at the wedge die entrance
P_1	Pressure at the wedge die exit
P_c	Critical pressure
P_i^*	Characteristic pressure of component i
P_r	Reference pressure, Pa
P_s, P_0	Gas saturation pressure and the environmental pressure
Q	Volumetric flow rate, cm^3
R	Gas constant, 1.987 cal/(gmol-K)
r	Number of sites occupied by mer
R_c	Radius of capillary die, cm
r_d	Radius of the dispersed droplet
r_i	Number of sites occupied by component i in solution state
r_i^0	Number of sites occupied by component i in pure state
s	Slope of the fitted apparent viscosity curve
T	Temperature, K
T_c	Critical temperature
T_g	Glass transition temperature, K
T_g'	Glass transition temperature of diluent
T_r	Reference temperature, K
v^*	Close packed volume
v_0	Limiting specific volume
v_f	Free volume
v_i^*	Closed packed volume of component i
W	Width of a wedge die, cm
$(\Delta T)_{bulk}$	Temperature increase in the wedge die
$\Delta G'$	Activation energy for foam cell nucleation
ΔP	Pressure drop
ΔP_{cap}	Pressure drop in the capillary
ΔP_{ent}	Pressure drop by the entrance effect
$\Delta\mu_i$	Difference of the chemical potential in two phases
T^*	Characteristic temperature
α	Constant of the 1st order temperature dependence, K
α_f	Free volume expansion coefficient, K
α_s	Free volume expansion coefficient of solvent, K
β	Constant of 1st order pressure dependence, Pa^{-1}
χ	Flory-Huggins interaction parameter
δ	Constant of pressure-concentration interaction, Pa^{-1}
δ_{12}	Interaction parameter in S-L EOS
ε	Constant of temperature-concentration interaction, K
ε^*	Interaction parameter per mer
ϕ_i	Volume fraction of component i in solution state
ϕ_i^0	Volume fraction of component i in pure state
ϕ_p	Volume fraction of polymer

ϕ_s	Volume fraction of diluent
γ	Interfacial tension
$\dot{\gamma}_{app}$	Apparent shear rate
$\dot{\gamma}_w$	True shear rate
η	True viscosity, Pa-s
η_0	Zero-shear viscosity
η_{app}	Apparent viscosity
η_{at}	Viscosity at atmospheric pressure, Pa-s
η_m, η_d	Viscosities of the matrix and particle
κ	Constant of temperature-pressure interaction, K/Pa
λ	Time Constant in Carreau model
θ	Converging angle of a wedge die
ρ	Density of a solution
ρ_c	Density at the critical point
ρ^*	Characteristic density
τ	Parameter in the generalized Cross-Carreau model
τ_w	Wall shear stress
ω	Constant of 2nd order concentration dependence
ξ	Constant of the 2nd order temperature dependence, K^2
ψ	Constant of 1st order concentration dependence
Ψ	Polymer Concentration in Kelley-Bueche equation
ζ	Constant of the 2nd order pressure dependence, Pa^{-2}

CHAPTER 1. INTRODUCTION AND OBJECTIVES

1.1. INTRODUCTION

Supercritical fluids (SCFs) have been used in a wide range of applications due to their unique properties, such as gas-like diffusivity and viscosity, and liquid-like density. These unique characteristics of SCFs have also been applied to the plastics industry. Fractionations of polymers, polymerizations in SCF media, and foaming processes are representative applications of SCFs to polymers. Specifically, the foaming processes related to this work, have been originated from food industry. A range of puffed food products such as cereal, pasta and confectionery products have been produced via the foaming technology. It has been noted that many plastic products produced by foaming processes are found in our surroundings. Due to poor mechanical properties, however, efforts for improving the properties have been performed, and microcellular foams having a small cell size, around 10 μm or below, were invented (Martini-Vvedensky, 1984). It should be noted that most of the microcellular foams have been produced using SCFs (Park and Suh, 1992, 1996a, 1996b).

One of the unique characteristics of SCFs is a tunable solubility behavior, and extensive studies related to the solubility of SCFs in polymers have been performed. Early studies have tested the solubility of SCFs in polymers using Henry's law. As indicated in Section 2.3, some of the research work published indicates that Henry's law is still valid up to high pressures and temperatures above the critical point of SCFs. Another approach has been developed using statistical thermodynamics. In this approach, the solubility of SCFs has been studied by equation-of-state (EOS) theories mostly based on the Flory-Huggins theory. One of the big advantages of the EOS theory is that it provides a P-V-T relationship of pure

polymers and polymer / SCF solutions. Based on literature recently published, the solubility of SCFs in polymers generally deviates from Henry's law at high pressures, and the solubility values can be estimated accurately using EOS theories when an interaction parameter between the polymer and the SCF is determined.

By dissolving a SCF into a polymer, it has been known that its rheological behavior is changed and viscosity reduction due to the dissolved SCF has been observed. However, the rheological behaviors of polymer / SCF solutions have not been clearly clarified due to experimental difficulties and theoretical complexities. The viscosity of a polymer melt depends on temperature and pressure, and an extensive study of the temperature and pressure dependencies has been carried out using a free volume concept since Doolittle's work (Doolittle, 1951). However, the viscosity of a polymer / SCF solution should be considered as a function of temperature, pressure, and the concentration of the SCF at the same time.

The viscosity of a polymer is a crucial factor in polymer processing. It affects the productivity, operating conditions, and the properties of the final products. In the case of polymer extrusion, for example, the viscosity affects the motor torque, heat generation due to the viscous dissipation, etc. Therefore, the viscosity change of a polymer due to the dissolution of a SCF should be clearly characterized for any application. By dissolving a SCF in a polymer blend during extrusion, the mixing process between two polymers will be changed due to the viscosity changes, which results in different blending morphologies.

1.2. RESEARCH OBJECTIVES

The work described in this thesis is focused on the extrusion of polymers and polymer blends in the presence of supercritical fluids. The first objective of this thesis is the investigation of the rheological behaviors of a polymer / SCF solution. Polystyrene and carbon dioxide are chosen for this study. It should be noted that two-phase flow during the viscosity measurement should be prevented. In order to prepare single-phase PS/CO_2 solutions, the solubility of CO_2 in PS at the operating temperature and pressure was determined. Efforts to understand the solution viscosity as a function of temperature, pressure, and concentration of CO_2 were made. The second objective of this thesis is the application of the viscosity change achieved by dissolving CO_2 in a polymer. Polymer blends whose morphology is affected by the viscosity of each component, are studied in this work using various extrusion systems including single-screw, twin-screw, and twin / single tandem extruders. It should be noted that the single / twin tandem extrusion system allows for preferential dissolution of CO_2 into the matrix and/or dispersed polymer phase. Polyethylene / polystyrene and polyethylene / polyamide 6 / polyethylene-g-maleic anhydride blends are chosen as non-reactive and reactive polymer blending systems, respectively. The third objective of this thesis is the investigation of extrusion behavior in the presence of a supercritical fluid. Design concepts for an experimental setup and an optimum screw configuration are studied.

This thesis is comprised of ten chapters including this introduction. Chapter 2 reviews literature related to this work. A survey on the properties and applications of SCFs, the solubility of SCFs, EOS theories, PE/PS and PE/PA blends was performed. Specifically, reviews for the viscosity of polymer / diluent systems are essential to understand the

viscosity behaviors of polymer / SCF solution in Chapter 5. Chapter 3 introduced materials and equipment commonly used in Chapter 5 through Chapter 8. Chapter 3 also includes preliminary experiments using a twin-screw extruder in the presence of supercritical CO_2. Chapter 4 examines the thermodynamics of polymer / supercritical CO_2 solutions. Two solubility estimation methods using Henry's law and Sanchez-Lacombe EOS theory were studied. Density estimation for pure components (pure polymer and CO_2) and their solutions was also carried out in this chapter for estimating volumetric flow rates. The estimated volumetric flow rates are used in the calculation of shear rate. Chapter 5 discussed PS/CO_2 solution viscosity as a function of temperature, pressure, and CO_2 concentration as well as shear rate. Cross, Carreau, and generalized Cross-Carreau models were employed to describe the shear-thinning behavior. The generalized Arrhenius equation for the zero-shear viscosity was used with these models to describe the solution viscosity. Chapters 6 and 7 examine the effects of supercritical CO_2 on the viscosity and morphology of PE/PS blends prepared in a twin-screw extruder and twin / single tandem extruder, respectively. Foamed structures and dispersed phase behaviors were investigated. Chapter 6 includes detailed methodology of the on-line measurement of the solution viscosity using a wedge die. In Chapter 8, reactive extrusion of PE/PA6/PE-g-MAH blending system was performed in the presence of supercritical CO_2 using various extrusion systems. Effects of the concentration of CO_2 and PE-g-MAH on the blending morphology were investigated. Finally, conclusions and recommendations and references were listed in Chapters 9 and 10, respectively.

CHAPTER 2. LITERATURE REVIEW

2.1. INTRODUCTION

A substance heated above its critical temperature and compressed above its critical pressure is known as a supercritical fluid (SCF). Such a fluid can move between the state of high density and that of low density without phase transition. Since a supercritical fluid can undergo continuous density changes, slight variations of temperature and/or pressure can also manipulate its thermodynamic and transport properties. Due to their unique properties, SCFs have been used in many fields such as food processing, pharmaceuticals, and the plastics industry. As pointed out by Johnston and Penninger (1989), most applications of SCFs are centered on separation processes. SCF science and technology dealt initially with extraction of simple molecules that dissolve in SCFs. The attention has shifted significantly to more complex molecules, undergoing much broader types of physical and chemical transformation. One of the main advantages of using SCFs is the ability to tune SCF solvent strength continuously from gas-like to liquid-like values through temperature and pressure changes. This adjustable nature of SCF dissolving power has been exploited for polymer processes such as extraction, and polymerization. However, supercritical fluids have hardly been applied to polymer processing operations such as extrusion and polymer blending. Recently, SCFs have been explored as processing aids to lower viscosity for processing applications, and the effect of supercritical CO_2 on the viscosity of polydimethylsiloxane has been studied by Gerhardt et al. (1992, 1994). As discussed in Chapter 1, the effects of SCFs on a polymer and its extrusion performance have not been clarified systematically. The rest of this chapter will review literature focused on the properties of SCFs, polymer / SCF

solutions, polymer rheological behavior, polymer blends and microcellular foaming processes.

2.2. SUPERCRITCAL FLUIDS AND THEIR APPLICATIONS

2.2.1. Supercritical Fluids

Homogeneous fluids are normally divided into two classes, liquids and gases. However, the distinction is not always clear because of the critical point at which the gas and liquid phases become indistinguishable. The critical point of a pure substance is thermodynamically defined by the conditions

$$\left(\frac{\partial P}{\partial V}\right)_T = 0 \quad and \quad \left(\frac{\partial^2 P}{\partial^2 V}\right)_T = 0 \tag{2-1}$$

where P is the pressure, V is the molar volume and T is the absolute temperature. Beyond this point, the fluid is called a supercritical fluid (SCF) rather than a gas or a liquid. A phase is generally considered to be a liquid if it can be vaporized by a reduction in pressure at constant temperature. A phase is considered a gas if it can be condensed by a reduction of temperature at constant pressure. Because the fluid region fits neither of these definitions, it is called neither a liquid nor a gas. Thus, a liquid can be changed to a gas and vice versa with no phase change. The critical point identified by the critical temperature and pressure is unique for any pure substance. The critical temperature and pressure represent the highest temperature and pressure at which a pure substance can exist in the vapor-liquid phase equilibrium. The critical points for a number of common fluids are given in *Table 2.1*.

SCFs show several unique characteristics such as solubility, density, diffusivity and viscosity. The unique solvating power of the supercritical fluid was first observed by Hannay

and Hogarth (1879). They found that increasing the pressure of an ethanol / inorganic salts system caused the inorganic salts to dissolve in ethanol and that decreasing the pressure caused the dissolved inorganic salts to precipitate "as a snow", when the mixture was heated above the critical temperature of ethanol. After their invention, there were many debates about the supercritical state and McHugh and Krukonis (1994) described the historical perspective of the early research and the debate associated with the supercritical state and the solubility power. They also discussed a number of generally accepted observations. As can be expected from *Eq. (2-1)*, the compressibility of a SCF is diverse. As the density becomes liquid-like, the SCF begins to act as a liquid solvent and the solvating power of a SCF is a function of the density. This solvating power which is able to manipulate such a wide range of densities allows for applications of SCFs as "tune-able" solvents. It should be noted that SCFs could be soluble in amorphous polymers as well as in liquids. Therefore, the mutual solubility of SCFs and liquids is seen in mixtures which contain SCFs.

Table 2.1. Critical constants for various common fluids (McHugh and Krukonis, 1994)

Substances	Critical Temperature (°C)	Critical Pressure (atm)
Carbon Dioxide	31.1	72.9
Ethane	32.2	48.2
Ethylene	9.3	49.8
Propane	96.7	42.0
Propylene	91.9	45.6
Benzene	289.0	48.3
Toluene	318.6	40.6
Water	374.2	217.7

The other unique characteristics of a SCF are the diffusivity and viscosity. The diffusivity and viscosity values are intermediate between those of the gas and the liquid as shown in *Table 2.2*. For example, the self-diffusion coefficient of carbon dioxide is about one or two orders of magnitude higher than the diffusivity of solutes in liquids (Paulaitis et al., 1983). The viscosity of carbon dioxide is an order of magnitude below that of typical viscosities of liquid organic solvents (de Filippi et al., 1980).

Table 2.2. Comparison of typical transport properties of fluid phases

Property	Liquid	SCF	Gas
Density (g/cm^3)	1	0.5 - 1	10^{-3} - 10^{-2}
Diffusivity (cm^2/s)	10^{-6}	10^{-3}	10^{-1}
Viscosity (Pa-s)	10^{-3} - 10^{-2}	10^{-5}	10^{-6}

Carbon dioxide (CO_2) is emphasized since it is the process fluid chosen for this work. CO_2 has been one of the classical and popular substances in supercritical fluid technology, and many studies have been performed about the critical point of CO_2 and its properties in the supercritical state. Michel and Michel (1936, 1937) and Michel et al. (1936, 1937) measured the isotherms of CO_2 between 0°C and 150°C and up to 3000 atm and near the critical point. A density-pressure diagram near the critical point, which is based on their results is shown in *Figure 2.1*. Much work for determining the critical point of CO_2 was reported by Wentorf (1956), Vicentini-Missoni et al. (1969), and Levelt Sengers and Chen (1972), and the critical points from their results are very close to one another. The critical conditions for CO_2 have been determined to be:

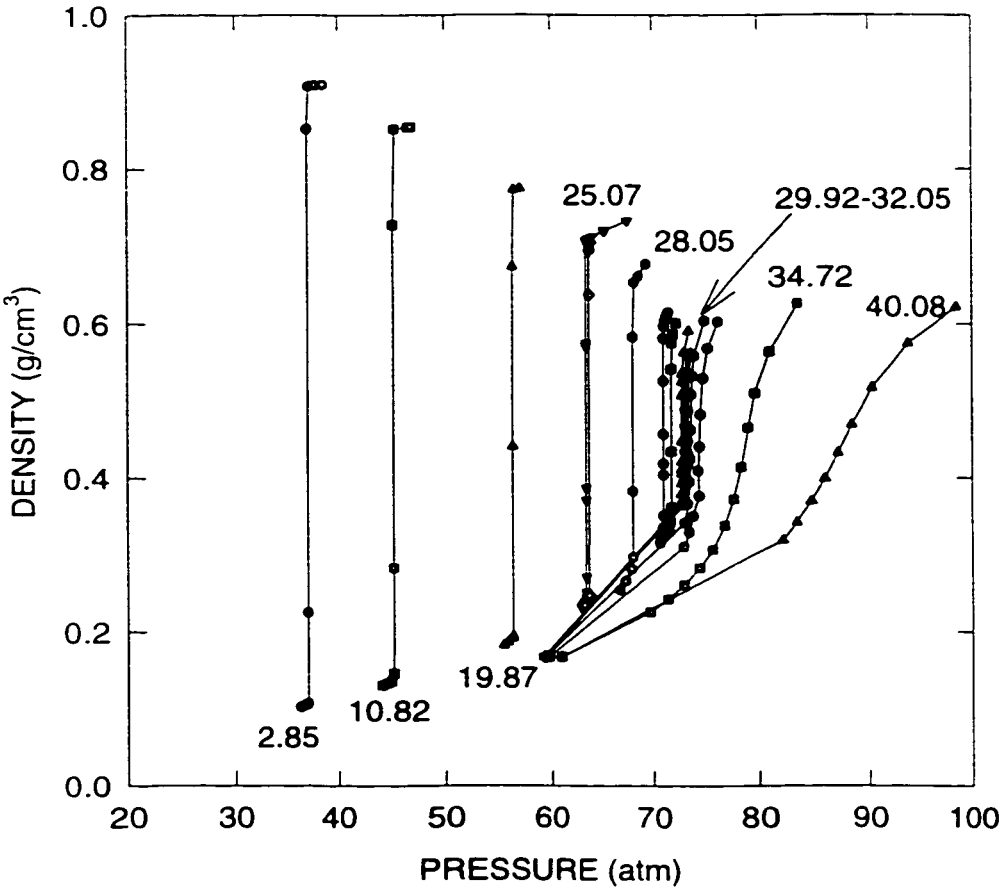

Figure 2.1. Density-pressure diagram of carbon dioxide near the critical point (Numbers indicate the temperature in °C).

$$T_c = 304.19 \text{ K}$$

$$P_c = 72.87 \text{ atm}$$

$$\rho_c = 0.468 \text{ g/cm}^3$$

The solvating strength of supercritical CO_2 can be described qualitatively by the solubility parameter. The dependence of the solubility parameter on temperature and pressure is similar to that of density behavior shown in *Figure 2.1*.

2.2.2. Applications of Supercritical Fluids

Due to their unique properties, SCFs have been used in a wide range of applications. Especially, the properties of gas-like diffusivity and viscosity, and liquid-like density combined with the tunable solvating power of a SCF have provided many applications. A few general categories of applications are discussed here. The application to foaming process will be reviewed separately in Section 2.2.3.

2.2.2.1. Separations

One of the major applications of SCFs is in separation processes using their unique solvating power. Funazukuri et al. (1985) studied the extraction of oil from used automotive tire using *n*-pentane, toluene and nitrogen. Poirier et al. (1987) reported the effect of temperature and pressure on the extracted oil yields from wood using methanol. Scholsky (1987) reviewed the principles of the separation process. The basic scheme is to pressurize the raw feed in a vessel, which is exposed to a supercritical solvent stream with a high selectivity for one of the components. This component dissolves in the supercritical solvent. The solvent is then removed and depressurized to precipitate the dissolved extract phase. Separation processes have been found in the food industry from the early 1980s. For

example. Pfizer began an operation of a hop extraction plant in 1985, and Kraft General Foods applied SCFs to a coffee decaffeination plant in 1987. Since 1985, numerous reports have been published on the use of SCF solvents to fractionate polymers with respect to molecular weight and chemical compositions. McHugh and Krukonis (1989) reviewed the literature on the fractionation using supercritical fluids. Patersen et al. (1987) published results on the isotactic polypropylene / supercritical pentane system. A study of the fractionation of poly(ethylene glycol) in supercritical carbon dioxide has been presented by Daneshvar and Gulari (1992).

2.2.2.2. Reactions and Polymerizations

SCFs have been used in chemical reactions and polymerization. The reasons for carrying out chemical reactions in SCFs are discussed by Clifford (1994). The most straightforward reason is that the control of phase behavior by pressure and temperature may allow reagents or products to be present either in one phase or two phases. For example, water that shows much less polar behavior in supercritical conditions can homogenize substantial amounts of non-polar organic compound, and make them available for reaction. The second reason is the fast diffusion rate. In SCFs diffusion coefficients are generally higher than in typical liquids as shown in *Table 2.2*. This can enhance the reaction rates. The other reasons are the varying solvent property and the environmental advantages.

These reasons for the chemical reactions are generally accepted in polymerization as explained by Kiran (1994). The general approach to the use of SCFs as reaction media in polymerization process is to adjust the pressure and temperature to control the precipitation thresholds for the polymer formed. Kumar and Suter (1987) investigated the precipitation polymerization of styrene in supercritical ethane at 12, 17 and 25 MPa at 333 K and reported

M_w=1017, 1063 and 1193 g/mol, respectively. Saraf and Kiran (1990) studied free radical polymerization of styrene in supercritical state and found a reduction in M_n by increasing the polymerization temperature. DeSimone et al. (1992) demonstrated the polymerization of fluoropolymers in supercritical CO_2. The fluoropolymers are generally insoluble in most solvents except chlorofluorocarbons (CFCs) which are environmentally hazardous. They tried to circumvent the environmental concerns by performing the polymerization of fluorinated acrylic monomers in supercritical CO_2. Watkins and McCarthy (1994) proposed a new route to polymer blends by carrying out a polymerization within supercritical fluid-swollen solid polymer substrates. The applications of SCFs in polymerization have been found not only in radical polymerization, but also in emulsion polymerization. Beckman and Smith (1990) investigated the inverse microemulsion polymerization of water-soluble acrylamide monomers in near-critical and supercritical alkane phases. They reported that the high pressure and low viscosity of the supercritical system could raise the reaction rate significantly and the removal of the supercritical continuous phase could be easily achieved, which led to produce very fine powder.

2.2.2.3. Particle Formation

The observation of the ultrafine powders resulting from the decompression of SCFs dates back to Hannay and Hogarth (1879), who were the first to report the precipitation of dissolved inorganic salts "as a snow" from ethanol above the critical temperature. More than a century elapsed after Hannay and Hogarth's work before Krukonis (1984) revived the interest in supercritical particle formation by demonstrating its potential for processing having a difficulty to make fine powders. As summarized by Debenedetti (1994), the most important advantages of the supercritical route to solid formation are the purity of the

products, the simplicity of the processes, the possibility of producing solid phases with unique morphology, the mildness of the operating conditions, and the wide range of materials that can be processed.

There are two principal techniques, Rapid Expansion of Supercritical Fluids (RESS) and Supercritical Anti-Solvent Process (SAS). The rapid expansion of supercritical solutions leads to loss of solvating power, and hence to solute precipitation. The rapid expansions are easily achieved in nozzles and capillaries. While the RESS generates the supersaturated state by the mechanical expansion, the SAS achieves it by introducing SCFs as anti-solvents. In the SAS process, the solid of interest is dissolved in a liquid, and a SCF having low solvating power with respect to the solute, but miscible with the liquid, is added to the solution. The dissolved SCF causes appreciable volumetric expansion which results in a decrease in the liquid's cohesive energy density, and the solute can be precipitated. In applications where fine powders are required, the RESS and SAS are able to allow processing at lower temperatures than conventional size reduction methods. At the same time, they form very fine, solvent free, and monodisperse powders.

2.2.3. Polymer Foams and Microcellular Foams

Incorporation of gases, not necessarily SCFs, into polymers has been used to produce polymer foams. Foaming processes may be found in the food industry as well as in the polymer industry. In the food industry, a range of puffed food products such as cereal, pasta and confectionery products with improved texture has been produced. In this section, however, only the polymer foaming process is discussed. Polymer foams can be generated in batch or continuous processes, from molten or solid materials, and before or after the shaping

process. The first commercial foam appeared between 1910 and 1920 (Madge, 1962). Since then, synthetic foams have been found in many areas such as comfort cushioning, insulation, packing and space filling. These conventional foams show relatively low mechanical properties due to their large cell size. As reviewed by Kim and Kim (1991), however, rigid foams show better mechanical properties because of the high strength-to-weight ratio. One of the rigid foams is a high density microcellular foam, which is characterized by cell density higher than 10^9 cells/cm^3 and a cell size smaller than 10 μm. Usually, a microcellular foam is produced by using SCFs.

Foaming with SCFs can be thought of as the opposite of a RESS particle formation process in its solute / solvent composition. Thus, the solute or polymer is the major phase in the foaming process. However, the principle of separating the two phases, solute or polymer and a SCF, is similar. Due to an applied thermodynamic instability, such as a depressurization or temperature increase, the SCF precipitates from the solution, and a cellular foam structure is finally produced. A microcellular plastic was originally developed by Martini-Vvedensky et al. (1984). Microcellular plastics were initially developed in batch processes. A polymer saturated with a high pressure gas is subjected to a thermodynamic instability induced by rapidly dropping the solubility of a gas in a polymer. The rapid solubility drop is achieved by a rapid change in pressure or temperature and as a consequence, the precipitated gas or SCF generates the cell structure.

2.2.3.1. Microcellular Foams - Batch Process

A typical batch process for producing microcellular structures was developed by Martini-Vvedensky et al. (1984). A polymer is saturated with a high pressure gas in a chamber, then the gas saturated-polymer is subject to a rapid pressure drop and a rapid

temperature increase resulting in cell nucleation and growth. The batch process for microcellular foams has been studied for the solid state of polymers. Wessling et al. (1994) investigated the saturated polycarbonate sheet in a high pressure CO_2 environment for 24 hours. The sheet was then immersed in a heated glycerol bath at 100°C. Despite being below the glass transition temperature of polycarbonate, the sheet was found to foam throughout with the exception of a dense unfoamed skin at the outer surface. They argued that the polymer becomes supersaturated with CO_2 during the heating step, and that the rapid mass transfer of CO_2 out of the sheet resulting in the unfoamed skin structure, takes place because the partial pressure of CO_2 outside the sheet is zero. Goel and Beckman (1994a, 1994b) studied microcellular foams of the PMMA / CO_2 system in a temperature range from 40°C to 80°C. A PMMA disc of 2 mm thickness and 18 mm diameter was pressurized in a closed chamber over 24 hours to ensure equilibrium sorption. The pressure was then rapidly dropped to atmosphere. In their experiments, the effects of temperature and pressure at equilibrium, and saturation time were studied. Smaller cells were obtained at a lower temperature, a higher pressure and a longer holding time.

The foaming process of a semicrystalline polymer was also studied by Kumar and Gebizlioglu (1992) and Doroudiani et al. (1996). Kumar and Gebizlioglu (1992) followed the process used by Martini-Vvedensky et al. (1984) for poly(ethylene terephthalate) system. They found, however, that the process resulted in foams with a large cell diameter of 100 μm. Doroudiani et al. (1996) used the same foaming method utilized by Wessling et al. (1994). Samples of polymers having various crystalline levels such as high density polyethylene (HDPE), polypropylene and poly(ethylene terephthalate) were studied. They found that increasing the crystallinity proportionally decreased the solubility of the

crystalline polymers. This indicates that sorption only take place in the amorphous region of polymers. Therefore, the resultant foam structures were found to be increasingly non-uniform as the crystallinity level increased due to the inhomogeneous dissolution and the subsequent nucleation of the CO_2.

2.2.3.2. Microcellular Foams - Continuous Process

Extrusion and injection molding have been studied for continuous foaming process. In order to produce a microcellular structure in a continuous process, two major processes, continuous formation of a polymer / gas solution and microcell nucleation, are essential. Park and Suh (1992, 1996a, 1996b) integrated these two steps in an extrusion process. They suggested a design of the continuous microcellular process using a single-screw extruder. Design of the overall extrusion process was presented. SCF was injected into the barrel and homogenized to a single-phase solution by dissolution. Creation of a single-phase polymer / SCF solution is governed by the degree of mixing and the diffusivity of the SCF. The required diffusion time for complete dissolution was estimated from diffusivity and striation thickness. About 10^9 - 10^{10} cells per cm^3 of unfoamed material were found in polypropylene, high impact polystyrene (HIPS) and acrylonitrile-butadiene-styrene terpolymer (ABS) when CO_2 was used as a blowing agent. However, 10^7 - 10^8 cells/cm^3 were found in PP and HIPS when N_2 was injected as a blowing agent. They pointed out that the critical parameters in the microcellular extrusion process are the solubility of the SCF, degree of mixing, and the processing temperature and pressure. Park and Suh (1993) presented the effects of the processing pressure and the injected gas amount on cell nucleation using a rapid pressure drop device.

Park et al. (1994) pointed out that one of the critical steps for continuous production of microcellular plastics was to achieve a constant gas to polymer weight ratio. Because the excessive SCF would result in the formation of undesirable voids in the polymer melt, only a soluble amount of gas must be injected into the polymer melt stream. They presented a metering device consisting of a porous metal for controlling the flow rate of CO_2 and a pump for building up a high pressure of CO_2.

Dey et al. (1994) studied the effect of physical blowing agents on the crystallization temperature of LDPE melt. The crystallization temperature was determined by monitoring the cooling behavior of unsaturated and saturated polymer melts. Depression of the crystallization temperature was observed in the presence of blowing agents such as CO_2 and argon. CO_2 was more effective in lowering the crystallization temperature than argon because CO_2 is more soluble than argon in the LDPE melt. They argued that the depression of the crystallization temperature could be explained by a similar mechanism as the freezing point depression in the conventional solvent / solute system. Jacob and Dey (1994) performed extrusion experiments for foaming PS by the addition of CO_2, N_2 and Ar. The effect of nucleating agents was investigated. They found that the use of a nucleating agent did not change the foam properties significantly, the cell size and the foam density. However, the use of an endothermic nucleating agent did stabilize die pressure fluctuations.

2.2.3.3. Processing Factors in Foam Formation

Research has been performed in order to clarify the effects of operating conditions on the cell structure. The cell formation and its structure are mainly dependent upon the nucleation and growth mechanisms, and therefore, most of research dealing with the

relationship between the operating conditions and the cell structure has been focused on those mechanisms.

It has been known that cells would be generated through two steps, cell nucleation and cell growth. Park and Suh (1992) defined the cell nucleation as the aggregation of a small number of dissolved molecules which spontaneously become energetically stable gas pockets, forming tiny domains of a second phase. And these small domains grow due to the diffusion of dissolved gas or SCF out of the melt phase. Cell nucleation can occur either homogeneously or heterogeneously. The homogeneous nucleation is the mechanism of molecular agglomeration and spontaneous transition to a growing cell. The homogeneous nucleation rate has been defined by Colton and Suh (1987):

$$N_{HOM} = C_0 f_0 \exp\left(-\frac{\Delta G'}{kT}\right) \tag{2-1a}$$

$$\Delta G' = \frac{16\pi\gamma^3}{3(P_s - P_0)^2} \tag{2-1b}$$

where N_{HOM} denotes the rate of nucleation, C_0 denotes the gas concentration, f_0 denotes the frequency factor of molecules joining the nucleating cluster, k is Boltzmann's constant, $\Delta G'$ is the activation energy, γ is the surface energy of the polymer, and P_s and P_0 denote the gas saturation pressure and the environmental pressure, respectively. Heterogeneous nucleation occurs in the presence of additives to the polymer melt phase, such as talc, finely divided metal particles (Lee, 1993), or rubber particles (Ramesh et al., 1994a, 1994b). Lee (1993) argued that the surface of nucleating agent creates small voids due to the incomplete wetting of the polymer melt and the voids act as nucleating sites. Heterogeneous nucleation has been observed in the foaming process of semicrystalline polymers due to the crystalline / amorphous interfaces. Once nucleation has occurred, by whatever mechanism, cell growth

can take place. The nucleation sites receive gas diffusing from the melt and forms a cell structure.

Based on *Eq (2-1b)*, a higher saturation pressure and lower environmental pressure lead to a lower activation energy barrier leading to a higher nucleation rate. Thus, a higher gas saturation pressure and lower nucleation pressure lead to a higher cell density. The effect of saturation pressure was experimentally verified by Kumar and Suh (1990). However, the effect of external pressure on the cell nuclei density does not agree with *Eq. (2-1b)* in their nitrogen-polystyrene system. They found that the external pressure under which nucleation takes place did not affect the number of cells in their experimental system, which allows them to uncouple the cell deformation process from the cell nucleation process. Park et al. (1995) observed the effect of pressure drop rate on the cell density. Various pressure drop rates were generated by the die geometry and the solution flow rate. The experimental results indicate that both the magnitude and the rate of pressure drop play an important role in microcellular processing of the high impact polystyrene (HIPS) / CO_2 system. The highest nucleation rate resulted in the highest cell density. It also affected cell growth because rapid nucleation led to rapid depletion of the dissolved gas. Shafi et al. (1996) simulated the effect of the environmental pressure, P_0. The study showed that lower nucleation pressures result in a slight increase in the total number of cells. A higher cell growth rate and larger final cell size were also observed due to less hydrostatic opposition to cell expansion. The result contradicts the experimental observation performed by Kumar and Suh (1990).

Another major factor affecting the cell structure of microcellular foams is temperature. The effect of temperature on the cell nucleation is not directly shown in *Eq (2-1a)* and *Eq (2-1b)*. Goel and Beckman (1994a, 1994b), however, demonstrated the effect of

temperature on the cell density in the PMMA / CO_2 system. They also compared the cell density values obtained from experiments with those from theoretical predictions. Both results showed that the cell density decreased with increasing temperature, even though the predicted value was slightly higher than the observed one. They explained the difference between the values using possible errors which could be involved in the prediction of the gas concentration and the surface energy in *Es.q (2-1a)* and *(2-1b)*. The effect of temperature on the cell density has been coupled with the concentration of gas since the solubility of gas would be affected by temperature. However, a polymer melt exhibits lower viscosity at higher temperature, which presents less of a physical impediment to cell growth, therefore, larger cells and lower cell densities are obtained at a higher temperature. In addition, lower viscosity leads to higher cell coalescence. Park and Cheung (1997) reported coalescence of cells during the foaming process of linear and branched polypropylene. The authors observed fast cell coalescence in the linear polypropylene, which might show a lower viscosity behavior.

The concentration of blowing agent has been known to be one of the major factors affecting the cell density. The cell density is expected to increase with increasing gas concentration since the nucleation rate is directly proportional to the amount of dissolved gas as shown in *E.q (2-1a)*. This has been verified experimentally by Park and Suh (1992, 1993), Park and Cheung (1997) and others.

Other factors such as shear rate (Lee, 1993) and saturation time (Goel and Beckmann, 1994a) have been investigated. Many studies concerning microcellular plastics have focused on the foaming mechanism and the foam properties. Lee (1995) suggested a non-isothermal viscoelastic cell model for the bubble growth during the continuous foam extrusion. Lee

(1996) proposed a simple experimental set-up consisting of a pressurized vessel with a capillary die in order to search for new blowing agent and additives. Dey et al. (1996) tried to obtain medium density polypropylene foams by injecting CO_2 into a single-screw extruder. Baldwin et al. (1996a, 1996b, 1996c) published on the foaming mechanism of poly(ethylene terephthalate) and the process design of a microcellular extrusion system.

2.3. POLYMER / SUPERCRITICAL FLUID SOLUTIONS

2.3.1. Solubility of Supercritical Fluids

As explained in Section 2.2.1, SCFs show unique solubility behaviors, a tunable solubility, and it has been known that a significant amount of SCF can be dissolved in a polymer phase. In this section, literature dealing with SCFs as the minor phase in solution with a polymer is reviewed, due to the interests in this study.

When the concentration of dissolved amount of gas is low, the gas solubility in a polymer at given conditions of temperature and pressure can be described by Henry's law:

$$c = HP \tag{2-2}$$

where P is the equilibrium gas pressure (atm), H is the Henry's law constant (cm^3-STP/g-atm), and c is the concentration of the gas in the polymer. Henry's law is based on the ideal solution state and an extremely dilute solution. It does not consider the interactions between the polymer and gas. Therefore, the solubility predicted from the Henry's law deviates from the actual solubility of gas in real solutions, especially at high pressures. In spite of its deficiencies, Henry's law has been used for polymer / diluent systems by many research groups. Very limited data for the solubility of gases in polymers were reported in the 1970s, and several early studies focused on the measurement of Henry's law constant.

Newitt and Weale (1948) measured the solubility and diffusivity of gases in polystyrene at high pressures. They determined the solubility by measuring the pressure drop due to gas sorption in the polymer in a closed and isothermal system of a fixed volume. For hydrogen and nitrogen, the solubility in polystyrene showed a gradual decrease with increasing temperature. Plots of the logarithm of solubility against 1/T in the range of 130-190°C were approximately linear, and from the data, heats of solution were determined.

Durrill and Griskey (1966) developed a technique to determine the solubility and diffusivity of gases in molten or thermally softened polymers. Systems studied include nitrogen, helium, carbon dioxide and argon in polyethylene, polyisobutylene, polypropylene, polystyrene and poly(methyl methacrylate). The solubility was determined by weighing the sample before and after saturation. The diffusivity was also determined by monitoring the pressure-time relations during the saturation process. They obtained Henry's law constants and diffusion coefficients for many systems including PS / CO_2 solutions at 188°C and up to 20 atm. The temperature dependence of the Henry's law constant was derived through an Arrhenius equation form.

$$H_1 = H_0 \exp\left(-\frac{E_s}{RT_1}\right) \tag{2-3}$$

In this expression, H_0 and H_1 denote the Henry's law constants (cm^3(STP)/g-atm), E_s is the heat of solution (cal/mol), and T_1 is the temperature (K). In order to predict the heat of solution, as indicated in *Eq. (2-3)*, Henry's law constant needs to be established at various temperatures.

Durrill and Griskey (1969) published the temperature dependence of both Henry's law constants and diffusivity for the same materials used in their previous study. Both

constants were described using Arrhenius equations. The heat of solution, E_s, and the activation energy for diffusion, E_d, were determined from experiments at different temperatures. They argued that there was no appreciable effect of pressure for both constants up to 300 atm.

Lundburg and Mooney (1969) measured the diffusivity and solubility of methane in polyisobutylene between 102°C and 188°C. Solubility varied little with temperature but showed a minimum between 127°C and 188°C. They also extended their experiments to the PE / methane and PS / methane systems. The solubility of all their systems showed a strong deviation from Henry's law with increasing partial pressure of gas. The deviation behavior was interpreted in terms of a Langmuir's sorption model.

Bonner and Cheng (1975) presented a technique for determining the equilibrium sorption of gases in polymers at elevated temperatures and pressures. They experimented using PE / nitrogen at 125°C and at various pressures up to 1700 psi. This technique consisted of the measurement of frequency changes due to gas sorption in a polymer layer coated on a piezoelectric quartz crystal. They argued that their results for the PE / nitrogen system agreed well with the literature even though their results below 300 psi did not seem accurate. Bonner (1977) published a review paper about the solubility of SCFs in polymers. Several experiments and theoretical considerations were introduced.

Gorski et al. (1983) published solubility of various fluorocarbon-blowing agents in polymers including polystyrene (PS), polyethylene (PE), polypropylene (PP), poly(vinyl chloride) (PVC), polycarbonate (PC), and poly(phenylene oxide) (PPO) over a broad range of temperature and pressure conditions.

Fleming and Koros (1986) measured mass sorption / desorption and volume expansion / consolidation for silicone rubber and polycarbonate at 35°C in the presence of CO_2 at pressures up to 900 psi. Different behaviors were observed for the partial specific volume of CO_2 in the rubbery and glassy media. In the rubbery media, the partial specific volume of CO_2 was similar to its value in low molecular weight solvents and showed little pressure dependence. For glassy polycarbonate, it was markedly lower than that in the rubbery material and showed a much stronger dependence on the external gas pressure. They also found a hysteresis effect in the sorption / desorption behaviors when comparing with the pressurization and depressurization of the glassy polymer in the presence of CO_2.

Wissinger and Paulaitis (1987) performed experiments for the sorption of CO_2 into several polymers such as PC, PS and poly(methyl methacrylate) (PMMA) over a range of temperature from 33 to 65°C and pressure up to 100 atm. Two distinct types of sorption behaviors were identified for glassy polymers. One was characterized by sorption that begins to level off and reaches a limiting value at elevated pressure. The other isotherm was characterized by sorption that continues to increase with pressure. They explained that the sorption behavior of CO_2 depended on the glass transition temperatures and pressures of polymer / gas solutions. When the experiments were performed below the glass transition temperature of the polymer / CO_2 solution, the sorption behavior showed a limiting value. When the experimental temperature exceeded the glass transition temperature of the polymer / CO_2 solution, the sorption increased continuously with pressure.

Sanchez and Rodgers (1990) suggested a method to predict the solubility of gases in liquid polymers, and they compared the solubility values calculated from the lattice fluid theory and the experiment using inverse gas chromatography (IGC). Henry's law constant

was shown to be a function of pure component parameters and the χ-parameter. By assuming that both the gas and polymer are non-polar, the interaction parameter of S-L EOS, δ_{12}, was reduced to zero. Consequently, the solubility could be predicted without any adjustable parameters. The resulting equation indicates that the molecular size of gas is an important parameter in determining the solubility and that the solubility should increase with the molecular size. In addition, the gas-polymer interaction energy plays a secondary role in determining the gas solubility, while pure component properties are dominant. They stated that this method was only applicable to the combinations of non-polar gases / non-polar polymers and polar gases / polar polymers when the pressure was very low. Rodgers and Sanchez (1993) extended this to polar / non-polar combinations of gas and polymer. By introducing Hansen's (1967) three-dimensional solubility parameter, a simple empirical expression was proposed for the interaction parameter in the Lattice-fluid theory, as a function of the Hansen's solubility parameter. Using this expression, they quantitatively predicted the solubility for all types of gas / polymer combinations without any adjustable parameters. However, this method is also applicable only at low pressures showing the ideal gas law.

An apparatus for the simultaneous measurement of solubility, density and viscosity of polymer solution was suggested by Sen and Kiran (1990a). They used a visual or optical observation for determining the solubility of a polymer in a solvent. They also measured the internal volume of the vessel and the mass of polymer solution for determining the density. The fall time of a cylindrical sinker was measured for measuring the viscosity.

The solubility of CO_2 in poly(vinyl acetate), PVAc, and poly(butyl methacrylate), PBMA, were measured by piezoelectric quartz sorption (Wang et al., 1994). They observed

that the solubilities of CO_2 in both polymers were approximately proportional to the pressure in the low pressure range. In the high pressure range, however, a deviation from the linear correlation toward higher solubility was observed.

Sato et al. (1996) measured the solubilities of carbon dioxide and nitrogen in polystyrene using a pressure decaying method at temperatures from 373.2 K to 453.2 K and pressures up to 20 MPa. The solubility isotherm of both gases increased almost linearly with pressure and it was observed that the solubility of carbon dioxide decreased with increasing temperature, while the solubility of nitrogen increased with temperature. Henry's law constants of PS / CO_2 and PS / N_2 solutions are in good agreement with those of Durrill and Griskey (1966). Sato et al. (1998) presented the solubility of these gases in polyolefins such as polypropylene and high-density polyethylene.

Kato et al. (1997) published CO_2 sorption isotherms of polystyrene / polycarbonate blending system at 25°C. Samples having various compositions were prepared by solution casting method. All sorption behaviors were interpreted using the dual-mode sorption which involved Henry's law and Langmuir sorption. CO_2 sorption behavior of the PS / PC blends was explained by the simple additive rule corrected for the degree of crystallinity of the PC component.

Recently, Kamiya et al. (1998) investigated the sorption and dilatation behaviors in PMMA / CO_2 system and Zhang et al. (1997) also published the sorption and swelling behaviors of PS-PMMA block copolymers. It was suggested that a swelling of the copolymer was adequately described using a linear relationship of the volume fraction of each pure component.

2.3.2. Empirical Correlation between Solubility Parameter and Critical Temperature

Attempts to predict the solubility of gases in polymers have been made empirically by correlating the solubility data with the critical temperature of gas. The early stage of these efforts focused on the correlation of data. However, the studies have moved toward combination with solution theories, such as the F-H theory and equation-of-state theories.

Stern et al. (1969) plotted the solubility data of twenty-eight gases and vapors in PE from literature. The logarithm of the solubility was found to be a linear function of $(T_c/T)^2$, where T and T_c indicate the experimental temperature and the critical temperature of the gas, respectively. The temperature range of their correlation was mainly below the critical temperatures of the gases used.

Stiel and Harnish (1976) experimentally obtained the solubilities of sixteen organic solutes, such as dichlorodifluoromethane, methylchloride, propane, n-pentane, benzene and toluene in molten polystyrene for temperatures from 135°C to 230°C and pressures up to 4 atm. They also found a linear relationship between the logarithm of the Henry's law constant and $(T_c/T)^2$. The temperature range of their correlation spanned across the critical temperatures of solutes.

Tseng et al. (1984) correlated the solubility of organic solutes in poly(vinyl acetate). Chloroform, methyl ethyl ketone, isopropyl alcohol, and toluene were used as solutes. Three empirical correlations were reported to predict the solubility of polar, aromatic, and nonpolar-nonaromatic solutes, respectively. For all cases, a linear relationship between the logarithm of the solubility and $(T_c/T)^2$ was shown. The solubility increased as the temperature decreased. The polar solutes exhibited the highest solubility whereas nonpolar-nonaromatic solutes showed the lowest one.

Tseng and Lloyd (1985a) published the solubility of organic solutes in poly(dimethylsiloxane) (PDMS) and polyisobutylene (PIB). They also analyzed the literature data. A better correlation was suggested by plotting the logarithm of the product of the solubility and the gas critical pressure and $(T_c/T)^2$. Tseng and Lloyd (1985b) also published data on the solubility of nonpolar and slightly polar organic compounds in LDPE, using the same correlation. Analysis was performed separately for two types of solutes, i.e., aliphatic and aromatic hydrocarbons.

Tseng et al. (1987) studied the solubility behavior and the thermodynamic interaction of nonpolar and slightly polar solutes / polybutadiene systems. They correlated the data with the linear relationship which was introduced by Tseng and Lloyd (1985a, 1985b), and tried to explain the solubility behavior using the interaction parameters from the F-H theory and the EOS theory. They argued that the EOS theory could explain better the temperature dependence of the thermodynamic interaction.

2.3.3. Equation-of-State Theory

Theoretical approaches for explaining and predicting the solubility of a gas in a polymer have been performed. These approaches originate from the prediction of pressure-volume-temperature relationship for a pure component, and are expanded to polymer / solute systems. The Flory-Huggins (F-H) theory (Flory, 1942 and Huggins, 1942) based on the lattice concept gives information about the solubility as well as the phase behavior, and it assumes that the volume and enthalpy of mixing are zero. The interaction parameter, χ, was introduced to correct the energetic effect of mixing. However, the χ-parameter was still assumed to be independent of composition and temperature. The solubility parameter for

regular solutions, which was developed by Hildebrand and Scott (1962) can be related to the χ-parameter because of their same physical meaning. The F-H theory has been modified to explain the behavior of irregular polymer solutions. Blanks and Prausnitz (1964) introduced the entropic contribution to the χ-parameter while Wilson (1964) modified the theory to explain local composition effects arising from the difference in intermolecular forces. In spite of modifications, the F-H theory fails to describe polymer solutions because it ignores the equation-of-state properties of pure components.

Sanchez and Lacombe (S-L) (1976, 1977, 1978) developed an equation-of-state (EOS) theory for pure fluids and for mixtures. This theory is based on the lattice fluid model, with empty sites, which are called holes. Each molecule occupies r-sites (r-mer) and there are unoccupied sites as well. These r-mers are randomly mixed with each other and with vacant sites. The holes differ from the F-H lattice theory because the density of the mixture can be varied by changing the fraction of holes in the lattice. The S-L EOS requires three pure component parameters to characterize a pure fluid and also one adjustable parameter, δ_{ij}. The adjustable parameter is related to the binary interaction to characterize a mixture. The pure component parameters can be determined by fitting pressure-volume-temperature data to the S-L EOS for a pure component. Some of characteristic parameters of the solution can also be determined by using mixing rules. However, the other parameters, such as the characteristic pressure and density, should be determined by combining the regression of the solubility data and an equation for chemical potentials.

Panayiotou and Vera (P-V) (1982) also derived an EOS. This EOS is very similar to the S-L EOS in that it is based on the lattice-hole theory. However, they developed a constant lattice site volume for all r-mers. They also introduced non-random mixing arising from the

interaction between molecules. This EOS theory was subsequently modified by Kumar et al. (1987), and High and Danner (1989, 1990). Kumar et al. (1987) simplified the P-V EOS for a multi-component mixture. High and Danner (1989, 1990) also developed a group contribution method for the estimation of the molecular parameter.

Kiszka et al. (1988) modeled the S-L EOS to the sorption behavior of high pressure gases in solid, amorphous polymers and molten polymers, and they determined the associated interaction parameter. Their systems involved polymers, such as poly(methylmethacrylate), silicone rubber, polyethylene, polyisoprene and polystyrene, and gases, such as CO_2, ethylene and methane. The interaction parameter, δ_{ij}, for their systems ranged from -0.019 to 0.136. They found that the S-L EOS could be used to effectively model the solubility of a high pressure gas in an amorphous or molten polymer. The volume dilatation of the polymer was also easily calculated.

Garg et al. (1994) studied the thermodynamics of polymer melts swollen with supercritical gases. The solubility of CO_2 in PDMS and 1,1-difluoroethane in PS was measured in wide ranges of temperatures and pressures where the gas was supercritical. The solubility data were correlated by the S-L EOS and P-V EOS theories with one adjustable interaction parameter, δ_{12}. The solubility behavior was well explained by these theories when the binary interaction parameter was allowed to depend on temperature. The behaviors of the swollen volume, the isothermal compressibility, and the thermal expansion coefficient for the mixtures were also well described by these two EOS theories.

Recently, Sato et al. (1996) measured the solubility of carbon dioxide in polystyrene and correlated the solubility using the S-L EOS with a temperature-dependent interaction parameter, and the experimental solubility behavior showed a good agreement with the

predicted solubility by S-L EOS theory. Henry's law constants for the PS/CO_2 and PS/N_2 systems are in good agreement with Durrill and Griskey's data (1966 and 1969). Zhang et al. (1997) also reported values of the interaction parameter in the S-L EOS for PS/CO_2 system at 35°C.

2.4. RHEOLOGICAL BEHAVIORS OF POLYMER AND POLYMER / SCF SOLUTIONS

2.4.1. Viscosity of Polymers

Viscosity is a material property which involves resistance to continuous deformation. One of the simplest types of rheological behaviors is the Newtonian behavior which shows a linear relationship between shear stress and shear rate. However, most polymers deviate from the Newtonian viscosity behavior due to various characteristics such as viscoelasticity and molecular weight distribution. In spite of the inherent complexity of polymeric materials, it has been known that the viscosity of a polymer can be varied with temperature, pressure, shear rate and molecular weight. In this section, literature dealing with the polymer viscosity is reviewed.

2.4.1.1. Temperature Dependence of Viscosity

The viscosity of a polymer melt has been found to be a strong function of temperature. Extensive studies have been carried out on the temperature dependence of viscosity. This relationship was originally proposed as an Arrhenius form by Tammann and Hessee (1926):

$$\log \eta = A' + \frac{B'}{T - T_0} \tag{2-4}$$

where A' and B' are constants, and T_0 is a thermodynamic second-order transition temperature. An alternative approach to understand the viscosity behavior of a pure liquid as a function of the free volume was also suggested by Doolittle (1951):

$$\log \eta = A'' + B'' \frac{v_0}{v_f} \tag{2-5}$$

where A'' and B'' are constants, v_0 is the limiting specific volume of a liquid, and v_f is the free volume. The free volume concept introduced by Williams et al. (1955) provides a theoretical basis for the WLF equation. By assuming that the free volume increases approximately linearly with temperature above the glass transition temperature, Doolittle's equation becomes the WLF equation:

$$\log \eta(T) = \log \eta(T_g) - \frac{(B/2.3 f_0)(T - T_g)}{(f_0/\alpha_f) + T - T_g} \tag{2-6}$$

where f_0 is the fractional free volume, v_f/v_0, at the glass transition temperature of polymer, and α_f is the expansion coefficient of the free volume. As indicated by Dealy and Wissbrun (1989), however, the WLF equation describes the temperature dependence of viscosity well only from T_g to above T_g+100. The temperature dependence of viscosity has been illuminated again using statistical thermodynamic theories. The statistical thermodynamic theories describe the *P-V-T* relationship of polymers. Therefore the theories might give a better prediction of the free volume.

2.4.1.2. Pressure Dependence of Viscosity

The pressure dependence of a polymer viscosity has also been studied extensively. Maxwell and Jung (1957) found that the effect of the hydrostatic pressure on the apparent viscosity of polyethylene and polystyrene was significant. They concluded that the effect of hydrostatic pressure should not be neglected in polymer processing involving high pressures.

Westover (1961) reported that an increase of the hydrostatic pressure from 2000 psi to 20000 or 25000 psi causes an increase in the apparent viscosity that corresponds to a reduction of about 50°C in the temperature of the polyethylene melt.

Duvdevani and Klein (1961) measured the pressure effect on the viscosity of low density polyethylene using a capillary rheometer and proposed an exponential relationship:

$$\eta = \eta_{at} \exp(bP) \tag{2-7}$$

where η_{at} denotes the viscosity at atmospheric pressure, b denotes a pressure coefficient which depends on temperature for each material. They reported that the pressure coefficient was in the vicinity of 3×10^{-5} psi^{-1}, and that it decreased by increasing the shear rate or temperature. The temperature dependence of the coefficient was small.

Matheson (1966) extended the free volume theory to account for the pressure dependence of the viscosity. It has been known that if the temperature and pressure of a liquid are increased simultaneously so as to maintain the specific volume of the liquid, the free volume approach predicts a constant viscosity. However, he argued that the free volume equation could not be applied to the pressure dependence of liquid viscosity because the limiting specific volume, v_0, increased with increasing temperature and decreased with increasing pressure.

Miller (1968, 1971) attempted a theoretical analysis to elucidate the effect of pressure on the Newtonian viscosity of polymeric liquids based on the free volume theory. Mathematical relationships between Newtonian viscosity and equilibrium P-V-T properties were reviewed and applied to η-P-T data. Choi (1968) determined the effect of hydrostatic pressure on polyethylene viscosity using an extrusion rheometer. It was reported that the

apparent viscosity was increased nearly fourfold as the average pressure in the barrel was raised from atmospheric to 24000 psi.

Casale et al. (1971), Penwell and Porter (1971), and Penwell et al. (1971) studied the effect of the pressure on the viscosity in order to explain the non-linearity in the relationship between the pressure drop along the capillary and the length-to-diameter ratio. The measured viscosity data were corrected using a pressure-viscosity model derived from the WLF equation. The corrected data agreed well with data obtained at atmospheric pressure using a Weisenberg rheometer.

Cogswell and McGowan (1972) combined Guzman's equation (1913) regarding the viscosity-temperature relationship and their own *P-V-T* equation in order to describe the effect of pressure and temperature on the viscosity. Kamal and Nyun (1973) also pointed out the importance of hydrostatic pressure effect on viscosity during polymer processing, and evaluated the effect on the viscosity of polystyrene in a capillary rheometer. Goldblatt and Porter (1976) compared the pressure coefficients predicted from theoretical approaches performed by Miller (1968), Matheson (1966) and Penwell et al. (1971).

While most of the early studies have used experimental *P-V-T* data to explain the free volume of polymers, Utracki (1983, 1985) introduced the statistical thermodynamics equation-of-state. In his studies, the free volume was described by Simha's (Simha and Somcynski, 1969) equation-of-state parameters, and an equation for the zero shear viscosity was proposed as a function of the free volume.

In order to generate high pressure in a capillary rheometer, a needle valve or a screw-type pin was attached at the exit of the capillary by Driscoll and Bogue (1990) and Baker and Thomas (1993). Extensive research work has been carried out by Kadijk and van den Brule

(1994) using a slit die. The pressure dependence of viscosity was determined using an Arrhenius type WLF equation for polystyrene, polypropylene and poly(acrylonitrile-butadiene-styrene) copolymer. They presented a slit die viscometer in order to generate high pressure and the Cross-Carreau model was applied for explaining the shear thinning behavior. They pointed out that the interaction between temperature and pressure is significant to describe the polymer viscosity.

2.4.2. Rheological Behavior of Polymer / SCF Solutions

Polymers containing SCF (or gas) or other types of diluent such as organic solvent and plasticizer has been extensively used, and the viscosity of the solution or mixture is important in many polymer processes. The viscosity of concentrated polymer solutions such as polymer / diluent and polymer / gas systems has been also interpreted by the free volume theory. Kelley and Bueche (1961) applied Doolittle's equation using a linear mixing rule of the fractional free volume. Using the WLF equation, the free volume of a polymer is

$$v_f = 0.025 + 4.8x10^{-4}(T - T_g) \tag{2-8}$$

In this relation 0.025 represents the free volume at the glass transition temperature. The additional term expresses the increase in the free volume due to the expansion of the polymer as the temperature is raised from T_g to T. If it is assumed that the free volume contributed by the diluent is added to that of the polymer, the free volume of the solution having a volume fraction of polymers, c, is

$$v_f = c[0.025 + 4.8x10^{-4}(T - T_g)] + (1 - c)[0.025 + \alpha_s(T - T_g')] \tag{2-9}$$

where α_s and T_g' are the thermal expansion coefficient and the glass transition temperature of the solvent, respectively. Based on *Eq. (2-9)*, an equation of the solution viscosity was

presented when the molecular weight of the polymer was greater than the critical entanglement molecular weight:

$$\eta = B\rho^{4} \exp\{c[0.025 + 4.8x10^{-4}(T - T_g)] + (1-c)[0.025 + \alpha_s'(T - T_g')]\} \quad (2\text{-}10)$$

where B denotes a constant and ρ denotes the concentration of polymer. However, Elmgren (1980) suggested that the fractional free volume deviates from the linear mixing rule; the fractional free volume is less than the free volume predicted the linear mixing rule and the difference between two free volumes is proportional to the volume fraction of polymer.

Polymer / gas solution systems have been also studied. Blyler and Kwei (1971) investigated the flow behavior of polyethylene melts with dissolved gases. Gases were introduced by decomposition of blowing agents. About 20% viscosity reduction at a constant shear rate was observed by adding 0.5 wt% gas in polyethylene. An analysis was presented based on Doolittle's equation for the viscosity and the free volume.

Bigg et al. (1976) published rheological properties of a polymer melt / blowing agent system to obtain foam properties and processing stability. They argued that the apparent viscosity-shear rate data for a polymer / blowing agent compound were independent of the temperature. The power-law index was observed to decrease from 0.33 to 0.27 by a blowing agent in polystyrene. The independence of viscosity on temperature was explained as a lubrication effect of the decomposed gas in the heterogeneous foamed mixtures.

Han and Villamizar (1978) carried out an experimental study to investigate the flow behavior of gas-charged polyethylene and polystyrene. A rectangular die with glass windows was used. As the melt approached the die exit, a curved pressure profile along the die was observed for the gas-charged molten polymer, while the polymer without a blowing agent showed a linear pressure profile. The bubble inflation pressure was determined by observing

the position and pressure profile at which gas bubbles started to grow. The bubble inflation pressure decreased with increasing melt extrusion temperature, and with increasing blowing agent concentration. The viscosity of gas-charged molten polymers decreased when the concentration of the blowing agent and the melt temperature increased. They also pointed out that rheological measurements of polymer / gas mixtures conducted with a plunger-type viscometer might be subject to serious criticism because the plunger-type viscometer could not guarantee a single-phase condition without allowing foaming inside the capillary. Phase separation, i.e., bubble formation, was involved as the mixture approached the capillary exit.

Oyanagi and White (1979) studied the bubble morphology and apparent rheological properties of polyethylene and polystyrene during foaming in extrusion. Generally, the extrudate swell increased with shear rate and by adding a chemical blowing agent. They found that an addition of 0.5 wt% blowing agent has a greater effect on the increase of swell than 1.0 wt% and 1.5 wt%. The viscosity reduction was observed at 190°C and 210°C, however, the viscosities were almost the same for their LDPE melt system with and without a blowing agent at 170°C.

As pointed out by Han and Villamizar (1978) in the early studies of polymer / gas solutions, experimental difficulties were also reported by Mendelson (1979, 1980) and Han and Ma (1983a). They focused on the phase separation behavior, i.e., bubble formation, which may be involved during the rheological measurements of polymer / gas solutions in a plunger type viscometer. In order to prevent the bubble formation as the solution approaches the capillary exit, Mendelson (1979, 1980) introduced a pressurized reservoir at the exit of a plunger-type capillary viscometer for preventing bubble formation. In his experiments on the polystyrene / ethylbenzene system, he prepared polymer / gas solutions in glass jars at room

temperature and then charged them into the barrel of the viscometer. Finally, these solutions were extruded to the pressurized chamber at an elevated temperature. This experimental technique is difficult to apply to molten polymer / gas mixtures because of the high temperature and pressure involved. Han and Ma (1983a, 1983b) published the rheological properties of mixtures of molten polymers and fluorocarbon blowing agents. They explained that the non-linear pressure profile in the capillary implied precipitation of the gas, and all their experiments were performed in the linear range of the pressure profile. The viscosity reduction factor (VRF) was defined as the ratio of the viscosity of polymer-blowing agent mixture to that of the polymer alone. In a second paper (1983b), they argued that VRF was independent of the shear rate and the temperature. It was only dependent upon the type of fluorocarbon blowing agent. They also investigated the foam extrusion characteristics of polyethylene and polystyrene with fluorocarbon blowing agents (Han and Ma, 1983c, Ma and Han, 1983) and correlated the extrudate swell ratio with the cell morphology.

Gerhardt (1994) and Gerhardt et al. (1997) used a capillary rheometer with a special loading assembly and a back pressure assembly. The back pressure assembly made the capillary rheometer a closed system, and the special loading assembly was used to keep an identical pressure and temperature in the vessel and the rheometer. The viscosity behavior of PDMS / supercritical CO_2 solutions was studied and the rheological measurements showed a viscosity reduction due to the dissolved gas. A composition-dependent shift factor was introduced to construct a master curve. While the magnitude of the viscosity was seen to decrease as the gas content increased, the onset of shear thinning was also shifted to higher shear rates. The author also determined the contribution from the dilution effect only in the total viscosity drop, in terms of iso-free volume experiments using low molecular weight

PDMS. High molecular weight PDMS was diluted with various amounts of a low molecular weight PDMS having the same density. Densities of pure components and solutions were predicted from the lattice fluid theory.

Kwag et al. (1996) published on the viscosity behaviors of PDMS and PS with dense or supercritical CO_2. Their experimental method was identical to those of Gerhardt (1994) and Gerhardt et al. (1997). Regarding the PS / CO_2 system, they stated that the solubility of CO_2 was lower than 4 wt% in PS under 12 MPa at 150°C. The composition-dependent shift factor was successfully used to construct master curves for the PS / CO_2 system as well as the PDMS / CO_2 system. The viscosity of PS can thus be reduced by two orders of magnitude with only 4.5% of dissolved CO_2 at 150°C. Bae and Gulari (1997) measured the solution viscosity of PDMS / CO_2 system at ambient temperature using a specially designed falling ball viscometer. The Kelley-Bueche free volume equation based on the additivity of free volumes of each component was modified by considering the compressibility effect on the free volume of polymer. They found that the modified theoretical equation was capable of predicting the solution viscosity with remarkable accuracy.

The rheological behavior of PS / blowing agent mixtures were studied by Gendron et al. (1996) in a co-rotating twin screw extruder equipped with a slit die. They maintained a sufficiently high pressure in the die by using two independently controlled gear pumps. HCFC and HFC were used as blowing agents. The shear stress-shear rate data were modeled by a modified Carreau equation containing four parameters. The zero shear viscosity, η_0, was used to predict T_g in the WLF equation. The predicted T_g of pure polystyrene was lower than its actual value. In order to explain the underestimated T_g, new values for two constants in the WLF equation were suggested. Gendron and Daigneault (1997) investigated the rheological

behavior of polystyrene and polypropylene with CO_2. The viscosity reduction resulting from the plasticizing effect of the blowing agent was related to the lowering of the glass transition temperature using a generalized Arrhenius type WLF model.

2.4.3. Viscosity Measurements of Polymer / SCF Solutions

Viscosity measurements of a polymer / SCF solution using conventional rheometers such as a capillary rheometer or a rotational rheometer are extremely difficult because the SCF must be prevented from vaporizing. As mentioned in the previous section, several studies have been performed by Mendelson (1979, 1980) and Gerhardt et al. (1994) to keep the SCF in solution at high pressure and high temperature. They introduced a special loading assembly and a back pressure assembly into a plunger type capillary rheometer. The need to make a plunger type capillary rheometer a closed system can be eliminated by on-line measurements of viscosity from the output stream of an extruder.

This thesis performed the on-line measurement of polymer / gas solution viscosities using capillary dies and a wedge die attached to single-screw or twin-screw extrusion systems. Therefore, literature related to the capillary and the wedge dies is reviewed in this section.

2.4.3.1. Capillary Die

One of the most popular rheometers for measuring the melt viscosity of a polymer is the capillary rheometer. A polymer melt is forced to flow by pressure, through a linear cylindrical capillary. For fully developed, steady-state, and laminar flow of incompressible Newtonian fluids, the wall shear stress, τ_w, the Newtonian shear rate, $\dot{\gamma}$, and the Newtonian viscosity, η, are given by

$$\tau_w = \frac{R_c}{2}\left(\frac{\Delta P}{L}\right) \tag{2-11}$$

$$\dot{\gamma} = \left(\frac{4Q}{\pi R_c^3}\right) \tag{2-12}$$

$$\eta = \frac{\tau_w}{\dot{\gamma}} \tag{2-13}$$

where ΔP is the driving pressure drop, R_c is the capillary radius, L is the capillary length and Q is the volumetric flow rate. The linear relationship between the shear stress and shear rate is no longer valid for non-Newtonian fluids because the shear stress is a function of shear rate. However, *Eqs. (2-12)* and *(2-13)* are still useful for defining the apparent shear rate, $\dot{\gamma}_{app}$, and the apparent viscosity, η_{app}. One of the most useful models for shear thinning fluids is the power-law fluid model. The shear stress is defined as follows:

$$\tau_w = K\dot{\gamma}_{app}^n \tag{2-14}$$

$$\dot{\gamma}_w = \left(\frac{3n+1}{4n}\right)\dot{\gamma}_{app} \tag{2-15}$$

where K is the consistency index and n is defined as the power-law index given by

$$n = \frac{d\ln\tau_w}{d\ln\dot{\gamma}_{app}} \tag{2-16}$$

Eqs. (2-15) and *(2-16)* are known as the Rabinowitsch correction.

In a capillary rheometer, the total driving pressure drop can be separated into two pressure drops: i.e., the entrance pressure drop, ΔP_{ent}, and the pressure drop in the capillary, ΔP_{cap}. ΔP_{ent} is the pressure drop which occurs before the onset of fully developed flow, at a certain length of capillary. Thus, the true wall shear stress can be calculated as follows:

$$\tau_w = \frac{\Delta P}{2(L/R_c + e)} \tag{2-17}$$

where e is the Bagley end correction related to ΔP_{ent} which can be obtained by extrapolation of ΔP against L/R_c at various shear rates. The Bagley end correction is considered to be negligible if L/D ratio of the capillary die is over 40 (Bagley, 1957).

2.4.3.2. Converging Die

The use of converging dies is almost universal in the extrusion of polymer melts. It has been found to reduce flow defects of the extrudate at operating pressures which are greater than those which would cause serious defects in a parallel die. These converging dies measure the viscosity at various shear rates at a fixed flow rate of a polymer melt. The slit die and linear capillary die by comparison, measure the viscosity at fixed shear rate determined by the flow rate of the polymer melts.

Cogswell (1972) analyzed the converging flow in terms of the extensional and simple shear flow in order to calculate the relationships between volumetric flow rate, pressure drop, and post extrusion swelling. He assumed simple shear, simple tension and a small bulk deformation. Mathematical expressions for the pressure drop of power-law fluids were derived and compared to the experimental data observed in a coni-cylindrical die. In addition, he also presented a mathematical derivation for a wedge shaped die.

Lenk (1978, 1979, 1981) introduced a simple method for the calculation of the pressure drop for a power-law fluid in dies with a wide slit profile and with vertical and/or lateral tapers. In order to simplify the analysis, the following assumptions were made:

(a) Dies with tapered angles could be considered as a series of infinitely small length slits.

(b) The parameters of the power-law fluids were constant in the range of shear rates determined by the dimensions of the converging dies.

(c) In the wedge die, edge effects were ignored.

The Rabinowitsch corrected equation for pressure drop in the wedge die with a constant width, w, and vertical taper angle, θ, is

$$\Delta P = \eta \cot\theta \frac{w^{-n}}{2n}\left(Q\frac{4n+2}{n}\right)^{n}(2h_1)^{-2n}\left[1-\left(\frac{h_0}{h_1}\right)^{-2n}\right] \tag{2-18}$$

where h_0 and h_1 are the heights from the center line at the die entrance and at the die exit, respectively. Q denotes the volumetric flow rate and n denotes the power-law index. In a circular truncated right cone die, the Rabinowitsch corrected equation for the pressure drop is

$$\Delta P = \eta \cot\theta \frac{2^{2n+1}}{3n}\left(Q\frac{3n+1}{\pi n}\right)^{n} r_1^{-3n}\left[1-\left(\frac{r_0}{r_1}\right)^{-3n}\right] \tag{2-19}$$

where r_0 and r_1 are the radius of die at the entrance and at the exit, respectively.

Forsyth (1976) reviewed the converging flow for various liquids including Newtonian and power-law fluids. He analyzed the flow using equations derived from the spherical coordinate system, and also presented various phenomena such as melt fracture and die swell, related to the converging flow. Yoo and Han (1981) carried out an experimental and a theoretical study to determine the stress distribution in viscoelastic polymeric melts in a converging channel. Shear stress and normal stress distributions were determined by measuring the wall normal stress and the stress birefringence in a tubular die with a 15° converging angle.

Lodge and de Vargas (1983) and Rauwendaal and Fernandez (1985) presented rheometers for on-line measurement of viscosity. Slit dies instead of converging dies, were

used in their research work. Since continuous extrusion processes require that the throughput of the extruder be kept constant, the slit die can measure the viscosity only at fixed shear rate. Considering the fact that the viscosity of a polymer melt is a function of shear rate, slit dies can not be used to measure the viscosity of non-Newtonian polymer melts.

Vlachopoulos and Scott (1985) presented approximate equations of the pressure drop for polymer melt flow through a slightly tapered die. They compared the results from the approximate equations and finite element calculations. They argued that the equations based on the lubrication approximation are valid for flows of polymer melts with three restrictions:

(a) Taper angles should be relatively small ($\theta \leq 15°$).

(b) Die length should be long enough to be able to ignore the entrance and exit pressure drops.

(c) Viscous dissipation effects should be negligible.

Kwon et al. (1986) conducted an experimental study with an extruder and conical dies of four different converging angles, and analyzed the results using a finite element method for a power-law fluid. They pointed out that the normal stress term becomes very important when the converging angle becomes large, especially at high flow rates. They also found that the Cogswell's formula (1972) overpredicts the pressure loss at high volumetric flow rates.

Pabedinskas (1992) used a wedge die to measure the viscosity at several shear rates simultaneously. Experiments were performed on controlled-rheology degraded polypropylene, using an on-line method. By using the wedge die, the dependence of the viscosity on the shear rate was measured without changing the polymer flow rate. *Eq. (2-18)* for power-law fluids derived by Lenk (1978, 1979, 1981) was used.

Binding and Jones (1989) analyzed data obtained from converging-flow rheometers for certain fluids showing a tension-stiffening behavior. Bersted (1993) evaluated the analysis of Cogswell (1972) and presented a refined analysis. Nguyen and Kausch (1995) discussed the polymer degradation in a transient elongational flow through a converging channel.

2.5. IMMISCIBLE BINARY POLYMER BLENDS

Polymer blends provide required material properties as an alternative way of new polymer synthesis. Polymer blends have been classified using different criteria such as the compatibility and the chemical reaction involved. The literature dealing with polymer blends is enormous, addressing lots of polymer blending systems. In this section, however, only two restricted areas, which relate to the dispersion of a minor phase in a matrix and the polyethylene / polystyrene blending system, are reviewed.

2.5.1. Size of the Dispersed Phase

The dispersion of one component in another one has been considered as one of the key factors to control the properties of polymer blends. The size and shape affect not only the mechanical properties, but also the rheological properties. For instance, a sharp tough-brittle transition was observed at a critical rubber particle size in nylon-rubber blends (Wu, 1985). When two immiscible polymers are blended during a melt process, one phase, which forms the dispersed phase, experiences breaking-up and coalescence. The two competing mechanisms determine the size and the shape of the dispersed phase, and the mechanisms are

dependent on several parameters such as interfacial tension, composition, and rheological properties.

Taylor (1932) proposed a formula that describes the size of an isolated particle as a function of the shear rate, the interfacial tension and the viscosity ratio.

$$r_d = \frac{c\gamma}{\eta_m \left(\frac{dv_x}{dy} \right) f(\eta_m/\eta_d)} \tag{2-20}$$

where r_d denotes the radius of the dispersed droplet, c is a constant, γ is the interfacial tension, η_m and η_d denote the viscosities of the matrix and particle, respectively, and dv_x/dy denotes the shear rate. The size of the dispersed particle decreases with decreasing interfacial tension, and with increasing viscosity of the matrix. *Eq. (2-20)* also predicts a decrease in the particle size when the viscosity ratio of the two components is approaching unity. It should be noted that the Taylor's formula is valid at very low concentration of Newtonian fluids. For the Newtonian fluids, no droplet deformation occurs under the simple shear field when the viscosity ratio is above 4.

Vanoene (1972) proposed two distinct modes of dispersion, stratification and droplet-fiber formation, when two viscoelastic polymers are mixed each other. He illustrated the stratification by investigating cross sections perpendicular to the flow direction of a PE / Ionomer (10/90) mixture. It was found that a lamellar structure is dominant except at very low shear rates. By increasing the concentration of polyethylene, droplet-fibril type dispersion was observed. It has been found that these two dispersion modes are independent of the magnitude of the shear stress and temperature. He also indicated that the interfacial tension and the viscoelastic properties of two phases affect the type of the dispersion mode.

Han and Kim (1975) performed an extensive experimental study on the dispersed two-phase flow of polymeric melts. As an incompatible polymer blending pair, polystyrene and high-density polyethylene were chosen. They extruded the blends through a circular tube die attached to a single-screw extruder, and measured the wall normal stress along the longitudinal direction of a capillary die. The wall normal stress allows one to determine the viscous and elastic properties of the blends. They found that both the viscosity and the elasticity of the blend go through a minimum and then a maximum at a certain blending ratio. However, when the viscosity shows the minimum, the elasticity approximately shows the maximum at that blending ratio. They explained this behavior using rheological characteristics of the matrix / dispersed morphology. They argued that the dispersed phase having lower viscosity would dissipate less of the energy while flowing through the die, which results in the higher elasticity and the lower viscosity behaviors in the blends.

Chin and Han (1979) studied droplet deformation theoretically in a steady extensional flow field, and performed an experimental study using a straight cylindrical tube. In their theoretical study, the effects of elasticity, viscosity, and interfacial tension of fluids were taken into account. Droplets were injected in the conical section in the centerline of the flow channel, and droplet deformation was observed. The viscoelastic droplets were less deformable than the Newtonian droplets.

The formation of a dispersed phase in incompatible polymer blends with a co-rotating twin-screw extruder was studied by Wu (1987). A master curve explaining the relationship between the dispersed phase and material properties was proposed.

$$\frac{\dot{\gamma}\eta_m D_d}{\gamma} = 4\,p^{0.84} \tag{2-21}$$

where $\dot{\gamma}$ is the shear rate, η_m is the matrix viscosity, D_d is the particle diameter, γ is the interfacial tension, and p denotes the viscosity ratio of the matrix and the dispersed phase, η_d / η_m. The positive sign applies for $p>1$, and the negative sign for $p<1$. As indicated *in Eq. (2-21)*, the size of the dispersed phase is directly proportional to the interfacial tension and ±0.84 power of the viscosity ratio. It should be noted that the minimum size of the dispersed droplets in *Eq. (2-21)* is obtained when the viscosity of the two polymers is the same. And the author observed the minimum size of droplets at $p=1$ in their polyester / ethylene-propylene rubber and nylon / ethylene-propylene rubber blending systems.

Favis and Chalifoux (1987) and Favis et al. (1987) examined the dispersed phase size as a function of the viscosity ratio and the torque ratio in polypropylene / polycarbonate blends. They found the dispersed phase size increasing by a factor of 3 to 4 times from $p=4.5$ to $p=17.3$. It should be noted that the minimum size was obtained at $p=0.15$ while Wu (1987) observed it at $p=1$. They pointed out that a significant particle disruption occurred at a viscosity ratio of $p=17.3$ unlikely a shear flow field of Newtonian systems which do not disrupt above $p=4$. The interpretation using a torque ratio, torque of the dispersed phase / torque of the matrix, was given to explain the dispersed behavior. The effect of the composition on the phase size was also investigated. By increasing the concentration of polycarbonate from 10 to 30%, the volume average diameter gradually increased from 3.7 μm to 5.9 μm. However, the minor phase becomes very sensitive to the concentration by increasing up to 40% due to particle-particle interactions. Palierne (1990) studied incompatible viscoelastic emulsions theoretically and derived a linear viscoelastic modulus of the emulsion system at arbitrary concentration and polydispersity of spherical dispersed particles. Sundararaj and Macosko (1995) studied the drop breakup and the coalescence in

polystyrene / polypropylene blends. The study showed a limiting dispersed particle size observed at very low concentration of the minor component. The final particle size increased with the dispersed phase concentration due to the increased coalescence. The particle size distribution was also broadened at higher concentration and also a comparison of the particle size to the Taylor's prediction was given. It has been found that Taylor limit underestimates the limiting particle size because it does not consider the elasticity of the droplets. They also investigated the effect of the shear rate on the dispersed size. The size increased by increasing the shear rate, and they explained the behavior using coalescence and viscoelasticity. Even though the effect of compatibilization was studied in their work, it is not reviewed here.

Sundararaj et al. (1995) investigated the evolution of the phase morphology of immiscible polymer blends. Pellets of the dispersed phase are stretched out into sheets, which break up into cylinders via different mechanisms. Three breaking-up steps from polymer pellets to the dispersed particles are suggested: 1) by stretching into cylinders with drops streaming off the end, 2) by extending sheets that forms fingers at the edges, and 3) by stretching into thin sheets that break up by forming holes. They presented a map showing the different regions of breakup. The map shows that sheets are formed easily when the Deborah number increased. Low enough shear rates lead to cylindrical shapes from the pellets.

The effect of elasticity on the dispersed drop diameter was predicted by Ghodgaonkar and Sundararaj (1996). The forces deforming a polymer droplet in a matrix are the shear force and the first normal stress of the matrix, and the deformation is resisted by the interfacial force and the first normal stress of the droplet. They showed that the size of the dispersed phase could be explained qualitatively by the force balance.

Scott and Joung (1996) investigated the viscosity ratio effect of immiscible fluids incorporated into polymer matrix during the compounding process. The viscosity ratio of polyethylene / polystyrene was varied form 0.7 to 0.003 by changing the molecular weight of both polymers. A critical viscosity ratio, which greatly retards softening of polystyrene, was found around 0.1.

Recently, Bourry and Favis (1998) investigated the effect of mixing procedures on the blending morphology for PS / HDPE blends. Three different feeding manners were applied: 1) both of HDPE and PS were added in the hopper of the twin-screw extruder, 2) HDPE was fed in the twin-screw extruder and PS was added as a melt using a single-screw extruder connected to the twin-screw extruder, 3) the PS melt stream was added to the downstream of the twin-screw extruder. Therefore, the cases 2 and 3 involves melt-melt mixing. It has been found that the size of the dispersed phase and the size distribution are independent of the mixing manners for all PS / HDPE compositions studied. They concluded that the blend morphology does not depend on the melting or softening step.

2.5.2. Polyethylene / Polystyrene (PE/PS) Blend

PE / PS binary blends have been studied since the early 1970s. These blends are of interest due to their immiscibility and the availability of compatibilizers. Early studies of such blends were mainly focused on rheological properties, morphologies and mechanical properties without compatibilizers. Since the 1980s, most studies have focused on the effect of compatibilizers (such as copolymers and reactive polymers), the degree of mixing, and the mechanical and rheological properties.

Han and Yu (1971) investigated the rheological properties of PS / PE and PS / PP blends using a capillary rheometer at 200°C. The effects of composition on the viscous and elastic properties were characterized by measuring the wall normal stress and the exit pressure, respectively. It was observed that the viscosities of PS / PE and PS / PP blends were lower than the viscosities of the pure components, and that a minimum value of viscosity of a two-phase system existed at a certain composition. They also reported a minimum value for melt elasticity at 10 wt% PS and a maximum value for melt elasticity at 90 wt% PS in the PS / PE blend system. They also found a finely dispersed morphology at the core of the extrudate, rather than at the edge of the extrudate.

Mechanical properties of PS / PE blends were studied by Barentsen and Heikens (1973). They reported that the yield strength and the tensile strength passed through a minimum at certain composition, and that an improvement of the properties was achieved by adding a small amount of PE-PS copolymer. They also investigated the impact strength behavior. All results reported in their work are the behaviors generally accepted for most polymer blends.

Han and Kim (1975) published results similar to those of Han and Yu (1971). The effects of temperature and shear stress on the viscosity and elasticity of PS / HDPE blends were investigated. At 200°C, the viscosity of PS is greater than that of HDPE; the viscosity of the blend goes through a minimum at a blending ratio of 55 wt% PS, and then goes through a maximum at a blending ratio of 20 wt% PS. By increasing the temperature up to 240°C, however, the viscosity of PS becomes lower than that of HDPE, and then the viscosity of the blend has no minimum, but still has a maximum at 20% PS. The elastic behavior of the blend also shows minimum and maximum values at certain compositions.

The droplet size of the HDPE phase (domains of 25/75 HDPE / PS blend) decreases as the melt temperature increases from 200°C to 240°C, while the droplet size of the PS phase (domains of 75/25 HDPE / PS blend) is not affected by either melt temperature or wall shear stress. It is suggested that the dispersion mode depend on the viscoelastic properties of the two-phase fluids.

The flow behavior of PS / PE blends through a capillary die was studied by Lee and White (1975). The difference in the composition across the extrudate was found through analysis of the capillary flow. A greater quantity of the lower viscosity component was mainly located in the surface region, rather than in the core region of the extrudate. Based on these experiments, the viscosity of the melt blend was suggested as a function of the volume fraction and the viscosity of each component.

Heikens et al. (1978) performed experiments for the mechanical properties, the morphology, and the effect of compatibilizers on PS / PE blends using a Brabender laboratory mixer. The behavior of the apparent particle dimensions was evaluated without compatibilizers. The domain sizes of PS-rich blends are smaller than those of PE-rich blends. Thus, the dispersed PE particles are smaller than dispersed PS particles when either component forms a very minor phase. This result is in general agreement with the Taylor's formula (1932), according to which the particle size is proportional to the interfacial tension between two components and is a function of the viscosity ratio and the shear rate. However, by increasing the concentrations of PE or PS, the size of the PE particles become larger than that of the PS particles. The overall blend viscosity and coalescence were applied to explain the phenomenon. Co-continuous phase behavior is found in the range of 30 to 60 wt% of PE.

Aref-Azar et al. (1980) studied the effect of the morphology on the crystallization characteristics. They argued that cylindrical rods of PE dispersed in PS were observed at a 50/50 composition of PE / PS. With PE in excess, the crystallization kinetics was insensitive to the morphology. However, when the PE phase forms a dispersed phase, it becomes dependent on the size and number of the spheres dispersed in PS matrix.

Min et al. (1984) performed an experimental study on the phase morphology, rheological properties and the processing behaviors for PS / HDPE blending system. The blends were prepared using a single-screw extruder and a static mixer. The dimensions of the dispersed phase varied from 1 to 5 μm in the products prepared from the static mixer, the cone-and-plate, and the capillary die, while the melt-spun fibers exhibited the dispersed phase dimensions as low as 0.35 μm. The shear viscosity and the principal normal stress difference, N_1, exhibited maximum and minimum when they were plotted to the composition. The shrinkage of PE extrudate was much higher than that of PS, and the additional small amount of PE in PS greatly increased its shrinkage. The shrinkage was measured using a hot silicon oil bath after the capillary die. The extrudate swell behavior was also investigated as a function of composition. It was found that the addition of PE to PS initially increased the extrudate swell and showed the maximum and minimum at the same compositions at which the normal stress difference showed maximum and minimum.

PS / PE blends involving a chemical reaction have been studied for the improvement of the blend properties. Baker and Saleem (1987) used oxazoline and carboxylic acid grafted to PS and PE, respectively. van Ballegooie and Rudin (1988) introduced dicumyl peroxide and triallyl isocyanurate to 50/50 wt% of PS / PE blends for a reactive extrusion using a counter-rotating twin-screw extruder. Dicumyl peroxide and triallyl isocyanurate were used

as coupling agents, and the PS was modified with a minor amount of ortho-vinylbenzaldehyde. Examination of the tensile properties was performed and the morphology arising from the reactive extrusion process was also investigated. Utracki and Sammut (1988) used a partially hydrogenated poly(styrene-b-isoprene) di-block copolymer as a compatibilizer for PS / LDPE blends. The rheological properties were examined using a Rheometrics Mechanical Spectrometer (RMS) with parallel plates. Recently, Yang et al. (1995a, 1995b), Harrats et al. (1995) and Li et al. (1995) published the PS / PE blends with various types of compatibilizers.

2.6. REACTIVE BLENDING OF POLYOLEFIN / POLYAMIDE

Reactive blending techniques have been used as a method to give compatibility to immiscible polymer blends. An extensive study including numerous general reviews has been performed. For instance, Bonner and Hope (1993) summarized the numerous methods for the compatibilization to four categories:

(a) Achievement of thermodynamic miscibility

(b) Addition of block and graft copolymers

(c) Addition of functional / reactive polymers

(d) *In situ* grafting / polymerization

All categories involve the modification of the polymer interfaces, which results in the change of the phase morphology and inter-phase adhesion. The reactive blending technique is corresponding to the third and fourth categories.

The polyolefin / polyamide (PO / PA) blends have been studied for increasing toughness of polyamide by adding low modulus polyolefin polymer. Due to their

immiscibility, the PO / PA blends show poor mechanical properties and efforts for increasing the compatibility have been carried out. Ide and Hasegawa (1974) studied the effect of maleic anhydride-grafted polypropylene in isotactic PP / PA6 blends. The improved dispersion behavior was observed, and they suggested a reaction mechanism between the maleic anhydride (MAH) and the terminal amine group (NH_2) of PA6 as shown in *Figure* 2.2. The chemical reaction resulting in the formation of PO / PA copolymer was verified by analyzing residual amine groups. It was found that the residual amine groups decreased with increasing maleic anhydride content on PP. Remarkable improvement in mechanical properties was observed.

In order to perform the extrusion experiment of PE / PA6 / PE-g-MAH blends in the presence of CO_2 in this thesis, literature focused on the reactive polyolefin (PO) / polyamide (PA) is reviewed in this section.

Hobbs et al. (1983) focused on the fractured toughness and the deformation mechanism of PA66 / PE-g-MAH blend. Over 0.4 percent of MAH was required for a good adhesion between two polymers. By increasing the MAH content, the volume averaged diameter of the dispersed PE-g-MAH phase decreased from 2.4 μm to 0.4 μm in PA66 / PE-g-MAH=70/30 blending ratio. Borggreve et al. (1988) studied the impact behavior of PA6 / EPDM-g-MAH blends

Park et al. (1990) reported the positive deviation from the linear mixing rule in the viscosity behavior of reactive PP / PA6 / PP-g-MAH blending systems at shear rate ($10\ s^{-1}$), while non-reactive PP / PA6 blends showed the negative deviation. They cited Han's (1981) suggestion: the positive deviation generally occurs either a strong interaction among the dispersed droplets or an interlocked blending morphology. The authors used the latter case

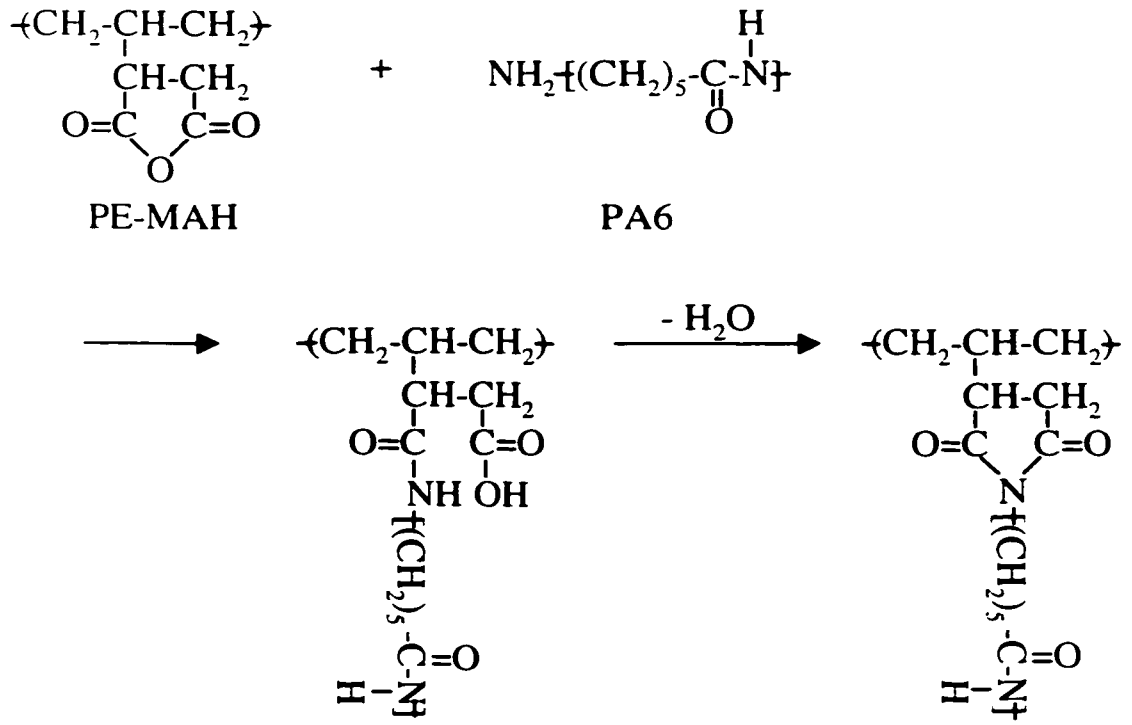

Figure 2.2. The Proposed reaction mechanism between PE-MAH and PA6 (Ide and Hasegawa, 1974)

for explaining their viscosity behaviors. Thus, they argued that the reaction between -MAH and $-NH_2$ induced a strong interaction between the two phases, and the blends became hard to flow, which result in the positive viscosity deviation.

Lavallee and Favis (1991) investigated the size of the dispersed phase in PE copolymer / PA6 at various mixing times and compositions. The PE copolymer is a random terpolymer consisting of 80% of PE and 20% of methacrylic acid and isobutyl acrylate. They applied the FTIR technique and SEM for the characterization. The size of the dispersed droplets reduced with increasing torque associated with the reaction between two polymers. They also presented that the control of the interfacial reaction allows for the preparation of a composite droplet morphology, and the sub-inclusion size and concentration can be controlled.

Hietaoja et al. (1994) studied the effect of viscosity ratio on the morphology of PA66 / PP blends when PP-g-MAH was used as a compatibilizer. They found the size reduction of dispersed PA phases by approaching the viscosity ratio to unity. However, no clear correlation between the viscosity ratio and the particle size was observed when PP was the dispersed phase. At the composition of PA20 / PP80, the number average particle size increased linearly from 1.7 μm at p=0.3 to 8.1 μm at p=2.2, and at PA80 / PP20, it varied from 4.2 μm to 6.1 μm in the range of the viscosity ratio of 0.5 to 3.1. They also pointed out that the dispersed phase was too fine to measure the individual particle size using SEM, and the particle size was discussed using the viscosity ratio of two polymers only when the compatibilizer was not used.

Dagli et al. (1994) performed a kinetic studies for the reaction between PA6 / PP in the presence of polypropylene-g-acrylic acid (PP-g-AA) which forms polypropylene-g-

anhydride (PP-g-AH) by dehydration reaction. They pointed out that the rotor speed affected the reaction kinetics significantly, whereas the temperature changes in the 15-20°C range had no effect.

Scott and Macosko (1994) investigated the morphology development from pellet-sized particles to submicron droplets for PA / ethylene-propylene rubber (EPR) blends. The investigation was carried out for non-reactive blends and reactive blends involving the amine-anhydride reaction. The major size reduction in the dispersed phase was found to occur at short mixing times: the volume average diameter of the dispersed phase was reduced form 4 mm (pellet size) to 1μm within the first 90 seconds of mixing in the reactive PA / EPR blends. They also observed that the interfacial chemical reaction reduced the dispersed phase size and made the size distribution narrow.

Lee and Yang (1995) performed the various mixing processes for clarifying the effect of PP-g-MAH on the PP / PA6 blends. They argued that the single step blending process led to a better morphological structure rather than the two step blending processes, first of PP-g-MAH with PP and then with PA6 or first of PP-g-MAH with PA6 and then with PP. The blends prepared from the latter two step blending process called as a reactive two step blend, led bigger dispersed particles than others. They explained that most of the PP-g-PA6 might reside in the PA6 phase, and little contribution to the size reduction was expected.

Gonzalez-Montiel et al. (1995) and Sathe et al (1996) investigate the morphology-property relationship for reactive PP / PA6 blends. Generally, a finely dispersed phase was obtained and better mechanical properties were observed when compatibilizers were used.

2.7. POLYMER BLENDS WITH A SUPERCRITICAL FLUID

Kung et al. (1997) tried to prepare polystyrene / polypropylene blends using supercritical CO_2. However, the method is not a conventional route for preparing the polymer blends. They prepared high-density polyethylene substrates by compression molding, and then made the substrate swollen with styrene monomer in the presence of supercritical CO_2 at 80°C and 240 atm. The gas-like diffusivity of supercritical CO_2 enhanced the infusion kinetics of styrene. Finally, the polymerization took place in the HDPE substrate. During the process the substrate remained in a solid state and the reaction was confined to an amorphous phase. They prepared samples up to 43 wt% of polystyrene. SEM analysis indicates that polystyrene exists throughout the sample.

Elkovitch et al. (1997) investigated the effects of carbon dioxide on poly(methyl methacrylate) / polystyrene blends having various viscosity ratios. They indicated a higher absorption of carbon dioxide in PMMA than in PS (Elkovitch et al., 1998), and expected the higher viscosity reduction in PMMA which made the viscosity ratio becomes closer. They argued that the domain size of the dispersed PMMA phase was reduced, which indicating a lower viscosity ratio.

CHAPTER 3. EXPERIMENTAL

3.1. INTRODUCTION

Extrusion of polymers and polymer blends in the presence of a supercritical fluid requires special techniques such as the injection and flow rate control of a SCF and the complete dissolution of the injected SCF. In this thesis, therefore, various extrusion system were utilized to clarify the effects of supercritical CO_2 on the polymer viscosity, foamed structure and blending morphologies of non-reactive and reactive polymer blends. In order to perform the experiments, several extrusion systems and devices were specially designed based on typical extruders, single-screw and twin-screw extruders. A general description of the equipment, materials and operating conditions is given in this chapter. Details such as design concepts for experimental setup, screw configurations, experimental conditions and procedures, will be discussed through Chapter 5 to Chapter 8 separately.

3.2. MATERIALS

3.2.1. Low Density Polyethylene

Low density polyethylene (LDPE, Novacor LF0219A by Nova Chemicals) was chosen not only for non-reactive PE / PS blends but also for reactive PE / PA6 blends. The average molecular weights and polydispersity were measured by Gel Permeation Chromatography (GPC) and are listed in *Table 3.1*. The shear viscosity was also measured using a Kayeness Galaxy V capillary rheometer at various temperatures and data shown in *Figure 3.1*.

3.2.2. Polystyrene

Polystyrene (PS, 101C by Nova Chemicals) was used for the measurement of polymer / CO_2 solution viscosity and non-reactive PE / PS blends. The average molecular weights and polydispersity were also measured by Gel Permeation Chromatography (GPC) and are listed in *Table 3.1*. The shear viscosity data are shown in *Figure 3.2*.

Table 3.1. Molecular weights and polydispersities of polyethylene and polystyrene

	M_n	M_w	M_w/M_n
PS	131000	374000	2.85
LDPE	38700	334000	8.64

3.2.3. Polyethylene-g-Maleic Anhydride

Polyethylene-g-Maleic anhydride (PE-MAH, Fusabond MB-226D by Dupont) was used for the reactive PE / PA6 blends. The concentration of -MAH in PE was known to be about 1.0 wt% from the resin supplier. No further characterization was performed. This resin was extruded to transform the acid group to anhydride before the blending experiment. FTIR spectra will be given at Chapter 8. The shear viscosity was also measured and is shown in *Figure 3.3*.

3.2.4. Polyamide 6

Polyamide 6 (PA6, Capron 8202 by Allied Signal Ltd.) was used for the reactive PE / PA6 blends. Due to the moisture sensitivity of polyamide, the resin was dried forfour hours at 80°C in a vacuum oven before the experiments. The shear viscosity is shown in *Figure 3.4*. It should be noted that the PA6 shows a lower viscosity than the other resin and that its behavior was Newtonian for shear rates up to 40 s^{-1}.

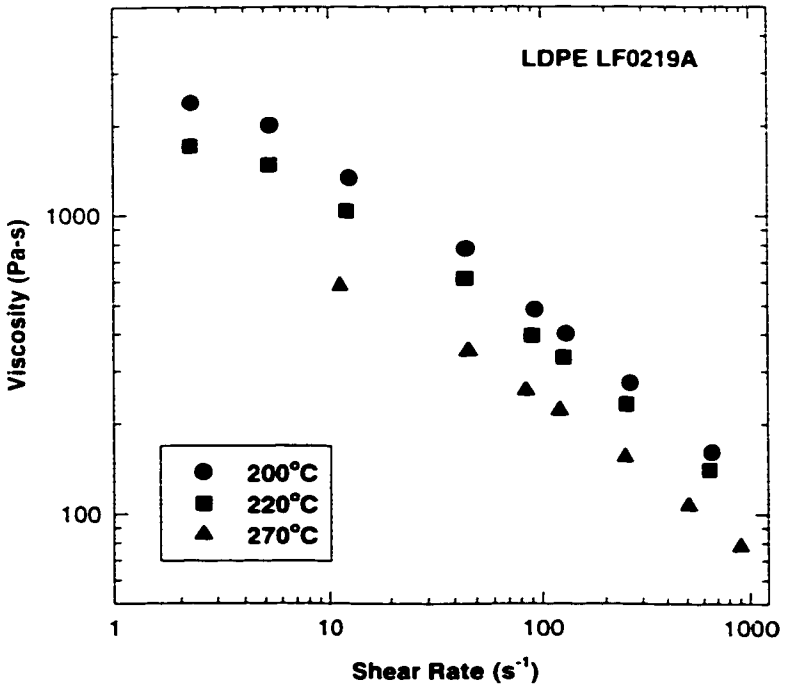

Figure 3.1. Viscosity of polyethylene at various temperatures

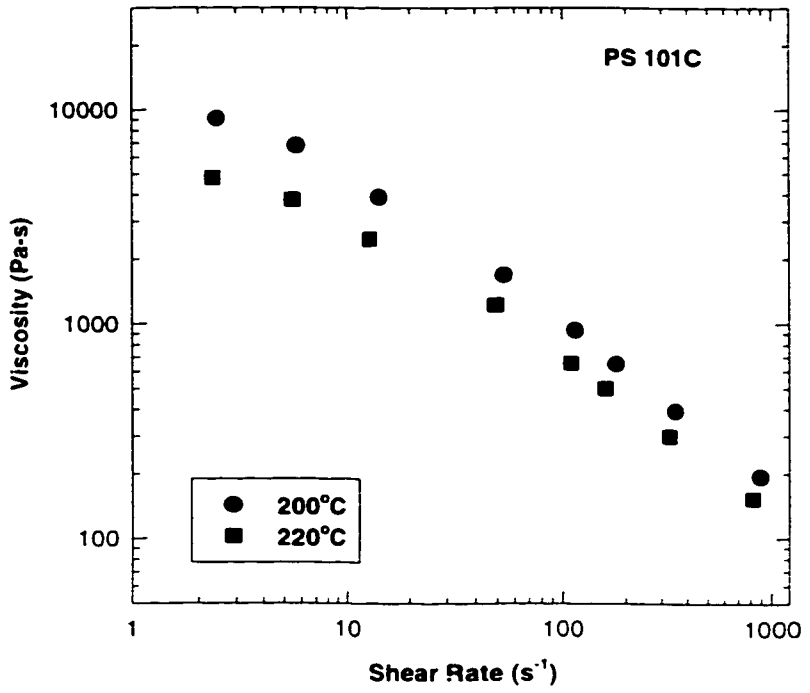

Figure 3.2. Viscosity of polystyrene at various temperatures

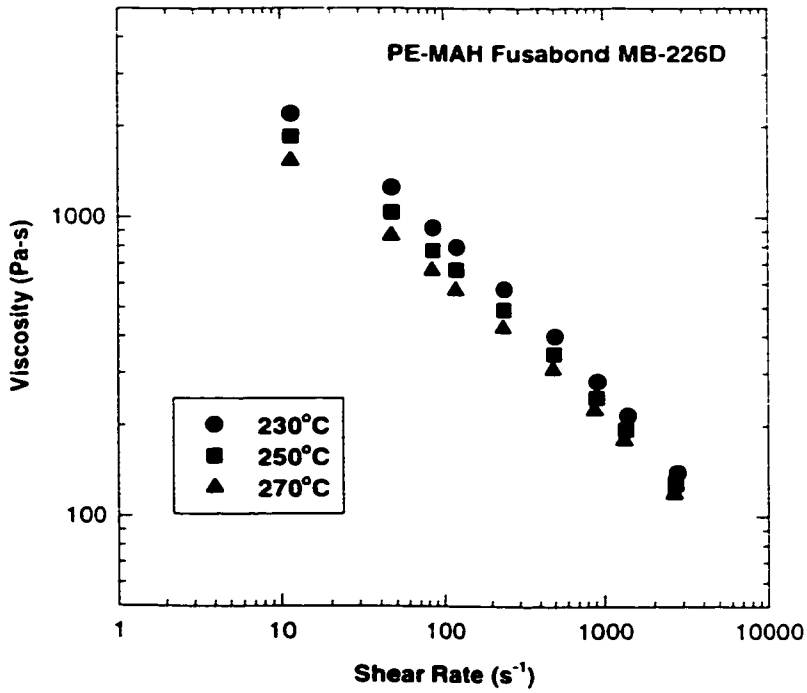

Figure 3.3. Viscosity of polyethylene-g-maleic anhydride at various temperatures

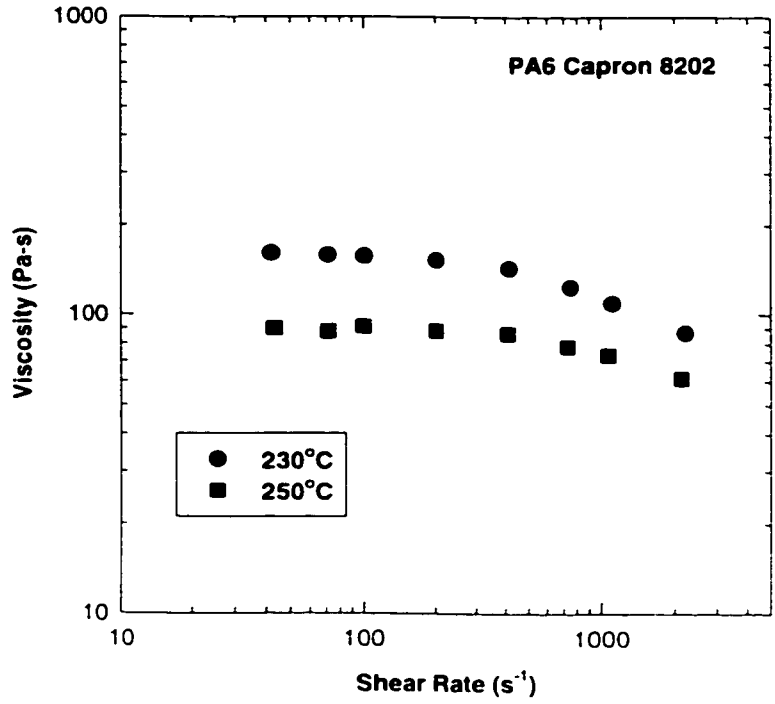

Figure 3.4. Viscosity of polyamide 6 at various temperatures

3.2.5. Supercritical Carbon Dioxide

Carbon dioxide (SFC grade by Air Products Corporation) was used as a supercritical fluid in the experiments. It was supplied 99.997% purity and an initial cylinder pressure of about 1900 psi. The cylinder was supplied with a high-pressure helium headspace, which helped maintaining the high pressure.

3.3. EQUIPMENT

3.3.1. Microcellular Extrusion System

The microcellular extrusion system used in these experiments consisted of a single-screw extruder equipped with a CO_2 injection port, static mixers, a capillary die and a high resistance nozzle. A schematic diagram of the microcellular extrusion system is shown in Chapter 5 along with a detailed description. This extrusion system was specially designed for producing foams having a microcellular structure. A single-screw extruder was used with a standard square pitch screw having a special mixing section. CO_2 was injected through an injection port into the metering section. At the end of the screw tip, static mixers were attached to enhance dissolution of CO_2 into the polymer melt.

In order to measure the viscosities of polymer / CO_2 solutions, capillary tube dies having 2.3 mm and 6.5 mm diameters were used. Also, several nozzles of different diameters and lengths were used for varying the pressure in the capillary tube die. The dimensions of these nozzles are given in *Table 3.2*. Nozzles A and B were used for the viscosity measurement of PS and nozzles C and D were used for the viscosity measurement of PS / CO_2 solutions. The temperatures of the die and nozzles were controlled by band heaters and PID controllers.

Table 3.2. Dimension of nozzles used in a microcellular extrusion system.

	Nozzle A	Nozzle B	Nozzle C	Nozzle D
Diameter (cm)	0.053	0.089	0.046	0.046
Length / Diameter Ratio	24	7	45	25

3.3.2. Leistritz LSM 30.34 Twin-Screw Extruder

The twin-screw extruder used in these experiments was a co-rotating and fully intermeshing extruder having 34 mm screw diameter and a L/D=30. The extruder has 10 barrel sections and the temperature of each section is controlled separately. Two barrel sections were equipped with two injection ports. These injection ports were used for injecting supercritical CO_2 and for connecting two flow streams in a twin-single tandem extrusion system. A polymer or dry blended polymer pellets were fed into the extruder by a K-tron F-1 series loss-in-weight feeder (LWFD5-200) regulated by a KDU controller. Depending on the experiment, a wedge die and/or a devolatilization section were used.

3.3.3. Haake Rheomix 252 Single-Screw Extruder

A Haake Rheomix 252 single-screw extruder was attached to the Haake Rheocord 90. In order to inject supercritical CO_2 into the barrel, pressure transducer port on the barrel was used and a special injection device was designed. However, the injection point was on the right end of the solid conveying section when a conventional single-screw configuration was used, as shown in *Figure 3.5(a)*. In this case, most of the injected CO_2 leaked through the feed hopper due to the incomplete melting and the low pumping capacity. Increase of the screw pumping capacity at the injection point and the early melting process are necessary for injecting CO_2 successfully. Therefore, a new screw was designed as shown in *Figure 3.5(b)*.

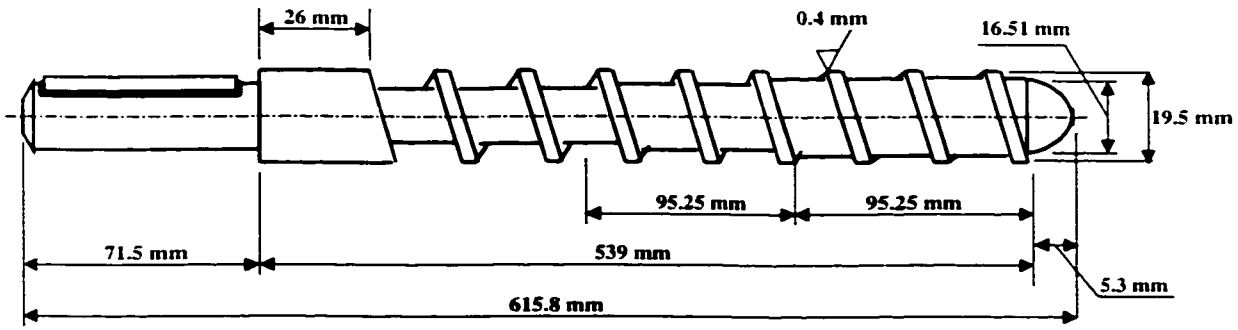

(a) Dimension of a conventional single-screw configuration

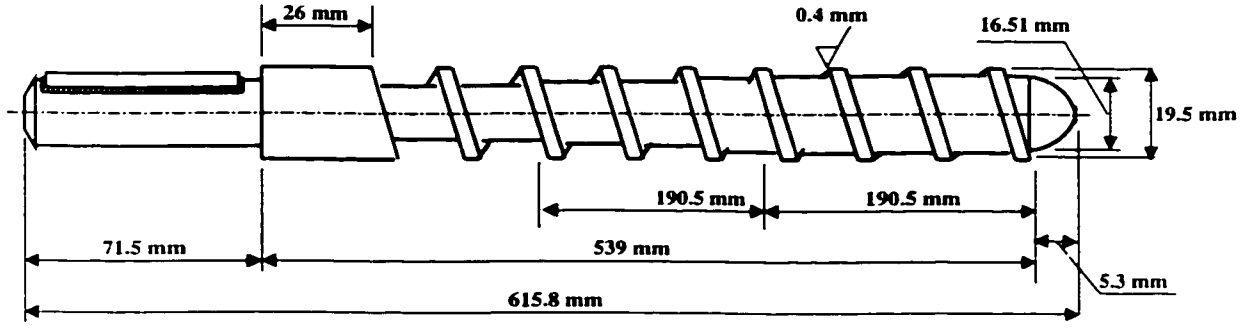

(b) Dimension of a single-screw configuration for injecting CO_2

Figure 3.5. Schematics of the screw configuration of a single-screw extruder

By increasing the length of the compression and metering sections, the CO_2 injection port was designed to be located at the end of the compression zone. Using the newly designed screw configuration, a successful injection of CO_2 was achieved. Thus, all injected CO_2 was dissolved into the polymer melt stream flowing downstream without any upstream leaking. Pellets were charged to the extruder by a Brabender FlexWall feeder via a vibrating feed hopper. The polymer flow rate was controlled by the screw speed.

3.3.4. Twin/Single Tandem Extrusion System

A twin/single tandem extrusion system was designed in order to carry out not only melt/melt blending experiments but also for the preferential dissolution of CO_2 into matrix and/or dispersed polymer phase. Depending on the use of the wedge die, devolatilization and the connecting location of two extruders, various configurations were designed. Detail schematics of the configurations are shown in Chapter 7.

3.3.5. ISCO Positive Displacement Pump

Supercritical CO_2 was injected using a positive displacement pump. Two models, 100DX and 260D, were used in this experiment, and their specifications are compared in *Table 3.3*. The pump is able to deliver fluid at a constant pressure mode and a constant volumetric flow rate mode. The pump cylinder was filled up first from a CO_2 cylinder and then pressurized to the desired setpoint in the constant pressure mode. During the experiment, the constant flow mode was used to meter a known volumetric rate of CO_2 into the polymer melt stream. The volumetric flow rate is converted to the mass flow rate using the CO_2 density predicted from the S-L EOS theory. The pump operating pressure should

always be maintained higher than the extruder barrel pressure. The pump was connected with an injection device using 1/8 inch tubing of 0.02 inch wall thickness.

Table 3.3. Comparison of two positive displacement pumps.

	ISCO-100DX	ISCO-260D
Cylinder Capacity (ml)	102.93	266.05
Pressure Range (psi)	10-10000	10-7500
Pressure Accuracy (%)	± 2.0	± 2.0
Flow Rate Range (min^{-1})	0.01μl-50ml	0.01 μl -107 ml
Flow Rate Accuracy (%)	± 0.5	± 0.5

3.3.6. SCF Injection Devices and a Connector for Tandem Extrusion System

Two injection devices, one for a twin-screw extruder and one for a single-screw extruder, were designed for injecting supercritical CO_2. The device for the twin-screw extruder is shown in *Figure 3.6.* A series of Swagelok compression fittings and a Leistritz liquid injection stem were used. The conventional Leistritz injection stem has a hollow space and two pinholes at the stem tip, and a liquid flows through the hollow space. Due to the high compressibility of a gas filled in the hollow space in the stem, however, the consistent injection of the gas could not be achieved. Therefore, the space volume should be minimized. The conventional Leistritz injection stem was replaced with another one having no hollow space. Thus, the controlled amount of CO_2 flows through the annular space between the threaded locking bolt and the stem instead of the hollow space. And the surface of the stem tip was grooved for gas channels.

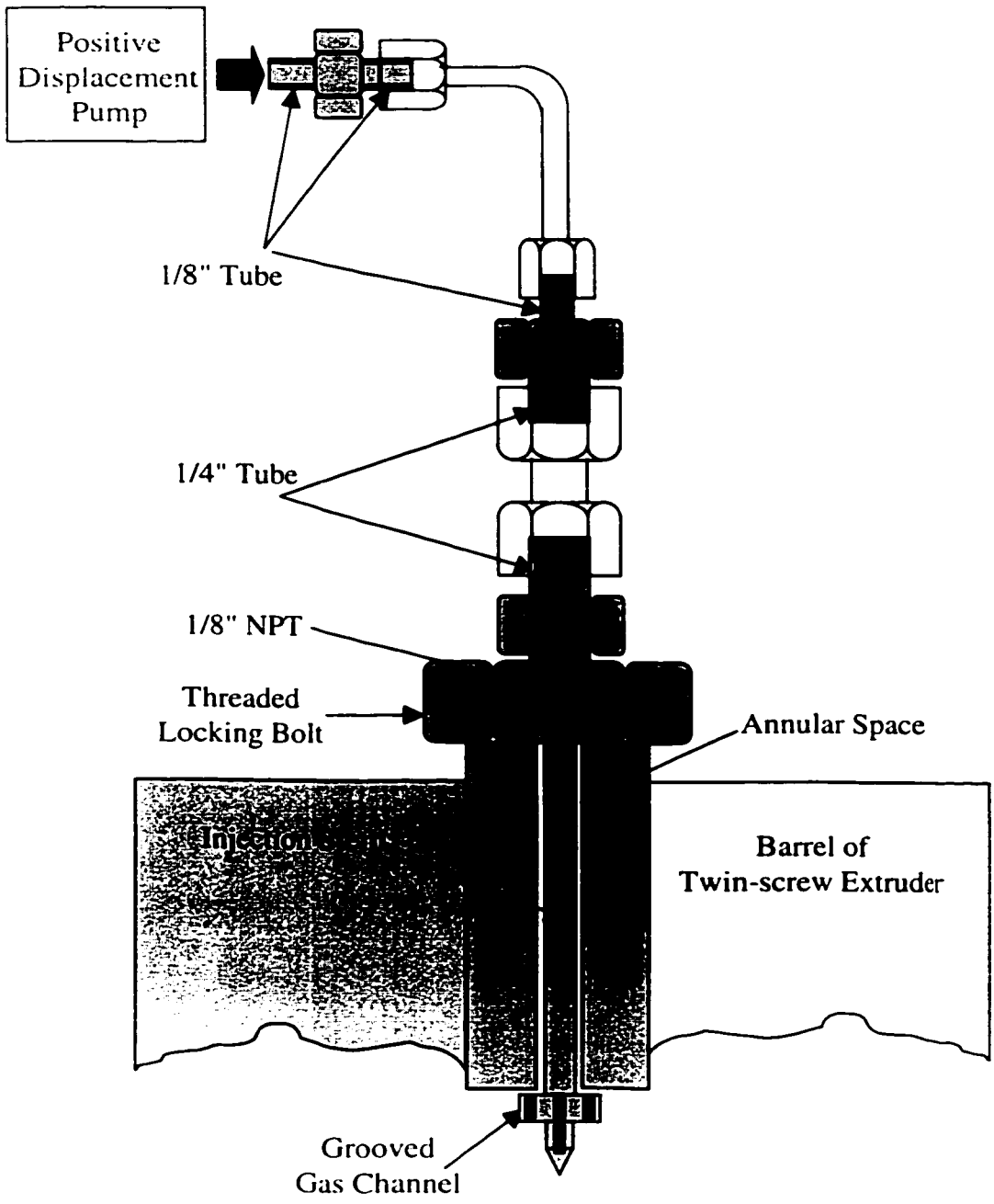

Figure 3.6. A CO_2 injecting device for a twin-screw extruder

As shown in *Figure 3.7*, the injection stem is inserted into the barrel through the locking bolt, and it seats in a narrow oval-shaped aperture. During the experiment, the extruder barrel at the CO_2 injection point is fully filled with polymer melts to generate the high pressure, and the injected CO_2 is directly swiped by the polymer melts and starts to dissolve.

An injection device for a single-screw extruder was also designed using similar concepts as in the injection device for the twin-screw extruder. However, a pressure transducer is attached to the injection device for measuring the barrel pressure, as shown in *Figure 3.8*.

A connector was designed for combining two polymer streams in the tandem extrusion system. The connector must stand high pressure because polymer/CO_2 solution should be maintained over the CO_2 solubility pressure. A series of tubing and Leistritz liquid injection hole were used as shown in ***Figure 3.9***. A heating tape was applied to the connector for controlling the polymer melt temperature.

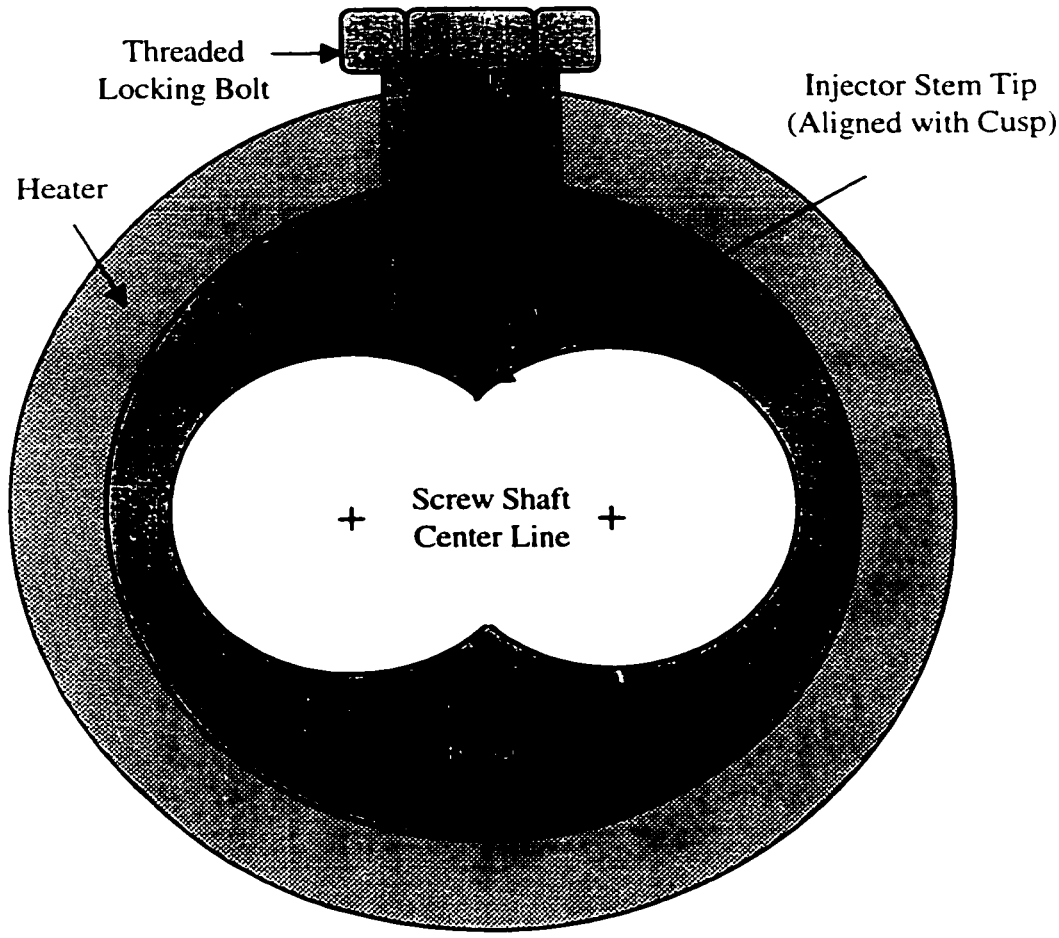

Figure 3.7. The barrel cross section of a twin-screw extruder showing the injector location

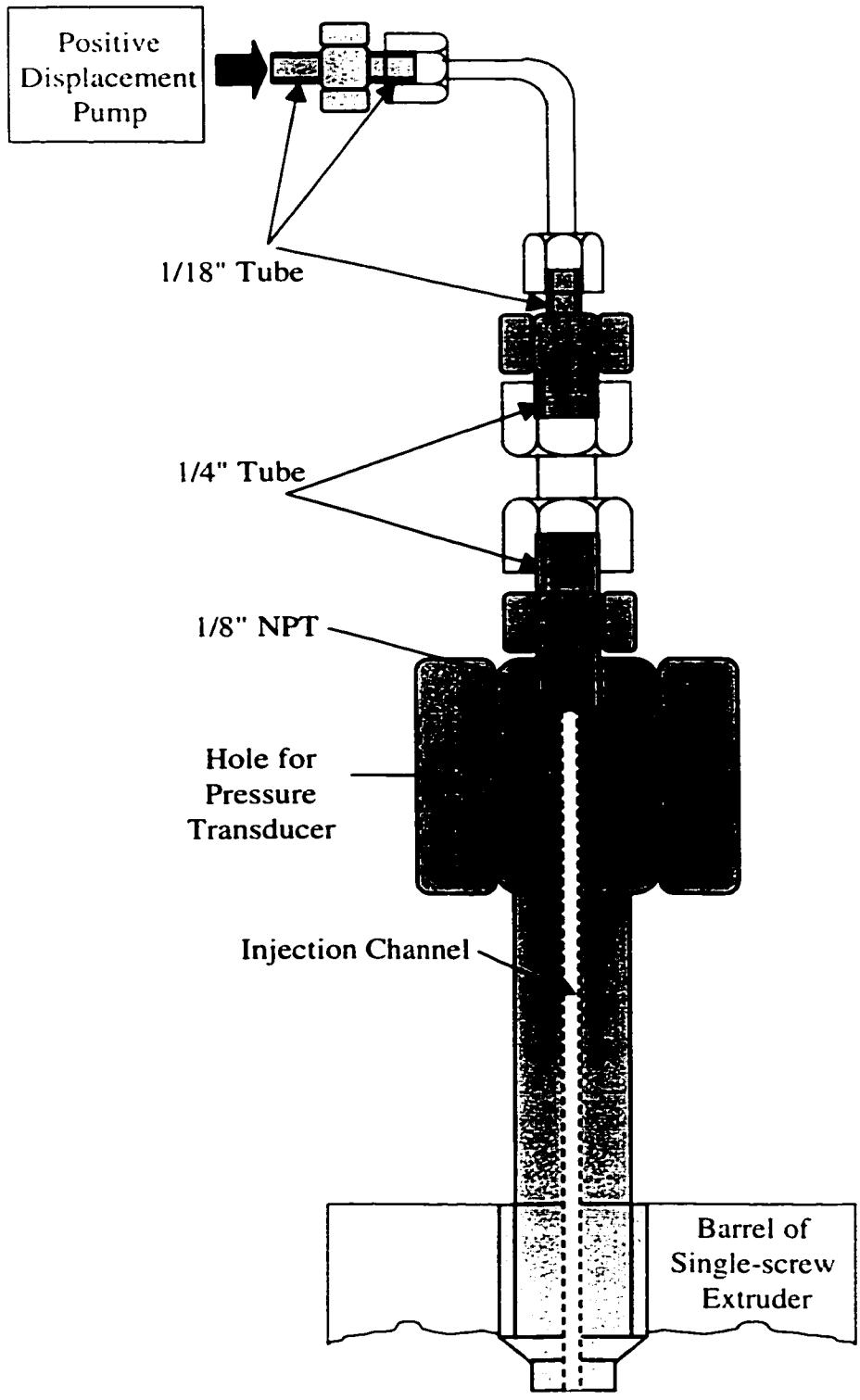

Figure 3.8. A CO_2 injecting device for a single-screw extruder

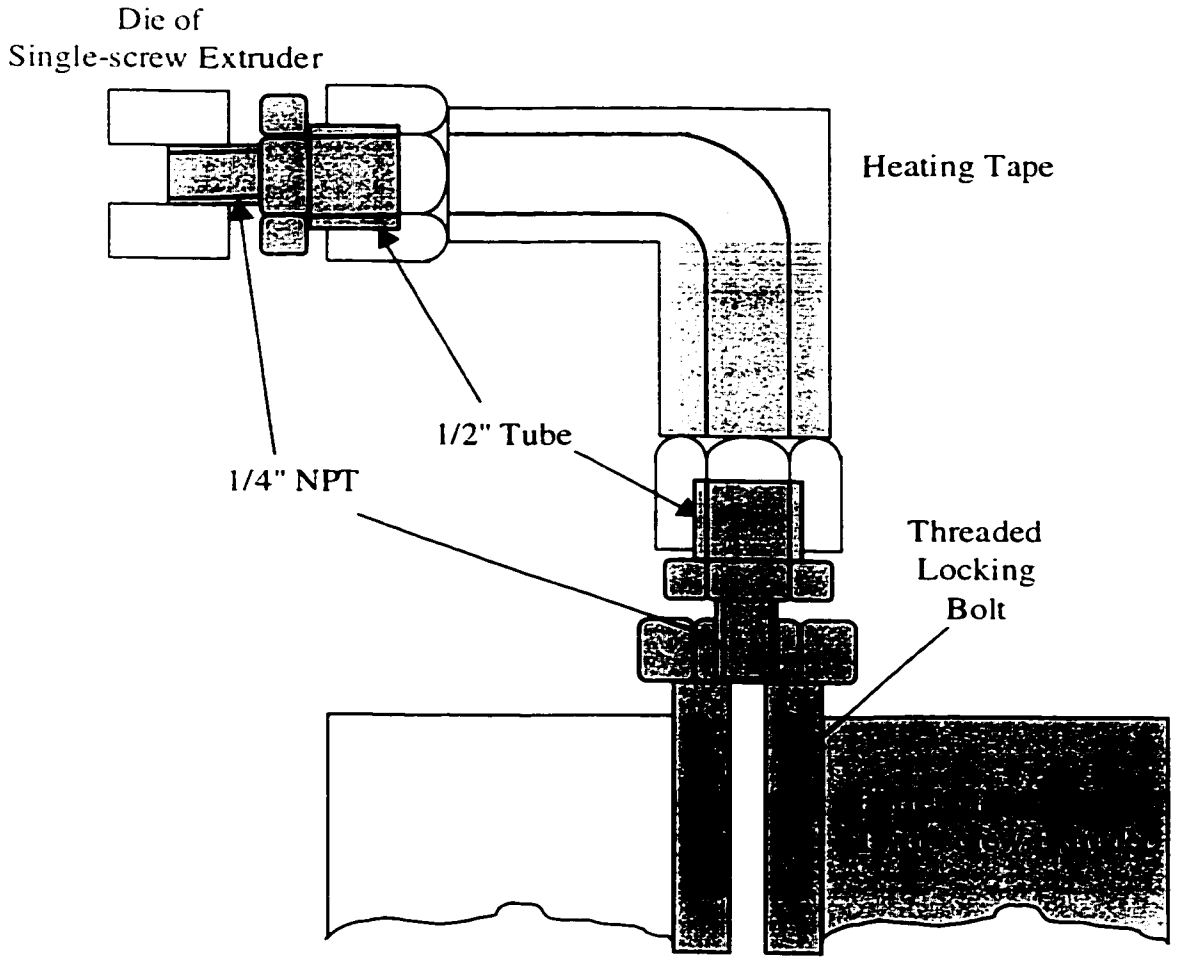

Figure 3.9. Schematic of the connector used in a twin/single tandem extrusion system

3.3.7. Opto22 Data Acquisition System

Analog signals from pressure transducers, a temperature probe, and the positive displacement pump, were converted to digital signals using an Opto22 control unit. The Opto22 unit basically consisted of a motherboard and input and output modules. The module selection is dependent upon the type of signals received or sent. All pressure transducers used had output signals between 0 and 33.3 mV full scale. For this application, Opto AD9T model covering 1-50 mV was chosen. Similarly, Opto AD7 and Opto AD12 were chosen for the temperature probe and the positive displacement pump, respectively. The converted digital signals were sent to the data-logging computer via an RS-232C cable.

The display and user interface for the data acquisition system was written using LabVIEW graphical program (Version 4.0). The digital signals were sampled 25 times per 6 seconds and displayed on the graphs. LabVIEW programs used in this study are shown in Appendix I.

3.4. CHARACTERIZATION

3.4.1. Capillary and Cone-Plate Rheometers

A Kayness Galaxy V capillary rheometer was used for measuring the shear viscosities of various polymers used. The capillary diameter and the L/D ratio used are of 0.03 inch and 40, respectively. Due to the high L/D value, the Bagley correction was not applied in *Figure 3.1* through *Figure 3.4*.

A cone and plate rheometer (Rheometric Scientific SR200) was also used for the viscosity measurement of polystyrene at low shear rates. Even though Cox-Merz (Cox and Merz, 1958) rule has been known, the measurement was performed at the steady shear mode

instead of the dynamic oscillation mode in order to compare the viscosities to the viscosities obtained from a capillary rheometer.

3.4.2. Linear Tube Die

Two linear tube dies having 2.3 mm and 6.5 mm diameters, were attached to the microcellular extrusion system for measuring the viscosity of unsaturated polystyrene and PS / CO_2 solutions. Schematics of the linear tube dies are shown in *Figure 3.10.* In order to minimize the entrance effect on the overall pressure drop, the L/D of the capillary die was chosen to be 40. A thermocouple was installed to measure and control the melt temperature. Two pressure transducers were also introduced to measure the upstream and downstream pressures. The upstream pressure transducer is located far from the tube entrance to ensure a fully developed flow.

3.4.3. Wedge Die Rheometer

A wedge die was used for measuring the viscosity of unsaturated and saturated polymers on line in the twin-screw extruder. Three pressure transducers (two Dynisco PT462-5M-6/18 and one PT462-7.5M-6/18) and a temperature probe (Dynisco MTS 922-6/24) were used for measuring the melt pressures and temperature, respectively. Dimensions of the wedge die are shown in *Figure 3.11.* The temperature of the wedge die was controlled using a band heater with 730W capacity, attached to a PID controller.

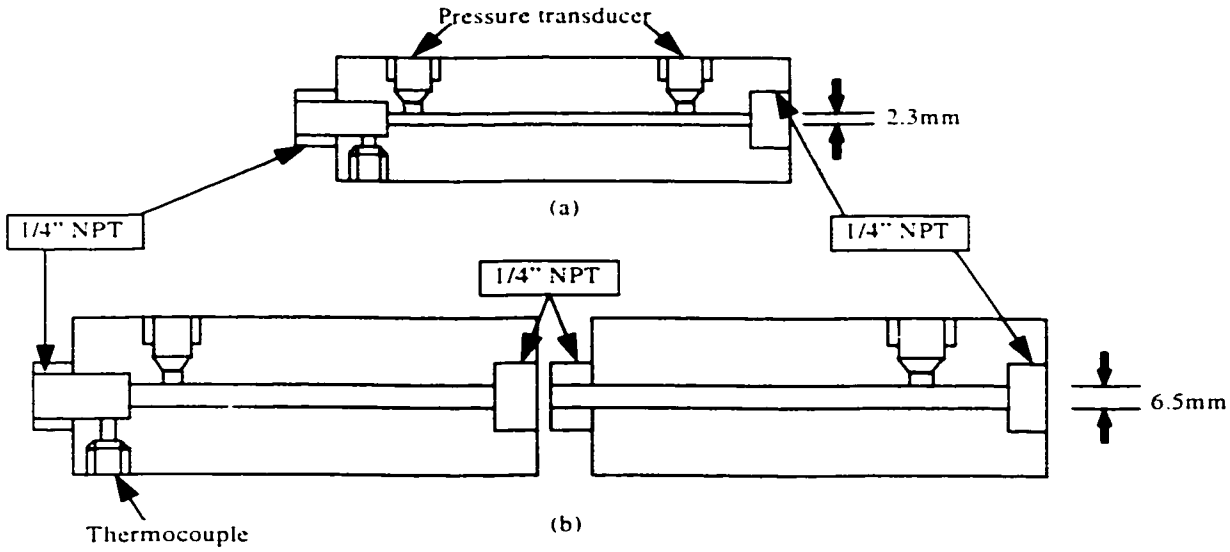

Figure 3.10. Schematic of linear tube dies attached to a microcellular extrusion system (a) D=2.3 mm, L/D=40 (b) D=6.5 mm, L/D=40

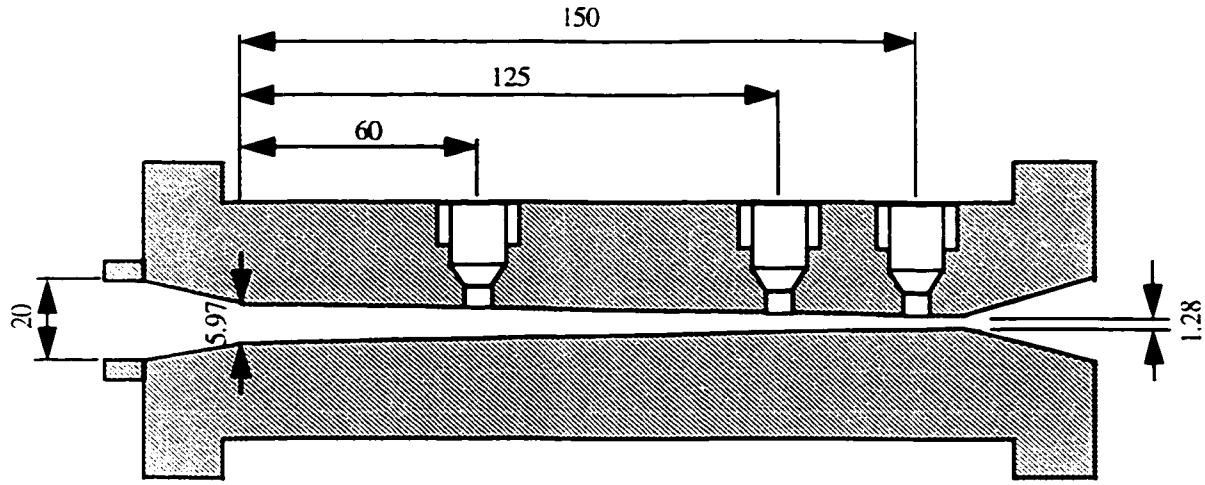

Figure 3.11. Dimension of the wedge die having 1.8° converging angle and 14 mm channel width (All dimensions are in mm).

3.4.4. Electron Microscopy

Foamed structure and blending morphology were analyzed by electron microscopes, scanning electron microscopy (SEM, JEOL JSM-840 and LEO 435 VP, Leo Elektronenmikroskopie) and transmitting election microscopy (TEM, JEOL JEM-100CX). Samples were fractured in liquid nitrogen and coated with gold for the SEM observation. TEM was used for PE / PA6 / PE-MAH blends. Due to the high interfacial strength of the reactive blends between PE and PA6 phases, the dispersed particles could not be clearly observed on the fractured surface even though the samples were prepared in liquid nitrogen. Therefore, a cryogenic microtoming technique at -120°C was used for TEM observation of the reactive PE / PA6 / PE-MAH blends. Ruthenium tetroxide vapor was used for staining the dispersed PA6 phases during 1 hr at room temperature.

3.4.5. GPC and FTIR

A high temperature Waters 150-CV Plus gel permeation chromatograph was used for analyzing the molecular weights of polyethylene and polystyrene used. The weight average molecular weights obtained were used for calculation in the S-L EOS.

FTIR (Nicolet 520) spectrometer was also used for following the reaction between PA6 and PE-MAH. Films from the blending samples were prepared using a Pasadena Hydraulics hot-press. In order to perform a quantitative study for the reaction conversion, PE and PE-g-MAH phases were extracted from the PA6 phase using boiling toluene and the PE / PE-g-MAH / toluene solution was cast on NaCl plates for preparing a thin film. The film was placed at 120°C for 3 hours in a vacuum oven for drying out the toluene and for transforming

the acid group to the anhydride group. Each sample was scanned 20 times in the range from 500 to 4000 cm^{-1}.

3.5. DESIGN OF THE TWIN-SCREW CONFIGURATION

Various twin-screw configurations were used for preparing polymer / CO_2 solutions in a twin-screw extruder and a twin/single tandem extrusion system. The preparation of polymer / CO_2 solutions can be achieved only at pressures above the solubility pressure. Even though the operating pressure is maintained over the solubility limit, the actual soluble amount of CO_2 might be less due to the limited residence time during the extrusion. The prepared solutions must be maintained over the solubility pressure through the extrusion process in order to prevent the precipitation of CO_2. Mostly, the conventional operating pressure of twin-screw extruders, however, is relatively low when it is compared to that of single-screw extruders. Therefore, special screw configurations are required not only for the pressure generation but also the stable injection of CO_2.

In this section, the design criteria of the twin-screw configurations are discussed. An example of the screw configurations is shown in *Figure 3.12*. The other screw configurations used in this thesis will be discussed in later chapters. As indicated in *Figure 3.12(a)*, the configuration of the initial steps including solid conveying, plasticization and melt conveying section are designed similarly to any conventional screw configuration. Thus, the initial few sections of the screw are given over to solids conveying and plasticization of the fed resin. The solid pellets are heated and plasticated in a series of kneading blocks. A relatively short section of kneading blocks is used in order to minimize the torque of driving-motor because a high torque generation from the fully filled downstream is expected. After the plasticization,

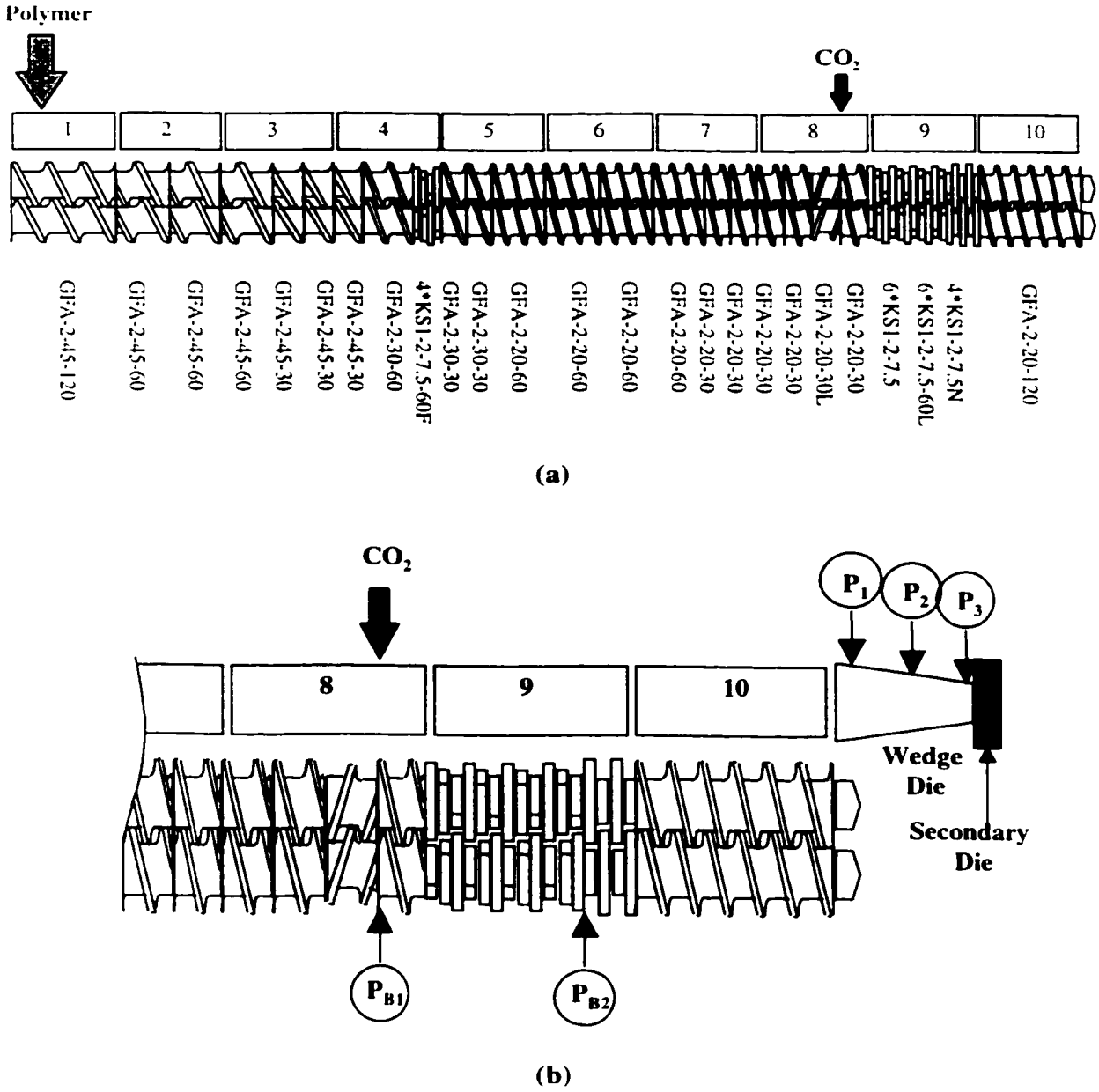

Figure 3.12. Schematic of a twin-screw configuration

a series of conveying screw elements is used for melt conveying and pressurizing. The screw pitch is decreased from 30 mm to 20 mm for more effective pressurization of the polymer melt stream.

This configuration in *Figure 3.12* was designed for preparing polymer / CO_2 and polymer blend / CO_2 solutions in a twin-screw extruder rather than in a twin/single tandem system. It should be noted that a wedge die and a secondary die are always attached to this configuration. Three main design concepts were applied to the configuration. First, the injected CO_2 should be prevented from leaking backward along the barrel. A reverse conveying element was positioned right before the CO_2 injection to generate a melt seal and prevent CO_2 backflow. Second, the barrel pressure after the CO_2 injection should be maintained over the solubility pressure. The high pressure was generated by controlling the flow resistance at the secondary die attached to the wedge die. The generated pressure level depends on the die opening area and the melt viscosity. Finally, an extensive mixing of the polymer melt and CO_2 is essential for the complete dissolution of supercritical CO_2 under a limited residence time. The extensive mixing was achieved using dedicated mixing elements as shown in *Figure 3.12(a)*. By introducing a series of kneading blocks, including neutral and left-handed staggered ones, the mixing performance was maximized. It should be noted that a screw element exhibiting less pressure fluctuation than a kneading block, is located at the CO_2 injection point.

3.6. PRELIMINARY EXPERIMENTS USING CO_2 IN A TWIN-SCREW EXTRUDER

In order to determine the optimum operating conditions when CO_2 was injected, the available processing variables such as the resin feed rate and the screw speed, were tested

using the screw configuration shown in *Figure 3.12* in preliminary experiments. A PE / PS blend (PE/PS = 80/20) was chosen as a test material and the barrel temperature was set to 120/188/188/188/188/188/188/188/188/188°C with the die at 188°C. Pressures at the barrel and the wedge die were monitored at various screw speeds and resin feed rates. The effects of each variable are described in this section.

3.6.1. Screw Speed

Maintaining the high pressure during the extrusion with CO_2 is critical because the injected CO_2 should be dissolved into the polymer in given residence time. Therefore, the effect of the screw speed on the pressure was investigated for PE / PS blending system, and the behavior at various screw speeds is shown in *Figure 3.13*. When the polymer feed rate was fixed at 100 g/min, the barrel pressure consistently decreased with increasing the screw speed, while the pressures at the wedge die remained relatively constant. This indicates that, as expected, higher screw speeds decrease the degree of fill due to the increased conveying capability.

3.6.2. Resin Feed Rate

The pressure behavior with the polymer feed rate was also investigated at 50rpm. As expected, all pressures at the barrel and the wedge die increased as the polymer feed rate increased, as shown in *Figure 3.14*. It should be noted that the barrel pressure increases faster than the wedge die pressures in the PE / PS=80/20 blending system. As a result, low screw speeds and high polymer flow rates are recommended to maintain high pressures during the extrusion.

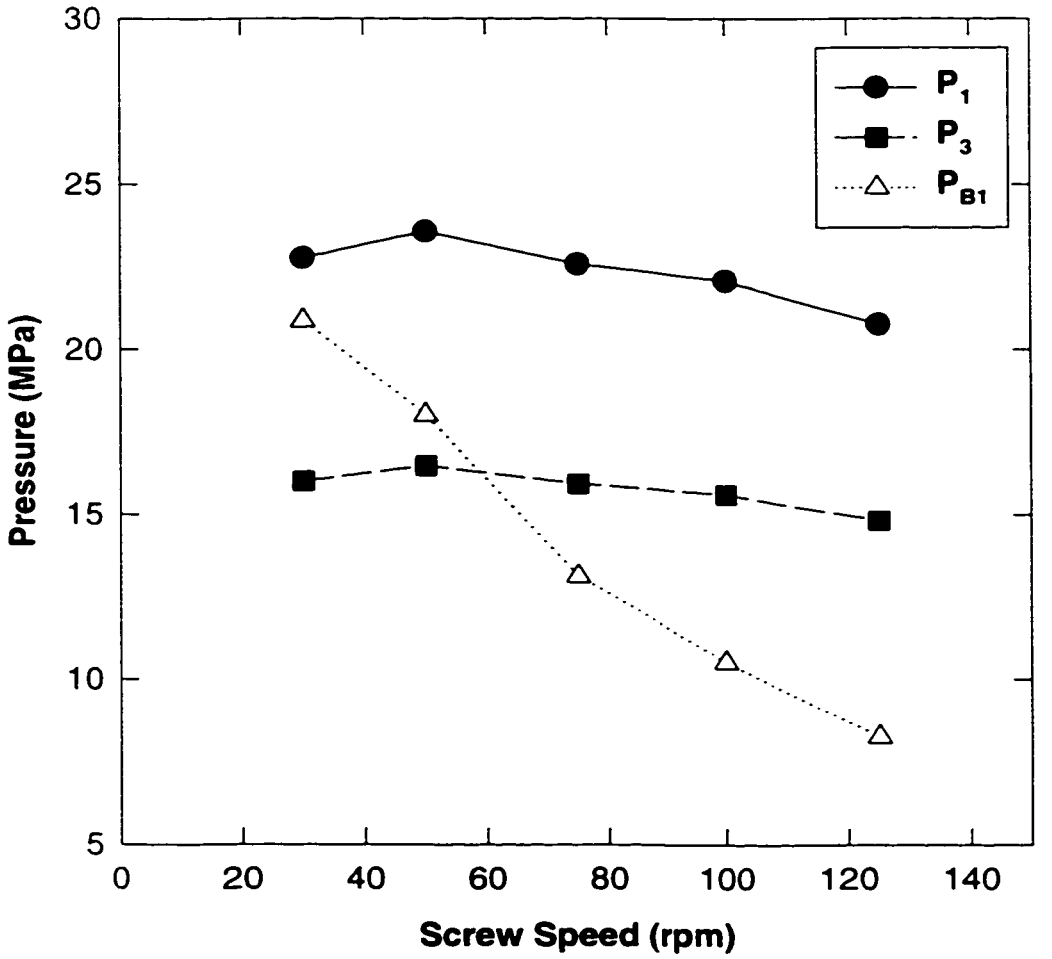

Figure 3.13. Pressure-screw speed relationship during extrusion (Feed rate=100 g/min)

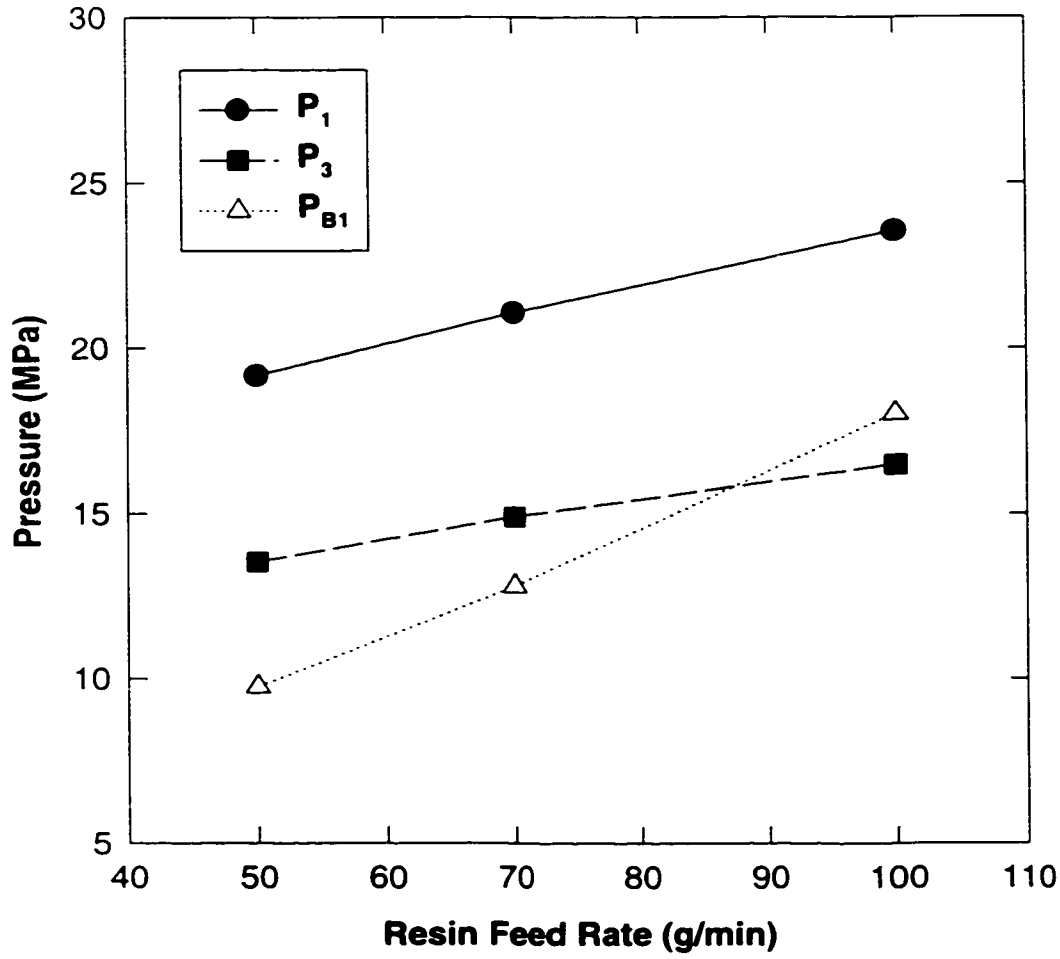

Figure 3.14. Pressure-resin feed rate relationship during extrusion ((PE/PS=80/20, 50 rpm)

3.6.3. CO_2 Concentration

The effect of the CO_2 concentration on the pressure were studied as well. Lower screw speed (50 rpm) and higher polymer feed rate (100 g/min) were used as recommended in the previous section. *Figure 3.15* shows an interesting phenomenon observed. The pressures at the wedge die decreased as the CO_2 content increased up to 7 wt% of CO_2. However, the pressure at the gas injection port in the barrel decreased only up to 3wt% of CO_2. When the injected gas amount increased more than 3wt%, the barrel pressure started to increase with the content of CO_2. This behavior can be understood by considering the solubility limit. The injected CO_2 might be completely dissolved up to 3wt% at given operating conditions. However, additional CO_2 injected might not be dissolved into the polymer if the solubility limit is exceeded. Two-phase mixtures would be generated, and the excess CO_2 just acts to pressurize the mixture, resulting in an increase of the barrel pressure. Therefore, the decrease in the die pressures might be associated with not only the viscosity reduction but also the lubrication effect of the excess CO_2.Thus, the decrease of the die pressure by increasing the CO_2 concentration up to 3 wt%, results from the viscosity reduction. However, the further decrease of the die pressure over 3 wt% of CO_2, results from both of the viscosity reduction and the lubrication effect of the excess CO_2.

As indicated in *Figure 3.15*, the pressure difference between P_1 and P_3 decreases with increasing CO_2 concentration. The pressure drop, P_1-P_3, along the wedge die is shown in *Figure 3.16*. Based on the wedge die principle (Lenk, 1978, 1979, 1981), the viscosity of a polymer is directly related to the pressure drop. Once again, however, careful consideration should be directed to the polymer / CO_2 solutions due to the possibility of the two-phase

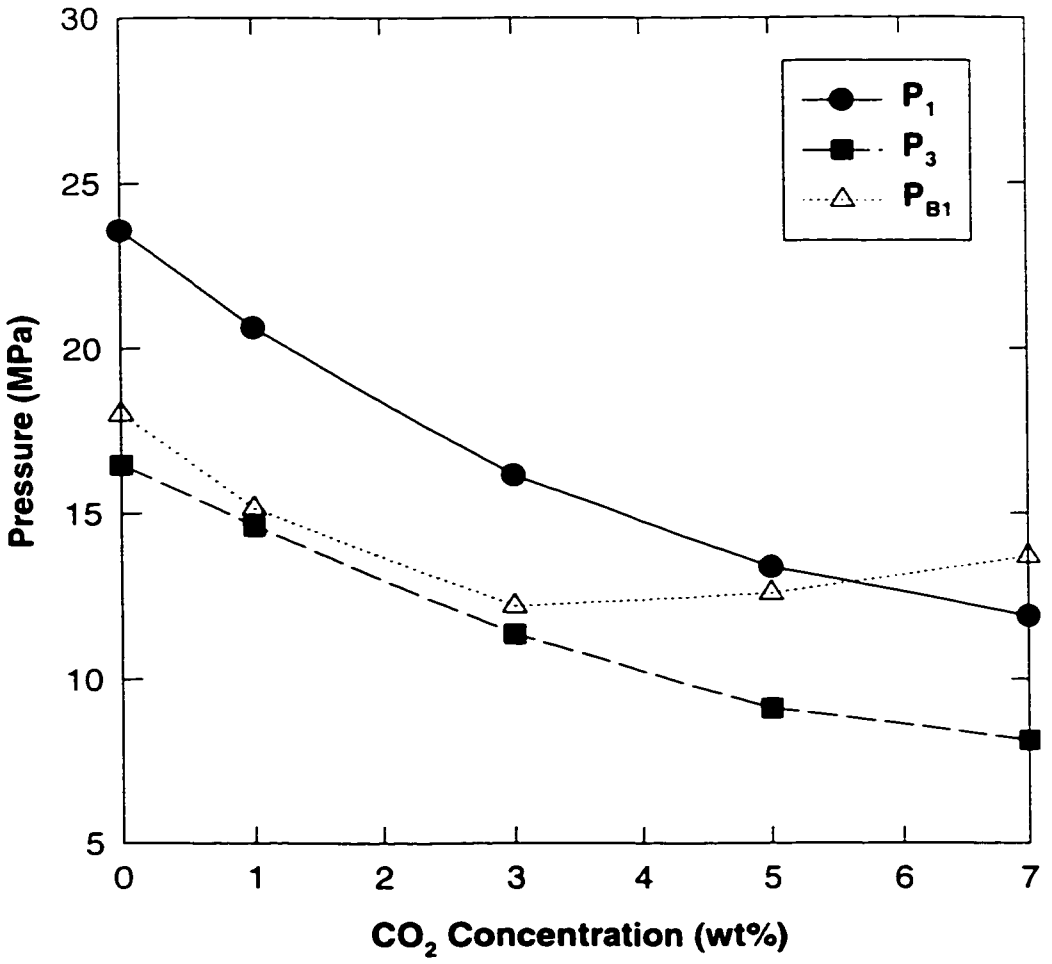

Figure 3.15. Pressure-CO_2 concentration relationship during extrusion (PE/PS=80/20, 100 g/min, 50 rpm)

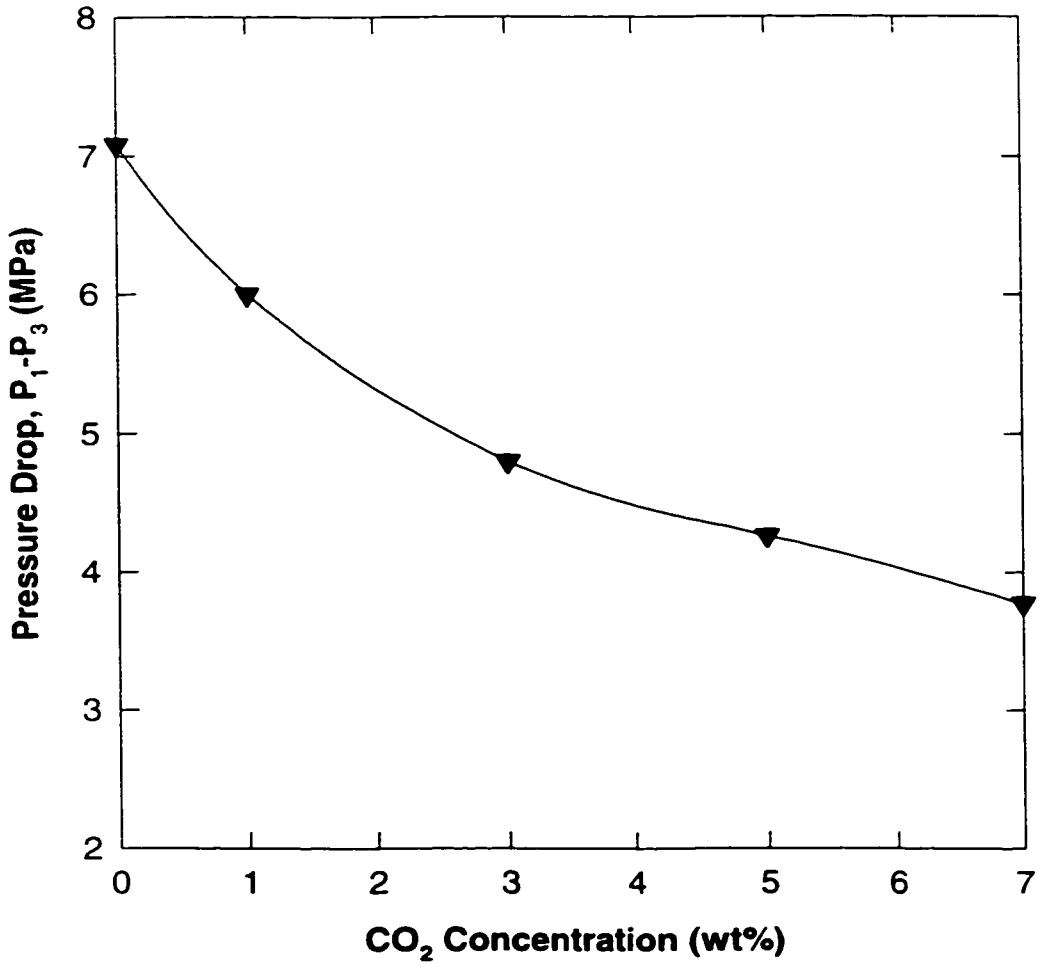

Figure 3.16. Pressure drop along the wedge die at various CO_2 concentrations (PE/PS=80/20)

flow. It should be noted that the viscosity calculation must be performed up to 3 wt% of CO_2 at this operating pressure level.

3.6.4. Extruder Operating Procedure and Data Acquisition

Based on the knowledge about the relationship between the pressure and operating conditions, an experimental run was carried out using the screw configuration shown in *Figure 3.12*. During this run, all pressures and temperature were monitored as shown in *Figure 3.17*. Polystyrene and the 3 wt% of CO_2 were used at the temperature profile of 120/200/260/260/260/260/260/260/260/260°C with the die at 260°C. The feed rate and the screw speed were fixed at 50 g/min and 50 rpm, respectively. The opening area of the secondary die attached to the end of the wedge die was manipulated to obtain a certain level of the pressure in the wedge die. "*A*", "*B*", and "*C*" in *Figure 3.17* denote the steady state zone, the decreasing and increasing points of the die opening area, respectively. In the beginning of the experiment, all pressures show fluctuations due to the startup transient prior to the first steady state condition. The pressure values (P_1, P_2, P_3) and the pressure drops (P_1-P_2 and P_2-P_3) were collected for the calculation of the solution viscosity. By decreasing the die opening area as indicated by "*B*", the second steady state was obtained, and the pressure values were collected as a different level of hydrostatic pressure. The barrel pressures and the pump pressure running at constant volumetric mode, show similar trends as the die pressures. It should be noted that all pressures including the barrel pressures are always maintained over the solubility pressure and the pressure drop between P_{pump} and P_{B1} determines the injected amount of CO_2. The pressure drops collected under various temperatures and hydrostatic pressures were used for the calculation of the solution viscosity, as well as for evaluating the

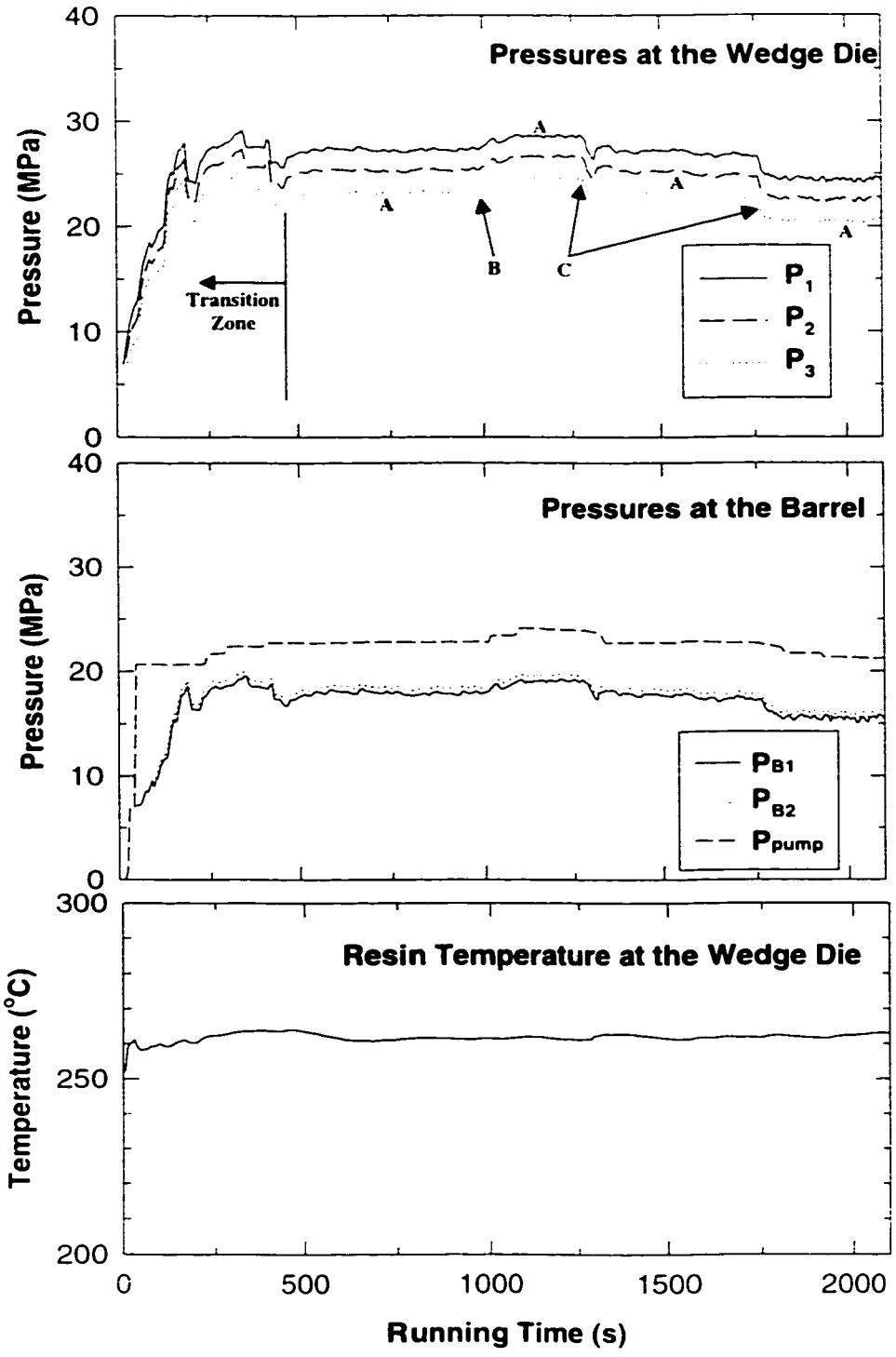

Figure 3.17. Monitoring the pressures and a temperature during the extrusion of PS with CO_2

effects of temperature and pressure on the viscosity. Detailed results and calculation procedures will be discussed through Chapter 5.

CHAPTER 4. THERMODYNAMICS OF POLYMER / SUPERCRITICAL CO_2 SOLUTIONS

4.1. ABSTRACT

Solubility of carbon dioxide and the density of pure components and polymer / CO_2 solutions are crucial factors in a polymer extrusion in the presence of supercritical CO_2. In this chapter, therefore, the solubility of CO_2 in polystyrene and polyethylene was estimated using Henry's law as a first approximation. The Henry's law constant at a certain temperature was calculated using a heat of solution, E_s. The heat of solution was also estimated from experimental solubility data in the literature. It was found that the solubility of CO_2 in polyethylene is higher than that in polystyrene. The Sanchez-Lacombe equation-of-state (S-L EOS) theory was introduced for predicting the *P-V-T* behavior of the pure components as well as the polymer / CO_2 solutions. The predicted densities of polystyrene and CO_2 agree well with the experimental data in the literature. However, the predicted density for PS/CO_2 solutions could not be compared since no data was found in the literature. The S-L EOS theory is able to predict not only the *P-V-T* relation but also the solubility of a gas, if the interaction parameter, δ_{12}, is known. The sensitivity of the interaction parameter on the solution density and the solubility of CO_2 was demonstrated.

4.2. INTRODUCTION

Viscosity measurement of polymer / supercritical solutions requires the complete dissolution of the supercritical fluid in the polymer during the measurement. It has been noted, as pointed out by Park et al. (1994), that any amount of gas injected over the solubility limit would result in the formation of undesirable voids in the polymer melt. Therefore, the

solubility of carbon dioxide in PS and PE should be known at the experimental temperature and pressure in this work.

The solubility of a gas in a polymer has been described using Henry's law as shown in *Eq. (2-2)*. It has been known, however, that Henry's law is valid only at low concentrations of an ideal gas. Therefore, the solubility predicted from Henry's law deviates from the actual solubility value. In spite of this deficiency, the solubility of supercritical fluids has been dealt with Henry's law in earlier studies. Specifically, the solubility of carbon dioxide in polystyrene and polyethylene is of interest in this work. Newitt and Weale (1948) reported the solubility of CO_2 in PS at 50 atm and 170°C. Durrill and Griskey (1966, 1969) measured the solubility of CO_2 in various polymers including PS and PE at 188°C. They argued no appreciable deviation from the linearity at up to 300 atm at this temperature. During two decades from Durrill and Griskey's measurements, data on the solubility of CO_2 in PS or PE have not been published. Wissinger and Paulaitis (1987) performed sorption experiments for PS up to 100 atm at a relatively low temperature, 65°C. Kwag et al. (1994) also published one data point for PS/CO_2 solutions at 12 MPa and 150°C. Recently, a rigorous study for the solubility was performed by Sato et al. (1996) who used a pressure decaying method over a quite wide range of temperatures and pressures, from 373.2 K to 453.2 K and up to 20 MPa. They observed a similar behavior as that observed by Durrill and Griskey (1966): the solubility isotherm of CO_2 decreased with increasing temperature, and the isotherm increased almost linearly with pressure. All solubility results for a polystyrene / CO_2 system found in literature are summarized *in Figure 4.1*. Except the results by Newitt and Weale (1948) and Kwag et al. (1994), the solubility generally decreased with increasing temperature, and it showed a linear relationship with pressure.

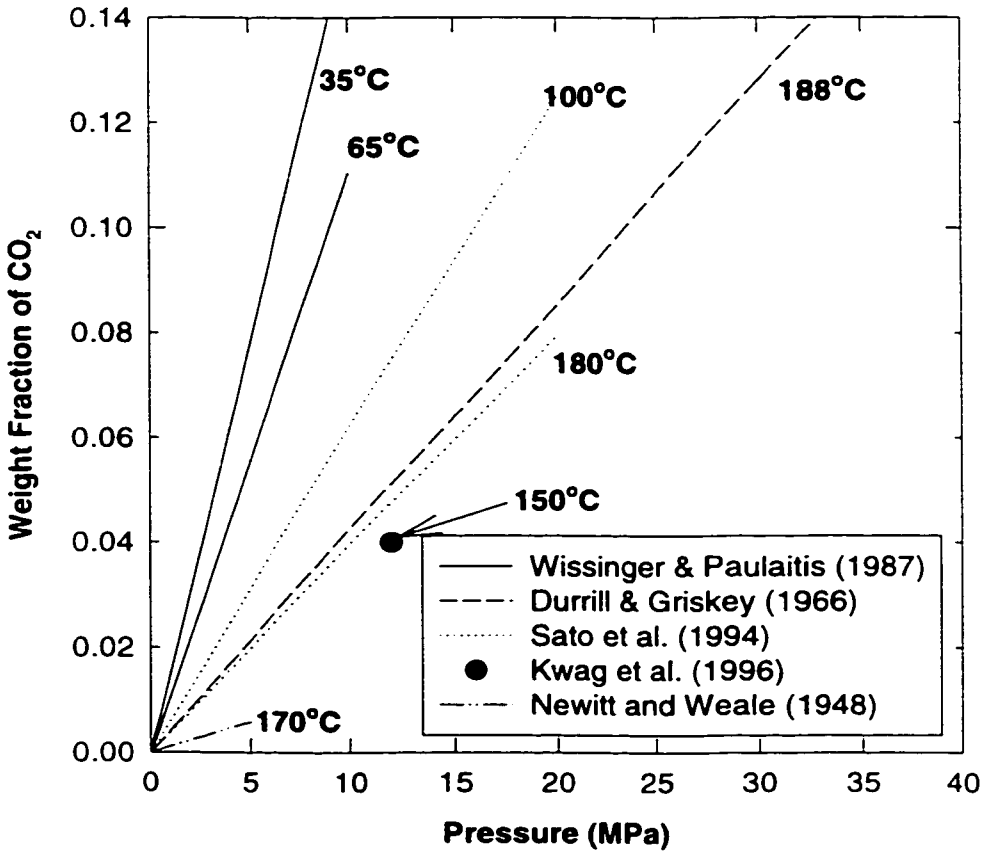

Figure 4.1. Solubility of CO_2 in PS at various temperatures published in the literature

The solubility of SCFs can also be predicted using equation-of-state theories. The primary purpose of the EOS theories was a prediction of the *P-v-T* relationship of a pure component. However, these were expanded to polymer/gas solution systems and the solubility prediction. Several equation-of-state theories have been developed by Flory (1965), Sanchez-Lacombe (1976, 1977, 1978) and Panayiotou-Vera (1982). The theoretical concepts of both theories are originated from the Flory-Huggins lattice fluid theory (Flory, 1942 and Huggins, 1942).

The Sanchez-Lacombe equation-of-state (S-L EOS) can be applied to pure fluids and to mixtures. This theory is based on the lattice fluid model with empty sites called holes. The S-L EOS requires three pure component parameters to characterize a pure fluid and one adjustable parameter, δ_{ij}. The adjustable parameter is related to the binary interaction to characterize a mixture. The Panayiotou-Vera equation-of-state (P-V EOS) is very similar to the S-L EOS in that it is based on the lattice-hole theory. However, the P-V EOS was developed based on a constant lattice site volume. The S-L EOS has been used for describing the solubility of a gas by many researchers (Kiszka et al, 1988, Garg et al., 1994, Sato et al., 1996, Zhang et al. 1997). Details including the solution systems and the value of interaction parameters were summarized in Section 2.3.

In this chapter, thermodynamics related to polymer / CO_2 solutions are discussed. Specifically, the solubility of CO_2 in PS and PE was predicted using Henry's law. The temperature dependence of the Henry's law constant is calculated using *Eq. (2-3)* and data in literature. The S-L EOS model is demonstrated to predict the density of pure components, CO_2 and polystyrene and PS/CO_2 solutions. The solubility of CO_2 in polystyrene is also estimated at various values of the interaction parameter.

4.3. SANCHEZ-LACOMBE EQUATION-OF-STATE THEORY

The lattice fluid theory derived by Sanchez and Lacombe (1978) is based on a system having N molecules and N_0 vacant sites. Each molecule occupies r sites (r-mer). When two pure components form an equilibrium solution state, the following equation of state can be defined from the chemical potential:

$$\tilde{\rho}^2 + \tilde{P} + \tilde{T}\left[ln(1-\tilde{\rho}) + \left(1-\frac{1}{r}\right)\tilde{\rho}\right] = 0 \tag{4-1}$$

where $\tilde{\rho}$ is the reduced density, $\tilde{P}$ is the reduced pressure, $\tilde{T}$ is the reduced temperature, and r is the number of lattice sites occupied by the r-mer. The reduced density, pressure and temperature are defined as

$$\tilde{\rho} = \frac{\rho}{\rho^*}, \quad \rho^* = \frac{M}{rv^*} \tag{4-2}$$

$$\tilde{P} = \frac{P}{P^*}, \quad P^* = \frac{\varepsilon^*}{v^*} \tag{4-3}$$

$$\tilde{T} = \frac{T}{T^*}, \quad T^* = \frac{\varepsilon^*}{\mathrm{R}} \tag{4-4}$$

where ρ^*, P^* and T^* are the equation of state parameters, ε^* denotes the interaction per mer, v^* is the close-packed mer volume, R is the gas constant, and M is the molecular weight of the r-mer. *Eq. (4-1)* can be applied to most low molecular weight substances such as gases and organic liquids. However, if the mer molecule is a polymer, then the number of lattice sites occupied by one molecule (r-mer) approaches infinity ($r \rightarrow \infty$). Therefore, *Eq. (4-1)* reduces to

$$\tilde{\rho}^2 + \tilde{P} + \tilde{T}\left[ln(1-\tilde{\rho}) + \tilde{\rho}\right] = 0 \tag{4-5}$$

4.4. RESULTS AND DISCUSSION

4.4.1. Solubility Estimation Using Henry's Law

Henry's law was used for predicting the solubility of CO_2 in PS and PE. In order to predict the solubility at the experimental temperature in this work, the temperature dependence of the Henry's law constant derived through an Arrhenius equation form was used as shown in *Eq. (2-3)*.

$$H_1 = H_0 \exp\left(-\frac{E_s}{RT_1}\right) \tag{2-3}$$

In this expression, H_0 and H_1 denote the Henry's law constants (cm^3(STP)/g-atm), E_s is the heat of solution (cal/mol), and T_1 is the temperature (K). The Henry's law constant at T_1 can be calculated from the heat of solution and Henry's law constant at a reference temperature. On the other hand, the heat of solution can also be calculated from two Henry's law constants obtained at different temperatures.

Henry's law constants of PE and PS, shown in literature, are listed in *Table 4.1*. As indicated in *Figure 4.1*, the solubility of CO_2 generally decreases with increasing temperature in both PS and PE. This trend is also indicated in *Table 4.1* as decreasing the Henry's law constant. It should be noted that the predicted solubility of CO_2 in PS is less than in PE due to the smaller Henry's law constant in *Table 4.1*. The heat of solution was calculated from the Henry's law constants at two different temperatures. It should be noted that the solubility obtained by Newitt and Weale (1948) shows much less solubility than the other solubility values. Therefore, their data were not included in the calculation of the heat of solution. As listed in *Table 4.1*, no big difference was found in the calculated heat of solution values for PS. However, the heat of solution in PE shows a big difference by taking the solubility data

of Durrill and Griskey (1966). Data published by Sato et al. (1996) were chosen for the prediction of the solubility at the experimental temperature in this work.

Table 4.1. Henry's law constants and heat of solutions from literature

Materials	Temperature (°C)	Henry's law constant (cm^3(STP)/g-atm)	Heat of Solution* (cal/mol)	Reference
PS	35	0.8	-2390	Wissinger and Paulaitis (1987)
	65	0.57		
	170	0.061		Newitt and Weale (1948)
	188	0.22	-2340	Durrill and Griskey (1966)
	100	0.322	-1900	Sato et al. (1994)
	180	0.205		
PE	188	0.275	-800	Durrill and Griskey (1966)
	160	0.39	-2238	Sato et al. (1996)
	180	0.34		
	200	0.313		

* calculated values in this work

Henry's law constants for CO_2 in PS and PE at 220°C are calculated using *Eq. (2-3)*, and the estimated solubilities are compared in *Figure 4.2*. In this calculation, the heat of solution by Sato et al. (1994, 1996), -1900 cal/mol for PS and -2238 cal/mol for PE, were chosen. *Figure 4.2* indicates that the solubility of CO_2 in PE is greater than that in PS. The estimated solubilities of CO_2 are about 5.0wt% and 8.1 wt% in PS and PE, respectively, at 15 MPa of pressure.

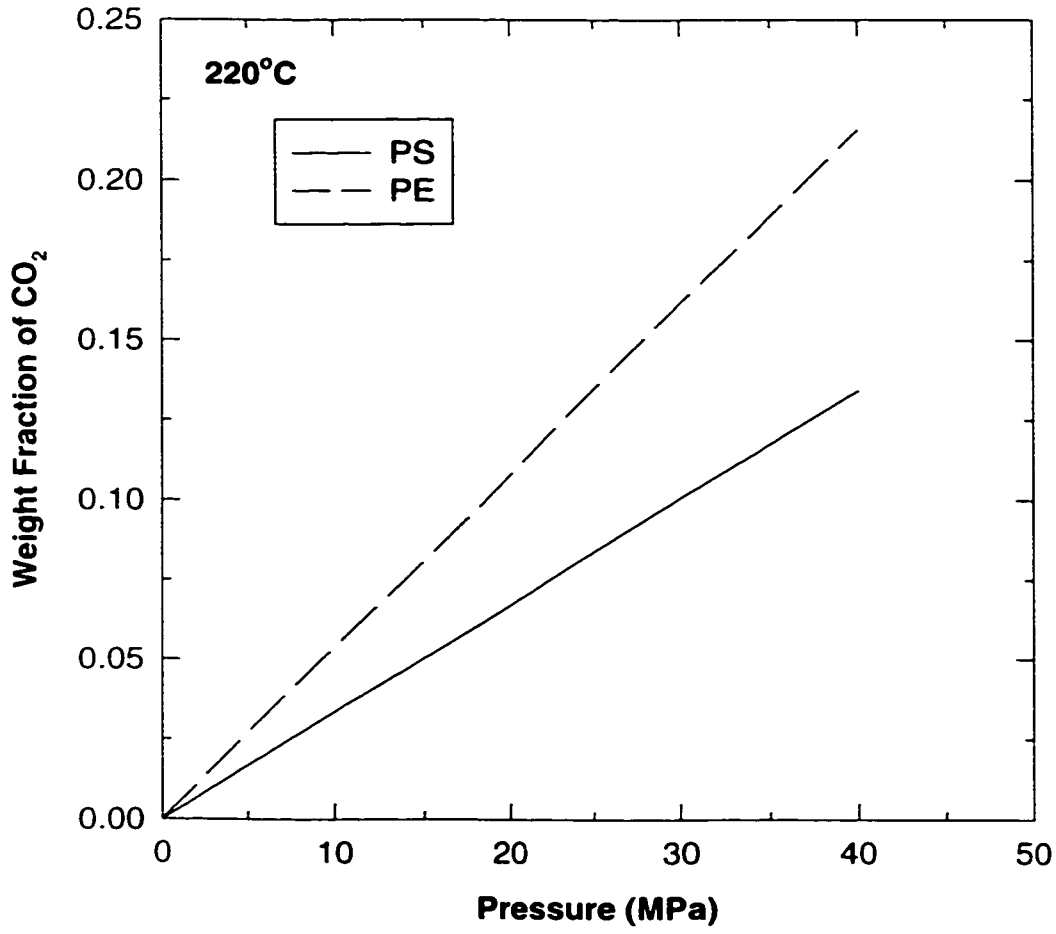

Figure 4.2. Predicted solubilities of CO_2 in PS and PE at 220°C

4.4.2. Characteristic Parameters and Density of a Pure Component

S-L EOS parameters, ρ^*, P^* and T^*, for each pure component such as carbon dioxide, polystyrene and polyethylene were determined using a non-linear least square method. These parameters are essential for applying the S-L EOS model to polymer / CO_2 solutions. The nonlinear least square regressions of *Eqs. (4-4)* and *(4-5)* for pure components to the experimental *P-v-T* data were carried out using a FORTRAN program (Program-1, Appendix II). The *P-v-T* data of PS by Quach and Simha (1971), LDPE by Olabish and Simha (1975), and CO_2 by Michels and Michels (1936, 1937) and Michels et al. (1936, 1937) were used for the non-linear regression. The pure component parameters are listed in *Table 4.2*. These pure component parameters are similar to those in the literature (Sanchez and Lacombe, 1976 and Garg et al., 1994)

Table 4.2. Estimated pure component parameters for PS, LDPE and CO_2

	PS	LDPE	CO_2
P^* (atm)	3523	4543	4388
T^* (K)	735	673	314.8
ρ^* (g/cm^3)	1.105	0.887	1.416
r	-	-	5.286

Based on the pure component parameters, the density of each component was calculated at various pressures and temperatures and the calculated densities were compared to the experimental values in the literature. *Figures 4.3* and *4.4* show the comparisons for carbon dioxide and polystyrene, respectively. These comparisons show that the calculated densities using the S-L EOS agree well with experimental data for both components.

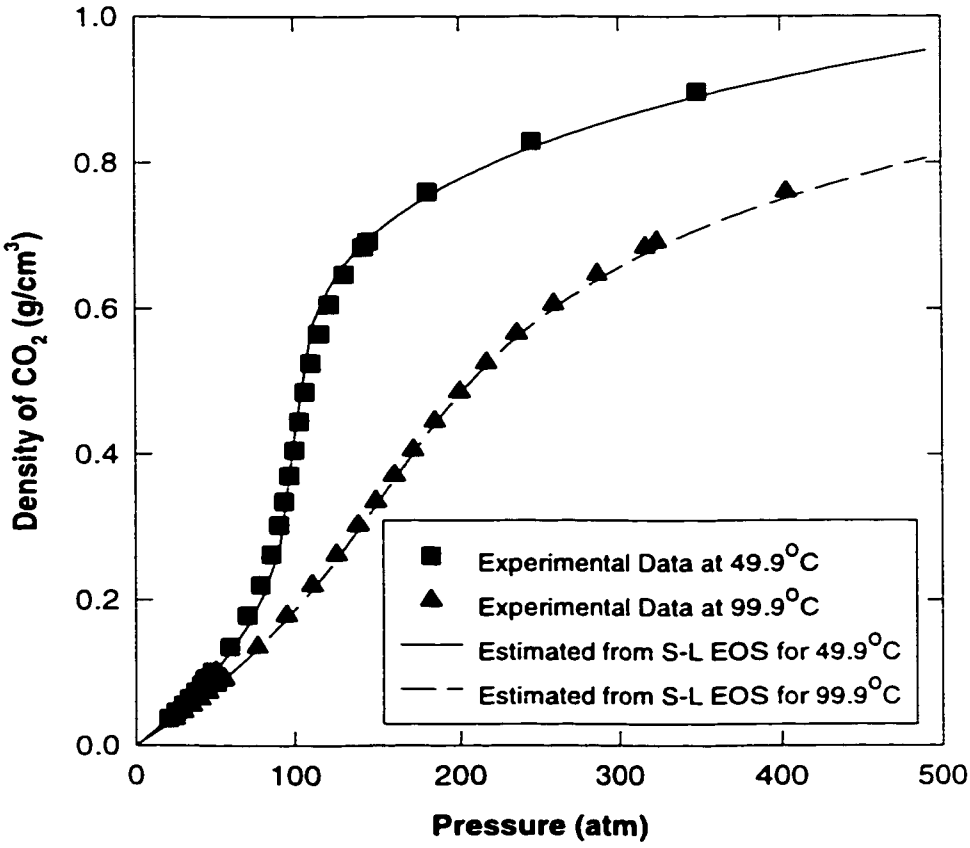

Figure 4.3. Comparison of the experimental and predicted densities of carbon dioxide (Experimental data by Michels and Michels, 1936, 1937 and Michels et al., 1936, 1937)

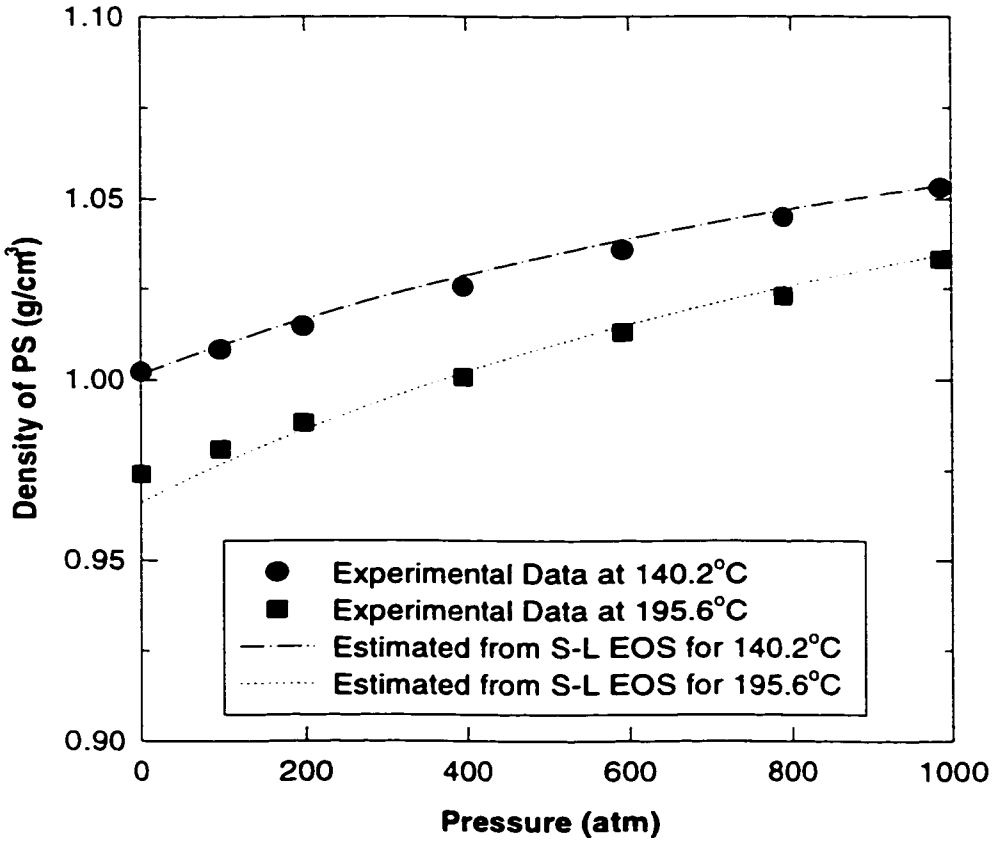

Figure 4.4. Comparison of the experimental and predicted densities of polystyrene (Experimental data by Quach and Simha, 1971)

A FORTRAN program (Program-2, Appendix II) was used for the density prediction. The CO_2 density predicted at room temperature is used in this work for calculating the injected mass flow rate of CO_2 during extrusion. Also, the densities of PS and LDPE are used for converting the mass flow rate to the volumetric flow rate in order to obtain the shear rate in a capillary and wedge die.

4.4.3. S-L EOS Theory for Polymer / CO_2 Solutions

The solubility of CO_2 in polystyrene and the solution density were estimated using the S-L EOS theory. In order to perform the experimental studies described in Chapter 5 to Chapter 9, the solubility of CO_2 should be known for preparing one-phase solutions during extrusion. Also, the estimated solution densities are used in the calculation of the volumetric flow rate.

The equation of state for a polymer / CO_2 solution is basically identical to that for a pure component. However, the polymer / CO_2 solution involves the non-ideal mixing due to the interaction between the two components. The interaction affects the characteristic parameters of each component. Therefore, all variables in *Eq. (4-1)*, such as $\tilde{\rho}$, $\tilde{P}$, $\tilde{T}$, and r, should be determined again for the solution using several combining rules. In addition, the interaction between CO_2 (component 1) and a polymer (component 2) should be considered.

The first combining rule is the conservation of the close-packed volume. If a molecule of component 1 occupies r_1^0 sites in its pure state and has a close-packed molecular volume of $r_1^0 v_1^*$, it occupies r_1 sites with v^* close-packed volume in the mixture. Then, the relationship of these two volumes becomes

$$r_1^0 v_1^* = r_1 v^* \tag{4-6}$$

The second rule states that the total number of pair interactions in the close-packed mixture is the same as the summation of pair interactions of the components in their close-packed pure state:

$$r_1^0 N_1 + r_2^0 N_2 = rN \tag{4-7}$$

where N_1 and N_2 are the number of molecules of component 1 and 2, respectively, N is the summation of N_1 and N_2, and r is the total occupied sites by both components in the mixture. From these two combining rules, the following relations can be obtained:

$$v^* = \phi_1^0 v_1^* + \phi_2^0 v_2^* \tag{4-8}$$

$$r = x_1 r_1 + x_2 r_2 \tag{4-9}$$

where ϕ_1^0 and ϕ_2^0 are the volume fractions of component 1 and 2 in their pure state, respectively. Also, x_1 and x_2 are the mole fractions of component 1 and 2, respectively. The third rule defines the characteristic pressure of the mixture as pairwise additive:

$$P^* = \phi_1^2 P_1^* + \phi_2^2 P_2^* + 2\phi_1\phi_2 P_{12}^* \tag{4-10}$$

$$P_{12}^* = (P_1^* P_2^*)^{1/2}(1 - \delta_{12}) \tag{4-11}$$

where ϕ denotes the volume fraction of the subscript component in the solution state and δ_{12} is the interaction parameter between the two components. The interaction parameter is the only parameter needed to completely characterize a binary mixture. It corrects the deviation of the characteristic pressure of the mixture from the geometric mean of the characteristic pressures of each component.

The solubility of CO_2 in a polymer at an equilibrium condition is calculated from the chemical potentials of the two phases. By assuming that the polymer is not dissolved in the

gas phase, the chemical potentials of CO_2 in the upper (gas) and the lower (polymer) phase are the same:

$$\mu_1^G(T,P) = \mu_1^P(T,P,\phi_1) \tag{4-12}$$

where the superscripts G and P denote the gas and polymer phase, respectively. The difference of the chemical potentials of CO_2 in the two phases is given by

$$\begin{aligned}\frac{\Delta\mu_1}{RT} = 0 = \ln\phi_1 + \left(1 - \frac{r_1}{r_2}\right)\phi_2 + r_1^0\tilde{\rho}X_1\phi_2^2 + \tilde{v}\tilde{\rho}\ln\tilde{\rho} - \tilde{v}\tilde{\rho}_1\ln\tilde{\rho}_1 \\ + r_1^0\left[-\frac{\tilde{\rho}-\tilde{\rho}_1}{\tilde{T}_1} + \frac{\tilde{P}_1(\tilde{v}-\tilde{v}_1)}{\tilde{T}_1} + \tilde{v}(1-\tilde{\rho})\ln(1-\tilde{\rho}) - \tilde{v}_1(1-\tilde{\rho}_1)\ln(1-\tilde{\rho}_1)\right]\end{aligned} \tag{4-13}$$

where $X_1 = (P_1^* + P_2^* - 2P_{12}^*)v_1^*/RT$.

Eq. (4-13) indicates that if we know the interaction parameter, δ_{12}, and P-v-T data of the solution, the equilibrium solubility of CO_2 in a polymer can be determined. On the other hand, if experimental solubility data in a certain range of temperature and pressure are available, the interaction parameter can be determined by a nonlinear regression of the solubility data to *Eq. (4-13)*. However, experimental solubility data are not available for many binary systems.

In order to predict the solubility isotherms, the characteristic parameters of the solution should be determined first. Pure component parameters were already determined in Section 4.4.2. The characteristic parameters for the solution were determined using the pure component parameters and the combining rules. A FORTRAN program (Program-1, Appendix II) was also used when the binary interaction parameter is assumed to be a constant. Using the characteristic parameters of the solution, the solution density at 220°C was calculated (Program-1, Appendix II), and it is shown in *Figure 4.5*. It should be noted that no interaction between PS and CO_2 was assumed in *Figure 4.5*. The solution density

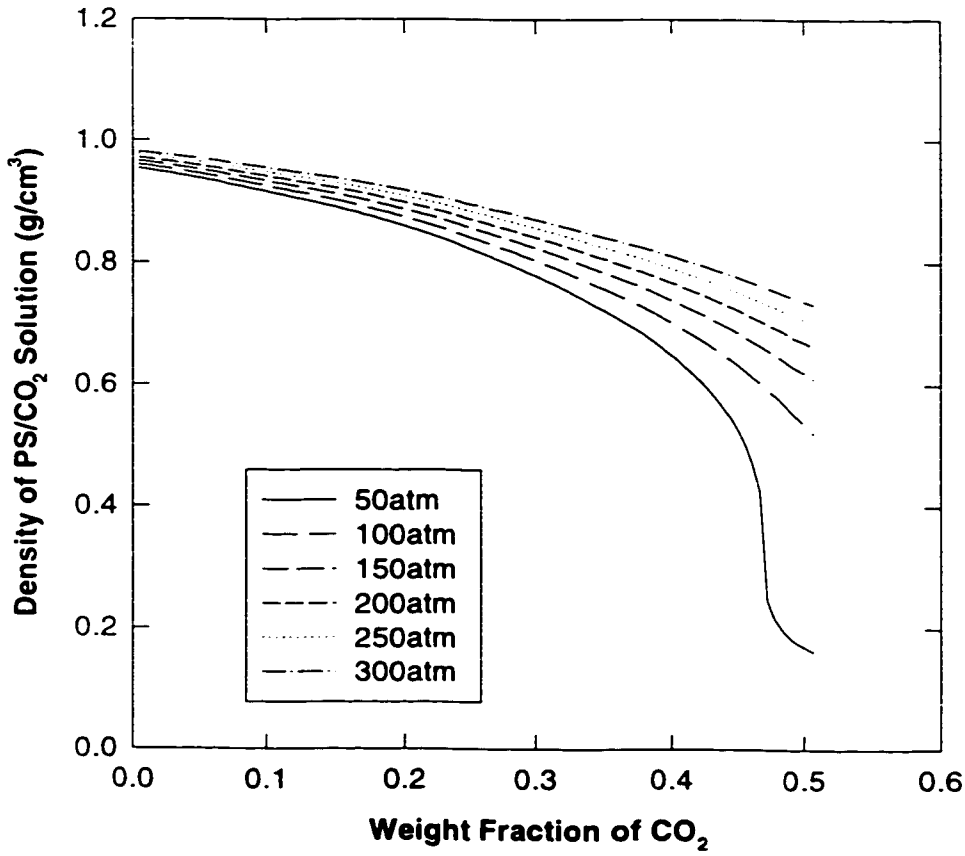

Figure 4.5. Estimated density of PS/CO_2 solutions at various pressures (at 220°C and δ_{12}=0)

decreases with increasing CO_2 concentration and it shows a higher sensitivity to pressure at higher concentrations of CO_2.

As indicated from the *Eqs. (4-1), (4-10)* and *(4-11)*, the solution density is a function of the binary interaction parameter as well as the content of CO_2. The sensitivity of the PS/CO_2 solution density on the interaction parameter was investigated in *Figure 4.6*. The solution density decreases as the interaction parameter increases. Therefore, the interaction parameter is essential to describe the solution density. It should be pointed out that the density variation due to the change of the interaction parameter is small at low concentrations of CO_2.

Once the characteristic parameters of pure components and their solutions are known, the solubility isotherm can be predicted based on the chemical potential equation, *Eq. (4-13)*. Another FORTRAN Program (Program-3, Appendix II) was used for the solubility isotherm. The solubility of CO_2 in polystyrene at 220°C was calculated at various levels of the interaction parameter. As shown in *Figure 4.7*, the dissolved amount of CO_2 increases with increasing pressure. It should be pointed out that the solubility shows a linear relationship with pressure when the interaction parameter is zero. Thus, the solubility is governed by Henry's law, which assumes an ideal solution. However, the isotherm starts to deviate from the linear relationship for increasing values of the interaction parameter. A positive interaction parameter reduces the solubility. It should be noted, as indicated in *Figure 4.7*, that the binary interaction parameter is a crucial variable in determining the solubility. For instance, the predicted solubility is changed from 3.2 to 10.6 wt% at 20.3 MPa when the interaction parameter decreased from 0.2 to zero.

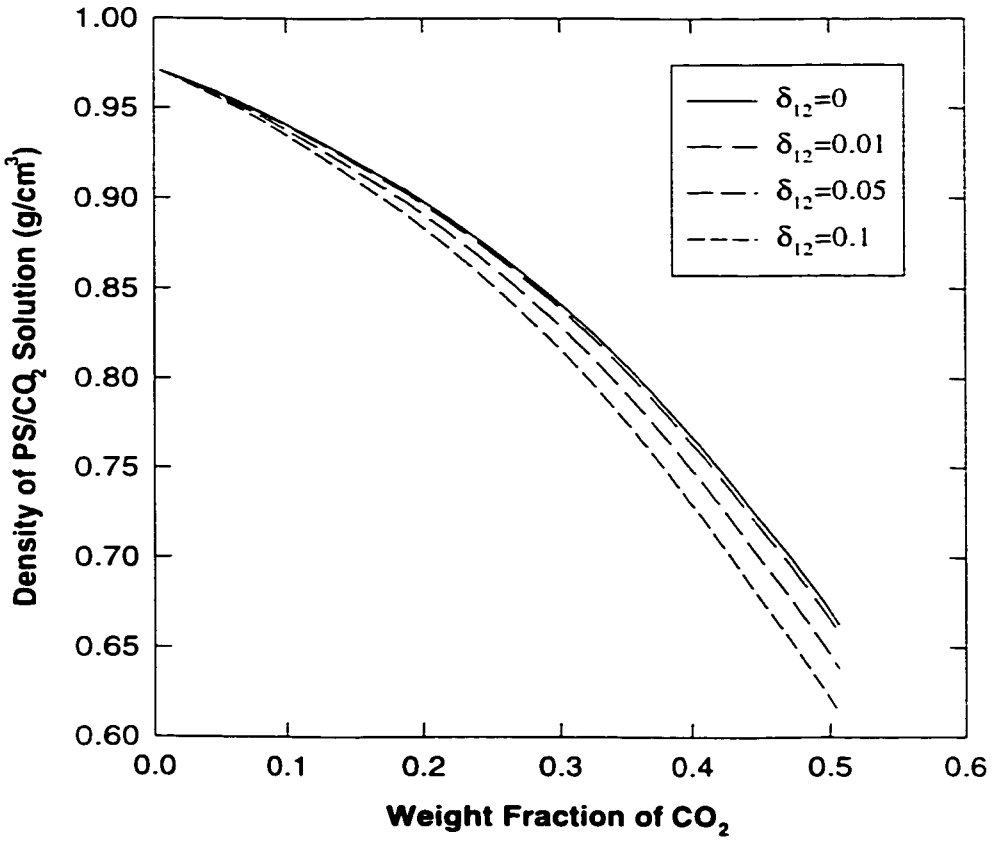

Figure 4.6. Estimated density of PS/CO_2 solutions at various binary interaction parameters (220°C and 200 atm)

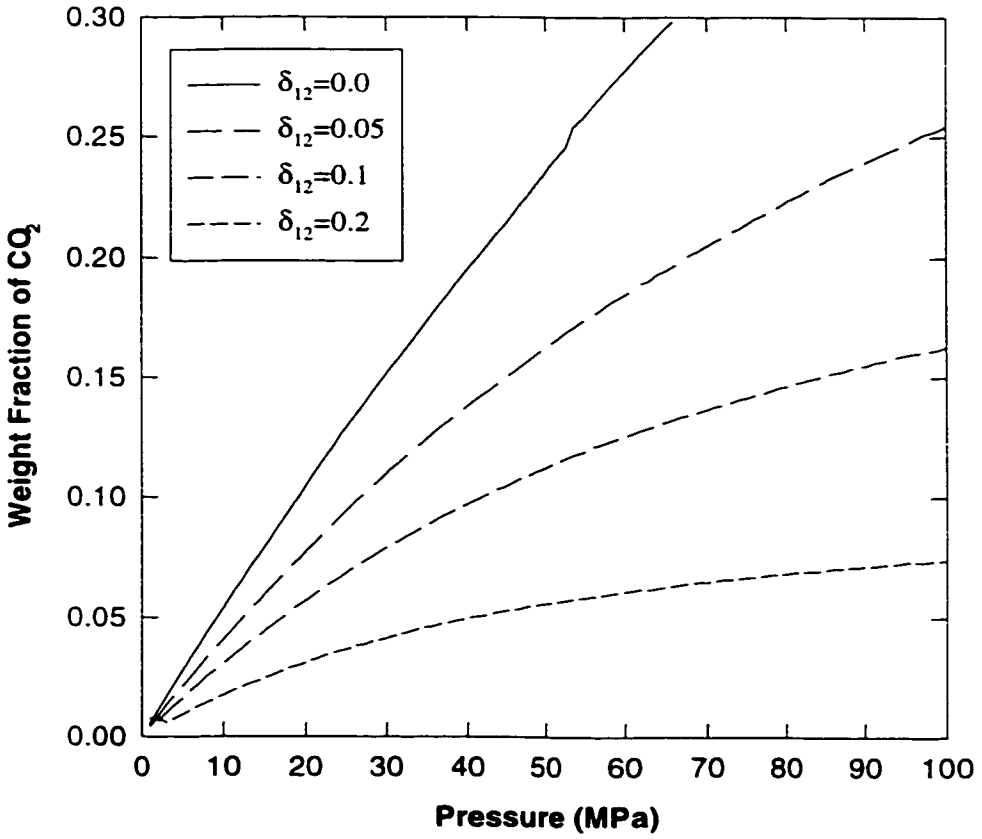

Figure 4.7. Prediction of the solubility of CO_2 in polystyrene at various interaction parameters (220°C)

The effect of temperature on the solubility of gas in a polymer was investigated. A decrease of the gas solubility with an increase in the temperature is also quite common for many polymer / gas systems. It has been known that the trend is valid in PS/CO_2 solution system (Durrill and Griskey, 1966, Sato et al., 1994). The predicted solubilities at various temperatures are shown in *Figure 4.8*. However, the predicted solubility using S-L EOS in this system fails to explain the temperature dependency. *Figure 4.8* indicates that the solubility increases with increasing temperature up to 75 atm. However, the opposite behavior was predicted over 75 atm. Therefore, the solubility isotherm implies the temperature dependence of the interaction parameter. It has been known that the interaction parameter is a function of temperature (Garg, 1993). It should be noted that the Sanchez-Lacombe EOS totally fails to explain the solubility nature as long as δ_{12} is assumed to be independent of temperature.

4.5. CONCLUDING REMARKS

The solubility of carbon dioxide in polystyrene and polyethylene was estimated using Henry's law as a first approximation. A higher solubility of CO_2 was observed in polyethylene than in polystyrene. The S-L EOS theory was demonstrated not only for estimating the properties of pure component parameters of polystyrene and carbon dioxide, but also for predicting the solubility isotherm and the solution density. The pure component parameters of CO_2, PS and PE were determined by applying a least squares method to the experimental density data in the literature and the obtained parameters were compared to the literature values. The densities of the pure components were also calculated. The solubility of CO_2 and the solution density were predicted at various interaction parameter values. It should

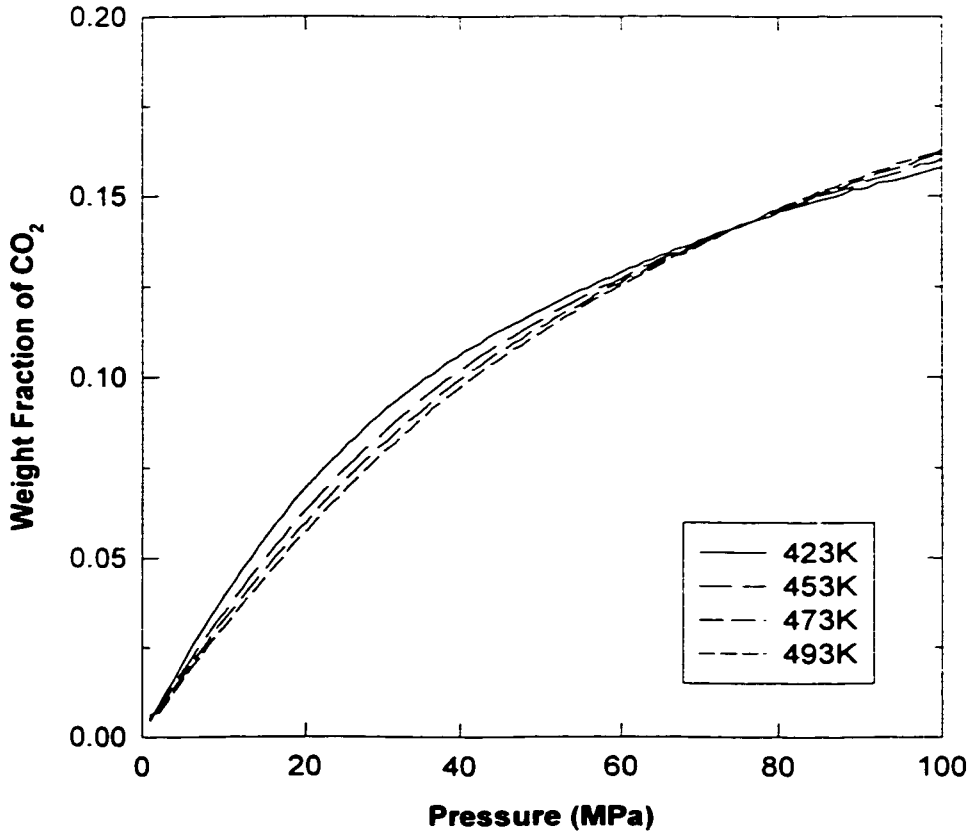

Figure 4.8. Predicted solubility of CO_2 in polystyrene at various temperatures (δ_{12}=0.1)

be noted that the density variation of the solution by changing the interaction parameter is small at the low concentrations of CO_2. Also, positive interaction parameter values led the lower solubility. The estimated solubility using the S-L EOS at zero interaction parameter followed the linear relationship with pressure like Henry's law which assumes an ideal solution. It was found that the interaction parameter is a crucial factor for estimating the solubility.

CHAPTER 5. EXTRUSION AND MODELING OF THE SHEAR VISCOSITY OF PS/CO_2 SOLUTIONS

5.1. ABSTRACT

This chapter presents a methodology to determine the melt viscosity of PS / supercritical CO_2 solutions using a linear capillary tube die mounted on a single-screw foaming extruder and a wedge die mounted on a twin-screw extruder. In both cases, CO_2 was injected into the extruder barrels and the content of CO_2 was varied in the range of 0 to 4 wt% using a positive displacement pump. Single-phase PS/CO_2 solutions were formed using a microcellular extrusion system and a twin-screw extruder, and phase separation was prevented by maintaining a high pressure in the capillary tube die and a wedge die, respectively. By measuring the pressure drop through the dies, the viscosity of PS/CO_2 solutions was determined on-line. The viscosities of neat PS melts measured at low and high shear rates using a cone-and-plate rheometer and a capillary rheometer, respectively, were also used in the modeling. The experimental results indicate that the PS/CO_2 solution viscosity is a sensitive function of shear rate, temperature, pressure, and CO_2 content. In order to mathematically describe the decrease of the shear viscosity due to the dissolved CO_2 in the PS melts, several theoretical models were considered. Cross, Carreau, and generalized Cross-Carreau models were employed to describe the shear-thinning behavior of PS/CO_2 solutions at various shear rates. The zero-shear viscosity in these models was derived in terms of the temperature, pressure and CO_2 content based on the free volume change due to these variables. Various forms of the zero-shear viscosity, including a generalized Arrhenius equation and a WLF equation, were studied. The modeling procedure and comparison of the model are presented in detail.

5.2. INTRODUCTION

In the processing of polymer / supercritical fluid (SCF) mixtures, the properties of the polymer are significantly affected by the presence of the SCF in the polymer. Particularly, the reduction of viscosity by the dissolved SCF has received a great deal of attention because it affects the processing conditions and the morphology of foamed products. The solubility of SCF in a polymer is also important because it provides guidelines to all the polymer processes containing SCFs. SCFs have been used in various fields such as food, pharmaceutical and plastics industries. Research on SCFs has centered around the separation processes in these fields. Initially, the SCF science and technology dealt primarily with extraction of simple molecules that dissolve in SCF and the attention has shifted significantly to more complex molecules, undergoing much broader types of physical and chemical transformation (Johnson and Penninger, 1989).

SCFs have also been used as blowing agents for foam products in polymer extrusion. CFCs, which have been the most popular blowing agents, are known to destroy the ozone layer, and have been replaced with other blowing agents such as HCFCs and inert gases. However, some polymer foams blown by HCFCs can be deteriorated by the chemical attack of the blowing agents. In contrast, the SCF physical blowing agents such as CO_2 are free from any criticisms on the ozone layer destruction and the chemical attack because of their inert properties.

Little work has been reported on the rheological properties of polymer / blowing agent mixtures (or solutions). Earlier studies on polymer / blowing agent mixtures have been carried out for polymer / CFCs or polymer / chemical blowing agent systems rather than for polymer / inert gas solutions. As reviewed in Chapter 2, several studies were reported on the

viscosity measurement of the polymer / gas mixtures in a plunger type viscometer (Blyler and Kwei, 1971, Bigg et al., 1976, and Oyanagi and White, 1979). Han and Ma (1983a, 1983b, 1983c) also published the rheological properties of LDPE/CFCs mixtures. As pointed out by Han and Villamizar (1978), rheological measurements of polymer / gas mixtures conducted with a plunger-type viscometer may be subject to serious criticisms because the plunger-type viscometer cannot guarantee a single-phase condition without allowing foaming inside the capillary. Phase separation, i.e., bubble formation, may be involved as the mixture approaches the capillary exit. Han and Ma (1983a) also explained that the non-linear pressure profile in capillary implies the vaporization of gas and all their experiments were performed in the linear range of the pressure profile.

Efforts have been made to prevent bubble formation in measurements of solution viscosities. A pressurized chamber was introduced by Mendelson (1980) at the exit of plunger-type capillary viscometer for preventing bubble formation. In his experiments, Mendelson (1980) prepared polymer / gas solutions in a glass jar at room temperature and then charged them into the barrel of the viscometer. Finally, these solutions were extruded to the pressurized chamber at an elevated temperature. This experiment is difficult to apply to molten polymer / gas mixtures because of the required high temperature and pressure. Recently, studies on viscosity measurements of polymer / SCF solutions were published by Gerhardt et al. (1994), Kwag et al. (1996) and Gendron et al. (1996). Gerhardt et al. (1994) and Kwag et al. (1996) used a capillary rheometer with a special loading assembly and a back pressure assembly. The back pressure assembly made the capillary rheometer a closed system, and the special loading assembly was used to keep the identical pressure and temperature in the vessel and the rheometer. Gendron et al. (1996) also measured the

viscosities of PS/HCFC and PS/HFC solutions using a commercial slit die rheometer mounted on an intermeshing co-rotating twin screw extruder. They maintained a sufficiently high pressure in the die by using two independently controlled gear pumps.

Viscosity reduction via gas dissolution can be explained by the dilution effect of polymer chains and the increased free volume. The relationship between the viscosity and the free volume of a polymer was first introduced by Doolittle (1951). Kelley and Bueche (1961) applied Doolittle's equation to a polymer / diluent system using a linear mixing rule of the fractional free volume. Gerhardt et al. (1994) and Kwag et al. (1996) introduced a modified Kelley-Bueche equation to include the dilution effect as well.

In order to calculate the viscosity of polymer / SCF solutions using the Kelley-Bueche equation, the fractional free volumes of the polymer and SCF should be known. Two methods are used to calculate these values. First, the fractional free volume (or density) of the polymer and polymer / SCF solution can be predicted from equation-of-state (EOS) theories such as the Sanchez-Lacombe (1977, 1978) and Panayiotou-Vera (1982) EOS. These EOS theories contain one adjustable binary interaction parameter for the polymer / SCF solutions. This interaction parameter can be estimated from the equilibrium solubility data. Second, the solution density at the equilibrium state can be directly measured in a Kratky (Wolf et al., 1989, Mertsch and Wolf, 1994) apparatus. Then, the fractional free volume can be calculated from the measured density of the solution and EOS theories. In order to use the EOS theory, the solution density should be measured at the equilibrium state. Thus, both methods need the solubility at the equilibrium state or the density of the solution measured at the equilibrium state.

An understanding of the rheological behaviors of polymer / SCF solutions is essential for production of a uniform cell structure in foam processing because cell nucleation and growth strongly depend on the viscosity of polymer / SCF solutions. Furthermore, the viscosity of polymer / SCF solutions is critically important in the design of foaming dies. Most viscosity measurements for polymer / SCF solutions have been performed by off-line methods. The off-line measurements for polymer / SCF solutions are not easy because of the precipitation of SCF. In off-line measurements, the solutions should be charged into the rheometer from the equilibrium vessel maintaining the high temperature and pressure. Consequently, special accessories such as a loading assembly and a back pressure assembly are required for preventing the two phase flow.

In this chapter, simple experimental setups that can effectively measure the viscosity of polymer / CO_2 solutions using extrusion systems are presented. As a case study, PS is used as the polymeric material. The viscosity of PS/CO_2 solution is measured at various shear rates and CO_2 contents. Since the pressure at which the viscosity is measured varies at different processing conditions, careful consideration was given to the effect of pressure on the solution viscosity. The effect of CO_2 content on the solution viscosity is also clearly elucidated. Finally, a simple theoretical model is developed to describe the viscosity of a PS/CO_2 solution as a function of shear rate, temperature, pressure, and CO_2 content. The purpose of this chapter is to present a procedure to determine the viscosity of a polymer / CO_2 solution by experimentally measuring the rheological parameters and theoretically modeling the results. The modeling procedures and the effects of T, P, and C on the polymer viscosity are discussed in detail. Based on the experimental data, the free volume concept and several rheological models were investigated to describe the Newtonian viscosity and the

shear thinning behavior of the PS melt and PS/CO_2 solutions. The adequacy of the various models to describe the experimental data was compared.

5.3. EXPERIMENTAL

5.3.1. Microcellular Extrusion System

5.3.1.1. Design of Microcellular Extrusion System

In order to measure the viscosity of a polymer / CO_2 solution, a rheological device is synthesized by attaching a linear capillary tube die to a foam extrusion line. First, a single-phase polymer / CO_2 solution is formed using a convective diffusion device (Park and Suh, 1996a and 1996b, Baldwin et al., 1996a). The polymer / CO_2 solution is then forwarded to the linear capillary die where the viscosity of polymer / CO_2 is measured by the capillary rheometer principle (Dealy and Wissburn, 1990), i.e., by measuring the pressure drop and the flow rate. If a two-phase polymer / CO_2 mixture flows into the capillary die, the measured viscosity cannot be the viscosity of the polymer / gas solution because of the secondary phase effects. Therefore, it is critically important to ensure that single-phase solution formation is complete before the solution reaches the upstream end of the capillary die.

A microcellular foam extrusion system is utilized to ensure complete solution formation in this study. A schematic of the microcellular extrusion system used is shown in *Figure 5.1*. First, a metered amount of gas is injected into the polymer melt in the extrusion barrel using a positive displacement pump. It should be noted that the injected gas amount should be less than the solubility limit at the processing temperature and pressure. The injected gas bubbles are well mixed with and dissolved in the polymer melt in a convective diffusion device that consists of a mixing element on the screw and static mixers.

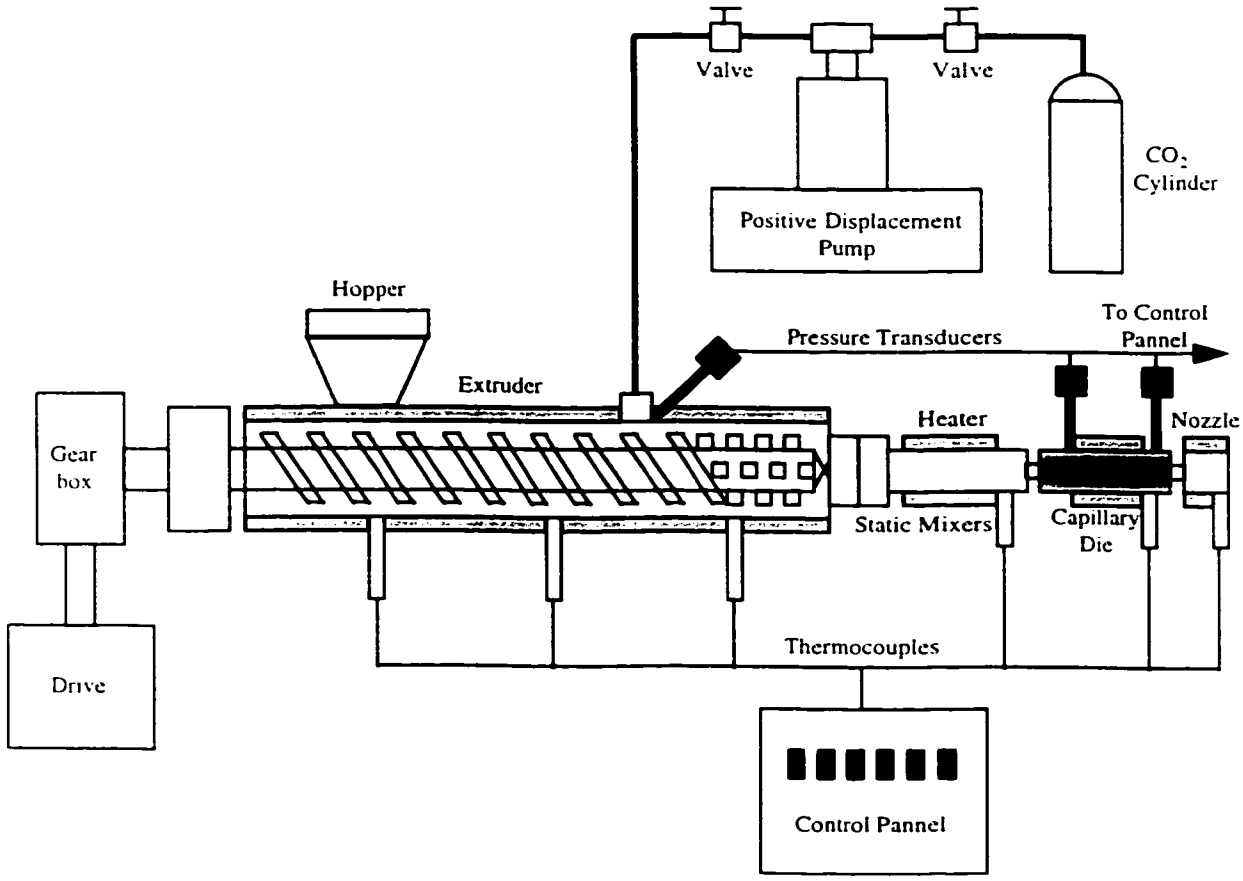

Figure 5.1. Schematic of the extruder setup for measurement of PS/CO_2 solution viscosities.

The procedure of dissolving the injected gas in the polymer melt is described in detail elsewhere (Park and Suh, 1996a, 1996b).

Another critical factor in the viscosity measuring system is that the pressure in the capillary die should always be maintained sufficiently high so that the concentration of gas dissolved in the polymer melt remains below the solubility of gas at the processing pressure. Since the lowest pressure in the capillary die is at the downstream, it is necessary to maintain the downstream pressure high enough to prevent the precipitation of CO_2 during viscosity measurement. The downstream pressure is controlled by varying the resistance of a nozzle die attached to the end of the capillary die, and the nozzle resistance is determined by its diameter and length.

Figure 5.2 shows a schematic of the linear capillary tube die designed to measure the viscosity of a polymer / CO_2 solution. In order to minimize the entrance effect, the L/D ratio is chosen to be 40 and the upstream pressure was measured far from the tube entrance. Then, the viscosity of a polymer / CO_2 solution can be determined using equations shown in Section 5.4.

5.3.1.2. Equipment of Microcellular Extrusion System

The extruder used in this experiment was a single-screw extrusion system (Brabender 05-25-000) driven by a 3.7 kW DC motor (Brabender Prep Center D-52T). A standard square pitch screw with a mixing section (Brabender 05-00-144) was used to enhance the convective diffusion. CO_2 was injected through an injection port into the metering section of the barrel using a positive displacement pump. At the end of the screw tip, static mixers (Omega FMX-8444I-S) were attached to enhance dissolution of CO_2 into the PS melt. The pressure at the barrel injection port was monitored by a pressure transducer (Dynisco PT462E-10M-6/18) to

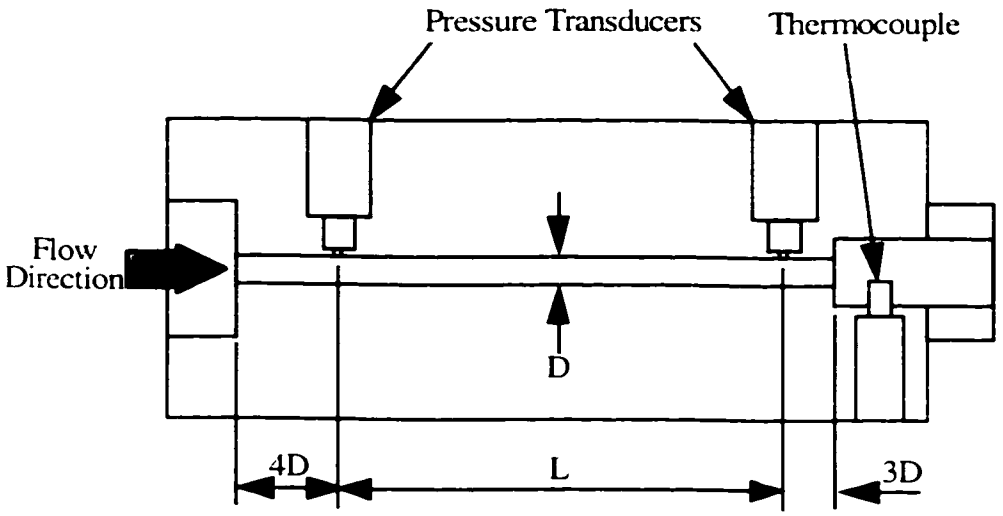

Figure 5.2. Schematic of the linear capillary tube die.

ensure consistent injection of CO_2.

Two capillary tube dies having 2.3 mm and 6.5 mm diameters were used in this study. A thermocouple was installed to measure and control the melt temperature. Two pressure transducers (Dynisco PT462E-10M-6/18) were installed to measure the upstream and downstream pressures. The temperature of the dies was controlled by band heaters and PID controllers (Omega CN9000A).

5.3.1.3. Experimental Conditions in Microcellular Extrusion System

The polymer used in this study was Nova 101C PS. PS was processed in the extruder at 220°C, and the polymer flow rate that affected the shear rate in the capillary die was controlled by the screw speed. The content of CO_2 in polymer was ranged from 0 to 4 wt%.

5.3.2. Twin-Screw Extrusion System

5.3.2.1. Design of a Twin-Screw Extrusion System

In order to prepare the PS/CO_2 solutions, a twin-screw extruder was specially designed and a high pressure was maintained during the measurements in order to prevent the precipitation of CO_2. Similar design concepts explained in the previous section (Section 5.3.1.1) were used for measuring the viscosities of neat PS melts and PS/CO_2 solutions using a twin-screw extruder, and the design criteria are also mentioned in Section 3.5. A schematic of the twin-screw extrusion system equipped with a CO_2 injection port and a wedge die is shown in *Figure 5.3*. Detailed wedge die dimension is shown in *Figure 3.11*.

5.3.2.2. Experimental Conditions in Microcellular Extrusion System

Detailed experimental conditions are shown in *Table 5.1*. Detailed procedures are well described by Lee et al. (1998) as well as in Chapter 6.

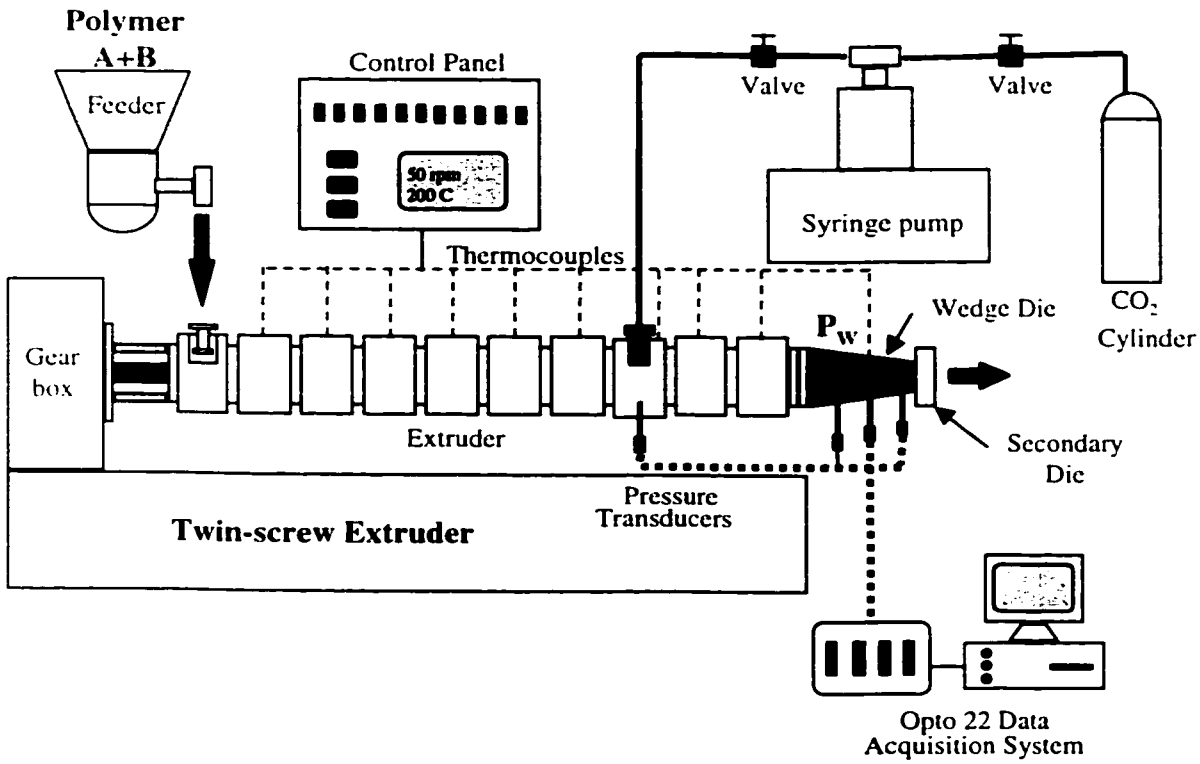

Figure 5.3. Schematic diagram of the twin-screw extrusion system

A commercial capillary rheometer and a cone-plate rheometer were also used for the viscosity measurement of the unsaturated PS. The cone-plate rheometer was operated in the steady shear mode for direct comparison with the capillary rheometer.

Table 5.1. Experimental conditions for the viscosity measurements

	Temperature (°C)	**Pressure (MPa)**	**CO_2 Content (wt%)**	**Shear Rate (1/s)**
Wedge Die Rheometer	203.3 - 271.4	6.3 - 29.1	0 - 4	40.1 - 316.6
Capillary Rheometer	200.0 - 260.0	2.0 - 19.2	0	4.2 - 3700
Cone-Plate Rheometer	220.0 - 260.0	0	0	2.25E-3 - 2.1

5.4. THEORETICAL MODELING

5.4.1. Modeling Equations

In order to properly describe the viscosity of a PS/CO_2 solution, the viscosity behavior should be characterized as a function of shear rate, temperature, pressure and dissolved amount of CO_2. The shear thinning behavior of PS/CO_2 solutions has been described by various models such as the Cross model (Cross, 1979), the Carreau model (Carreau, 1968) and the generalized Cross-Carreau (C-C) model (Hieber and Chiang, 1992). These models can be expressed in the same form:

$$\eta = \eta_0 / \left[1 + (\eta_0 \dot{\gamma} / \tau)^a\right]^{(1-n)/a} \tag{5-1}$$

where η, η_0, and $\dot{\gamma}$, indicate the viscosity, zero-shear viscosity, and shear rate, respectively. The constants τ, a, and n in this model are unique characteristics of the polymeric material and determine the shape of the master curve plot, η/η_0 versus $\eta_0\dot{\gamma}$. *Eq. (5-1)* reduces to the

Cross model when $a = 1 - n$, to the Carreau model when $a = 2$, and to the generalized C-C model when a and n are independent.

The effects of temperature, pressure, and dissolved CO_2 on the viscosity can be explained using the change in the free volume (Lee et al., 1999). Doolittle (1951) described the zero-shear viscosity of a polymer as a function of the free volume:

$$\eta_0 = A' exp(B'/f) \tag{5-2}$$

where A' and B' are constants, and f is the fractional free volume. The dependence of the fractional free volume on the temperature, T, is described by Fox and Flory (1954):

$$f = f_g + \alpha_f (T - T_g) \tag{5-3}$$

where f_g is the fractional free volume at glass transition temperature, T_g, and α_f is a constant. The pressure dependence of the viscosity has also been investigated. Some studies dealt with the pressure effect on the viscosity by revealing the glass transition temperature-pressure relationship instead of the free volume-pressure relationship (Miller, 1971 and Penwell et al., 1971). The empirical relationship between viscosity and pressure has been proposed as (Penwell et al., 1971):

$$\eta_{0,P} = \eta_{0,P=0} exp(\beta'' P) \tag{5-4}$$

where η_0 and $\eta_{0,P=0}$ are the zero-shear viscosities at pressures, P and $P=0$, respectively, and β'' is a constant. The increase in the zero shear viscosity due to a pressure increase may be interpreted as a decrease in the molecular mobility because of a reduction of the free volume.

It is well known that the free volume of a polymer is also changed by the dissolution of a diluent. Kelley and Bueche (1961) simply assumed the linear additivity of the fractional free volume Efforts to theoretically estimate the free volume of a polymer and a polymer / diluent solution have been developed by Sanchez and Lacombe (1976) and Panayiotou and

Vera (1982). The equation-of-state (EOS) theory successfully predicts the free volume of a pure polymer based on the *P-v-T* diagram. For polymer / diluent systems, however, the EOS theories require an adjustable parameter explaining the interaction between the two components.

The change of the free volume in a polymer / CO_2 solution due to variations of the temperature, pressure, and dissolved CO_2 affects the mobility of polymer molecules, thereby affects the shear viscosity of the solution. Kadijk and van den Brule's extensive experimental results (1994) confirmed that when the temperature and pressure were varied, the viscosity of a polymer was changed only through the zero-shear viscosity without affecting the material constants, and that the shape of the viscosity versus shear rate curve was not changed. In the same manner, it is expected that the effect of gas concentration on the viscosity of a polymer / CO_2 solution will be reflected only through change of free volume and the resultant change in the zero-shear viscosity. One may contemplate that the viscosity of CO_2 itself and/or the interactions between the polymer and gas molecules would affect the viscosity of polymer / CO_2 solution. However, since the viscosity of polymer melt would be much higher than the viscosity of CO_2 and the interaction between polymer and CO_2, it is believed that the viscosity of a polymer / CO_2 solution would be governed by the viscosity component of the polymer melt which is determined by the free volume of polymers. In other words, it is speculated that the dissolved CO_2 will contribute the viscosity of a polymer / CO_2 solution only by changing the free volume of polymer melt as in the case of temperature and pressure.

For a polymer / CO_2 solution, the fractional free volume can be mathematically expressed as a power law series in terms of temperature (T), pressure (P), and CO_2 concentration (C):

$$B'/f = \alpha'/(T-T_r) + \beta'(P-P_r) + \psi'(C-C_r) + \kappa'(P-P_r)/(T-T_r) + \delta'(P-P_r)(C-C_r) + \varepsilon'(C-C_r)/(T-T_r) + \xi'/(T-T_r)^2 + \varsigma'(P-P_r)^2 + \omega'(C-C_r)^2 + (higher\ order\ terms) \quad (5\text{-}5)$$

where T_r, P_r and C_r are reference values of temperature, pressure, and CO_2 concentration, respectively, and α', β', ψ', κ', δ', ε', ξ', ζ', and ω' are constants. By taking up to the first order terms or the second order terms in *Eq. (5-5)* and rearranging the constants, the zero-shear viscosity can be approximated as:

$$\eta_0 \approx A\exp[\alpha/(T-T_r) + \beta P + \psi C] \quad (5\text{-}6a)$$

$$\eta_0 \approx A\exp[\alpha/(T-T_r) + \beta P + \psi C + \kappa P/(T-T_r) + \delta PC + \varepsilon C/(T-T_r) + \xi/(T-T_r)^2 + \varsigma P^2 + \omega C^2] \quad (5\text{-}6b)$$

where A, α, β, ψ, κ, δ, ε, ξ, ζ, and ω are constants. The viscosities measured for neat PS melts and PS/CO_2 solutions are fully described by determining all the parameters involved in *Eq. (5-1)* and *Eq. (5-6)*. A non-linear regression using a quasi-Newtonian method is used for estimating the parameters, and all experimental data are fit to a master plot, η/η_0 versus $\eta_0\dot{\gamma}$.

5.4.2. Modeling Procedures

Detailed procedures for modeling the viscosities of PS melts and PS/CO_2 solutions are described below:

(1) Measurement of the viscosity of neat PS melt:

(1-a) Capillary rheometer: The apparent viscosity of unsaturated PS melt is measured at various temperatures and pressures using a capillary rheometer. The temperature is controlled in the range of 200°C to 260°C. The *L/D* ratio of the capillary die is chosen to be 40 to minimize the contribution of the entrance pressure loss. In order to

determine the effect of pressure on the viscosity, the pressure in the capillary should be measured. In this study, the arithmetic mean value of the inlet and outlet pressures of the capillary rheometer is chosen to represent the pressure in the capillary.

(1-b) Cone-and-plate rheometer: In order to obtain the Newtonian (or zero-shear) viscosity of PS melt, a cone-and-plate rheometer is used. The shear rate is varied from 2.25E-3 s^{-1} to 2.1 s^{-1} at a temperature in the range of 220°C to 260°C.

(1-c) Wedge die rheometer: The viscosity of neat PS melt is also measured using a wedge die at various temperatures, pressures, and shear rates.

(2) Measurement of the viscosity of PS/CO_2 solution:

The viscosity measurement of PS/CO_2 solutions is performed only with the linear capillary die and the wedge die. By measuring the pressure drops, the apparent viscosity is calculated at various concentrations of CO_2 as explained by Lee et al. (1998). The concentration of CO_2 is controlled up to 4 wt% using a positive displacement pump. As explained in the literature (Pabedinskas et al., 1991), the wedge die is capable of measuring the viscosity at various shear rates covering over a decade for a fixed polymer flow rate. In this study, however, only the viscosity value at the shear rate obtained where the centered pressure transducer is located, was taken for modeling. The pressure drop ratio between upstream and downstream of the wedge die can be expressed as a function of power law index, volumetric flow rate and the die dimensions. It should be noted here that the pressure transducers measure the sum of the hydrostatic pressure and the wall normal stress as pointed out by Han (1976). In order to use the pressure readings to *Eqs. (5-5)* and *(5-6)*, the normal stress contribution to the pressure readings should be eliminated. In this work, however, the wall normal

stress in our experimental conditions was small compared to the hydrostatic pressure. Therefore, the readout pressures from the pressure transducers are simply taken for the viscosity modeling in this Chapter. Further discussion on the normal stress contribution on the pressure readings in addressed in Section 5.5.2.1.

(3) Rabinowitsch correction:

The viscosity curves of η_{app} versus $\dot{\gamma}_{app}$ obtained from the capillary rheometer and the wedge die are converted into the true viscosity curves of η versus $\dot{\gamma}$ using the Rabinowitsch correction (Dealy and Wissburn, 1990).

(3-a) Rabinowitsch correction for the capillary rheometer: The Rabinowitsch correction of the viscosity obtained from the capillary rheometer is given by the following equations:

$$\dot{\gamma} = [(3s+1)/4s]\dot{\gamma}_{app} \quad and \quad \eta = [4s/(3s+1)]\eta_{app} \tag{5-7}$$

where the local power law index, s, is calculated by fitting a power law equation for three points (one point of interest and its neighboring two points). The local power law index at the end of the viscosity curve is taken to have the same value as its neighboring points.

(3-b) Rabinowitsch correction for the wedge die: The apparent viscosity measured from the wedge die is transformed into the true viscosity using the following equations:

$$\dot{\gamma} = [(2s+1)/3s]\dot{\gamma}_{app} \quad and \quad \eta = \eta = [3s/(2s+1)]\eta_{app} \tag{5-8}$$

where the local power law index, s, is calculated from the ratio of two pressure drops through the wedge die (Pabedinskas et al., 1991).

(4) Parameter estimation and master curve generation:

(4-a) Parameter estimation for neat PS melts: The true viscosity data obtained from three different kinds of rheometers for neat PS melts are fit to the proposed viscosity equations, *Eq. (5-1)* and *Eq. (5-6)*, using non-linear regressions. In *Eq. (5-6)*, all terms related to the concentration are ignored. By taking various values of the parameter "a" in *Eq. (5-1)* and by taking different terms in *Eq. (5-6)*, all relevant parameters are determined for the Cross, Carreau and generalized Cross-Carreau models. Finally, a master curve of η/η_0 versus $\eta_0\dot{\gamma}$ is generated for each model. The relative contribution of each term on the zero shear viscosity (for example, the 1st order dependence of temperature on the viscosity) is estimated using the parameters determined. For the non-linear regression, a quasi-Newtonian method is applied using a commercial software (Statistica).

(4-b) Parameter estimation for PS/CO_2 solutions including neat PS melts: All viscosity data for neat PS melts and PS/CO_2 solutions are used for the parameter estimation, and the viscosity data are listed in Appendix IV. All parameters including the terms related to the CO_2 concentration are estimated by the same procedures explained in (4-a).

5.5. RESULTS AND DISCUSSION

5.5.1. Microcellular Extrusion System

5.5.1.1. Measurements of PS Melt Viscosities at Various Shear Rates

The viscosity of the PS melt was measured first without adding any CO_2 at various shear rates. In order to investigate the effect of pressure (Kadijk and vanden Brule, 1994 and Westover, 1961) on the viscosity of unsaturated PS, the resistance of the nozzle attached to the end of the capillary die was varied in the experiments. *Figure 5.4* shows the apparent viscosities of the PS melt measured at various shear rates with three different resistance nozzles (*Table 3.2*): a high resistance nozzle (Nozzle A) of a length 1.27 cm and a diameter 0.053 cm, a low resistance nozzle (Nozzle B) of a length 0.62 cm and a diameter 0.089 cm, and no (resistance) nozzle.

The number shown at each point represents the average of the two pressures measured in the capillary die. A relatively higher average pressure was observed at a higher shear rate because a higher upstream pressure was required to induce a higher flow rate (i.e., higher shear rate) for a given nozzle. It was also observed that the viscosity measured at the same shear rate varied considerably as the (average) pressure changed. This indicates that the pressure dependence of the PS melt viscosity is significant as observed by others (Kadijk and van den Brule, 1994).

The experimental data after Rabinowitsch correction were fitted to the generalized Cross-Carreau, *Eq. (5-1)*, and the first order generalized Arrhenius equations, *Eq. (5-6a)*. The zero-shear viscosity in *Eq. (5-6a)* can be rewritten with a zero CO_2 content (i.e., $C = 0$) for the unsaturated PS melt as follows:

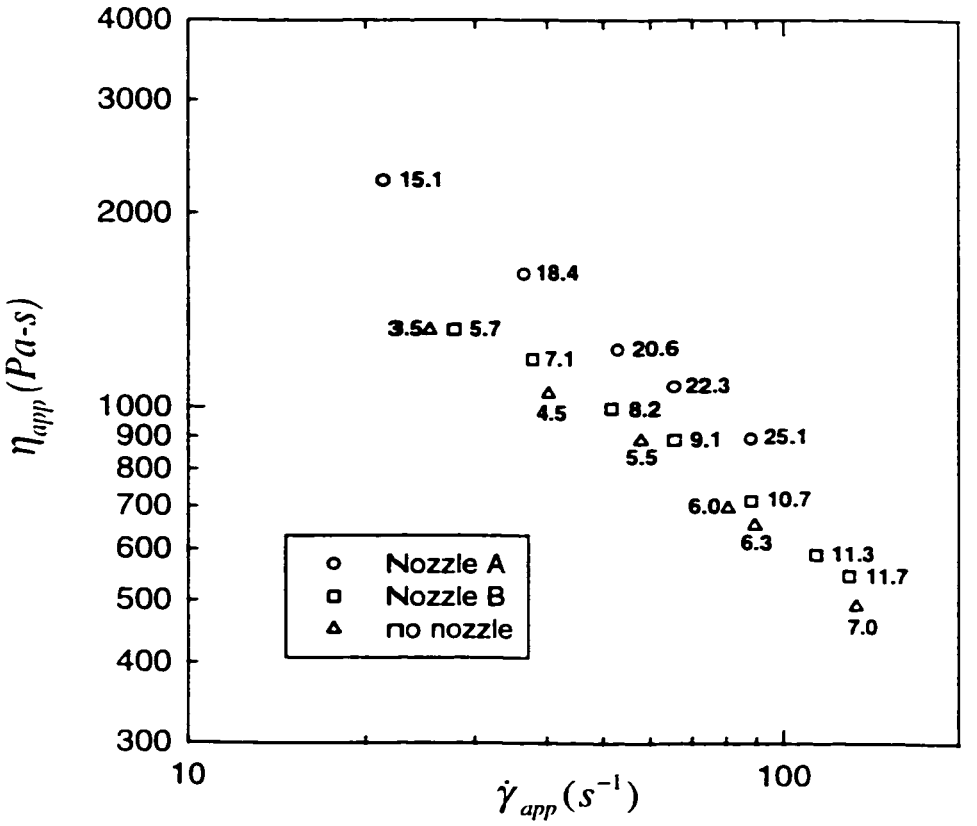

Figure 5.4. Apparent viscosities of unsaturated PS melt measured with Nozzle A, Nozzle B and without nozzle. The number indicate the average die pressure in MPa.

$$\eta_0 = A\exp\left(\frac{\alpha}{T - T_r} + \beta P\right) \tag{5-9}$$

All the material constants in *Eqs. (5-1)* and *(5-9)* were determined using a least squares method based on the Marquardt-Levenberg algorithm (Levenberg, 1944 and Marquart, 1963) and the values of these estimated parameters were

$$(A,\ T_r,\ \alpha,\ \beta,\ \tau,\ n,\ a)$$

$$= (0.5541,\ 332.7\ \text{K},\ 1206\ \text{K},\ 7.971\text{E-}8\ \text{Pa}^{-1},\ 46200\ \text{Pa},\ 0.168,\ 1.479) \tag{5-10}$$

A master curve of η/η_0 versus $\eta_0\dot{\gamma}$ based on these parameters is plotted in *Figure 5.5*. The master curve shown in *Figure 5.5* indicates that the proposed models of *Eqs. (5-1)* and *(5-9)* describe the pressure effect well for the PS melt viscosity.

5.5.1.2. Measurements of PS/CO_2 Solution Viscosities at Various Shear Rates and CO_2 Contents

The viscosity of the PS/CO_2 solutions was measured at various shear rates and CO_2 contents. The CO_2 contents used in these experiments were 2, 3 and 4 wt%. The measured viscosities of PS/CO_2 solutions are shown in *Figure 5.6* together with the unsaturated PS melt viscosities. The average pressure is also indicated at each measured data point. Nozzles C and D in *Table 3.2* were used for the PS/CO_2 solutions. The experimental results indicate that the viscosity of PS/CO_2 solutions strongly depends on the shear rate, the CO_2 content, and the processing pressure. It was observed that the viscosity of PS/CO_2 solutions tended to decrease as the CO_2 content increased. However, the obtained solution viscosity data had a significant scatter at each shear rate due to the pressure difference as in the case of unsaturated PS melt viscosities. As a consequence, it was very hard to extract the effects of the CO_2 content and pressure variations on the PS/CO_2 solution viscosity from the scattered

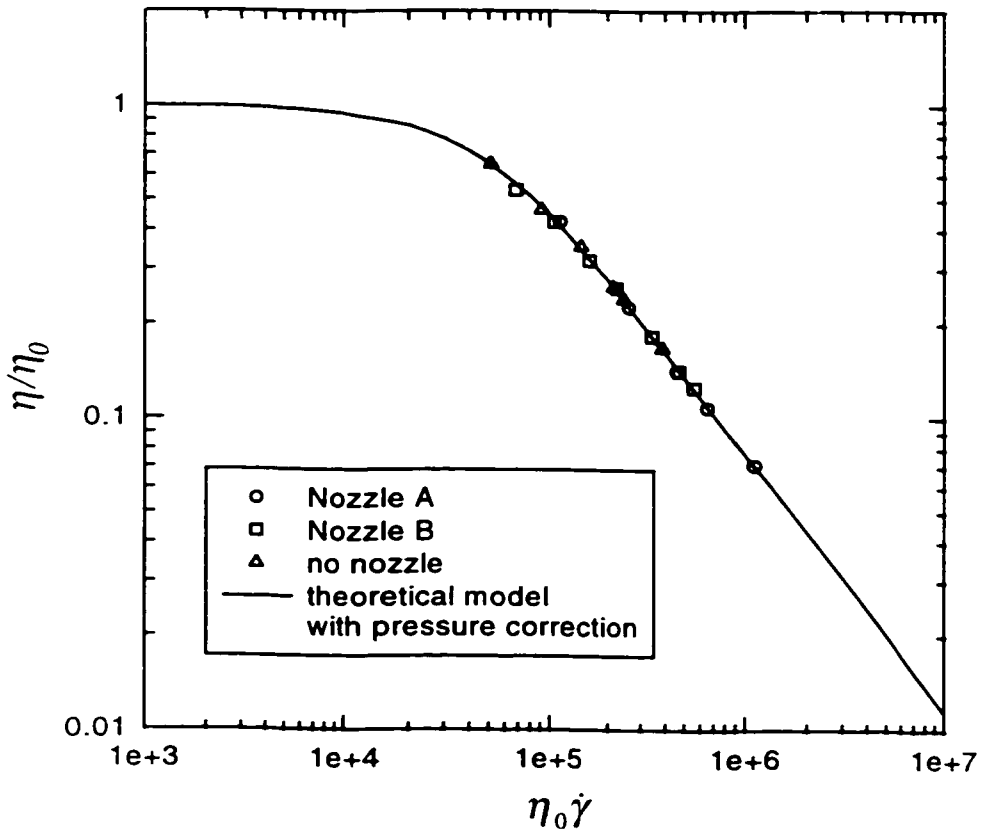

Figure 5.5. A master curve of η/η_0 versus $\eta_0\dot{\gamma}$ for unsaturated PS melt with pressure correction.

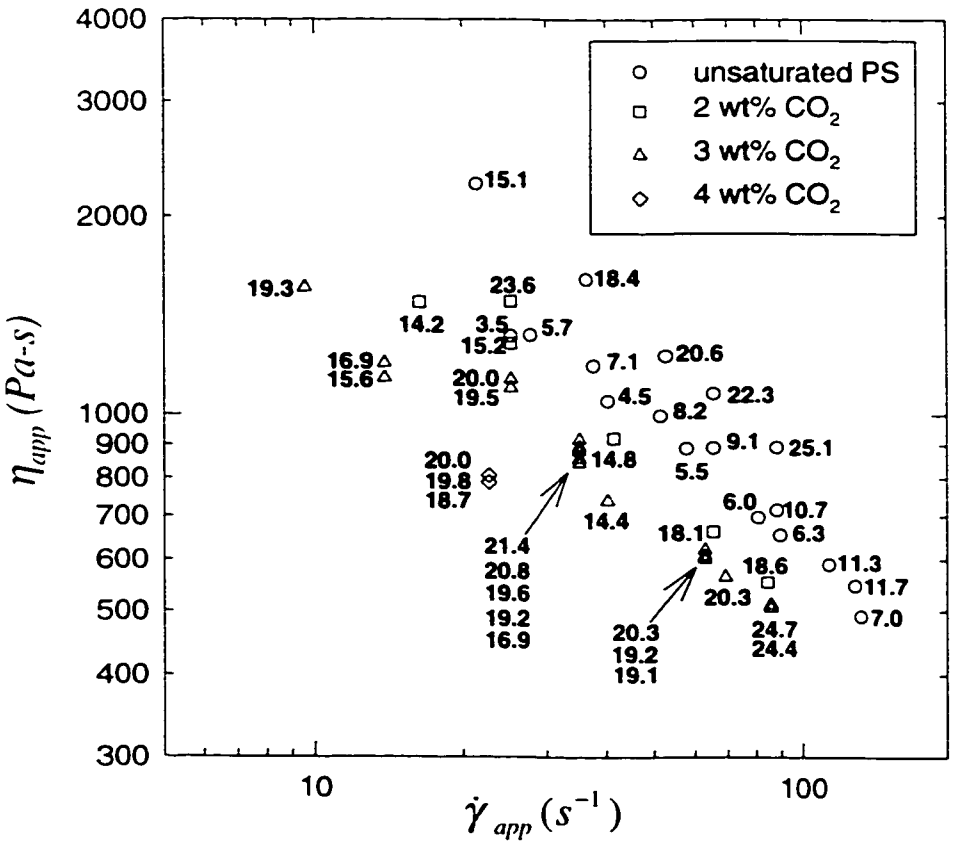

Figure 5.6. Apparent viscosities of unsaturated PS and PS/CO_2 solutions at various shear rates and CO_2 contents. The number indicate the average die pressure in MPa (T=220°C).

data shown in *Figure 5.6*.

In order to distinguish the effect of the CO_2 content on the PS/CO_2 solution viscosity clearly, the pressure dependence of the solution viscosity was eliminated by using *Eq. (5-9)*. A master curve of η/η_0 versus $\eta_0\dot{\gamma}$ based on *Eq. (5-1)* is plotted in *Figure 5.7* using the parameters shown in *Eq. (5-10)*. It may be noted that *Figure 5.7* assumed that the effect of pressure on the viscosity of PS/CO_2 solution was the same as that of the unsaturated PS melt. A decrease of the viscosity with increasing concentration of CO_2 is clearly illustrated in this figure.

It may be noted that the plasticizing effect of the dissolved CO_2 was more dominant than the effect of the hydraulic pressure applied on the PS/CO_2 system for dissolving the gas. In other words, when CO_2 was dissolved in the PS matrix under pressure, the viscosity drop due to the dissolved gas was much more than the viscosity increase due to the applied pressure which was required to dissolve CO_2 in the polymer. Therefore, the resultant viscosity of the PS/CO_2 solution was usually lower than that of the polymer. However, if the pressure in the capillary die is much higher than the solubility pressure, the viscosity of a polymer / gas solution can be higher than that of the polymer.

It was also noticeable that the decreased viscosity of the PS/CO_2 solutions tended to show a less shear-thinning behavior at low shear rates compared to the unsaturated PS melt. Similar tendencies were observed with an increase in temperature or a decrease in pressure (Hieber and Chiang, 1992, and Kadijk and van den Brule, 1994) as implied from the generalized Cross-Carreau equation. Despite the less shear-thinning behavior of PS/CO_2 solutions at low shear rates, the slope of the viscosity curve at high shear rates was not

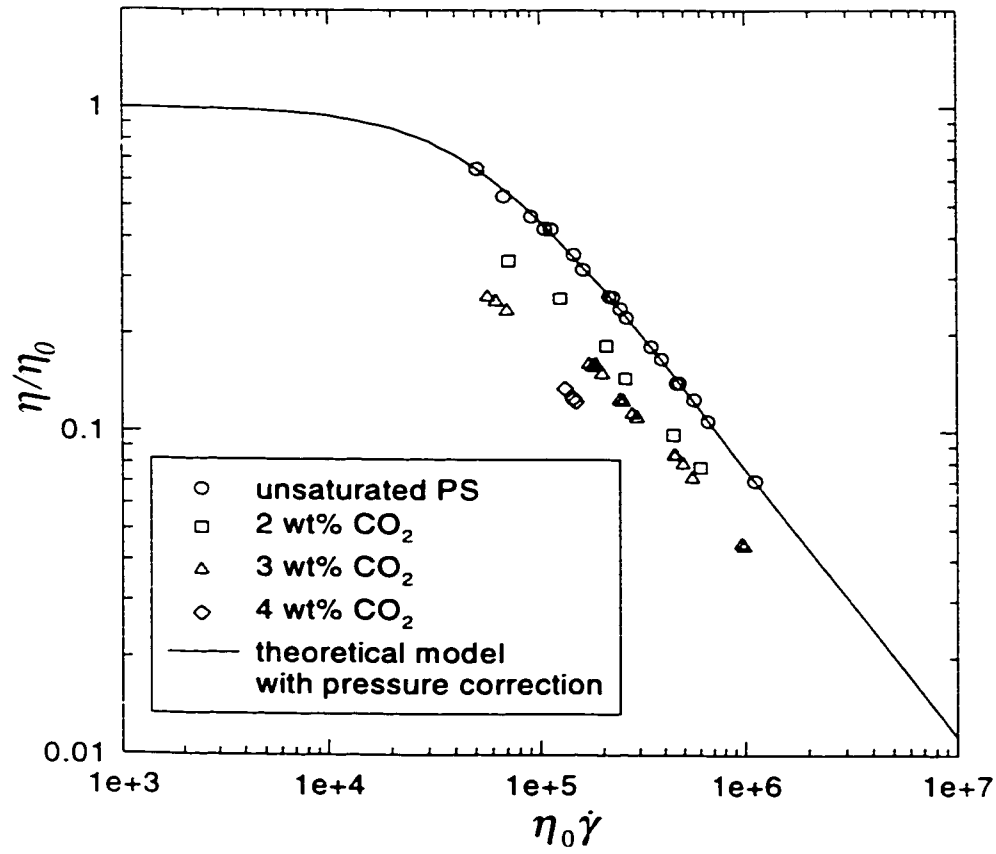

Figure 5.7. Pressure-corrected viscosities of unsaturated PS and PS/CO_2 solutions.

changed. This implies that the decrease of viscosity can be modeled as a simple downward shift in the high shear rate region.

When all the results were fitted into the generalized Cross-Carreau (*Eq. (5-1)*) and first order generalized Arrhenius (*Eq. (5-6a)*) equations, a master curve of η/η_0 versus $\eta_0\dot{\gamma}$ was formed (*Figure 5.8*) which accommodated the effects of the CO_2 concentration as well as the pressure. In this curve fitting, the material parameters in *Eqs. (5-1)* and *Eq. (5-6a)* were again determined using all the data points shown in *Figure 5.6*. The values of the estimated parameters were

$(A, T_r, \alpha, \beta, \psi, \tau, n, a)$

$= (0.8298, 341.1\ \text{K}, 1272\ \text{K}, 6.032\text{E-}8\ \text{Pa}^{-1}, -66.51, 23160\ \text{Pa}, 0.265, 1.877)$ (5-11)

The newly estimated parameters with pressure and concentration correction were slightly different from those obtained with pressure correction only. This means that the shape of the master curve was slightly changed.

Figure 5.8 illustrates that all the data points in *Figure 5.6* for the unsaturated PS and PS/CO_2 solutions at various CO_2 concentrations were successfully shifted to the master plot. Thus, the effects of pressure and CO_2 concentration on the viscosity could be described adequately by combining the generalized Cross-Carreau model and generalized Arrhenius equation. It was noted that the concentration coefficient of viscosity, ψ, was a considerably negative value as expected. It was also noted that the pressure coefficient, β, of pure PS in this study was higher than those obtained by Cogswell and McGowan (1972) and Kadijk and van den Brule (1994). This seemed to be mainly due to the pressure range difference: since this study was directed to foam applications, the pressure range in the experiment was 0.1 MPa to 25 MPa whereas the pressure ranges in Cogswell and McGowan's (1972) and Kadijk

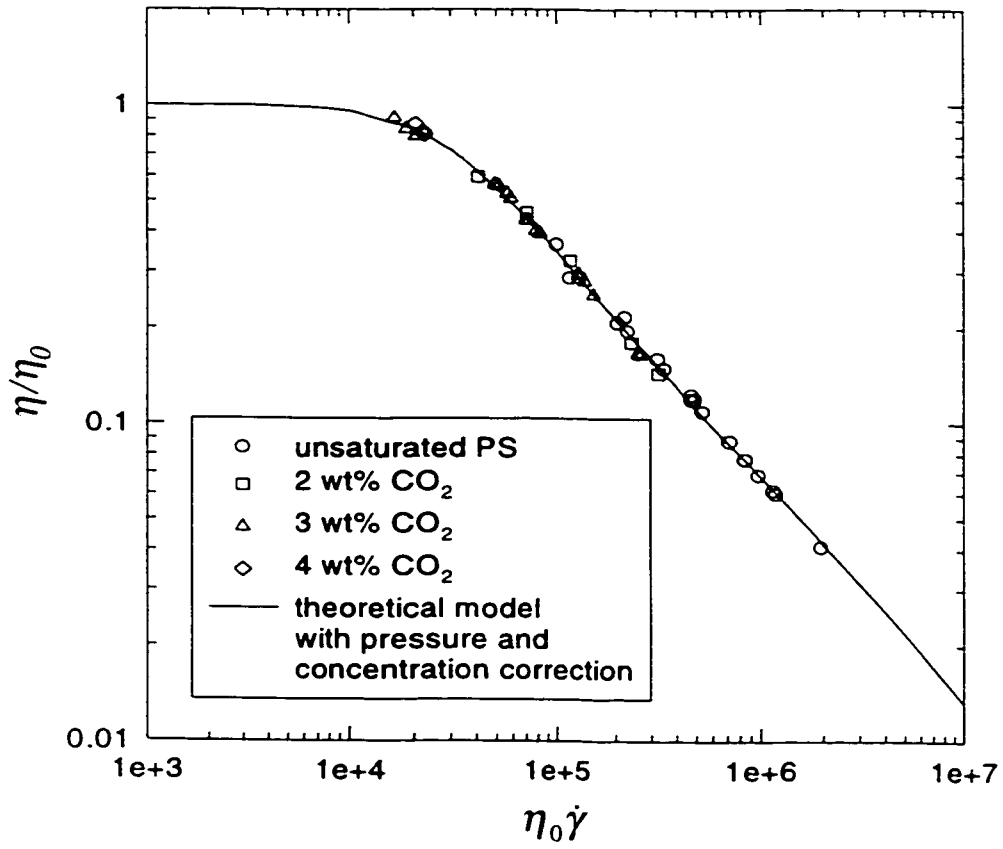

Figure 5.8. Pressure and concentration corrected viscosities of unsaturated PS and PS/CO_2 solutions.

and van den Brule's (1994) studies were 0.1 MPa to 140 MPa and 20 MPa to 100 MPa, respectively.

There was a difficulty in elucidating the effect of pressure on the viscosity. As mentioned earlier, the pressure shown in *Figure 5.6* indicates the average of the upstream and downstream pressures. Since the pressure changes along the capillary die, the effect of pressure on the apparent viscosity is not straightforward and the arithmetic average taken as the representative pressure may involve some errors. Because the pressure change is larger for a higher shear rate, the error involved in taking the average pressure to calculate the effect of pressure on the viscosity will be greater for a higher shear rate. Further study is required to quantify the pressure dependence of the viscosity of polymer / CO_2 solutions at each flow rate.

5.5.1.3. Estimation of the Solubility of CO_2 in PS

It has been emphasized that the downstream pressure of the capillary die should be high enough to prevent bubble formation in the capillary die. However, when precipitation of CO_2 occurred due to a low pressure in the die, an interesting phenomenon was observed. Let us consider the 3% CO_2 solution case. At a fixed apparent shear rate of 13.8 s^{-1}, the processing pressure was reduced step by step. In the beginning, because of the hydraulic pressure effect, the solution viscosity decreased as the downstream pressure decreased up to the solubility pressure. In this case, the amount of gas dissolved in the polymer was fixed, and therefore, the viscosity was governed by the hydraulic pressure effect alone. However, when the pressure was further decreased below the solubility pressure, precipitation of CO_2 began and the content of CO_2 dissolved in the PS matrix was reduced. Because the dissolved gas content decreased, the viscosity of the polymer / gas solution increased. This reduction in

the plasticization effect of gas now caused an increase in the viscosity of the polymer / gas mixtures, even though a second phase was formed and the viscosity tended to decrease due to the formed second phase. In other words, the viscosity increased as the pressure was further decreased below the solubility pressure. This is well depicted in *Figure 5.9*. When the CO_2 contents were 2 and 4 wt%, similar results were obtained: the viscosity initially dropped as the pressure decreased up to the solubility pressure; when the pressure was further decreased, the measured viscosity increased. A similar observation was reported by Gendron et al. (1996). They found decrease of the viscosity with an increase in the pressure and also used the solubility to explain that phenomenon.

If the observed minimum die exit pressures in *Figure 5.9* were the solubility pressure for each CO_2 content, the corresponding CO_2 content would be the solubility of CO_2 in the polymer at the minimum die exit pressure. *Figure 5.10* shows this approximately estimated solubility at each pressure, and it is compared with the theoretically or experimentally predicted values from the literature. For the prediction of the solubility for PS/CO_2 system at 220°C, the heat of solution obtained from Durrill and Griskey (1966, 1969) was used. It turned out that the solubility estimated from our experiments was lower than the predicted values. When the solubility of CO_2 in PS at elevated temperatures is measured, this point will be clarified.

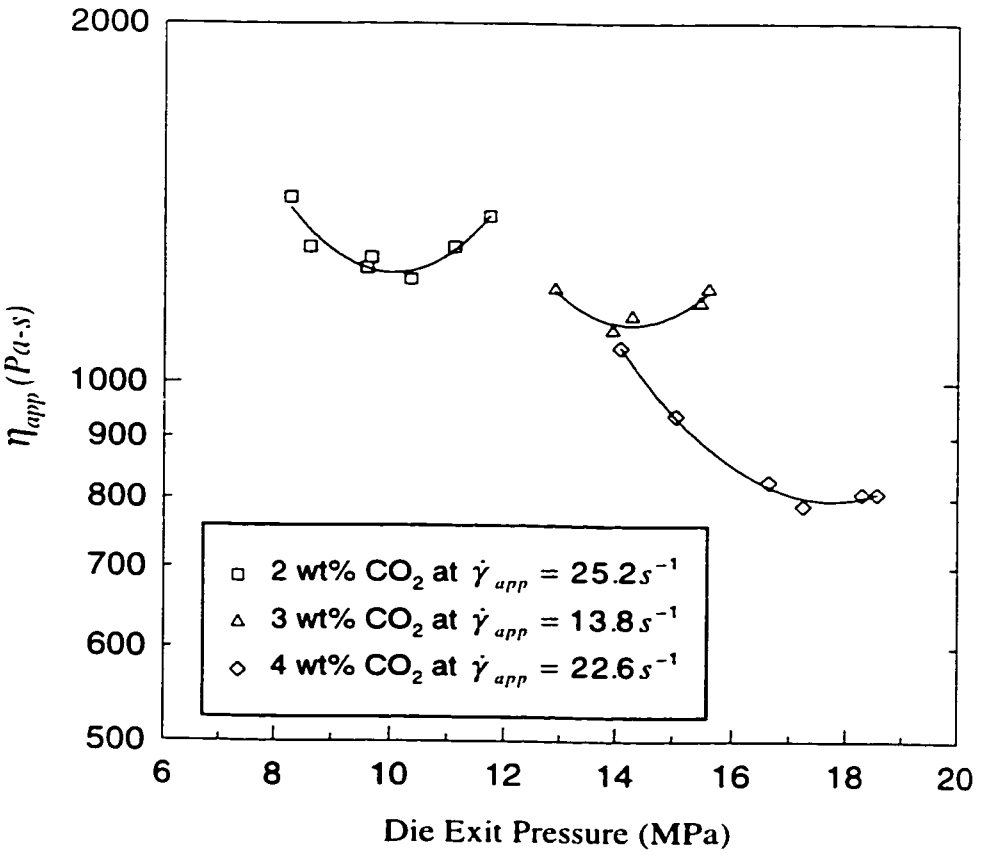

Figure 5.9. Variation of viscosity as a function of the die exit pressure at 220°C.

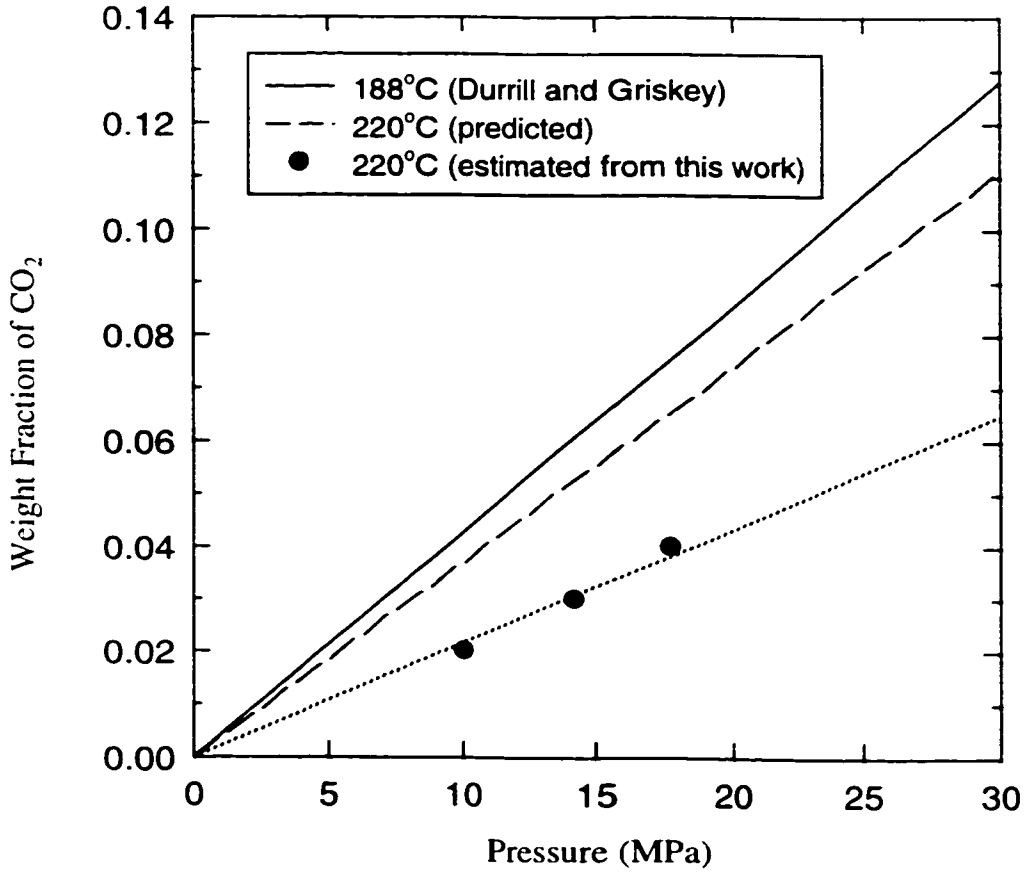

Figure 5.10. Comparison of the estimated solubilities of CO_2 in PS.

5.5.2. Twin-Screw Extrusion System

5.5.2.1. Measurements of Viscosity

The viscosities of the unsaturated and saturated PS melts were measured using three rheometers at various experimental conditions (*Table 5.1*). As shown in *Figure 5.11*, the viscosity data of neat PS melts show a Newtonian viscosity behavior at low shear rates, and a shear thinning behavior at high shear rates. It should be noted that the viscosities obtained from the capillary rheometer and the wedge die were measured at relatively high pressures while those obtained from the cone-plate rheometer were measured at atmospheric pressure. Therefore, as in *Figure 5.11*, the viscosity data measured from the capillary rheometer and wedge die show higher values than the viscosities measured from the cone-and-plate rheometer at low shear rates. These deviations were properly addressed by considering the effect of pressure on the viscosity in modeling.

The viscosities of PS/CO_2 solutions were also measured at various temperatures, pressures, and CO_2 concentrations. The experimental results are shown in *Figure 5.12*. The experimental results indicate that the effect of each variable is very difficult to determine because of the many variables involved. In order to clarify the individual effect of each variable, the viscosities shown in *Figures 5.11* and *5.12* were fit to various viscosity models, *Eq. (5-1)*, and the generalized Arrhenius equation, *Eq. (5-6b)*.

It may be noted that the value measured from the pressure transducers included the wall normal stress in addition to the actual pressure (Han, 1976). Therefore, although the hole pressure effect was removed by flush-mounting of the pressure transducers, a certain degree of error was involved in the pressure measurements. However, this error was believed to be small because the normal stresses in the experimental conditions were calculated to be

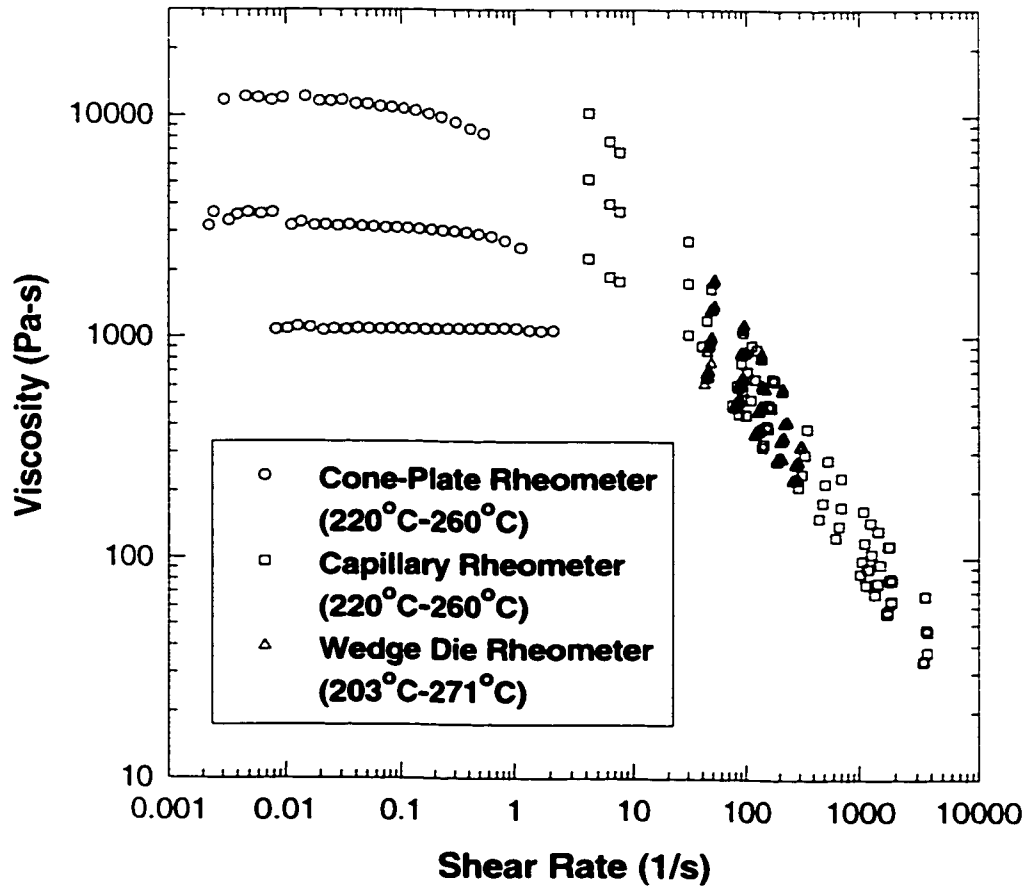

Figure 5.11. Viscosity of unsaturated PS measured using various rheometers.

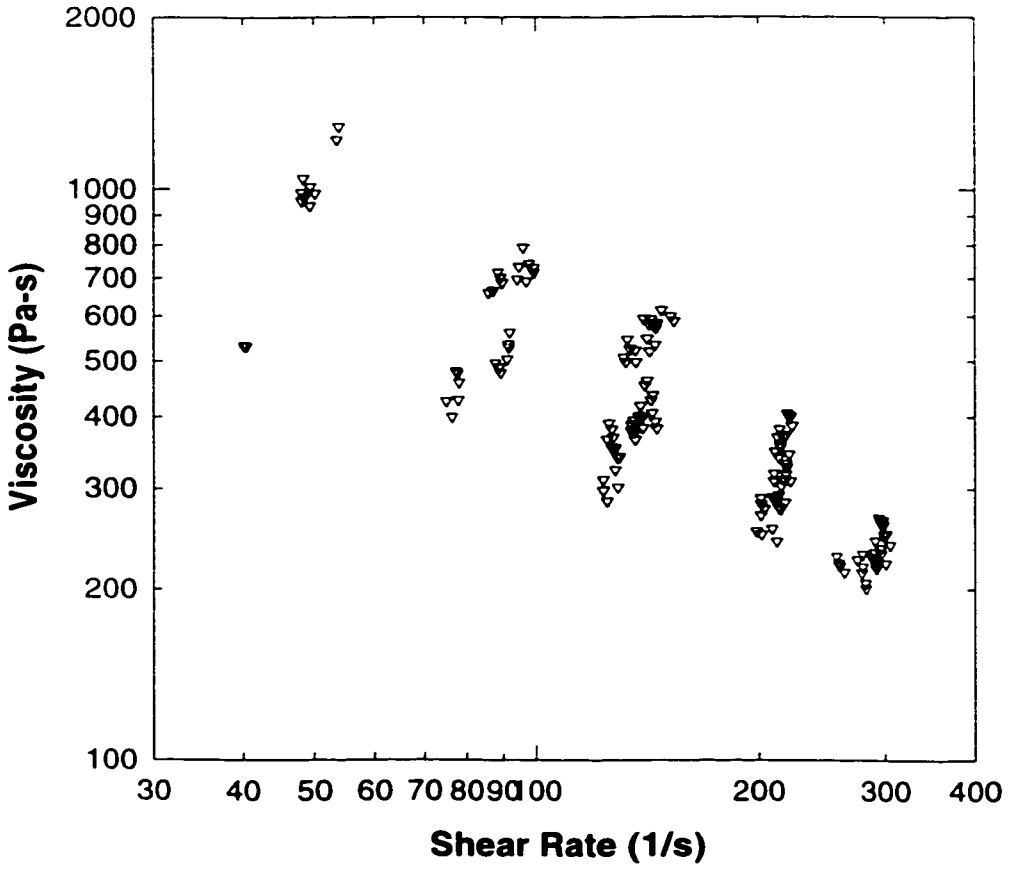

Figure 5.12. Viscosity of PS/CO_2 solutions at various T, P and CO_2 content.

in the range of 300 to 700 KPa according to the in-house simulation based on Leonov model (Leonov, 1976, Leonov et al., 1976, Leonov and Prokunin, 1980, Zatloukal et al., 1999), while the total pressure readings are in the range of 3.5 to 24.7 MPa.

5.5.2.2. Comparisons of Various Viscosity Models

Three viscosity models (i.e., the generalized Cross-Carreau (C-C), Cross, and the Carreau models) were compared by determining the parameters in *Eqs. (5-1)* and *(5-6b)*. First, comparison was made for the neat PS melts. All parameters except the CO_2 concentration dependency in *Eqs. (5-1)* and *(5-6b)* were estimated by non-linear regression as described in the Section 5.4.2. The master curves of η/η_0 versus $\eta_0\dot{\gamma}$ generated based on these parameters for each viscosity model were plotted and are shown in *Figures 5.13* and *5.14*. It should be noted that the residual sum of the squares (RSS) of the generalized C-C model is smaller than the RSSs of the other two models, indicating that the generalized C-C model gives the best description of the viscosity behavior of neat PS melts. *Figure 5.13* illustrates that all the viscosity data for the neat PS melts were reasonably well shifted to the master plot when the three models were used. This indicates that the effects of temperature, pressure and CO_2 concentration, and their interactions on the viscosity could be described adequately by combining the Cross Carreau, or the generalized C-C model and generalized Arrhenius equation. These viscosity models are compared each other in *Figure 5.14*. The Carreau model shows a sharp transition from the Newtonian viscosity region to the shear thinning region due to its high "*a*" value. The sharp transition leads to a poor agreement with the experimental data as indicated in *Figure 5.13(b)*. However, the generalized C-C model and the Cross model show broader transitions leading to a good agreement with the experimental data.

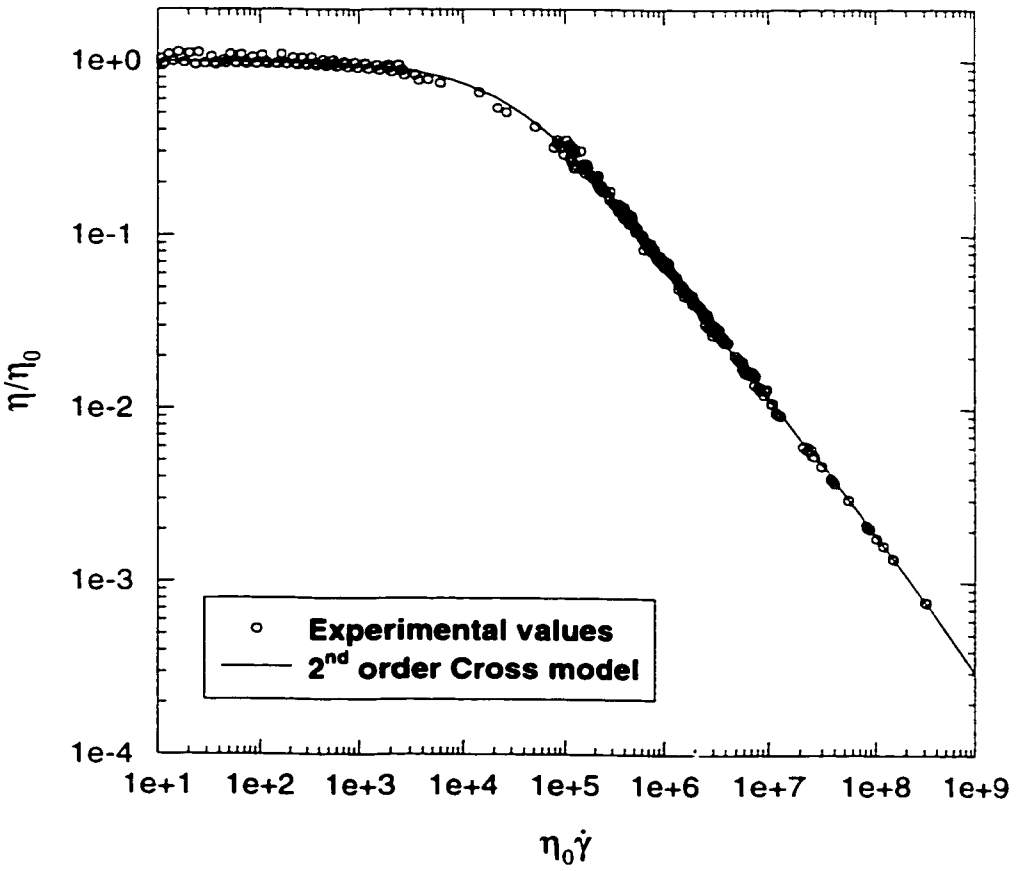

Figure 5.13(a). Master plot for unsaturated PS, Cross model

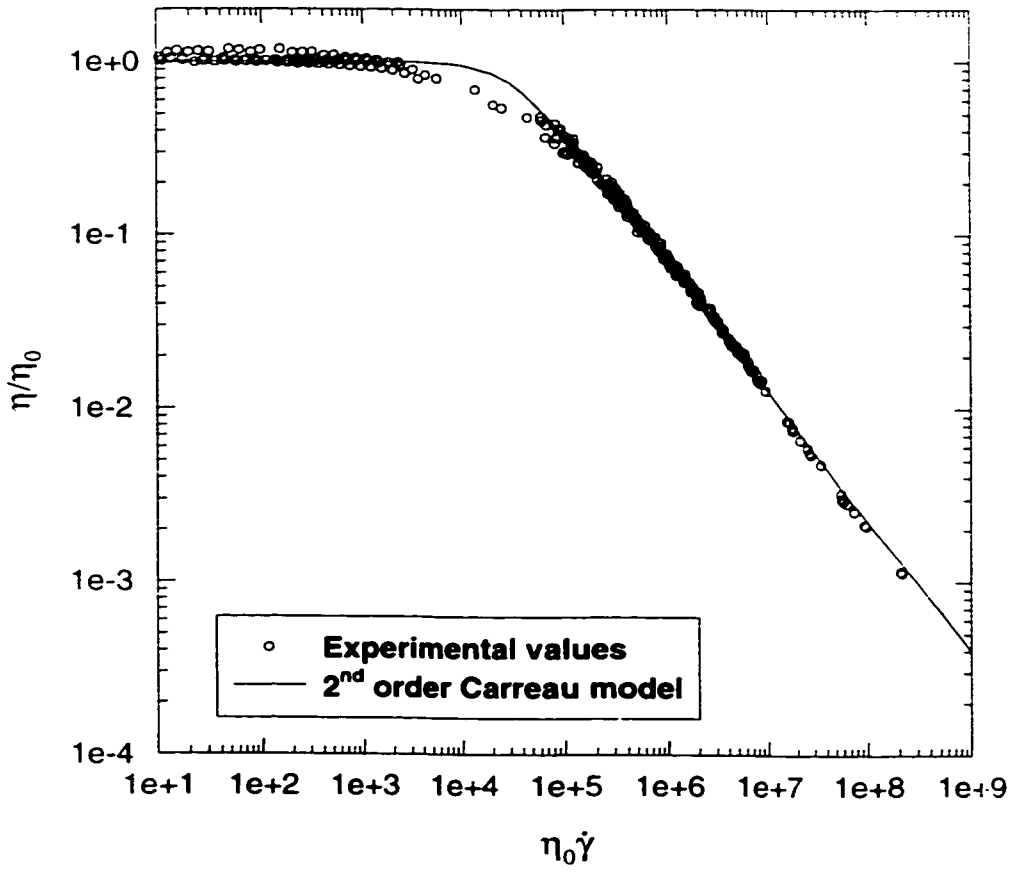

Figure 5.13(b). Master plot for unsaturated PS, Carreau model

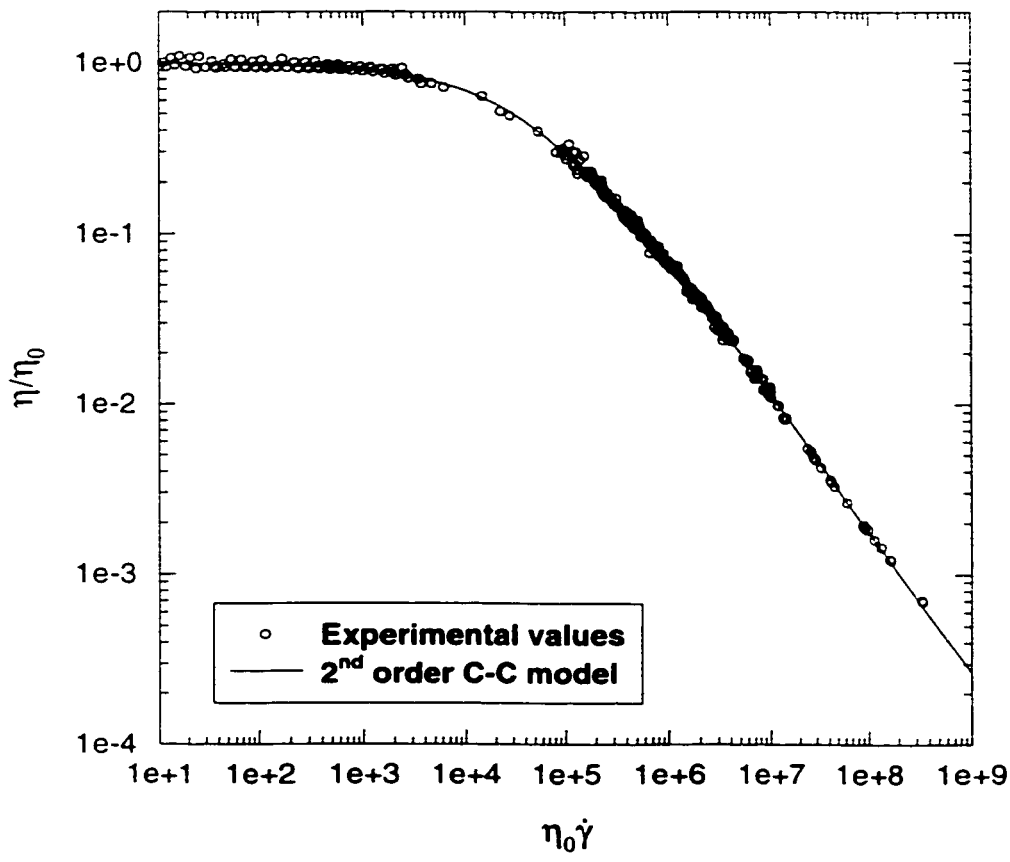

Figure 5.13(c). Master plot for unsaturated PS, Generalized Cross-Carreau model

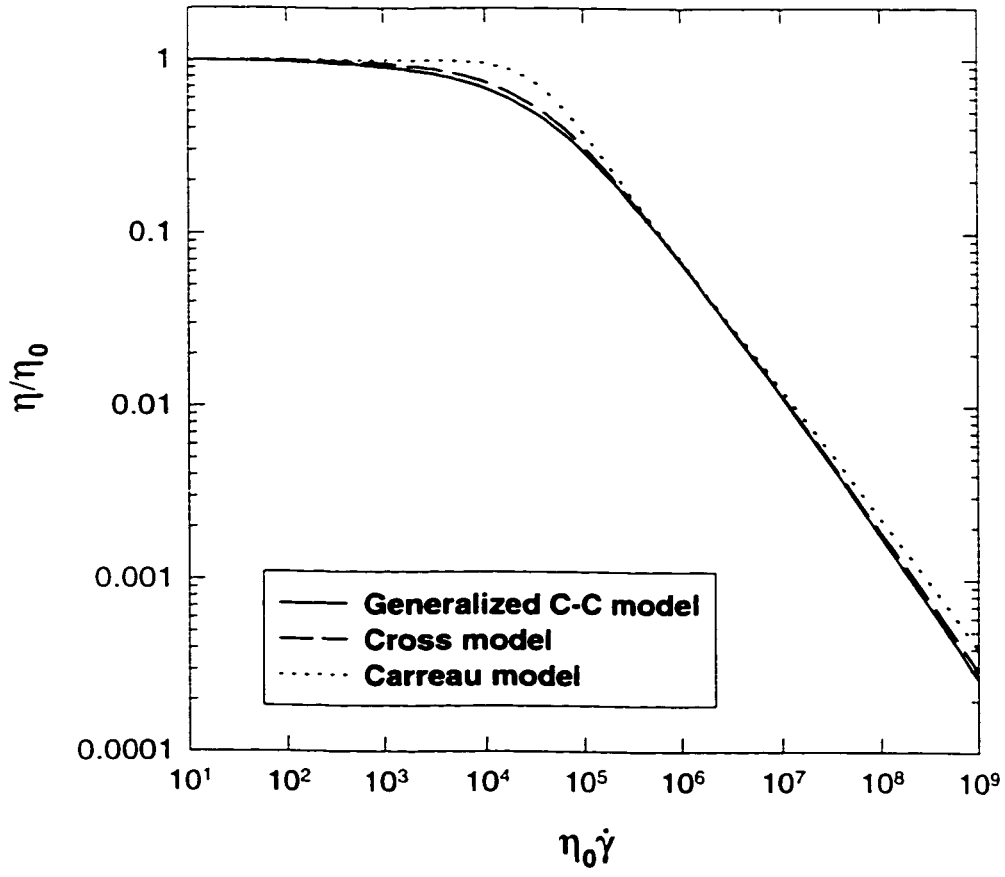

Figure 5.14. Comparison of various viscosity models for unsaturated PS.

Second, all the viscosity data for PS melts and PS/CO_2 solutions are used together for modeling, and the results are shown in *Figures 5.15* and *5.16*. All parameters involved in *Eqs. (5-1)* and *(5-6b)*, including the concentration dependency, were determined by the non-linear regression. As in the case of the neat PS melts only, the viscosity behaviors of PS melts and PS/CO_2 solutions are best described by the generalized C-C model. In addition, the transition behaviors in the models for all neat PS melts and PS/CO_2 solutions are similar to those in the models for the neat PS melts only. It is noted that the material constant, a, of the generalized C-C model is close to that of the Cross model; thus, the viscosity behavior of PS melts and PS/CO_2 solutions follows the Cross model more closely than the Carreau model. A similar result has been published by Hieber and Chiang (1992) for a commercial neat polystyrene melt.

5.5.2.3. Effects of T, P, C and Their Interactions on the Solution Viscosity

The effects of temperature, pressure, CO_2 content and their interactions were investigated by calculating the relative contribution of each term over the range of experimental conditions. *Table 5.2* shows the estimated parameter values for the neat PS melts, and *Table 5.3* for all the neat PS melts and PS/CO_2 solutions. As shown by the RSS values, consideration of the interaction terms increased the accuracy of the fits significantly. For instance, by including the interaction and higher order terms from the generalized Arrhenius equation of *Eq. (5-6b)*, the RSS for the generalized C-C model decreased from 0.9728 to 0.6818 for PS melts and decreased from 1.6374 to 0.8937 for PS melts and PS/CO_2 solutions. This agrees with the results of Kadijk and van den Brule (1994) who found that the WLF form including the P-T interaction term describes the zero shear viscosity of a pure PS melt well.

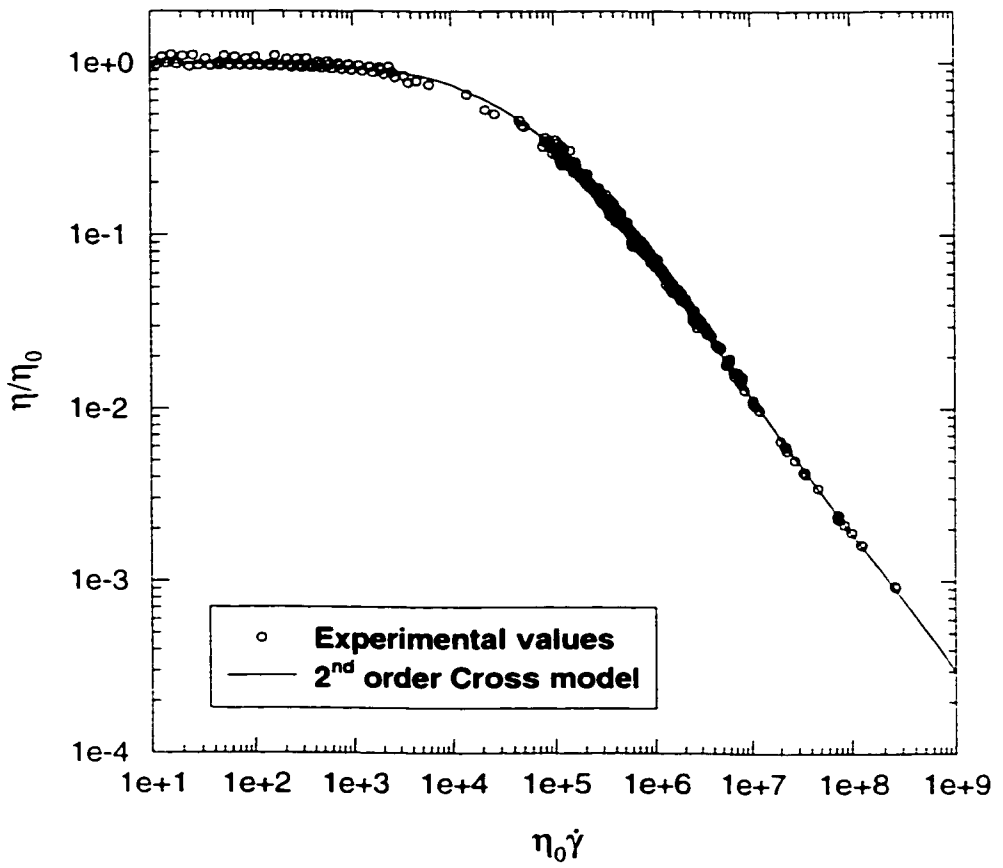

Figure 5.15(a). Master plot for unsaturated PS and PS/CO_2 solutions, Cross model

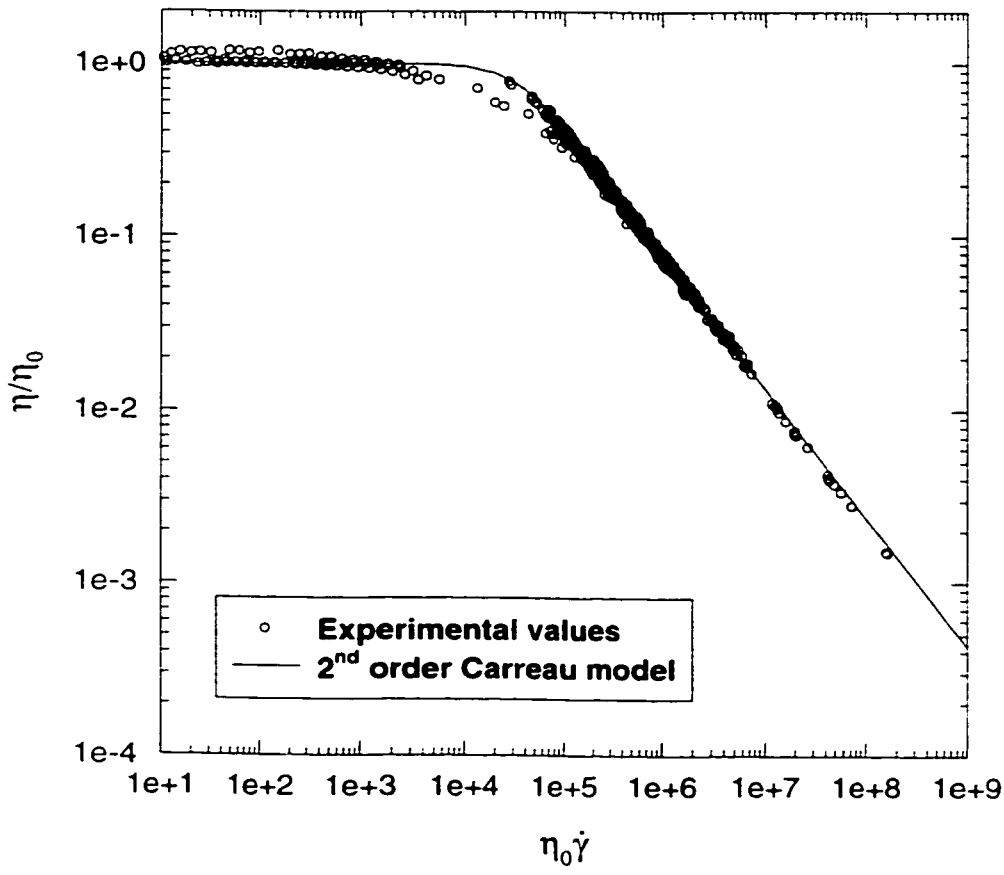

Figure 5.15(b). Master plot for unsaturated PS and PS/CO_2 solutions, Carreau model

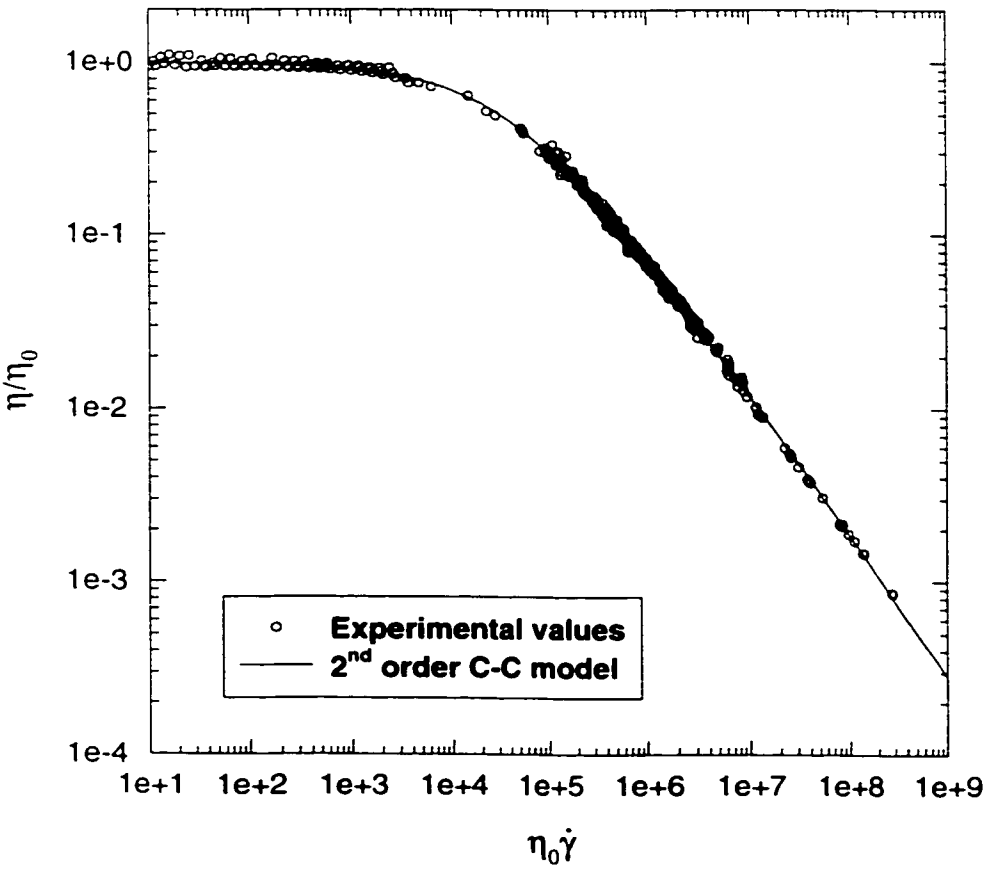

Figure 5.15(c). Master plot for unsaturated PS and PS/CO_2 solutions, Generalized Cross-Carreau model

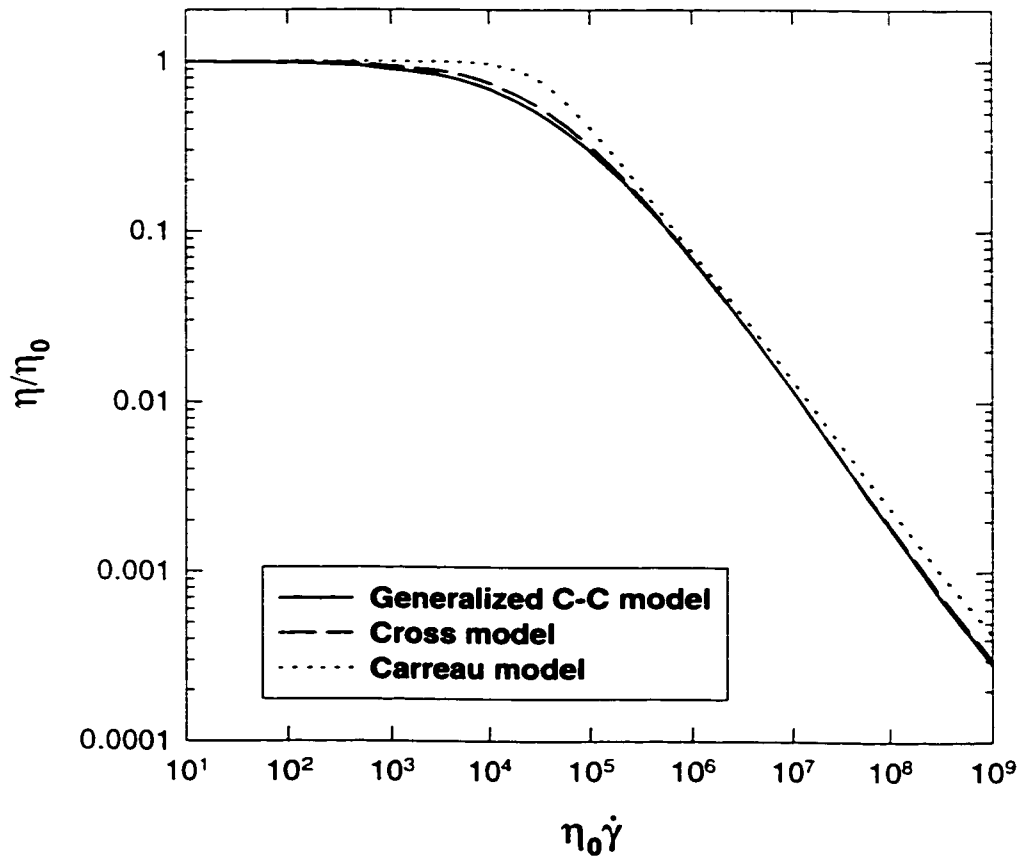

Figure 5.16. Comparison of various viscosity models for unsaturated PS and PS/CO_2 solutions

Table 5.2. Parameter estimations of various viscosity models for unsaturated PS

	Cross Model			Carreau Model			C-C Model		
	1st order	1st order + Interactions	1st order + Interactions + 2nd order	1st order	1st order + Interactions	1st order + Interactions + 2nd order	1st order	1st order + Interactions	1st order + Interactions + 2nd order
n	0.1844	0.1983	0.1992	0.2385	0.2532	0.2525	0.1784	0.1845	0.1793
a	1-n	1-n	1-n	2	2	2	0.7809	0.7324	0.6782
τ	42959	41715	39784	29797	27404	28973	44760	46236	45044
A	9.7E-4	1.9E-4	6.6E-5	1.1E-8	1.0E-5	5.3E-8	1.8E-3	1.06E-3	4.7E-4
α	4048.3	4883.5	5507.2	12420	6776.5	10902	3738.0	3929.8	4343.2
Tr	243.5	219.8	202.2	41.1	166.5	73.5	254.0	250.1	237.6
β	4.92E-8	1.76E-7	1.89E-7	4.8E-8	1.9E-7	1.99E-7	4.98E-8	1.72E-7	2.0E-7
ψ	-	-	-	-	-	-	-	-	-
κ	-	-3.93E-5	-3.76E-5	-	-4.94E-5	-7.6E-5	-	-3.4E-5	-3.2E-5
δ	-	-	-	-	--	-	-	-	-
ε	-	-	-	-	-	-	-	-	-
ξ	-	-	-22.31	-	-	22.2	-	-	-0.035
ζ	-	-	-9.7E-16	-	-	6.9E-16	-	-	-1.7E-15
ω	-	-	-	-	-	-	-	-	-
RSS	0.9792	0.8156	0.7632	2.2415	2.1448	2.1279	0.9728	0.7905	0.6818
R^2	0.99790	0.99825	0.99836	0.99519	0.99540	0.99543	0.99791	0.99830	0.99854

Table 5.3. Parameter estimations for PS melt and PS/CO_2 solutions using various viscosity models

	Cross Model			Carreau Model			C-C Model		
	1st order	1st order + Interactions	1st order + Interactions + 2nd order	1st order	1st order + Interactions	1st order + Interactions + 2nd order	1st order	1st order + Interactions	1st order + Interactions + 2nd order
n	0.1868	0.1875	0.2055	0.2372	0.2531	0.2495	0.1958	0.1893	0.1813
a	1-n	1-n	1-n	2	2	2	0.8753	0.7403	0.6684
τ	41091	42052	38866	30479	28412	32695	38826	45292	45879
A	5.1E-4	4.0E-5	1.7E-4	1.8E-5	1.8E-6	2.3E-5	7.9E-5	5.4E-3	2.62E-4
α	4506.7	5834.0	4918.9	6539.7	8073.0	6263.0	5619.7	3130.0	4661.6
Tr	225.7	192.8	219.3	168.2	134.0	178.6	192.5	278.1	228.1
β	5.3E-8	2.2E-7	2.2E-7	4.6E-8	1.6E-7	1.1E-7	5.2E-8	1.7E-7	2.5E-7
ψ	-53.1	-43.2	-57.3	-50.1	-33.3	-18.2	-51.1	-37.9	-68.2
κ	-	-5.7E-5	-4.5E-5	-	-4.6E-5	-4.1E-5	-	-3.1E-5	-4.7E-5
δ	-	1.9E-7	8.4E-7	-	-1.3E-7	-1.3E-6	-	1.41E-7	1.3E-6
ε	-	-1384.1	-1532.3	-	-3491	-1.815	-	-1875.5	-949.8
ξ	-	-	10.27	-	-	-3.644	-	-	-8.69
ζ	-	-	-9.5E-16	-	-	1.82E-15	-	-	-1.51E-15
ω	-	-	20.2	-	-	100.9	-	-	7.51
RSS	1.6600	1.0449	0.9733	2.7889	2.5929	2.4936	1.6374	1.0078	0.8772
R^2	0.99686	0.99802	0.99816	0.99472	0.99509	0.99528	0.99690	0.99807	0.99834

Statistical investigation of the estimated parameters was carried out. The 2nd order generalized C-C model for the pure PS melt and PS/CO_2 solutions, was chosen for the significance tests of the overall regression model and the individual parameters. First, overall significant test was performed based on the total viscosity data (419 data points) to investigate the validity of the regression model, and ANOVA table is shown in *Table 5.4*. As indicated in *Table 5.4*, the null hypothesis (βi=0) should be rejected by *F*-test. Thus, the 2nd order generalized C-C model is significant with 99% confidence level. Second, the significance level of each parameter involved in *Eq. (5-6b)* was investigated using a partial *F*-test and the results are shown in *Table 5.5*. (+) and (-) signs in *Table 5.5* indicate whether the corresponding term is considered in the regression model or not. In order to calculate the confidence level of each parameter, a covariance matrix is required. In this study, however, the covariance matrix could not be calculated. Therefore, a partial *F*-test method derived from linear regression was used as an approximation. It should be noted, however, that the partial *F*-test could provide an approximate confidence level in the non-linear regression (Draper and Smith, 1998). As shown in *Table 5.5*, 11 partial regression models were tested for determining the significance of parameters, and three parameters representing the P-T, P-C interactions and the second order temperature dependence were not significant at a 95% confidence level.

In order to clarify the effect of each term on the zero shear viscosity, the maximum and minimum values of each term were calculated (*Tables 5.6* and *5.7*). The difference between maximum and minimum values of each term indicates its relative contribution to the zero shear viscosity. For neat PS melts, as shown in *Table 5.6*, the P-T interaction and the 2nd

Table 5.4. ANOVA table for the 2nd order generalized C-C model

	Sum of Square (S.S)	Degree of Freedom	Mean Square (M.S)
Regression	530.8720	13	40.8363
Residual	0.8937	406	0.0022
Total	531.7657	418	1.2722
$F_{obs}=MS_{Regression}/MS_{residual}=18562$ $F_{13,406,0.01}\approx 2.3$			

order pressure terms were not negligible in all models, while the 2nd order temperature term hardly affected the zero shear viscosity. For PS melts and PS/CO_2 solutions, the P-T interaction, P-C interaction, and 2nd order pressure terms were not negligible in the C-C model. The significance of each term in *Table 5.7* generally agrees with the significance of each term calculated in *Table 5.5* except the P-C interaction, when the 2nd order C-C model was considered. The difference in the significance level of the P-C interaction might be related to the approximated *F*-test in the non-linear regression. For the Cross and Carreau models, the C-T interaction and the 2nd order concentration terms were also significant. This means that the concentration terms behave nonlinearly. It should also be noted that the 2nd order temperature terms are small for all the models, indicating that the first order of the inverse temperature term describes the zero shear viscosity behavior well.

Finally, the effect of each parameter was investigated qualitatively using a sensitivity analysis. A variation of one parameter equivalent to the variation of the other parameter can be determined from the model. As a simple calculation, for example, dissolving 1 wt% of CO_2 was equivalent to increasing the pressure by 9.8 MPa when the 1st order Arrhenius approximation was applied with these experimental conditions. The relationships of T-P and

Table 5.5. Significance test of each parameter in the 2nd order C-C model using partial *F*-test

Model	α	β	ψ	κ	δ	ε	ξ	ζ	ω	RSS	Comparisons	F_{obs}	$f_{r1, r2, 0.05}$
1	+	-	-							7.83484	Models 1 and 4	777.8	2.01
2	+	+	-							7.80762	Models 1 and 2	6.8	2.01
3	+	-	+							4.27416	Models 1 and 3	8938.0	2.01
4	+	+	+							1.63741	Overall model	777.8	2.01
5	+	+	+	+	-	-				1.02767	Models 4 and 5	244.0	1.94
6	+	+	+	+	+	-				1.02459	Models 5 and 6	1.25	1.83
7	+	+	+	+	-	+				1.02672	Models 6 and 7	0.4	1.83
8	+	+	+	+	+	+				1.00778	Overall model	4.0	1.83
9	+	+	+	+	+	+	+	-	-	1.00424	Models 8 and 9	1.63	1.8
10	+	+	+	+	+	+	+	+	-	0.87811	Models 9 and 10	58.2	1.72
11	+	+	+	+	+	+	+	-	+	0.99371	Models 9 and 11	4.9	1.72
12	+	+	+	+	+	+	+	+	+	0.87718	Overall model	29.3	1.72
Significant at a 95% confidence level	Yes	Yes	Yes	Yes	No	No	No	Yes	Yes				

Table 5.6. Relative contribution of each term in various viscosity models for unsaturated PS

		$\alpha/(T-Tr)$	βP	φC	$\kappa P/(T-Tr)$	δPC	$\varepsilon C/(T-Tr)$	$\xi/(T-Tr)^2$	ζP^2	ωC^2
Cross (1^{st} order)	Max	17.63	1.43	-	-	-	-	-	-	-
	Min	13.45	0.005	-	-	-	-	-	-	-
Cross (Interactions)	Max	19.27	5.12	-	-0.012	-	-	-	-	-
	Min	15.04	0.018	-	-4.514	-	-	-	-	-
Cross (2^{nd} order)	Max	20.32	5.50	-	-0.011	-	-	-2.0E-4	-9.9E-6	-
	Min	16.09	0.019	-	-4.038	-	-	-3.0E-4	-0.82	-
Carreau (1^{st} order)	Max	28.75	1.40	-	-	-	-	-	-	-
	Min	24.67	0.005	-	-	-	-	-	-	-
Carreau (Interactions)	Max	22.10	5.53	-	-0.013	-	-	-	-	-
	Min	17.92	0.019	-	-4.688	-	-	-	-	-
Carreau (2^{nd} order)	Max	27.28	5.79	-	-0.016	-	-	1.4E-4	0.58	-
	Min	23.14	0.020	-	-5.534	-	-	1.0E-4	7.1E-6	-
C-C (1^{st} order)	Max	17.06	1.45	-	-	-	-	-	-	-
	Min	12.86	0.005	-	-	-	-	-	-	-
C-C (Interactions)	Max	17.62	5.01	-	-0.012	-	-	-	-	-
	Min	13.35	0.017	-	-4.436	-	-	-	-	-
C-C (2^{nd} order)	Max	18.44	5.82	-	-0.011	-	-	-3.7E-7	-1.7E-5	-
	Min	14.15	0.02	-	-3.953	-	-	-6.3E-7	-1.44	-

Table 5.7. Relative contribution of each term in various viscosity models for PS and PS/CO_2 solutions

		α/ (T-Tr)	βP	φC	κP/ (T-Tr)	δPC	εC/ (T-Tr)	ξ/ $(T-Tr)^2$	ζP^2	ωC^2
Cross (1st order)	Max	18.21	1.54	0	-	-	-	-	-	-
	Min	14.13	0.005	-2.124	-	-	-	-	-	-
Cross (Interactions)	Max	20.81	6.40	0	-0.016	0.221	0	-	-	-
	Min	16.59	0.022	-1.728	-5.916	0	-0.197	-	-	-
Cross (2nd order)	Max	19.38	6.40	0	-0.014	0.978	0	1.6E-4	-9.8E-6	0.032
	Min	15.12	0.022	-2.292	-5.158	0	-0.241	9.7E-5	-0.80	0
Carreau (1st order)	Max	21.44	1.34	0	-	-	-	-	-	-
	Min	17.38	0.005	-2.004	-	-	-	-	-	-
Carreau (Interactions)	Max	23.80	4.66	0	-0.011	-0.151	0	-	-	-
	Min	19.66	0.016	-1.332	-3.947	0	-0.412	-	-	-
Carreau (2nd order)	Max	21.26	3.20	0	-0.011	-1.510	0	-2.7E-5	1.54	0.161
	Min	17.11	0.011	-0.728	-4.050	0	-0.0003	-4.2E-5	1.9E-5	0
C-C (1st order)	Max	20.02	1.51	0	-	-	-	-	-	-
	Min	15.96	0.005	-2.044	-	-	-	-	-	-
C-C (Interactions)	Max	16.05	4.95	0	-0.012	0.164	0	-	-	-
	Min	11.75	0.017	-1.516	-4.625	0	-0.385	-	-	-
C-C (2nd order)	Max	19.02	7.28	0	-0.015	1.510	0	-8.7E-5	-1.6E-5	0.012
	Min	14.73	0.025	-2.728	-5.581	0	-0.155	-1.4E-4	-1.28	0

T-C are not simple due to their interactions and the unique mathematical form of the temperature dependence, *1/(T-Tr)*. The relationships can be estimated by solving an equation obtained from the exponential function of *Eq. (5-6b)*. When the 1st order C-C model was applied, for instance, a temperature increase from 200°C to 210°C was equivalent to 1.35 wt% dissolution of CO_2 or a 13.3 MPa decrease of pressure. However, an increase from 260°C to 270°C was corresponding to 0.9 wt% dissolution of CO_2 or 8.7 MPa decrease of pressure.

5.6. CONCLUDING REMARKS

The viscosities of neat PS melts and PS/CO_2 solutions were measured using various rheometers and the measured data were interpreted as a function of temperature, pressure, concentration of CO_2 and shear rate. In order to model the shear thinning behavior of the viscosity, the Cross, Carreau and generalized Cross-Carreau viscosity models were used. As a case study, a PS/CO_2 system was studied while the CO_2 content was varied from 0 to 4 wt%. Careful attention was paid to maintain a single-phase polymer / CO_2 solution in the capillary die and the wedge die by ensuring the completion of polymer / gas solution formation before it entered the dies and by maintaining a high pressure at the downstream end of the dies. A generalized Arrhenius equation for describing the zero shear viscosity was proposed. The generalized C-C model gives the best description of the viscosity behavior of PS melts and PS/CO_2 solutions. By analyzing the sensitivity of each term using the generalized Arrhenius equation, the effects of individual parameters such as temperature, pressure, concentration of CO_2 and their interactions were elucidated. The 1st order terms of all parameters and the 2nd order term of pressure including the interaction terms had

significant effects on the zero shear viscosity under these experimental conditions. Quantitative comparisons between parameters were discussed by calculating the relative contribution of each term. Finally, the solubility of CO_2 in the PS melt was estimated based on understanding of the competing mechanisms of the hydraulic pressure effect and the plasticization effect of gas on the viscosity as the precipitation of CO_2 occurred in the capillary die attached to the microcellular extrusion system.

CHAPTER 6. EXTRUSION OF PE/PS BLENDS WITH SUPERCRITICAL CO_2 USING A TWIN-SCREW EXTRUDER

6.1. ABSTRACT

A twin-screw extruder was used for the extrusion of polyethylene / polystyrene blends in the presence of supercritical carbon dioxide. The effects of dissolved supercritical carbon dioxide on the viscosity and blend morphological properties were investigated. The viscosities of the blend / CO_2 solutions were measured using a wedge die mounted on the extruder. A considerable reduction of viscosity was found when CO_2 was dissolved in the blend. It was observed that the dissolution of CO_2 into PE/PS blends, regardless of the CO_2 content used, led to decreased shear thinning behavior resulting in an increase of the power law index from 0.29 to 0.34. The cell structure of foamed PE/PS blends showed a typical dependence on pressure and CO_2 concentration, with higher operating pressures and CO_2 content leading to a smaller cell size. Also, it was noted that the size of the dispersed PS phase in the PE/PS blends decreased by increasing the CO_2 concentration, and that the dispersed PS phase domains were highly elongated in the direction normal to the cell radius.

6.2. INTRODUCTION

It is well known that the final properties of polymer blends can be affected by many factors, such as the properties of each blend component, interfacial tension, blend morphology, and types of compatibilizers used. Therefore, whenever a polymer blend is designed, these factors should be given special consideration. The viscosity of each polymer blend component is one of the crucial parameters influencing the blend morphology. When two polymers are mixed with one another, the relationship between the size of the minor

phase and the viscosity ratio of the blend components can be qualitatively predicted by Taylor's formula (1932) which describes the domain size as a function of the interfacial tension, the shear rate, and the viscosity ratio. Heikens et al. (1978) investigated polyethylene / polystyrene (PE/PS) blends and showed that the size of the dispersed phase generally followed Taylor's formula. PE/PS binary blends have been studied since the early 1970s. These blends are of interest due to their immiscibility and the use of certain compatibilizers. Rheological behavior, morphology, crystallization behavior and the effect of compatibilizers on PE/PS blend properties have been published as summarized in Section 2.5.2. A review of these studies shows that the size of the dispersed phase was highly dependent on the processing conditions and generally varied from 2 to 20 μm when compatibilizers were not used.

Free volume is a very important concept that has been used extensively to explain certain rheological properties, such as the viscosity, of polymer melts, solutions, and blends. This concept has also been applied to polymer / gas mixtures in foaming processes. The viscosity reduction observed when a gas is dissolved in a polymer was described by Blyler and Kwei (1971) who introduced an analysis based on Doolittle's equation (1951) in order to describe the rheological behavior of a polyethylene / blowing agent system. Several other studies have examined the rheological properties of polymer / gas solution systems employing either chemical agents, or hydrofluorocarbons (CFC) as blowing agents, as reviewed in Section 2.4.2. Gerhardt et al. (1994) studied the viscosity behavior of polydimethylsiloxane (PDMS) / supercritical carbon dioxide solutions and Kwag et al. (1996) also reported on the viscosity behavior of PS/CO_2 systems. It was found that the

viscosity of PS could be reduced by two orders of magnitude with only 4.5 wt% of dissolved CO_2 at 150°C.

Supercritical fluids (SCFs) have also been used as blowing agents for foam products in polymer extrusion (Jacob and Dey, 1994, Dey et al., 1996, Park and Suh, 1996(a), Park et al., 1995, Baldwin et al., 1996a). Most chemical blowing agents such as azodicarbonamide (AZ) and dinitrosopenta-methylenetetramine (DNTP) leave some residues in the polymer phase. For example, AZ decomposes to 32% of gas and 68% of residue (Throne, 1996). The residues deteriorate the quality of the final foam products. CFCs, which are other popular blowing agents, are known to destroy the ozone layer and they have been replaced with other blowing agents such as HCFCs and inert gases. However, some polymer foams blown by HCFCs can be also deteriorated by the chemical attack of the blowing agents. In contrast, the SCF physical blowing agents such as carbon dioxide, are free from any criticisms on the destruction of the ozone layer and the chemical attack because of their inert nature.

Although the viscosity of a polymer can be dramatically changed by dissolving a SCF and although the viscosity of polymers is a crucial factor for polymer blends, it seems that no applications of SCFs to polymer blends have been published. Most studies dealing with polymer / SCF solutions have rather focused on the solubility of SCFs, the viscosity reduction of pure polymers and foaming applications.

In this chapter, the effect of supercritical CO_2 on the rheological behavior and on the morphology of PE/PS blends has been studied using a twin-screw extruder system. The viscosity of PE/PS blends has been measured at various CO_2 concentrations, and the effect of processing parameters on the size of the dispersed PS phase and cell structure have been investigated at various extrusion conditions and CO_2 concentrations.

6.3. EXPERIMENTAL

Complete dissolution of SCF in the PE/PS blend is critical before viscosity measurements are performed as pointed out in Chapter 5. It has been shown previously (Park et al., 1995, Lee et al., 1997) that by maintaining the melt pressure above the solubility limit results in the formation of a single phase PS/CO_2 solution in a single-screw extruder. This was accomplished by assessing the effect of pressure on viscosity and on cell nuclei density for PS/CO_2 foams. Based on similar measurements, it is believed that a single phase system (blend / CO_2) is achieved in this work due to the superior mixing performance of the twin-screw extruder and the high pressures used.

In order to dissolve CO_2 in the blend in a twin-screw extruder, an optimum screw configuration was determined based on several design concepts:

(a) At the injection point of CO_2, pressure fluctuations inside the barrel should be minimized for a stable injection. Use of conveying screw elements is recommended rather than that of kneading discs.

(b) Injected CO_2 should be prevented from leaking upstream. This is achieved by a melt seal which can be generated using a reverse conveying screw element.

(c) The pressure downstream of the CO_2 injection point should be maintained sufficiently high above the solubility pressure, to ensure that CO_2 remains dissolved in the polymer phase. For that purpose, the barrel pressure can be manipulated through the die resistance.

(d) Although the mixing capability of a twin-screw extruder is much higher than that of a single-screw extruder, an array of kneading discs was used to ensure complete dissolution of CO_2.

In order to measure the viscosity of the flowing polymer / SCF solution, a converging wedge die with three pressure transducers was used to allow for viscosity measurements at various shear rates for a given flow rate. Conventional slit dies and capillary dies by comparison, measure the viscosity at a fixed shear rate determined by the flow rate of the polymer melt. The pressure in the wedge die was controlled by varying the opening area/resistance of a secondary die attached downstream.

6.3.1. Equipment and Materials

The extruder used in this study is a Leistritz LSM 30.34, intermeshing and co-rotating twin-screw machine having a 34 mm screw diameter. Polymers were fed by a K-tron feeder (LWFD 5-200), and CO_2 was injected into the extruder through an injection port on the barrel using a syringe pump. The pressure at the barrel injection port was monitored by a pressure transducer (Dynisco PT462-5M-6/18), and three other transducers (one Dynisco PT462-7.5M-6/18, two Dynisco PT462-5M-6/18) were installed in the wedge die for pressure measurements. The temperature of the blend/CO_2 solutions was measured using a fiber optic melt temperature transducer (Dynisco MTS 922-6/24) at the end of the wedge die.

In this study, Nova Chemicals 101C PS and Nova Chemicals LF0219A LDPE were used at a blend ratio of LDPE/PS 80/20. Material data were listed in Chapter 3. CO_2 was supplied by Air Products with 99.997% purity. The polymer feed rate was varied from 50 to 100 g/min, and a relatively low screw speed of 50 rpm was used in order to minimize the heat generation in the barrel. The solution temperature in the wedge die was maintained between 193°C and 196°C, and the content of CO_2 in the polymer was controlled below 5% by weight. A schematic diagram of the entire extrusion system is shown in *Figure 6.1*. The screw configuration shown in *Figure 3.12* was used in this chapter.

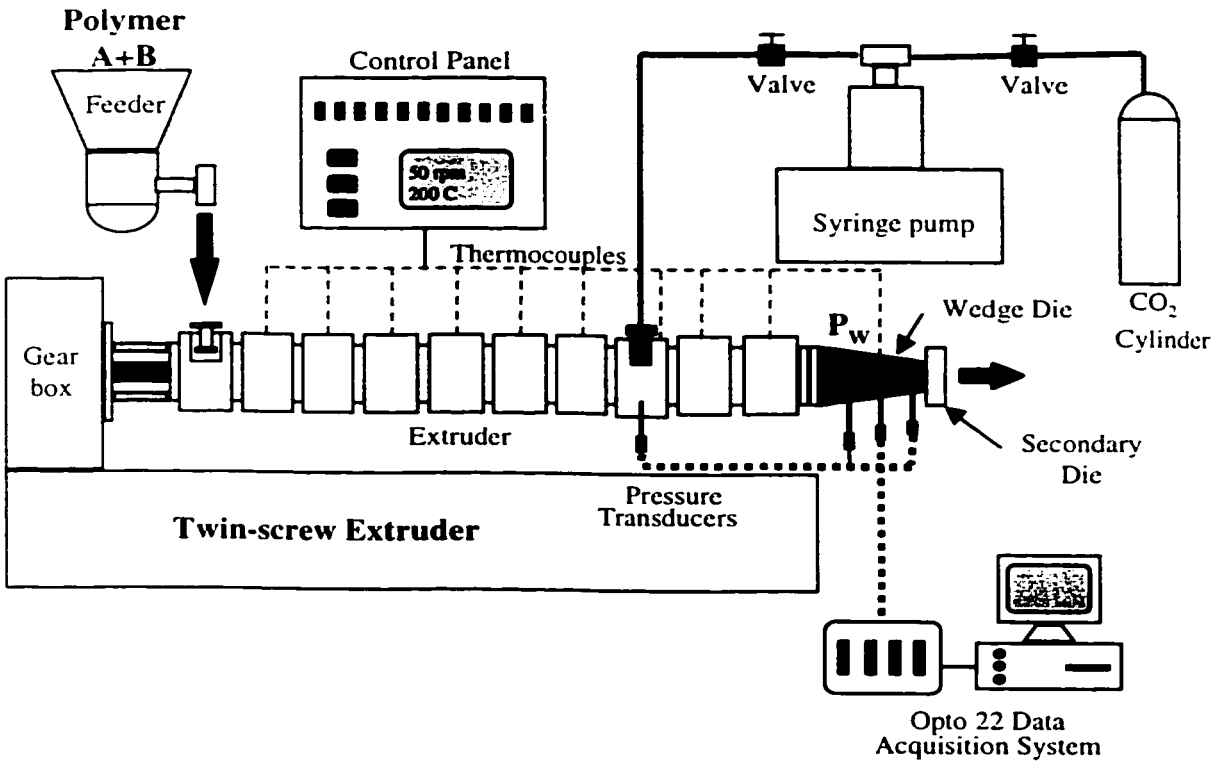

Figure 6.1. Schematic diagram of the twin-screw extrusion system

6.3.2. Procedures

First, a metered amount of CO_2 is injected into the polymer melt in the extruder barrel using the syringe pump. The injected gas amount is controlled at a level less than the solubility limit at the processing temperature and pressure. The polymer feed rate is controlled by the feeder, and the two polymers are blended by tumbling before loading into the feeder. The injected CO_2 bubbles are well mixed with and dissolved in the polymer melt blend while they flow downstream through a set of screw and kneading disc elements. The barrel pressure at the injection point is monitored for a stable injection of CO_2. The blend / CO_2 solution formed flows into a wedge die equipped with three pressure transducers and a temperature sensor. All signals from the die are monitored through an Opto 22 data acquisition system. The pressure in the wedge die is controlled by a secondary die attached downstream. The secondary die is specially designed to easily control the flow resistance by changing its opening area. Finally, the extruded foamed filament is cooled in a water bath and sampled for investigating the cell structure and the blend morphology. In order to investigate the cell structure and the morphology of the dispersed PS phase, a scanning electron microscope (SEM, JEOL JSM-840) was used. All foamed filaments were fractured in liquid nitrogen and coated with gold for the SEM analysis.

6.4. RESULTS AND DISCUSSION

6.4.1. Wedge Die Calculation

Converging dies have been used extensively in polymer melt extrusion and the principles of converging flows have also been applied to the design of rheometers for on-line viscosity measurements. Converging conical and wedge dies are capable of measuring the

viscosity at various shear rates, for a fixed polymer flow rate. By comparison, slit and linear capillary dies, measure the viscosity at fixed shear rates determined by the polymer flow rate. Flow analysis calculations for converging flows have been reported in the literature (Section 2.4.3.2). Cogswell (1972) analyzed the flow in terms of the extensional and simple shear flow components while Lenk (1978, 1979, 1981) introduced several simplifying assumptions when the converging angle was small and equations for pressure drop calculation through conical and wedge dies were derived for a power law fluid. Pabedinskas (1992) used this simple method to measure on-line the viscosity of controlled-rheology degraded polypropylenes.

In this section, the pressure drop of a Carreau fluid and the temperature increase of a power-law fluid through a wedge die were investigated. If the experimental shear rate is low and the flow behavior deviates from the power-law region, the pressure drop for a power-law fluid derived by Lenk (1978, 1979, 1981) can not be used. In addition, if the temperature increase due to the viscous heating through the wedge die is significant, the non-isothermal effect should be considered in the viscosity calculation. Therefore, these two cases are tested in this section.

6.4.1.1. Pressure Drop of a Carreau Fluid

The pressure drop of a Carreau fluid was derived during the flow through the wedge die shown in *Figure 6.2*. The viscosity of the Carreau fluid is

$$\eta = \eta_0 \left[1 + (\lambda\dot{\gamma})^2\right]^{\frac{n-1}{2}} \tag{6-1}$$

where η_0 is the zero-shear viscosity, λ is the characteristic relaxation time, and n is the power-law index. The analytical equations for the pressure drop, P_0-P_1, are shown in *Eqs. (6-2)* and *(6-3)*. The detailed derivation procedures are shown in Appendix III.

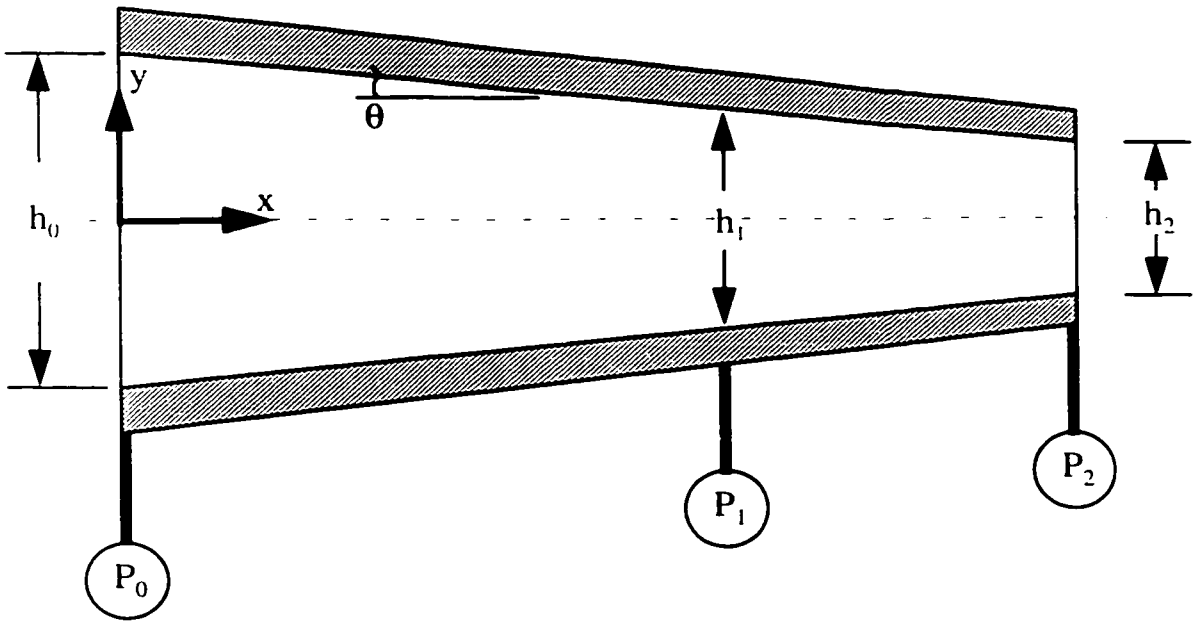

Figure 6.2. Schematic diagram of wedge die having a constant width, *W*.

Case 1 (when $\left(\frac{6Q\lambda}{wh_1^2}\right)\left(\frac{2n+1}{3n}\right)<1$):

$$-\Delta P=\frac{6\eta_0 Q}{\tan\theta}\left(\frac{2n+1}{3n}\right)\left[\frac{1}{w^2}\left(\frac{1}{h_1}-\frac{1}{h_0}\right)+\frac{1}{2w}\left(\frac{1}{h_1^2}-\frac{1}{h_0^2}\right)\right]+\frac{6\eta_0 Q}{\tan\theta}\left(\frac{2n+1}{3n}\right)$$
$$\left\{\sum_{k=1}^{\infty}\left(\prod_{s=1}^{k}\frac{2s-1-n}{2}\right)\frac{(-1)^k}{k!}\left(\frac{6Q\lambda}{w}\right)^{2k}\left(\frac{2n+1}{3n}\right)^{2k}\right. \tag{6-2}$$
$$\left.\left[\frac{1}{w^2}\left(\frac{1}{4k+1}\right)\left(\frac{1}{h_1^{4k+1}}-\frac{1}{h_0^{4k+1}}\right)+\frac{1}{2w}\left(\frac{1}{4k+2}\right)\left(\frac{1}{h_1^{4k+2}}-\frac{1}{h_0^{4k+2}}\right)\right]\right\}$$

Case 2 (when $\left(\frac{6Q\lambda}{wh_1^2}\right)\left(\frac{2n+1}{3n}\right)>1$):

$$-\Delta P=\frac{6\eta_0 Q}{\tan\theta}\left(\frac{2n+1}{3n}\right)^n\left(\frac{6Q\lambda}{w}\right)^{n-1}\left[\frac{1}{w^2}\left(\frac{1}{2n-1}\right)\left(\frac{1}{h_1^{2n-1}}-\frac{1}{h_0^{2n-1}}\right)+\frac{1}{w}\left(\frac{1}{2n}\right)\left(\frac{1}{h_1^{2n}}-\frac{1}{h_0^{2n}}\right)\right]$$
$$+\frac{6\eta_0 Q}{\tan\theta}\left(\frac{2n+1}{3n}\right)\left\{\sum_{k=1}^{\infty}\left(\prod_{s=1}^{k}\frac{n-2s+1}{2}\right)\frac{1}{k!}\left(\frac{6Q\lambda}{w}\right)^{n-2k-1}\left(\frac{2n+1}{3n}\right)^{n-2k-1}\right.$$
$$\left.\left[\frac{1}{w^2}\left(\frac{1}{2n-4k-1}\right)\left(\frac{1}{h_1^{2n-4k+1}}-\frac{1}{h_0^{2n-4k+1}}\right)+\frac{1}{w}\left(\frac{1}{2n-4k}\right)\left(\frac{1}{h_1^{2n-4k}}-\frac{1}{h_0^{2n-4k}}\right)\right]\right\} \tag{6-3}$$

where Q denotes the volumetric flow rate of a polymer or polymer / CO_2 solution, n is the power law index, K is the consistency index, and h_0 and h_1 are the heights at the die entrance and exit, respectively. As shown in *Eqs. (6-2)* and *(6-3)* the governing equations are divided into two cases by the value of $\left(\frac{6Q\lambda}{wh_1^2}\right)\left(\frac{2n+1}{3n}\right)$ in order to integrate the binomial series function.

Using material data such as n, η_0, λ, and the die dimension, the pressure drops along the wedge die can be calculated for the Carreau fluid. By increasing λ value, *Eq. (6-1)*

reduces to the power-law model. The calculated pressure drops of the Carreau and the power-law fluids are shown in *Figure 6.3*. n=0.264, K=21130 Pa-s^n, η_0=5010 Pa-s, and λ=0.1798 s were used as material data for polystyrene. It should be noted that the Carreau model prediction was obtained by the expansion up to the 4th term. *Figure 6.3* indicates that the pressure drop predicted by the Carreau model is less than that of the power-law model at low shear rates, while the two pressure drops are similar in high shear rate. This means that the predicted viscosity of PS using the Carreau model will be lower than that using the power-law model.

It should be noted that the pressure drop estimated by the Carreau model in the wedge die, diverges near the shear rate of $\left(\frac{6Q\lambda}{wh_1^2}\right)\left(\frac{2n+1}{3n}\right)=1$. The governing equations of the pressure drop, *Eqs. (6-2)* and *(6-3)*, diverge to $+\infty$ or $-\infty$ when the degree of the expansion, k, is an even or odd number, respectively. There is a shear rate range in which the viscosity cannot be estimated by measuring the pressure drop. This is defined as "the dead shear rate zone" in this study. The range of the dead shear rate zone is a function of the time constant, λ, and the volumetric flow rate, Q. The sensitivity of the dead shear rate zone was investigated by changing the time constant, and the results are shown in *Figure 6.4*. It should be noted, by definition, that the increase of the time constant results in the decrease of the onset shear rate showing the shear-thinning behavior. By increasing the time constant of a polymer, the range of the dead shear rate moves to lower shear rate. Thus, the dead shear rate zone is related to the onset shear rate showing the shear-thinning behavior.

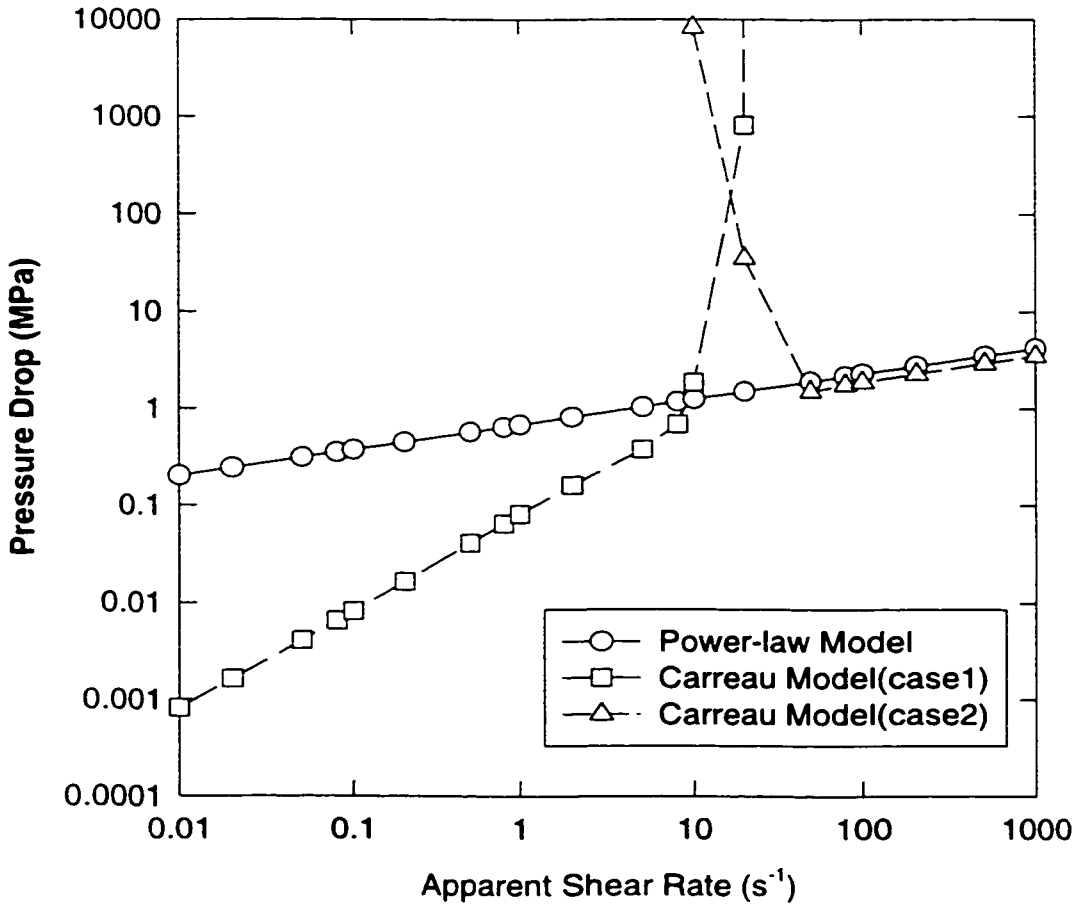

Figure 6.3. Comparison of the predicted pressure drops for polystyrene using Carreau and power-law models

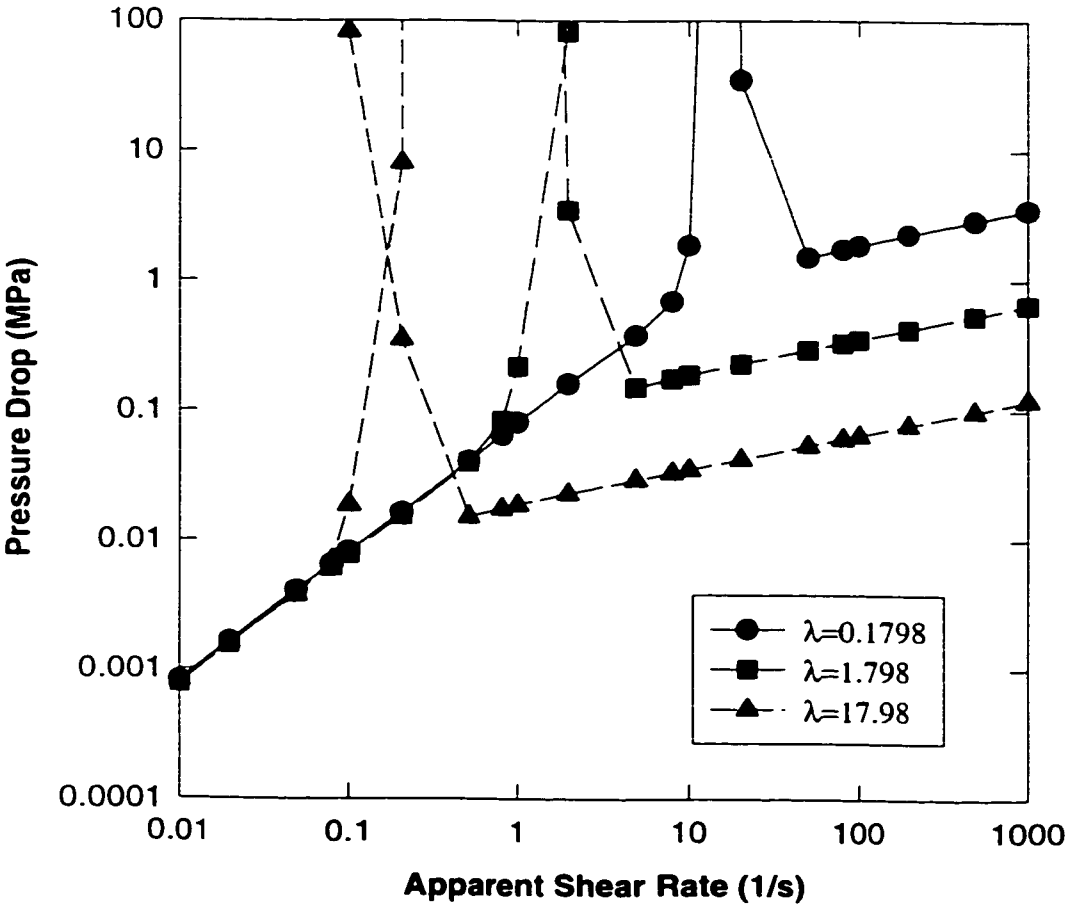

Figure 6.4. Behaviors of the dead shear rate at various time constants

In this chapter, all viscosity measurements were performed at the shear rates showing the power-law behavior. The Rabinowitsch-corrected pressure equation of the power-law fluid in the wedge die is

$$\Delta P = \frac{K}{\tan\theta}\left(\frac{6Q}{W}\frac{2n+1}{3n}\right)^n\left[\frac{1}{2n}\left(\frac{1}{h_2^{2n}}-\frac{1}{h_0^{2n}}\right)+\frac{1}{W(2n-1)}\left(\frac{1}{h_2^{2n-1}}-\frac{1}{h_0^{2n-1}}\right)\right] \tag{6-4}$$

By measuring three pressures, P_0, P_1, and P_2, two pressure drops, $\Delta P_{0\text{-}1}$ and $\Delta P_{1\text{-}2}$, are determined. Then, the pressure drop ratio between the two sections is

$$\frac{\Delta P_{0-1}}{\Delta P_{1-2}} = \frac{\left(\frac{6Q_{0-1}}{W}\frac{2n+1}{3n}\right)^n\left[\frac{1}{2n}\left(\frac{1}{h_1^{2n}}-\frac{1}{h_0^{2n}}\right)+\frac{1}{W(2n-1)}\left(\frac{1}{h_1^{2n-1}}-\frac{1}{h_0^{2n-1}}\right)\right]}{\left(\frac{6Q_{1-2}}{W}\frac{2n+1}{3n}\right)^n\left[\frac{1}{2n}\left(\frac{1}{h_2^{2n}}-\frac{1}{h_1^{2n}}\right)+\frac{1}{W(2n-1)}\left(\frac{1}{h_2^{2n-1}}-\frac{1}{h_1^{2n-1}}\right)\right]} \tag{6-5}$$

where $\Delta P_{0\text{-}1}$ and $\Delta P_{1\text{-}2}$ are pressure drops and $Q_{0\text{-}1}$ and $Q_{1\text{-}2}$ are volumetric flow rates upstream and downstream of point 1 in the wedge die, respectively. *Eq. (6-5)* is only function of the volumetric flow rates and the power law index.

The volumetric flow rates can be calculated from the mass flow rate and the density of the blend / CO_2 solution. The density may be considered constant for pure polymer melts, however, the density variation of the polymer / gas solution with pressure is higher than that of a pure polymer. The solution density estimated from S-L EOS theory was used in this chapter. The detail procedures for the density estimation were explained in Chapter 4. The interaction parameter between each polymer and CO_2 was assumed to have a constant value of 0.01 because the dependence of solution density on the interaction parameter is very small. As indicated in Section 4.4.3 and *Figure 4.6*, the solution density of PS/CO_2 solution does not change significantly specially when the CO_2 concentration is low.

By determining the volumetric flow rates using solution density and mass flow rate, the power law index, n, can be calculated from *Eq. (6-5)* and then the consistency index, K, can be obtained from *Eq. (6-4)*. Finally, the Rabinowitsch-corrected solution viscosity is

$$\eta = K\left(\frac{2n+1}{3n}\right)^{n-1}\left(\frac{6Q}{Wh^2}\right)^{n-1} \tag{6-6}$$

6.4.1.2. Temperature Increase in the Wedge Die

The effect of viscous dissipation on the polymer temperature in the wedge die was investigated. An equation for the temperature difference between the die entrance and the die exit was derived, and the derivation procedures are also shown in Appendix III. The power-law model was used for the derivation because the viscous dissipation is usually small at low shear rates and the experimental measurement of the viscosity was performed up to the shear rate of 1000 s^{-1}. The wall of the wedge die was assumed as an adiabatic wall. The equation for the temperature difference, $(\Delta T)_{bulk}$, is

$$(\Delta T)_{bulk} = \frac{1}{2n\tan\theta}\left(\frac{1}{3^n}\right)\left(\frac{K}{\rho c_p}\right)\left(\frac{2n+1}{n}\right)^n\left(\frac{6Q}{wh_1^2}\right)^n\left[1-\left(\frac{h_1}{h_0}\right)^{2n}\right] \tag{6-7}$$

where K is the consistency index of the power-law model, ρ is the density, and c_p is the specific heat of polymer melt. *Eq. (6-7)* indicates that the temperature increase is proportional to the n power of apparent shear rate at the die exit. The estimated temperature increases between 1st and 3rd pressure transducers of the wedge die are shown in *Figure 6.5*. The temperature increases for both polymers are below 1°C up to 1000 s^{-1} of shear rate. Therefore, the viscous dissipation effect on the viscosity was ignored in this chapter.

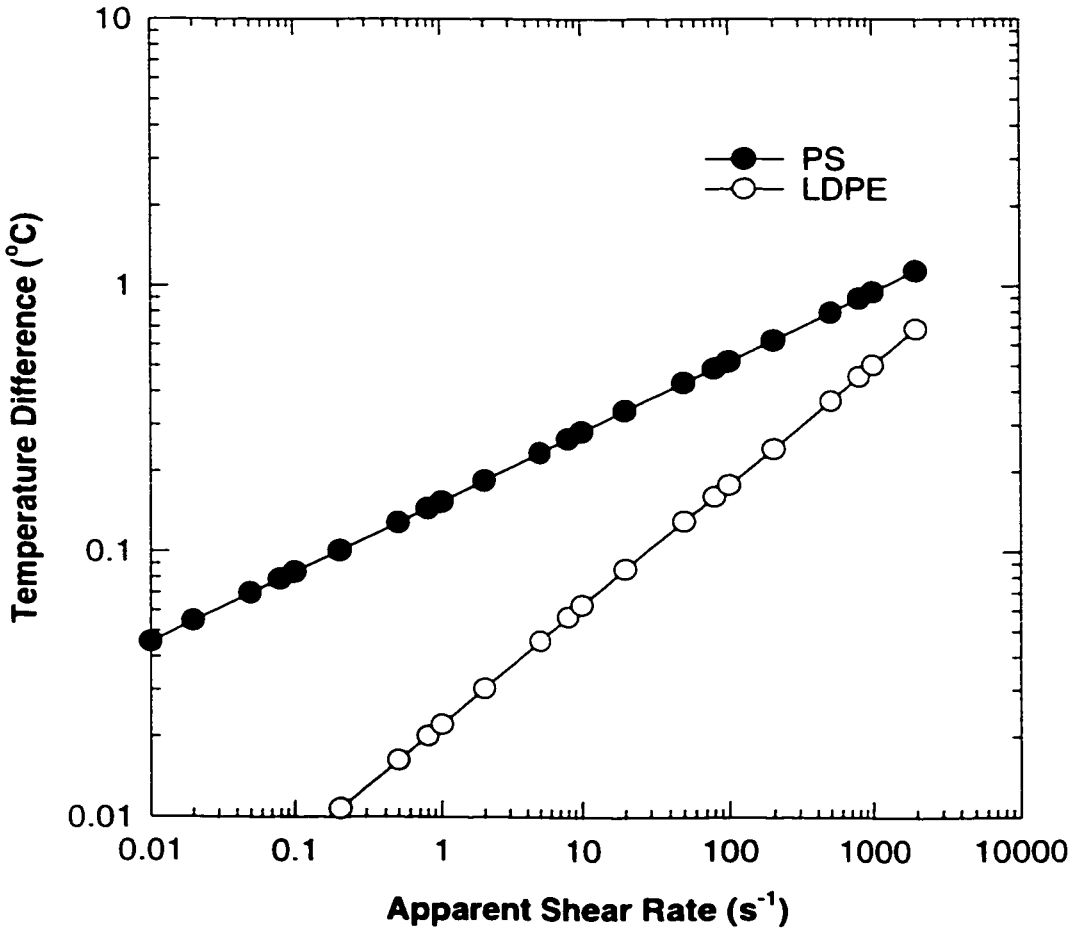

Figure 6.5. Prediction of the temperature increases due to the viscous dissipation in a wedge die

6.4.1.3. Sensitivity of Viscosity on the Polymer Density

The sensitivity of the viscosity variation to the density was demonstrated. Although the S-L EOS gives an accurate estimated density values for PDMS/CO_2 system (Garg et al., 1994), a certain level of error might be involved in the density prediction for PE/PS/CO_2 systems. Therefore, a sensitivity study was carried out by changing the density values. Density values predicted by the S-L EOS were varied by ± 5% and the result is shown in *Figure 6.6*. It was found that the calculated power-law index was unaffected while the consistency index was slightly increased (less than 5%). However, such variations in density would require pressure fluctuations in the order of 500 atm. Since such pressure fluctuations are not encountered in our experiments, it is believed that the effect of the estimated density value on the viscosity calculation is not significant.

6.4.2. Viscosity of (PE/PS) Blend / CO_2 Solutions

The viscosity of PE/PS blends containing CO_2 was measured using the wedge die shown earlier. The CO_2 content was varied from 0 to 5 wt%. The viscosities of a PE/PS blend and several PE/PS/CO_2 solutions measured at various shear rates are shown in *Figure 6.7*. A reduction in the viscosity was observed for PE/PS/CO_2 solutions compared to the pure PE/PS blend. In general, the PE/PS/CO_2 viscosity tended to decrease as the CO_2 content increased. All viscosity data in *Figure 6.7* are Rabinowitsch-corrected values, and they are normalized to 195°C using the temperature shift factor as suggested by Rauwendaal (1990). Also, the mean pressure for each curve was controlled in the range of 19.2 ± 0.3 MPa in order to eliminate the effect of pressure on the viscosity.

It can be seen that typical shear thinning behaviors were observed for the PE/PS/CO_2 solutions as well as for the PE/PS blend. It should be noted, however, that the shear-thinning

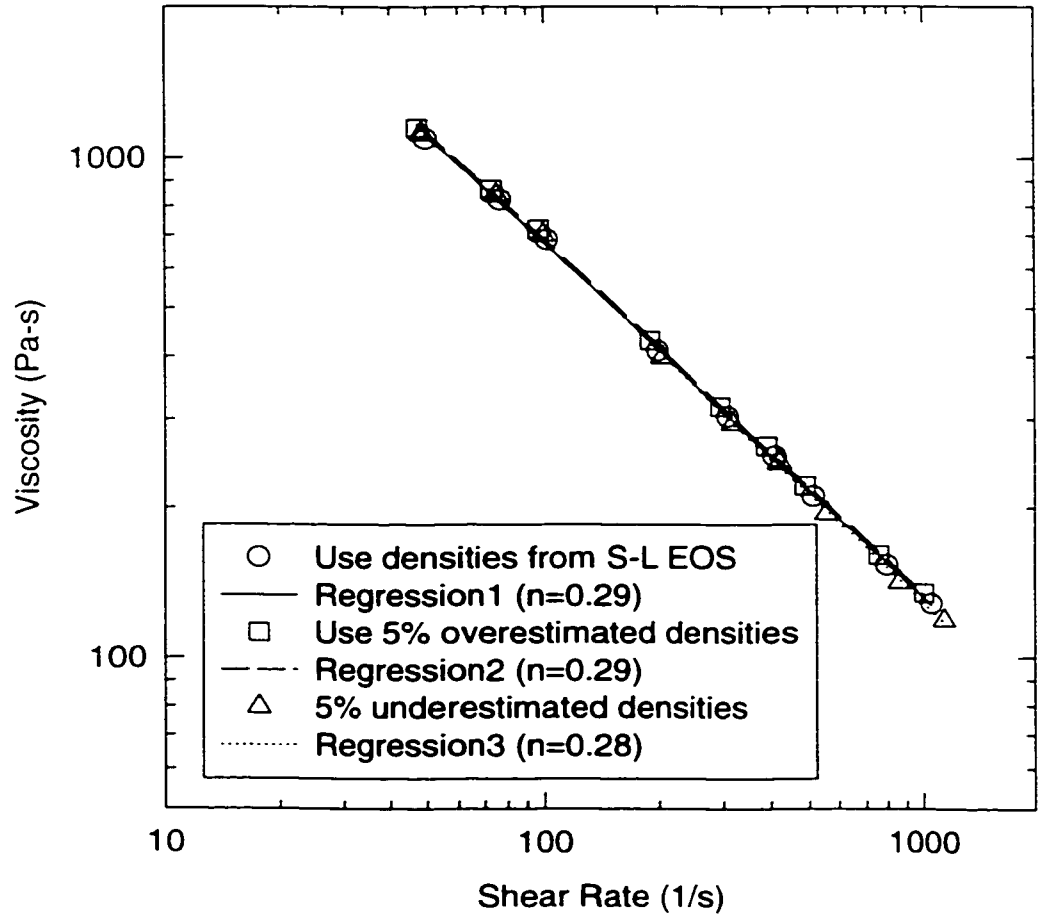

Figure 6.6. Sensitivity of the polymer density on the viscosity

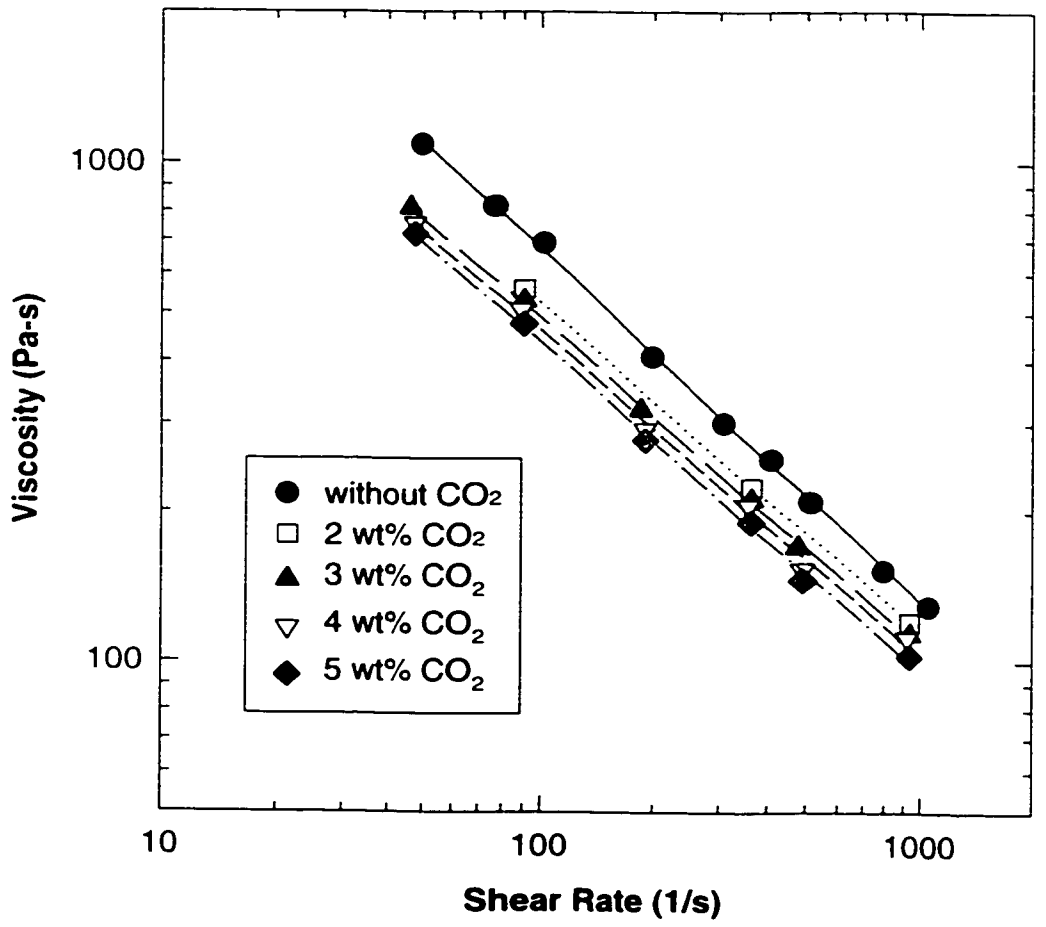

Figure 6.7. Rabinowitsch-corrected viscosity of PE/PS/CO_2 solutions, at 195°C.

behavior of PE/PS/CO_2 solutions is less than that of the pure PE/PS blend. In order to investigate the shear-thinning behavior, the power law index values were computed and they are plotted in *Figure 6.8*. It is observed that dissolution of CO_2 into the PE/PS blend, results in an increase of the power law index. However, it seems that the CO_2 content does not significantly affect the power law index value (about 0.34) for PE/PS/CO_2 blends. Bigg et al. (1976) have reported that the power law index decreased from 0.33 to 0.27 after compounding with a blowing agent in their PS system. However, it is ambiguous whether their polymer / blowing agent mixture was a single phase or not. The increase of the power law index value observed in ***Figure 6.8*** may be explained in terms of the temperature and free volume effects on viscosity. It is well known that the power law index increases with increasing temperature for most polymers (Bird et al., 1987). However, a temperature increase means an increase of the free volume of the polymer. A free volume increase, which reduces the glass transition temperature, can also be achieved by the dissolution of a gas into a polymer (Beckman and Porter, 1987, Wissinger and Paulaitis, 1987, Gendron et al., 1996). Therefore, the temperature increase and the dissolution of a gas into a polymer have an equivalent effect on viscosity and shear thinning behavior, which explains the data in *Figure 6.8*.

6.4.3. Morphology of PE/PS Blends

Upon exiting the die, the extruded polymer / gas solutions were found to foam. The cell morphology of the foamed extrudate filaments of PE/PS blends was investigated by SEM. It is well known that the operating pressure affects the cell size in foaming processes (Park and Suh, 1996a, Throne, 1996). It is also known that the cell density and size depend on the content of the dissolved blowing agent with the cell density (cells/cm^3) increasing with

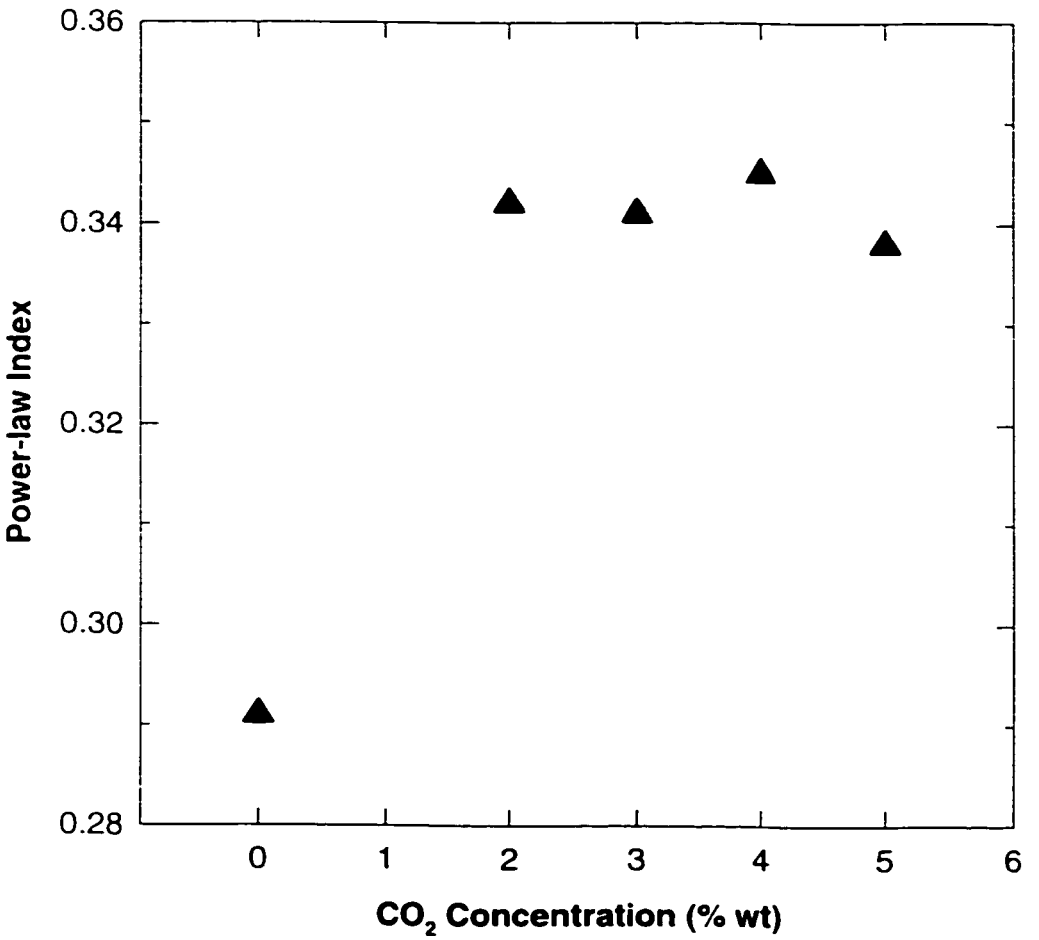

Figure 6.8. Effect of CO_2 concentration on the power-law index of PE/PS/CO_2 blends.

an increase in the gas content (Park et al., 1994). On the other hand, since the average cell size decreases as the cell density increases, the cell size decreases with an increase in the gas content (Park et al., 1995, Throne, 1996). As shown in *Figure 6.9*, these behaviors were observed for the PE/PS blend systems. The first three micrographs in *Figure 6.9* show how the cell size changes with the mean pressure in the wedge die. The cell size is dramatically reduced by increasing the die pressure at a constant concentration of CO_2 (3 wt%). The last three micrographs in *Figure 6.9* show that the cell size decreases with an increase in the CO_2 content at a constant die pressure (19.2 MPa). In order to determine the cell size and the distribution behavior, the foamed sample collected at 5 wt% of CO_2 and 19.2, *Figure 6.9(f)*, was investigated using an image analyzer (Optimas 5.1, Optimas Corporation) and the result is shown in *Figure 6.10*. The foamed sample was microtomed at -30°C for SEM observation, and several SEM images having different magnifications were taken for the quantitative analysis. As indicated in *Figure 6.10*, the mean cell diameter (number average) is 10.7 μm, which indicates the microcellular structure.

The blending morphology was also investigated for the PE/PS and PE/PS/CO_2 filaments. The size of the dispersed PS phase is compared at various CO_2 contents in *Figure 6.11*. The fracture surfaces are perpendicular to the flow direction, and correspond to the area between cells as schematically shown in *Figure 6.11(a)*. As explained before, the domain size of the PS phase in a PE matrix has been reported to vary from 2 to 20 μm when no compatibilizers are used. In this experiment, the dispersed PS phase has a size of 2-10 μm when the blend was prepared without the injection of CO_2 as shown in *Figure 6.11(b)*. However, when CO_2 was used, the size of the dispersed PS phase was reduced dramatically as shown in *Figure 6.11(c)* and *(d)*: the number average diameter of the dispersed PS phase is

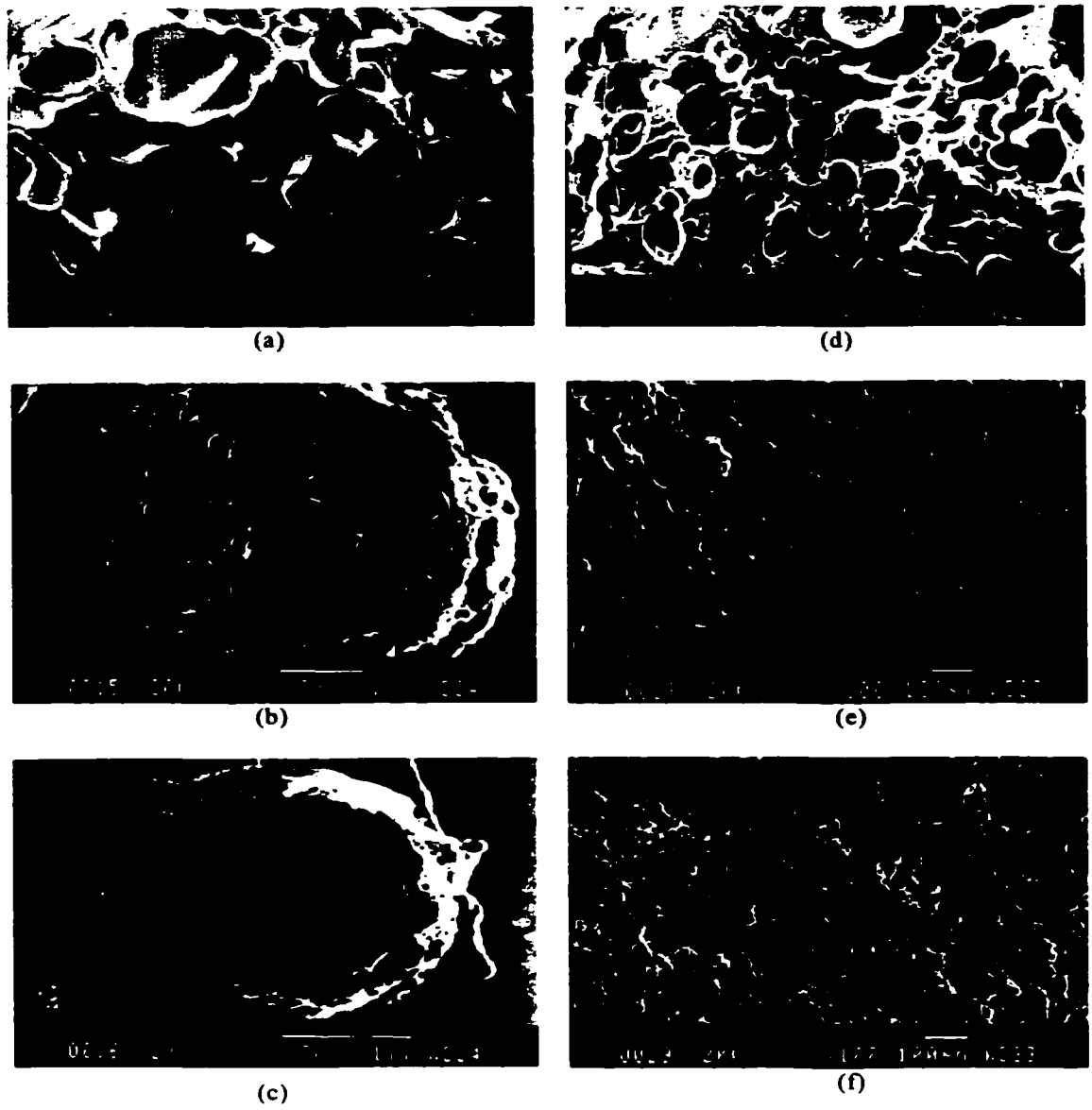

Figure 6.9. SEM photographs of PE/PS blends at:
- constant CO_2 content (3 wt% CO_2): (a) 15.2 MPa (b) 18.9 MPa (c) 22.1 MPa,
- constant die pressure (19.2 MPa): (d) 3 wt% CO_2 (e) 4 wt% CO_2 (f) 5 wt% CO_2

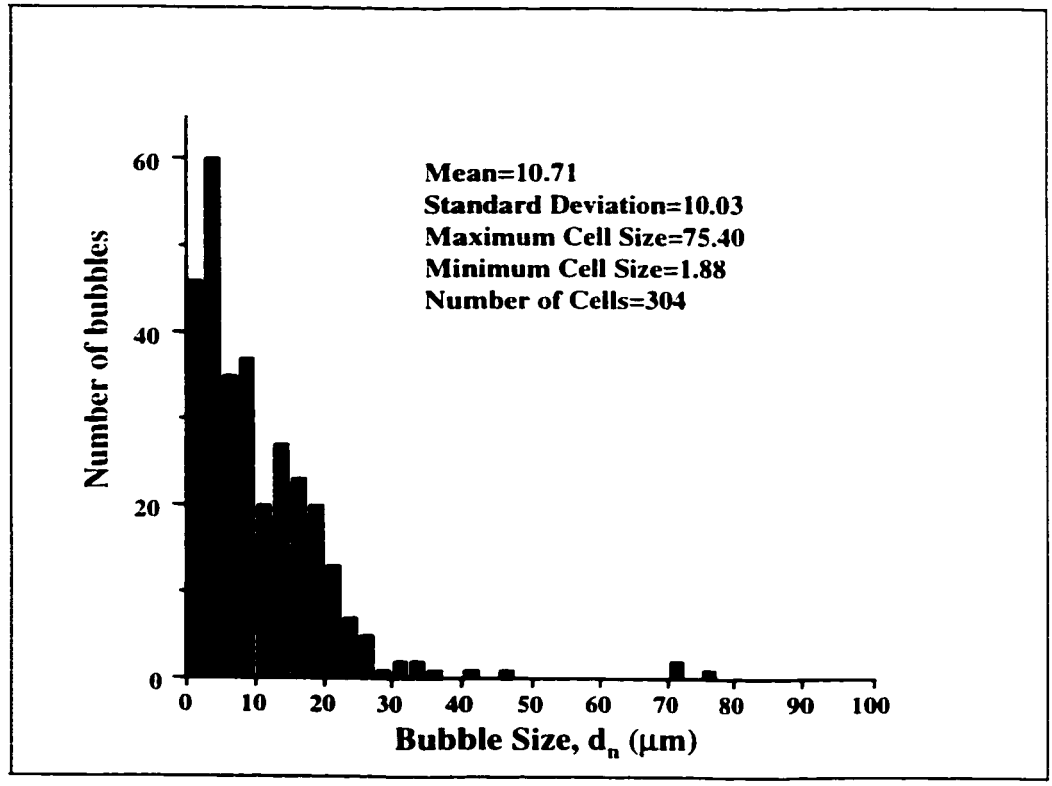

Figure 6.10. Cell size distribution of a foamed PE/PS=80/20 blend (5 wt% of CO_2 and 19.2 MPa)

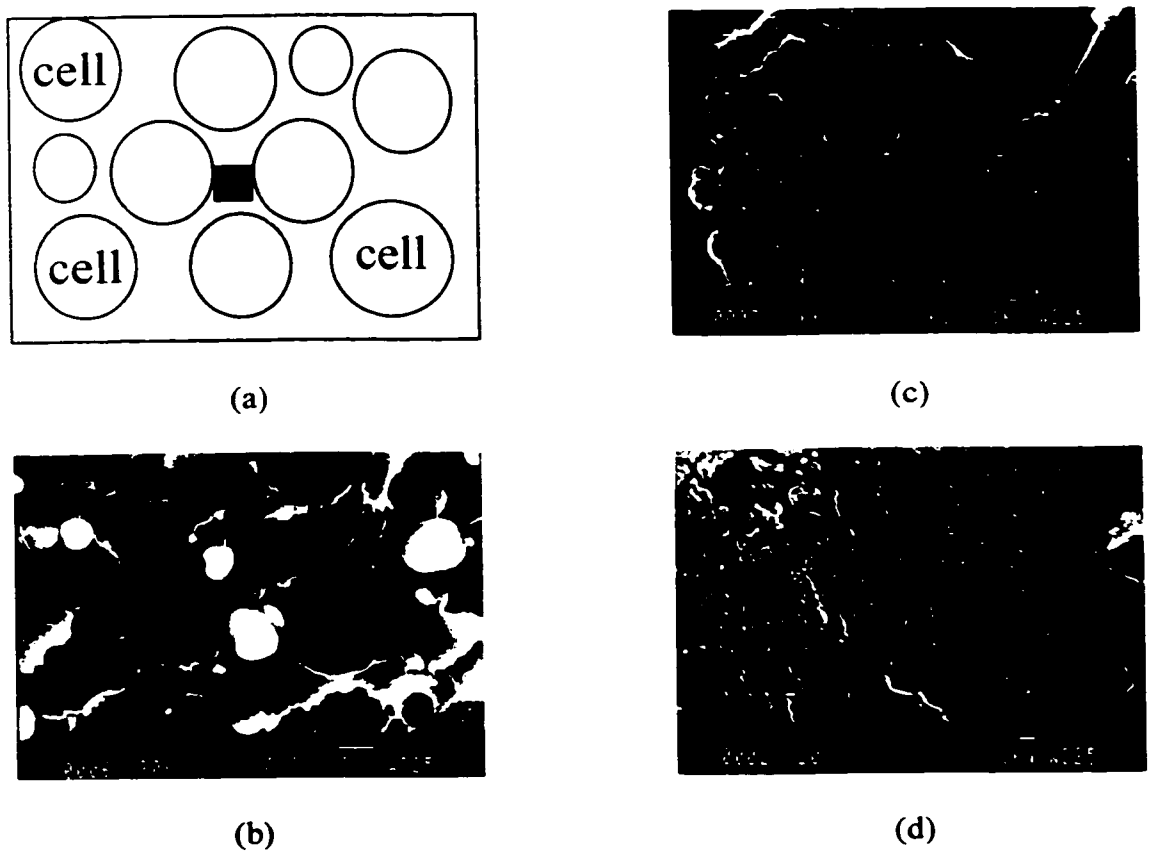

Figure 6.11. SEM photographs of the PE/PS blends at various contents of CO_2 (19.2 MPa) (a) Schematic diagram of fracture surface. Photographs b, c, d correspond to black square. (b) 0 wt% CO_2 (c) 3 wt% CO_2 (d) 5 wt% CO_2

0.78 μm when 5 wt% of CO_2 was dissolved in the blend . The size reduction of the dispersed PS phase was also observed on the cryo-microtomed surface as shown in *Figure 6.12* (SEM photographs in *Figure 6.12* were taken at Institut fur Polymerforschung Dresden e. V., Germany). In *Figure 6.11*, it should be noted that the fracture surfaces of the PE/PS/CO_2 blends were quite flat when they were compared to the PE/PS blend. This fracture characteristic implies that the crack penetrated the dispersed PS phase instead of the interface between PE and PS. This could be attributed to extensive elongation of the dispersed PS domains in the flow direction and subsequent extensive increase of interfacial area. In order to test this assumption of the elongated morphology, fracture surfaces parallel to the flow direction were prepared as shown in *Figure 6.13(a)*. An interesting morphology was observed for the PE/PS/CO_2 blends. While the PS domain in the PE/PS blend maintained a spherical shape (*Figure 6.13(b)*) as in the fracture surfaces reported in *Figure 6.11*, the PS domains in the PE/PS/CO_2 were highly elongated as shown in *Figure 6.13(c)*. PS domains were found to elongate between the CO_2 cells. This seemed to suggest that the size reduction of the PS domain might be due to the compression between the cells. Finally, it was observed that although the die pressure affected the cell size, it did not affect the size of the dispersed PS domains.

6.5. CONCLUDING REMARKS

The effects of dissolved supercritical CO_2 on the rheological and morphological properties were investigated for PE/PS blends in a twin-screw extruder. A considerable reduction in the viscosity was observed for PE/PS/CO_2 solutions, and the power-law index was found to increase when CO_2 was used in the blends. The cell structure of foamed

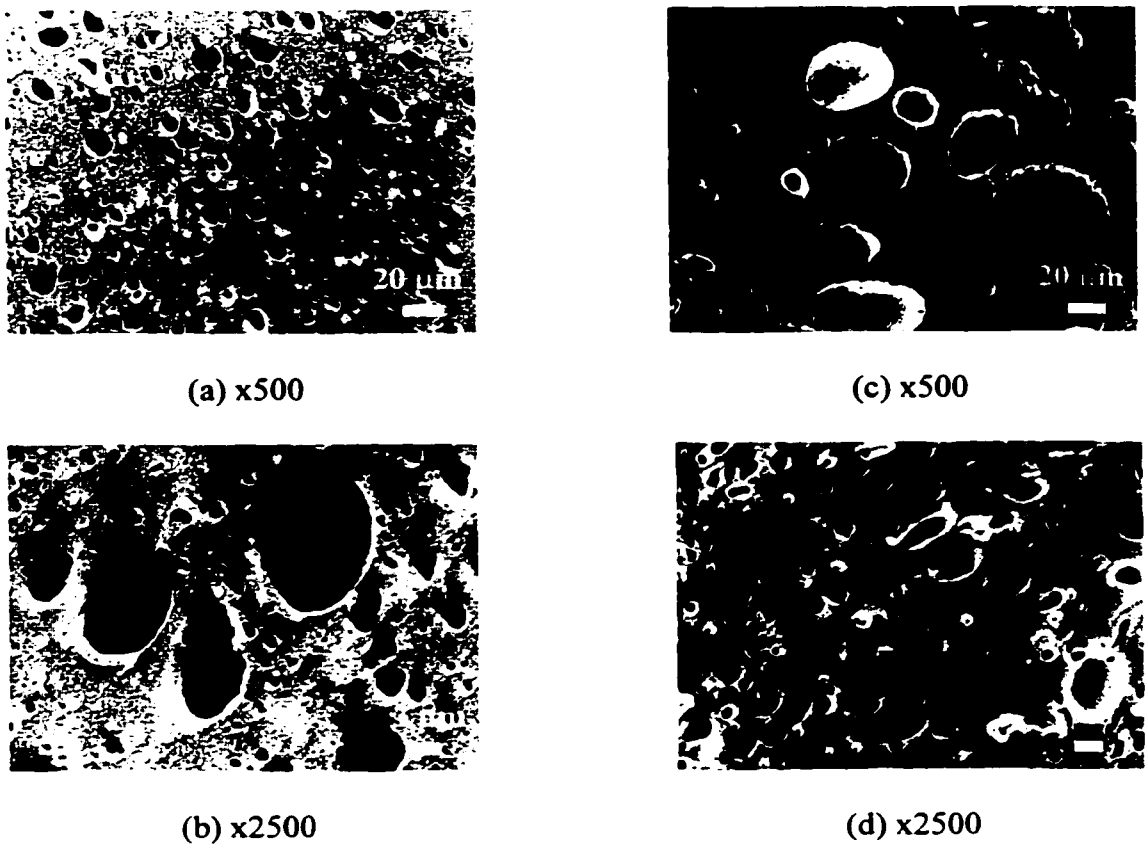

(a) x500 (c) x500

(b) x2500 (d) x2500

Figure 6.12. SEM photographs of the cryo-microtomed and etched PE/PS blend (a) and (b):without CO_2, (c) and (d): 5 wt% of CO_2

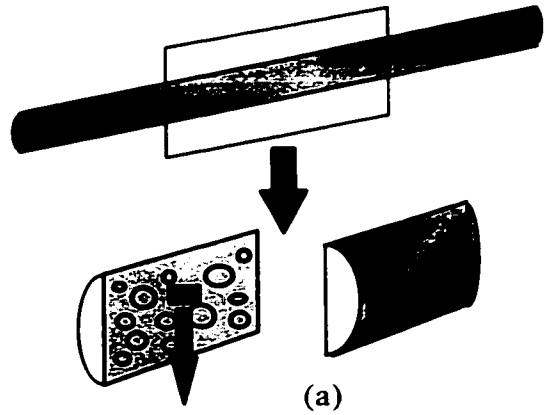

(a)

(a)

(b)

(c)

Figure 6.13. SEM photographs of the PE/PS blends fractured parallel to the flow direction (19.2 MPa)
(a) Schematic diagram showing the fracture surface (b) 0 wt% CO_2 (c) 3 wt% CO_2

filaments was observed at various contents of CO_2 and pressures. The cell structure of the PE/PS blends showed the same behavior observed for pure polymers. Higher operating pressures and CO_2 content led to smaller cell size and it was found that CO_2 cells produced elongated cylindrical PS domains. The size and shape of the dispersed PS phase were also investigated, and while the size of these PS domains decreased by increasing the CO_2 content, it was not affected by the operating die pressure.

CHAPTER 7. EXTRUSION OF PE/PS BLENDS WITH SUPERCRITICAL CO_2 USING TANDEM EXTRUSION SYSTEMS

7.1. ABSTRACT

Various extruder configurations including twin/single tandem extrusion system were designed for investigating the effects of dissolved supercritical carbon dioxide on the viscosity and morphological properties of polyethylene, polystyrene and their blends. The viscosities of the polymer / CO_2 and the blend / CO_2 solutions were measured at various concentrations of CO_2 and PE/PS blending ratios using a wedge die mounted on the twin-screw extruder. The effect of CO_2 on the morphology of PE/PS blends was also investigated using a twin/single screw tandem system. This system allowed for preferential dissolution of the CO_2 into the matrix and/or dispersed polymer phase. By introducing devolatilization to the tandem system, the morphological behaviors of PE/PS blends were investigated on unfoamed filaments. In general, the mixing between two polymers was improved by the dissolution of CO_2. The size reduction of the dispersed phase was successfully explained using the viscosity ratio of the two polymers. Finally, the interface between foamed and unfoamed polymer was studied in a bilayer structure produced by using a special configuration the tandem system.

7.2. INTRODUCTION

Extensive studies for polystyrene / polyethylene blends have been carried out as a typical immiscible blend system as reviewed in Section 2.5.2. The literature review shows that the degree of mixing between two polymers highly depends on the processing conditions and the size of the dispersed phase generally varies from 2 to 20 μm when compatibilizers

are not used. And the size of the dispersed phase has been reported up to sub-micron order when compatibilizers were used.

Several parameters, such as composition, viscosity and elasticity ratio, interfacial tension and shear stress have been used for explaining the size of the dispersed phase in immiscible blending systems. Taylor (1932) proposed a formula that describes the size of the dispersed phase as a function of the shear rate, the interfacial tension and the viscosity ratio. Vanoene (1972) studied the effect of viscosity and elasticity ratio for a mixture of immiscible fluids. Wu (1987) reported that the dispersed particles become larger when the viscosity ratio increases above unity or decreases below unity. Favis and Chalifoux (1987) investigated the effect of viscosity ratio on polypropylene / polycarbonate blends. They reported that the size of the dispersed phase was minimized when the viscosity ratio of the dispersed phase and the continuous phase was 0.15 in their blending system.

Several papers have been published on applications of SCFs to polymer blends. The sorption behavior of CO_2 was investigated in polystyrene / polycarbonate blending system by Kato et al. (1997). Elkovitch et al. (1998) reported the effect of CO_2 on a PMMA/PS blend. They reported that the size of the dispersed PMMA phases decreased by dissolving CO_2 into the blend in their experiments using a high pressure mixing vessel. They argued that the smaller dispersed phase was obtained due to the higher sorption of CO_2 into the PMMA phase, which leads to the closer viscosities between two polymers. Also, Lee et al. (1998) performed experiments for PE/PS blends with supercritical CO_2 using a twin-screw extruder. They measured the solution viscosity on-line and investigated the foamed structure and the dispersed morphology. They found a considerable viscosity reduction for PE/PS=80/20 blend by dissolving supercritical CO_2 and clarified the behavior of the cell structure of the PE/PS

blends: higher operating pressure and CO_2 content led to smaller cell size. They also found the dispersed PS phase highly elongated in the direction normal to the cell radius.

In this chapter, a PE/PS blending system was investigated in the presence of supercritical CO_2 using various extrusion configurations. These configurations were specially designed for the study of the rheological and morphological behavior of this system. Viscosities of PS, PE and their blends at various blending ratios were measured at various concentrations of carbon dioxide using a twin-screw extruder (Configuration I). Morphological studies were also performed using the other extrusion systems (Configurations II, III and IV). The tandem system allowed for preferential dissolution of CO_2 into the matrix and/or dispersed polymer phase.

7.3. DESIGN OF EXPERIMENTAL SETUP

7.3.1. Extrusion Using a Twin-screw Extruder (Configuration I)

First, experiments were performed in a twin-screw extruder. The extruder and the screw configurations are identical to the configurations used in Chapter 6 (*Figure 6.1* and *3.12*). In this case, two polymers were blended by tumbling before loading into a feeder. It has been shown previously that by maintaining the melt pressure above the solubility limit can result in the formation of a single-phase polymer / CO_2 solution in a single-screw extruder (Park et al., 1995, Park and Suh, 1996a). This was accomplished by assessing the effect of pressure on viscosity and on cell nuclei density for PS/CO_2 foams. Based on similar measurements, it is believed that a single-phase system (blend / CO_2) was achieved in this work. Detailed experimental procedures were explained in Chapter 6. In this experimental setup, the injected CO_2 precipitates at the exit of the secondary die. Thus, as the solution

approaches the die exit, the pressure decreases and the specific volume of CO_2 increases. Therefore, the extrusion speed of the filament was highly increased. Also, the solution experienced an elongational flow in a wedge die even though the converging angle was low (0.9°). As a result, the elongational flow led to a highly elongated dispersed phase in this configuration (Lee et al., 1998)

7.3.2. Extrusion Using a Twin/single Tandem Extruder System (Configurations II, III and IV)

In Configuration II, two extruders, a single-screw extruder and a twin-screw extruder, were connected as shown in *Figure 7.1*. A metered amount of CO_2 was injected into the single-screw extruder using a syringe pump and dissolved into the polymer melt. In order to achieve complete dissolution of CO_2, a special single-screw having a long metering zone was designed. The solution was fed into the barrel of the twin-screw extruder through a connector. The connector, equipped with a temperature controller, was specially designed for high pressure use. While a polymer / CO_2 solution was prepared in the single-screw extruder, the other polymer was fed into the twin-screw extruder and plasticized. The two polymer streams were blended in the twin-screw extruder. An optimum screw configuration was designed for generating high pressure and high mixing performance in a section of the twin-screw extruder, and it is shown in *Figure 7.2(a)*. The high pressure section consisted of left-handed screw elements and a combination of kneading discs. Right after the high pressure section, a series of right-handed screw elements were located in order to precipitate the dissolved CO_2 from the polymer blend. The precipitated CO_2 was vented out before the die exit as indicated in *Figure 7.1*. It should be noted that, in Configuration II, a die having a low resistance was used instead of the wedge die to minimize the elongational flow.

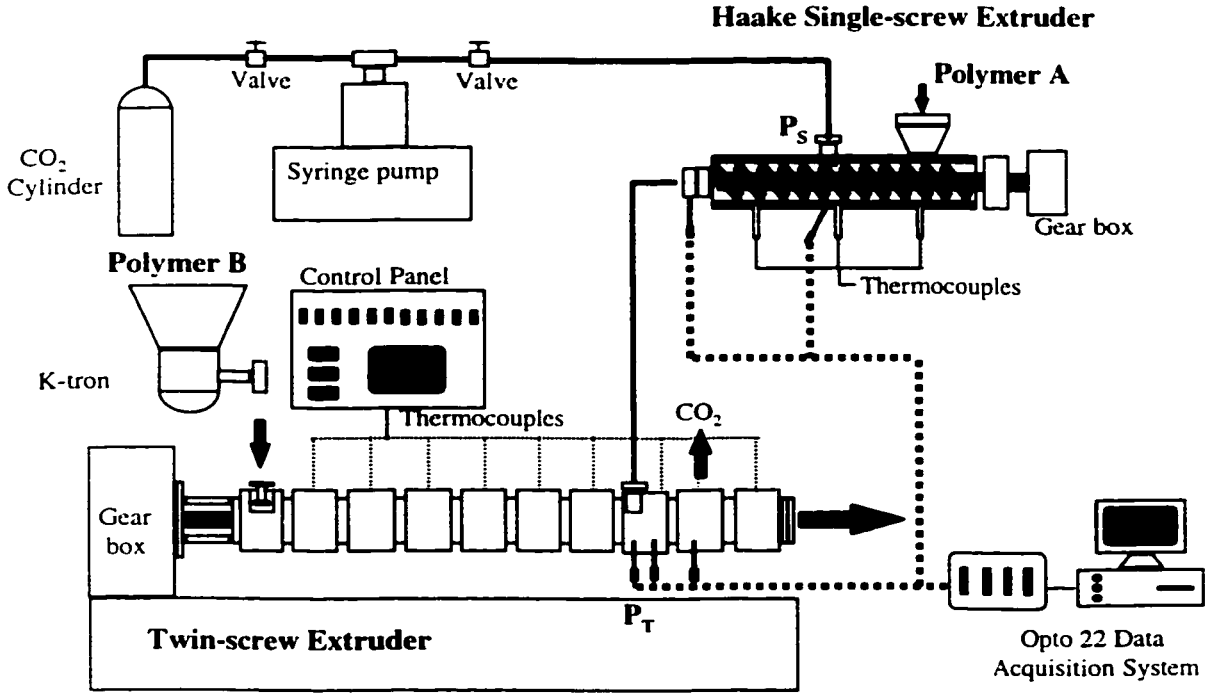

Figure 7.1. Schematic diagram of a twin/single tandem system (Configuration II)

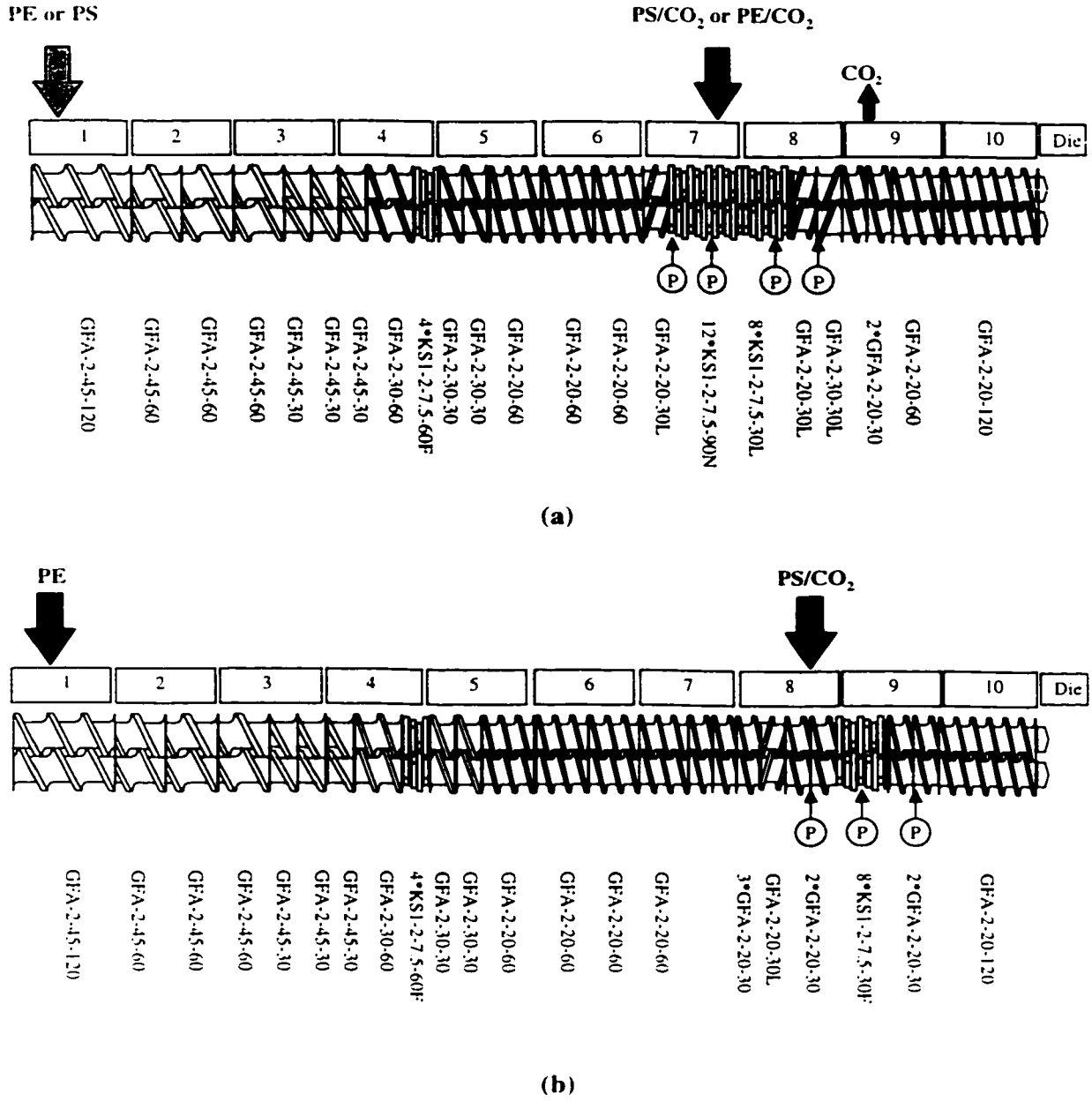

Figure 7.2. Screw configurations for various tandem extrusion system (a) for Configuration II, (b) for Configuration IV

In Configuration III, the polymer / CO_2 solution prepared in the single-screw extruder was connected to the other stream at the wedge die attached to the twin-screw extruder as shown in *Figure 7.3*. By injecting the polymer / CO_2 solution into the other polymer stream at the wedge die, no mixing between two polymer streams was involved and a bilayer structure could be obtained in the extrudate. The same screw configuration (*Figure 3.12*) used in the twin-screw extruder (Configuration I) was used.

Configuration IV has a similar extruder configuration and experimental procedures to Configuration III. However, the single-screw extruder was connected to the barrel of the twin-screw extruder instead of the wedge die as indicated in ***Figure 7.4***. A secondary die was also used for maintaining the high pressure in the wedge die. It should be noted that the temperature of the polyethylene stream in the twin-screw extruder was controlled around 140°C. However, the temperature of PS/CO_2 solutions in the single-screw extruder was about 200°C. After combining the two streams, a moderate mixing was taken place using a screw configuration shown in ***Figure 7.2(b)***.

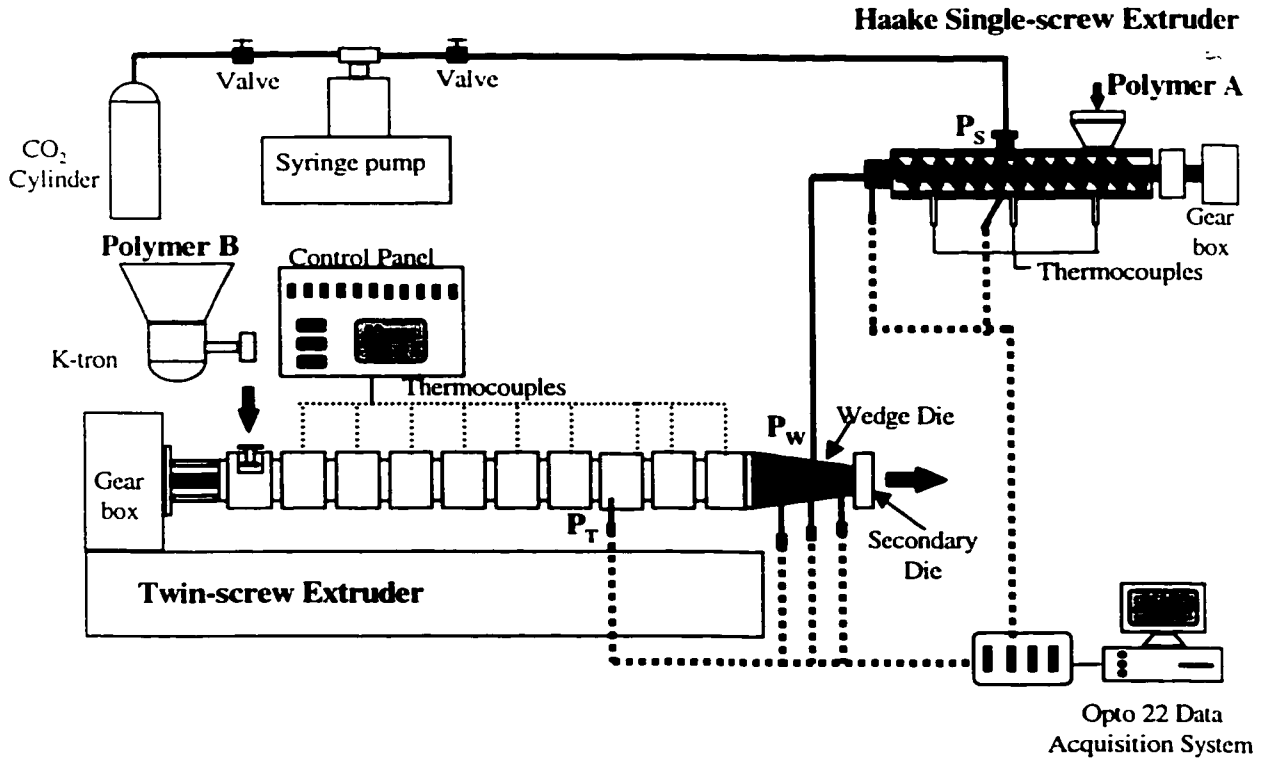

Figure 7.3. Schematic diagram of a twin/single tandem system (Configuration III)

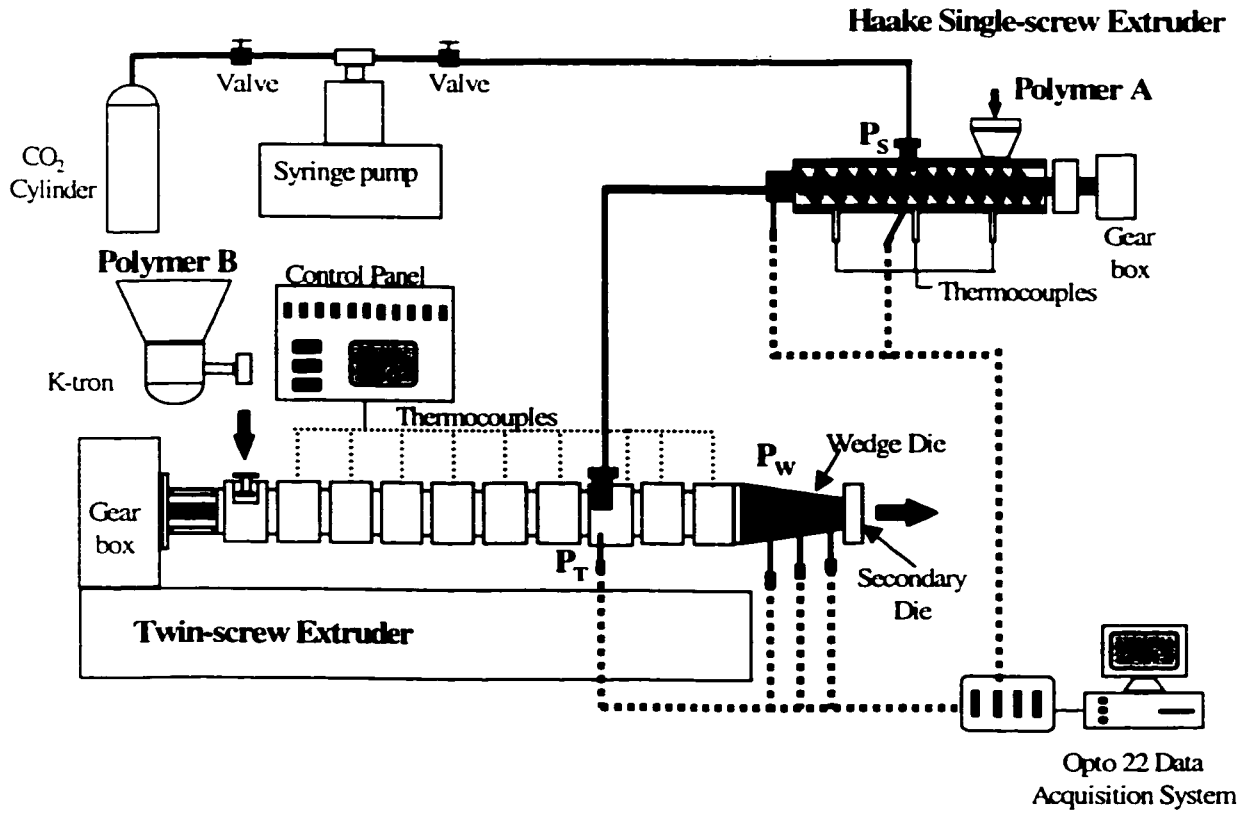

Figure 7.4. Schematic diagram of a twin/single tandem system (Configuration IV)

7.4. EXPERIMENTAL

7.4.1. Equipment and Procedures

The extruders used in this study were a Haake Rheomix 252 single-screw extruder and a Leistritz intermeshing and co-rotating twin-screw machine having a 34mm screw diameter. The screw geometry of the single-screw extruder was specially designed for preparing polymer / CO_2 solutions, as shown in *Figure 3.5(b)*. Polymers were fed into the twin-screw extruder by a K-tron feeder, and into the single-screw extruder by a Brabender FlexWall feeder. CO_2 was injected into the extruder through an injection port (*Figure 3.8*) on the barrel of the single-screw extruder using a syringe pump. During experiments, all pressures at the single-screw extruder, the twin-screw extruder and the wedge die were monitored through an Opto 22 data acquisition system using LABVIEW programs in Appendix I. Finally, the extruded filament was cooled in a water bath and sampled for investigating the blending morphology. A scanning electron microscope was used and all filaments were fractured in liquid nitrogen and coated with gold for the SEM analysis. Some filaments were etched using toluene to dissolve out the PS phase.

7.4.2. Experimental Conditions

The detailed experimental conditions are listed in *Table 7.1* for each configuration. The screw speed of the twin-screw extruder was fixed at 50 rpm. However, the screw speed of the single-screw extruder was controlled for a constant feed rate because the feed rate in a single-screw extruder depends on the pressure at the die. P_T, P_S and P_W in *Table 7.1* denote the pressure values at the various locations of the twin-screw extruder, the single-screw extruder and the wedge die, respectively, as indicated in *Figures 7.1*, *7.3* and *7.4*.

Table 7.1. Experimental conditions at various equipment configurations

Config-uration	PE/PS Ratio	Fed polymer		Screw speed (rpm)		Pressure (MPa)			Measure-ments
		Twin	Single	Twin	Single	P_T	P_S	P_W	
I	100/0, 80/20, 50/50, 20/80, 0/100	PE/PS		50		10.3 - 17.2		13.8 - 27.6	Viscosity, Cell structure, Blend morphology
II	90/10, 83/17, 50/50, 17/83	PE or PS	PS or PE	50	15-25	13.8	22.7		Blend morphology
III	60/40	PE	PS	50	17		22.7	20.7	Cell structure, Blend morphology
IV	90/10	PE	PS	35	25	15.6	22.0	20.4	Cell structure, Blend morphology

7.5. RESULTS AND DISCUSSION

7.5.1. Viscosity Measurement of Polymer / CO_2 Solutions

The viscosities of polymers and their blends were measured at various concentrations of CO_2 using the Configuration I shown in *Table 7.1*. The shear viscosity data of PS/CO_2 and PE/CO_2 solutions are shown in *Figure 7.5*, respectively. The experiment for the viscosity measurement using a wedge was followed by the method explained in Chapter 6 (Lee et al., 1998). All viscosity data were Rabinowitsch-corrected values, and they were normalized to 195°C using a temperature shift factor. Also, the mean pressure for each curve was controlled in the range of 19.2 $\pm$ 0.3 MPa in order to eliminate the effect of pressure on the viscosity. As indicated in *Figure 7.5*, a reduction in the viscosity was observed by dissolving CO_2 into the

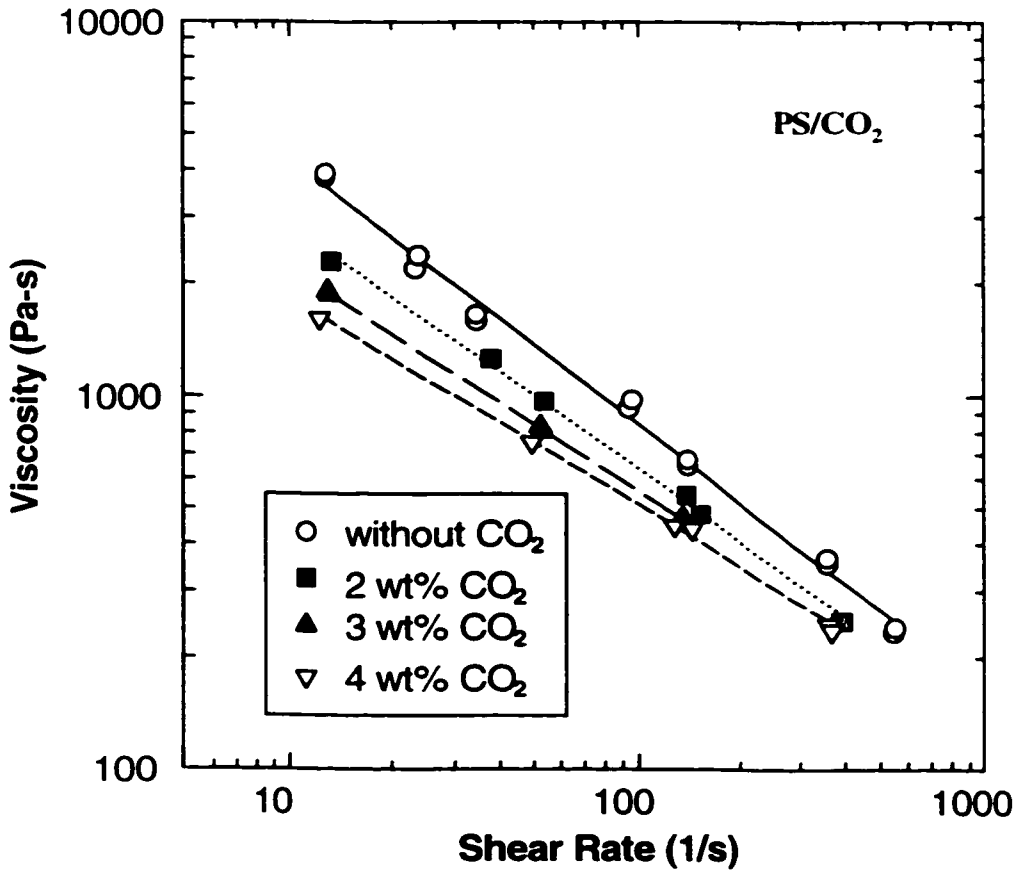

Figure 7.5(a). Shear Viscosity data of polymer / CO_2 solutions: (a) PS/CO_2 solutions

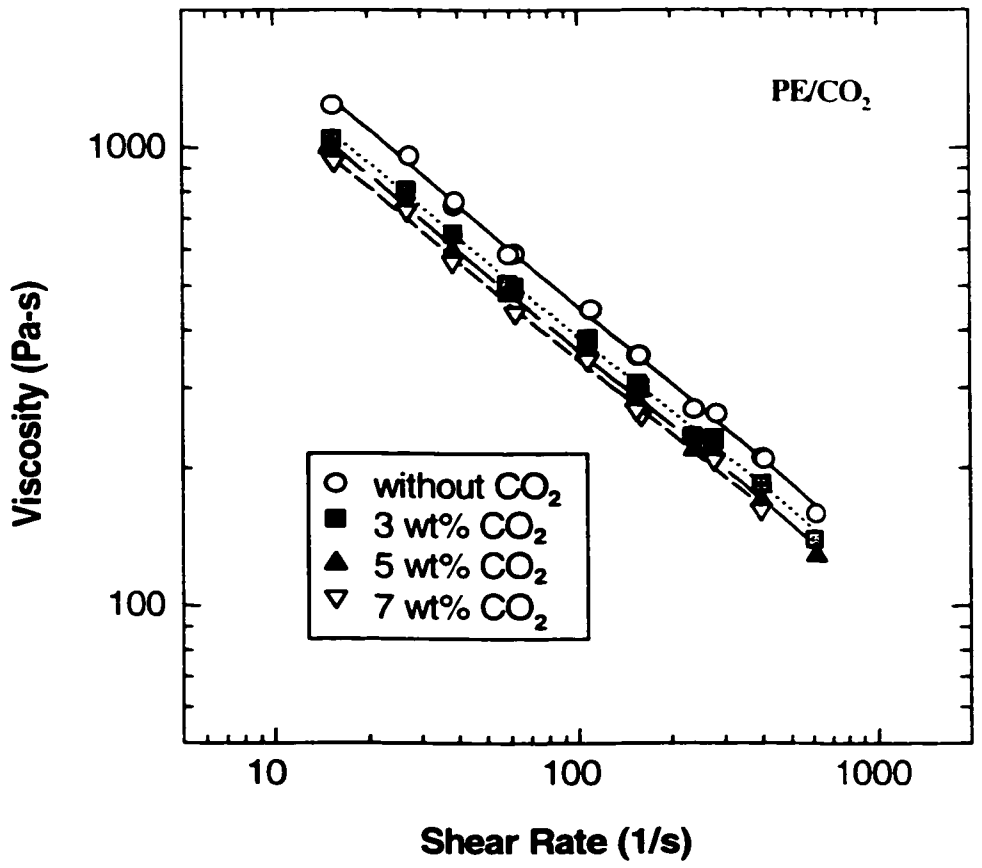

Figure 7.5(b). Shear Viscosity data of polymer / CO_2 solutions: (b) PE/CO_2 solutions

polymers. In general, the solution viscosities tended to decrease as the CO_2 content increased. It should be noted, however, that the viscosity reduction of the PS/CO_2 solutions (*Figure 7.5(a)*) is more than that of the PE/CO_2 solutions (*Figure 7.5(b)*). As explained in Chapter 6, the temperature increase and the dissolution of a gas into a polymer can be understood to have an equivalent effect on the free volume. In these experiments, the working temperature is closer to the glass transition temperature of PS than that of PE. As a result, the higher viscosity reduction in PS/CO_2 solutions can be explained. It should be noted that the (PE/PS) blend / CO_2 solution also showed similar viscosity behaviors as shown in *Figure 7.6*. The mean pressure in *Figure 7.6* was controlled in the range of 19.2 $\pm$ 1.1 MPa. Higher content of PS in the blend led to higher reduction in the viscosity. It should be noted, however, that the viscosity reduction of the blend / CO_2 solutions was in between those of the PS/CO_2 and the PE/CO_2 solutions.

7.5.2. Morphology of PE/PS Blends in a Twin-screw Extruder (Configuration I)

The blending morphology was investigated for the PE/PS blends at various blending ratios and concentrations of CO_2 using Configuration I. In the case of a blend having dispersed PS phase (PE/PS=80/20), the difference in the blending morphologies between unsaturated and saturated PE/PS blends were already compared in Chapter 6: the dispersed PS domains were highly elongated to the flow direction by dissolving CO_2, which results in a subsequent increase in interfacial area. In this chapter, a similar behavior was observed at blending ratio of PE/PS=20/80. *Figure 7.7* shows the blending morphology of PE/PS=20/80 blends at various concentrations of CO_2 when the fracture surfaces are perpendicular to the flow direction. The size of the dispersed PE phase was generally reduced by increasing the

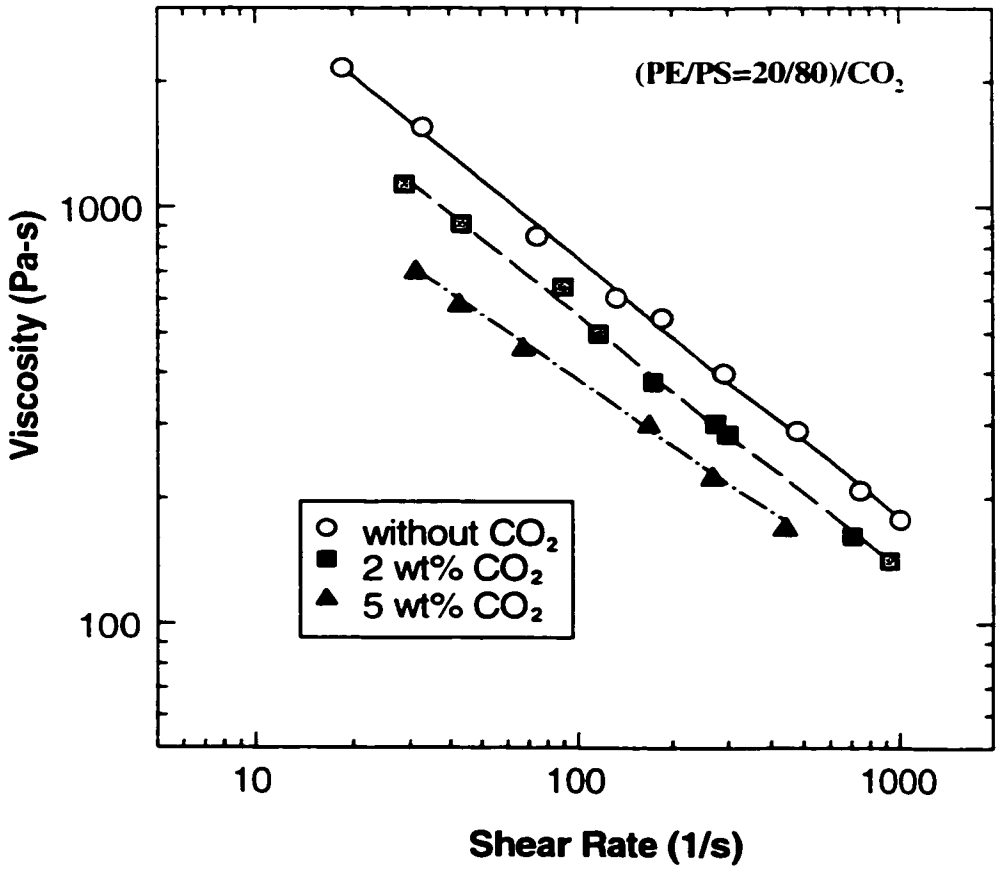

Figure 7.6(a). Shear Viscosity data of polymer blend / CO_2 solutions: (a) PE/PS(20/80)/CO_2 solutions

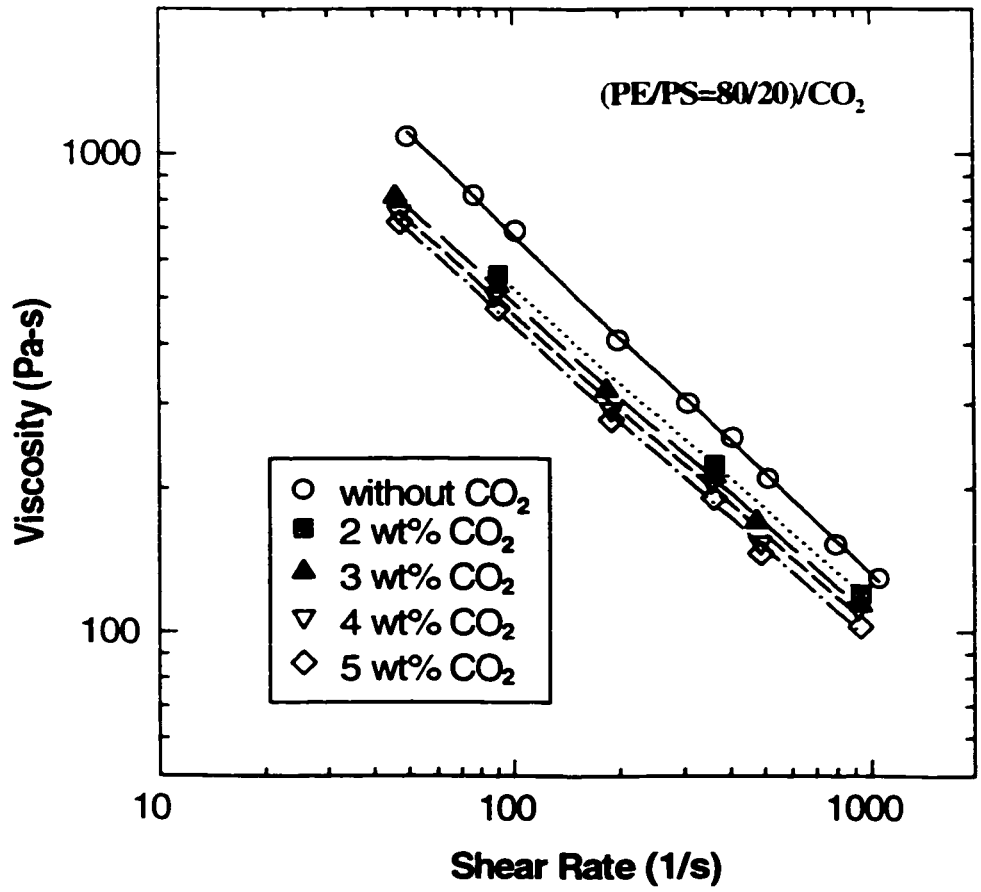

Figure 7.6(b). Shear Viscosity data of polymer blend / CO_2 solutions: (b) PE/PS(80/20)/CO_2 solutions

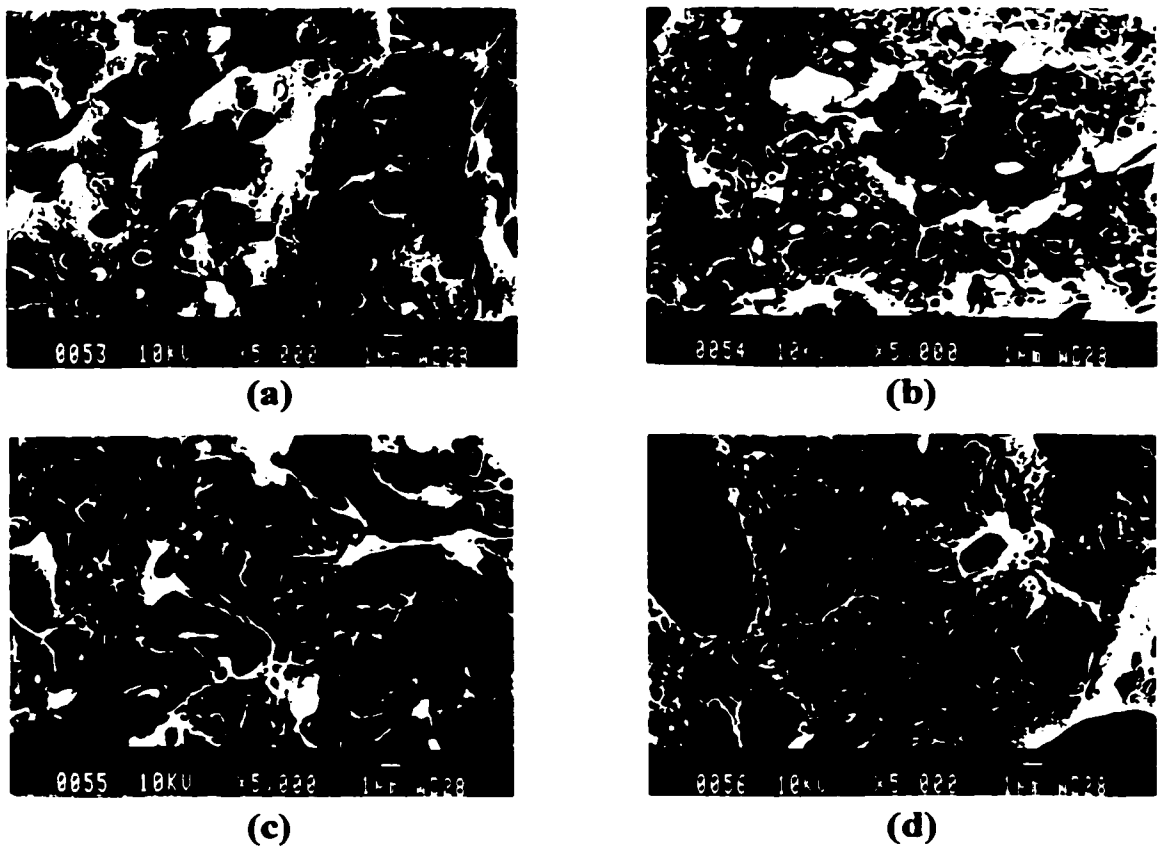

Figure 7.7. SEM photographs of PE/PS (20/80) blends at various contents of CO_2: (a) 0 wt% CO_2 (b) 2 wt% CO_2 (c) 3 wt% CO_2 (d) 4 wt% CO_2

concentration of CO_2. It should be noted, however, that the size of the dispersed PE phase was not reduced dramatically as shown in the dispersed PS phase reported in Chapter 6. The size of the dispersed PE particles will be further discussed with non-foamed blending morphology obtained from a tandem extrusion system in Section 7.5.3.

An interesting behavior was found in the PE/PS=20/80 blending ratio. During the extrusion when CO_2 was not used, the minor component, PE, was mainly found at the surface of the cooled strand. The morphology was verified using SEM for the surface of the filament. In order to prepare the SEM specimen, the surface area and core area of the filament were separately dissolved in toluene and the PE phases were separated by centrifuging. As indicated in *Figure 7.8(a)* and *7.8(c)*, the PE phase collected from the core of the filament formed the dispersed phase regardless of the amount of CO_2 (0% vs 4%). However, it was observed that the PE phase collected from the surface of the filament showed different morphologies. The PE phase looks like continuous even at a content of 20 wt% when CO_2 is not dissolved (*Figure 7.8(b)*). This behavior has been widely observed in polymer melt processing, and is known as a skin-core effect due to the viscosity difference (Paul and Newman, 1978). The phase separation due to the skin-core effect, however, was significantly reduced when CO_2 was used. Thus, no continuous PE phase was observed at the surface of the filament as shown in *Figure 7.8(d)*. It is believed that the viscosity ratio of the two polymers affects the morphology of polymer blend / CO_2 solutions. By dissolving CO_2 in PE/PS blend system, the viscosities of two polymers are closer to each other. Based on *Figure 7.5*, the viscosity ratio of PE (dispersed phase) and PS (continuous phase), η_m/η_m, was increased from 0.37 to 0.62 at the 10 s^{-1} of shear rate by dissolving 4 wt% of CO_2. The PE/PS=50/50 blends were also obtained at various concentrations of CO_2 using

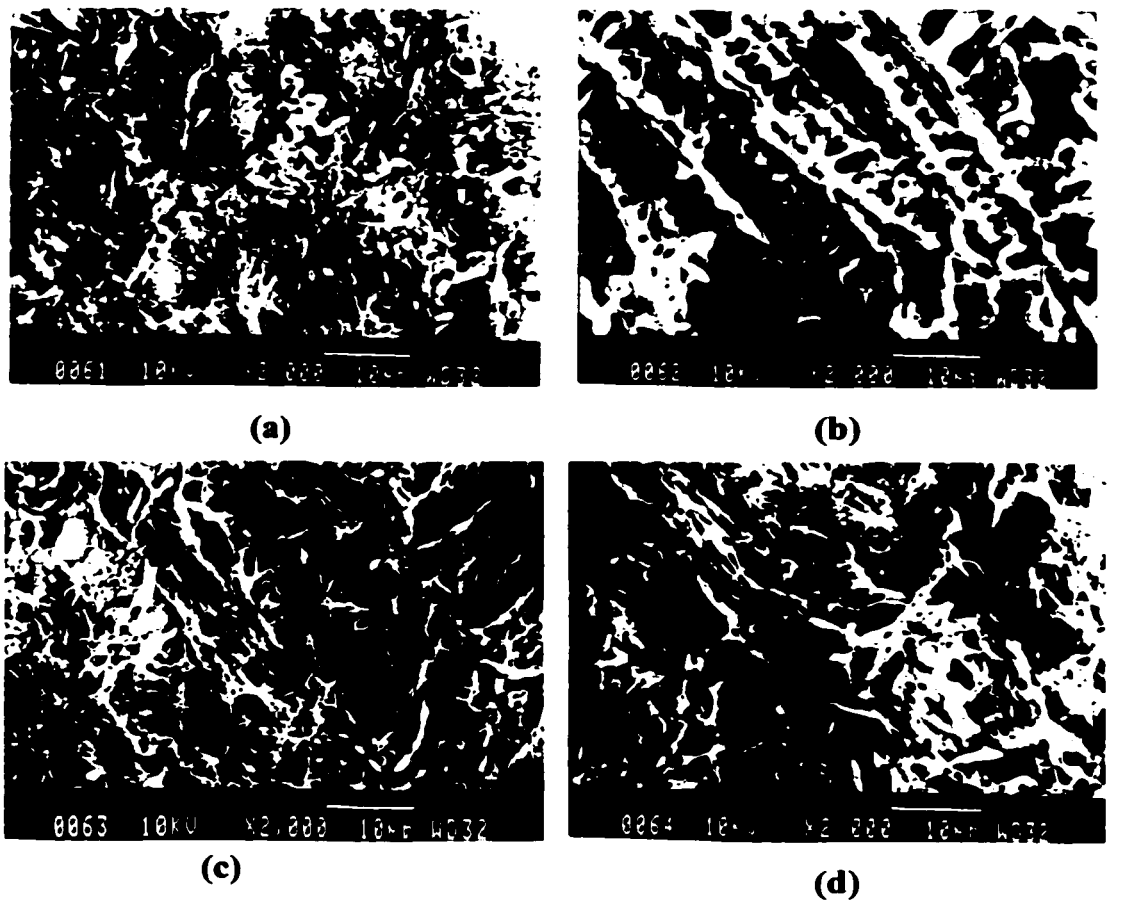

Figure 7.8. SEM photographs of PE/PS (20/80) blend after etching using toluene for the filament surface
(a) core, 0 wt% CO_2 (b) surface, 0 wt% CO_2 (c) core, 4 wt% CO_2 (d) surface, 4 wt% CO_2

Configuration I. However, it was very difficult to clarify the effects of supercritical CO_2 on the blending morphology at this blending ratio due to the co-continuous phase structure.

7.5.3. Morphology of PE/PS Blends in a Tandem System (Configuration II)

In order to investigate the effect of CO_2 on the blend morphology without foaming, a tandem extrusion system (Configuration II) having a devolatilization section was specially designed as shown in *Figure 7.1*. While the polymer / CO_2 solutions experienced the elongational flow in the Configuration I due to the converging wedge die and the rapid expansion of CO_2 at the die exit, the elongational flow was minimized in the Configuration II. It is very difficult to determine the actual size of the dispersed phase in the foamed and elongated morphology obtained from the Configuration I. In order to clarify the effect of CO_2 on the polymer blend, the injected CO_2 was vented after the mixing process. In order to prevent coarsening of the dispersed phase after the CO_2 ventilation, the screw mixing action was minimized. Thus, extensive mixing was carried out only in the high-pressure section. As explained in the experimental section, the high-pressure section in the twin-screw extruder was built using a series of left-handed screw and kneading discs. After the devolatilization section, the polymer blends were extruded through the low resistance die.

When the blending ratio was controlled to be PE/PS=90/10 and when the concentration of CO_2 was controlled to be 0, 5 and 10 wt% based on PS (0, 0.5 and 1.0 wt% based on total polymer), the blending morphologies are compared in *Figure 7.9*. In this case, the viscosity reduction occurred only in the PS phase in the single-screw extruder. Thus, the viscosities of two polymers were getting closer at the early stage of the mixing process. Based on *Figure 7.5*, the viscosity ratio of the dispersed and the continuous phase (η_d/η_m)

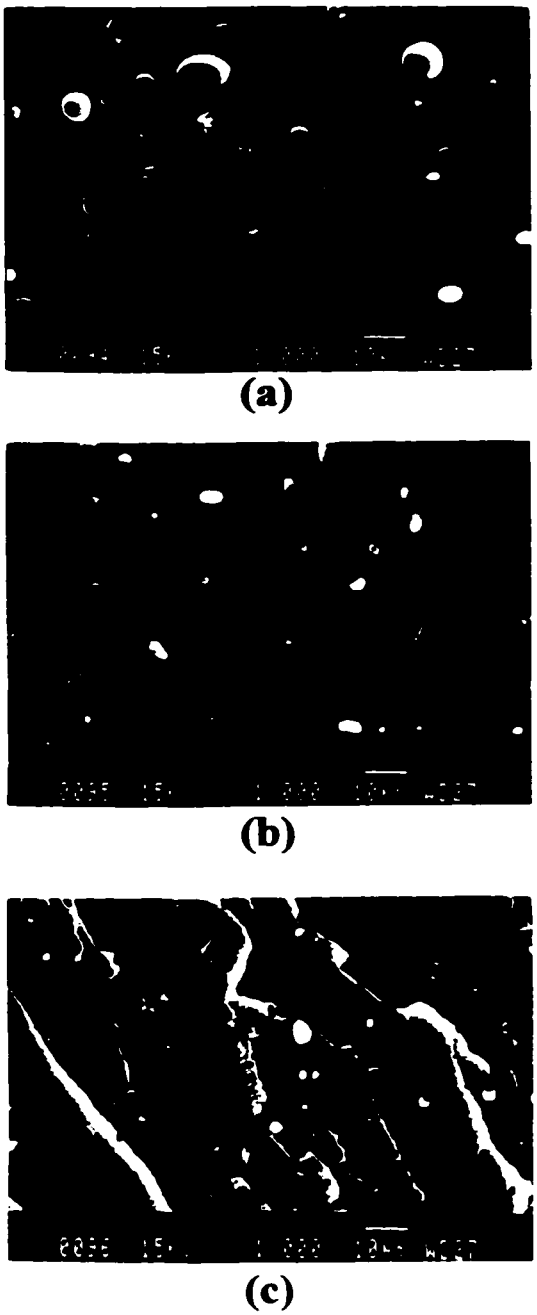

Figure 7.9. Morphologies of PE/PS (90/10) blends obtained from Configuration II at various concentrations of CO_2
(a) 0 wt% CO_2 based on PS (b) 5 wt% CO_2 based on PS (c) 10 wt% CO_2 based on PS

was reduced from 2.69 to 1.14 at 10 s^{-1} of shear rate by dissolving 5 wt% of CO_2. SEM photographs in *Figure 7.9* indicate that by injecting CO_2 the size of the dispersed PS domains decreased from about 10 μm to 2 μm.. It should be noted, however, that no significant differences were observed between 5% and 10% (*Figure 7.9(b)* and 7.9*(c)*). This behavior of the size of the dispersed PS phase of (PS/CO_2)/PE blends can be explained using a solubility limit. At the operating pressure (13.8 MPa) the solubility of CO_2 in PS is known to be 4.7 wt% at 180°C (Sato et al., 1996). Even though we injected up to 10 wt% of CO_2 based on PS, no further decrease in the viscosity of PS was expected after the solubility limit. There is a chance that the excess CO_2 dissolves in the PE phase during the mixing of the two streams. However, the dissolution of the excess CO_2 might be small because of the very short mixing time. Even though some amount of the excess CO_2 is dissolved in the PE phase, the viscosity reduction of the PE matrix will be little as expected in *Figure 7.5(b)*. The reduction of the dispersed phase size at various concentrations of CO_2 was also observed at different blending ratio (PE/PS=83/17). A similar result for the size of the dispersed phase was observed.

Finally, the (PE/CO_2)/PS blending system was investigated at PE/PS=17/83. The PE/CO_2 solution was prepared in the single-screw extruder at various concentrations of CO_2 (0, 5 and 10 wt% based on PE) and the results were shown in *Figure 7.10*. This experiment generated the viscosity reduction in PE phase. It should be noted, however, that the difference in the size of the dispersed PE phase was not observed. As explained in the previous section, less difference in the viscosity ratio was observed by dissolving CO_2 in PE phase than in PS phase. It is believed that the small difference in the viscosity ratio does not significantly affect the size of the dispersed PE phase.

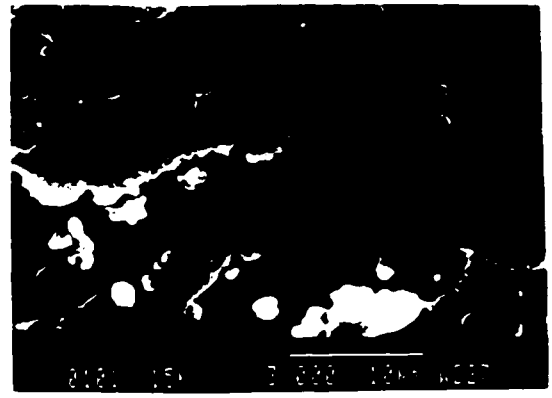

(a)

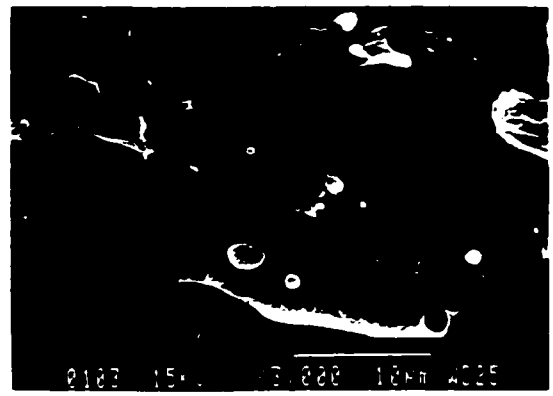

(b)

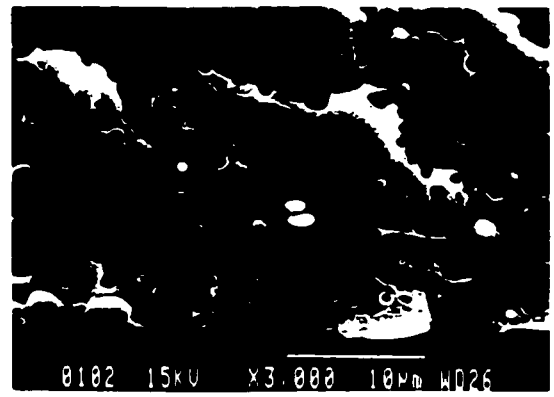

(c)

Figure 7.10. Morphologies of PE/PS(17/83) blends obtained from Configuration II at various concentrations of CO_2
(a) 0 wt% CO_2 based on PE (b) 5 wt% CO_2 based on PE (c) 10 wt% CO_2 based on PE

For the explanation of the blending behavior, the change of the interfacial tension by dissolving supercritical CO_2 should be considered because the surface tension of SCFs is known to be zero. Thus, the dissolution of supercritical CO_2 in PE/PS blends might affect the interfacial tension between PS and PE, which would result in a change of the size of the dispersed phase based on Taylor's formula (Taylor, 1932). In addition, dissolved small molecules such as organics and gas act as interface lubricants. The lubrication effect will also affect the stress for breaking up the dispersed phase. However, no experimental evidence is available for interfacial tension and lubrication due to the dissolution of supercritical CO_2. In this chapter, therefore, the viscosity ratio of two polymers was only employed for a qualitative explanation for the size reduction of the dispersed phase even though the possible effects of the interfacial tension and lubrication might be involved.

From the experiments for the (PS/CO_2)/PE and (PE/CO_2)/PS blending systems, it can be concluded that the viscosity ratio of two polymer streams at the early stage of the mixing process affects the blending morphology. It should be noted that the coarsening of the dispersed phase after the ventilation occurred even though the mixing action after the ventilation was minimized. Therefore, the effect of CO_2 on the size of the dispersed phase in polymer blending system might not be clearly distinguished due to the coarsening process. Furthermore, the dissolution of CO_2 might cause changes of the material properties such as interfacial tension and phase behavior. Therefore, the explanation of the size of the dispersed phase using only the viscosity ratio may not be sufficient to clarify the morphological behavior of this blending system. In spite of the coarsening process and the possibility of the material property change, the effect of CO_2 on the blending morphology has been observed

and the morphology has been qualitatively explained using the viscosity ratio and possible effects of interfacial tension in this experiment.

7.5.4. Morphology of PE/PS Blends in a Tandem System (Configuration III)

The tandem system was designed for the preferential dissolution of CO_2 into a specific polymer phase during the blending experiments. Especially, Configuration III was designed for investigating the interface between a saturated and an unsaturated polymer stream. A polymer / CO_2 solution was prepared using a single-screw extruder and the solution was added to the other polymer stream at the center of the wedge die attached to the twin-screw extruder. This configuration allows minimization of the mixing between the two streams. In this work, the PS/CO_2 solution was prepared using the single-screw extruder as a minor component (40 wt%), and added to the PE stream (60 wt%) plasticized in the twin-screw extruder. Both streams were prepared at 200°C. The concentration of CO_2 was controlled at 5 wt% based on the amount of PS. The combined stream was extruded through the die exit and quenched in a water bath. A SEM photograph of the combined stream is shown in *Figure 7.11*. The foamed structure was observed only in the PS phase while the PE phase was unfoamed. In the middle of the PS phase, the cell showed a typical microcellular structure having cells sized about 10 μm. However, the cell size increased up to 100 μm at the interface of two polymers. It has been known that the cell density and size depend on the content of the dissolved blowing agent with the cell density (cells/cm^3) increasing with an increase in the gas content (Throne, 1996). On the other hand, since the average cell size decreases as the cell density increases, the cell size decreases with an increase in the gas content (Park et al., 1995, Park and Suh, 1996a). Thus, the variation of the cell size shown in

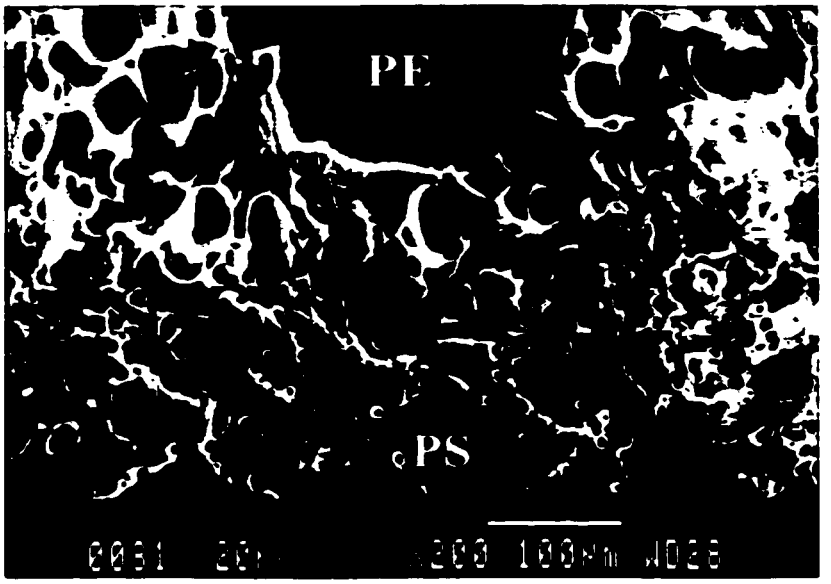

Figure 7.11. SEM photograph of the interface between the foamed PS / unfoamed PE sample

Figure 7.11 is due to the variation in the CO_2 concentration. The dissolved CO_2 diffuses from the PS phase to the interface or to the other phase during the contact in the wedge die.

7.5.5. Morphology of PE/PS Blends in a Tandem System (Configuration IV)

Configuration IV was designed for investigating the foaming and blending behaviors when the preferential sorption was achieved at different temperatures between the two streams. A PS/CO_2 solution was prepared in the single-screw extruder at the barrel temperature of 200°C. The PS/CO_2 solution was mixed with polyethylene flowing in the twin-screw extruder at a lower temperature. The temperature of 140°C was the minimum temperature in the torque range of the twin-screw extruder. The two streams were blended moderately using the screw configuration shown in *Figure 7.2(b)*. By using a wedge die and a secondary die, the polymer blend was successfully foamed at the high pressure as shown in *Table 7.1*. The blending morphology and the foaming structure were investigated using the SEM. The viscosities of PE and PS at each extrusion temperature are measured using a capillary rheometer, and shown in *Figure 7.12*. It should be noted that the viscosity of PS at 200°C is close to that of PE at 140°C. Thus, two polymers would be blended with the same viscosity at the early stage of the mixing when CO_2 was not dissolved in the PS stream. And then the viscosity of PS will increase gradually during the mixing with PE stream at 140°C. When CO_2 is dissolved in PS, the PS/CO_2 solution viscosity will be lower than the PE viscosity at the early stage of the mixing. The blending samples with or without CO_2 were observed, and SEM photographs are shown in *Figure 7.13*. It should be pointed out that the blending ratio of PE to PS is 90/10 and the concentration of CO_2 is 3 wt% based on PS (about 0.3 wt% based on the total polymer). As indicated in *Figure 7.13(a)*, the phase

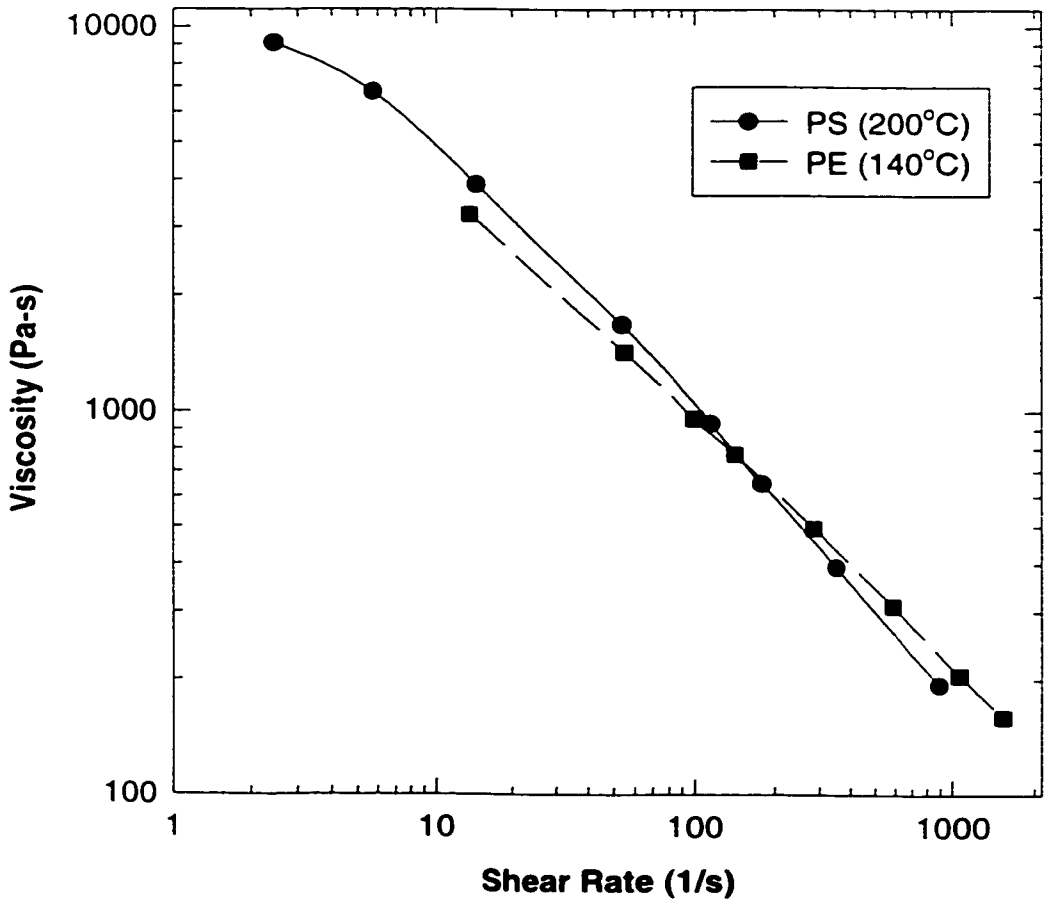

Figure 7.12. Viscosities of PS and PE at their extrusion temperatures

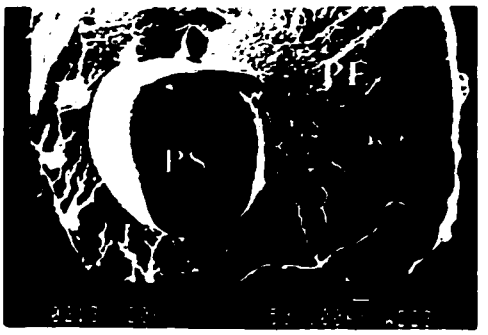

(a) x50

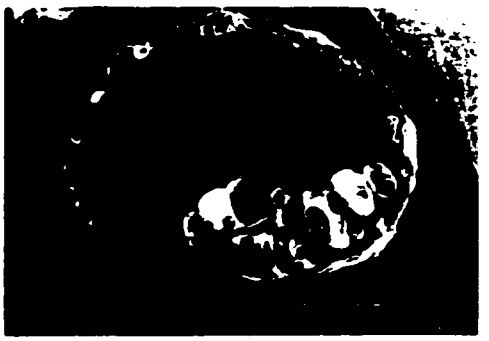

(b) x30

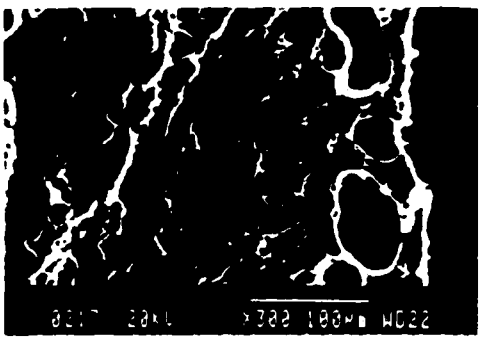

(c) x300

Figure 7.13. Morphologies of PE/PS (90/10) blends obtained from Configuration IV (a) 0 wt% CO_2 (b) 3 wt% CO_2 based on PS (c) 3 wt% CO_2 based on PS (etched with toluene)

separation due to the skin-core effect was observed without CO_2. When CO_2 was injected, however, the macroscopic phase separation was not observed. Thus, the injected CO_2 leads a better mixing between PS and PE. In order to investigate the dispersed phase, the PS phase was removed using toluene. After the etching, it is shown that the PS particles are well dispersed through the fracture surface as shown in *Figure 7.13(c)*.

Another interesting behavior was also observed in *Figure 7.13(b)*. The foamed structure is shown only on the surface instead of the interior of the stand. This behavior is very difficult to explain because the behavior of the injected CO_2 into PS is not clearly explained during the blending process. Regardless of where CO_2 is dissolved, in the PS phase or in both of the PE and PS phases, however, it is considered that the injected CO_2 well spread out through the strand because the PS phase is well blended with PE as indicated in *Figure 7.13(c)*. Therefore, the foaming behavior mainly occurred at the surface might be explained using the difference of CO_2 expandability: CO_2 dissolved in the interior of the strand is suppressed to expand while CO_2 on the strand surface can easily expand due to the free surface. Thus, CO_2 could be easily expanded at the surface rather than in the middle due to the strain constraint. The constrained foaming process is considered as a one of the major reasons of the foaming behavior shown in *Figure 7.13(b)*.

7.6. CONCLUDING REMARKS

The effects of supercritical CO_2 were investigated during the extrusion of PE, PS and their blending systems using a twin-screw extruder and twin/single tandem systems. Three different extruder configurations were designed in order to clarify the effect of CO_2 on the blending system. From Configuration I, the viscosity measurement of polymer / CO_2

solutions and the blending morphology from the foamed structure were investigated. The viscosity reduction of PS was greater than that of PE, and the viscosity reduction of the blend / CO_2 solutions was in between those of the PS/CO_2 and the PE/CO_2 solutions. The size of the dispersed PE phase obtained from the Configuration I was generally reduced by increasing the concentration of CO_2. Also, the effect of CO_2 on the blending morphology was investigated without foaming process through Configuration II. The size of the dispersed PS domain in the (PS/CO_2)/PE blending system decreased when 5 wt% of CO_2 in PS was injected. However, no further decrease was observed by increasing the concentration of CO_2 up to 10 wt%. This behavior was discussed quantitatively using a solubility limit and a viscosity ratio and possible effects of the interfacial tension. The phase separation due to the skin-core effect was significantly reduced at PE/PS=20/80 blend when CO_2 was used. The behaviors of the dispersed phase and the skin-core phase separation were successfully explained using the viscosity ratio of two polymers, even though material properties such as interfacial tension might be changed by the dissolution of CO_2. In general, the mixing between polyethylene and polystyrene was improved by dissolving CO_2. Using the Configuration III, the interface between foamed and unfoamed polymer was investigated. Finally, PE and PS were blended using Configuration IV when the viscosities of the two polymers are close together at the early stage of the mixing. Once again, the improved mixing was observed by dissolving CO_2 in this configuration. An interesting foamed structure was observed and discussed using the strain constraint and the PS particle dispersion.

CHAPTER 8. REACTIVE EXTRUSION OF PE/PA6/PE-g-MAH BLENDS WITH SUPERCRITICAL CARBON DIOXIDE

8.1. ABSTRACT

Reactive extrusion of a polyethylene / polyamide-6 / polyethylene-g-maleic anhydride system was performed in the presence of supercritical carbon dioxide. Effects of the polyethylene-g-maleic anhydride (PE-g-MAH) and the dissolved carbon dioxide on the viscosity and the blending morphology were investigated. Experiments were carried out using a twin/single screw tandem system equipped with devolatilization, which allowed the preferential dissolution of CO_2 into the matrix and/or dispersed polymer phase and chemical reaction after melt-melt mixing. By introducing devolatilization to the tandem system, the morphological behaviors of the blends were investigated on unfoamed filaments. It was found that the addition of a small amount of polyethylene-g-maleic anhydride to polyethylene / polyamide-6 (PE/PA6) blends causes an increase of blend viscosity, which results from the reaction between PA6 and PE-g-MAH. The reaction was verified by observing an imide peak at 1701 cm^{-1} using FTIR. The size of the dispersed PA6 phase decreased by increasing the concentration of PE-g-MAH. It was found that the injected CO_2 affects the size of the dispersed phase when the concentration of PE-g-MAH was low (5 wt%).

8.2. INTRODUCTION

Polyethylene / polyamide-6 / polyethylene-g-maleic anhydride (PE/PA6/PE-MAH) blends have been studied for increasing toughness of polyamide by adding low modulus polyolefin polymers. Due to their immiscibility, the blends show poor mechanical properties

without any interfacial treatment. Therefore, efforts for increasing the compatibility have been carried out. PA6/EPDM-g-maleic anhydride and PA66/maleated EPR systems have also been studied by Ban et al. (1988). Lavallee and Favis (1991) investigated the size of the dispersed phase in PE copolymer/PA6 at various mixing times and compositions. The size of the dispersed droplets reduced with increasing torque associated with the reaction between two polymers. Ide and Hasegawa (1974) studied the effect of maleic anhydride-grafted polypropylene in isotactic PP/PA6 blends, and an improved dispersion behavior and remarkable improvement in the mechanical properties were observed.

Studies for the reaction mechanism between anhydrides and polyamides have been performed by many researchers. Ide and Hasegawa (1974) suggested a mechanism between the maleic anhydride and the terminal amino group of PA6 as shown in *Figure 2.2*. Scott and Macosko (1994) argued the secondary amide salt as the intermediate in the reaction to form the cyclic imide in a melt processing. They observed two broad peaks at 1635 and 1568 cm^{-1} of the secondary amide salt in the blends of styrene-maleic anhydride copolymer and amine terminated butadiene-acrylonitrile copolymer. They also indicated that the reaction to form the secondary amide salt is fast while the cyclic imide is formed slowly. Marechal et al. (1995) also reported on the formation of imide and the decrease of the amine chain end concentration in the reaction between PA6 and poly(metaxylene adipamide) with anhydrides. Sanchez-Valdes et al. (1998) investigated the reaction of linear low-density polyethylene-grafted maleic anhydride and PA6. They also observed a peak at 1704 cm^{-1} associated to the stretching of imide functionality.

In this chapter, a PE/PA6/PE-g-MAH blending system is investigated in the presence of supercritical CO_2. In most of the reactive extrusions using conventional extruders such as

single-screw or twin-screw extruders, two polymers start to react with each other right after the plasticization. In order to investigate the effect of supercritical CO_2 on the reaction, however, the reaction should be confined to a specific section containing the supercritical CO_2 at high pressures. Therefore, a twin/single tandem extrusion system allowing the melt/melt mixing is used for this reactive blending system. The effect of PE-MAH on the morphology and the reaction between amide and maleic anhydride at various concentration of CO_2 are studied using FTIR and electron microscopy. Also, the rheological behavior is also studied on-line using a wedge die.

8.3. EXPERIMENTAL

8.3.1. Equipment and Procedures-Batch Mixer

Preliminary experiments for the reaction between PE-g-MAH and PA6 were performed in a Haake Rheomix 3000 batch mixer. Two roller rotors were used to mix the polymer melt. It should be noted that the two rotors have a different rotation speed for increasing the shear mixing. Thus, one rotates at 2/3 of the major rotor speed. The batch mixer was heated and the torque cell was calibrated prior to the experiments. The dry-blended PE-g-MAH/PA6 or PE/PA6 was fed in the Rheomix and mixed at 240°C and 50 rpm of the major rotor for the duration of 30 minutes. The blending ratio of the two polymers and the total loaded amount of polymers were fixed at 20 wt% of PA6 and 200g, respectively. During the experiments, all conditions including the melt temperature and motor torque were monitored. Polymer resins were dried at 120°C during 6 hours in a vacuum prior to the experiments. Samples were taken at various reaction times and analyzed using FTIR.

8.3.2. Equipment and Procedures-Tandem Extrusion System

A twin/single tandem extrusion system was used and schematic diagrams of the extrusion system and the screw configuration are shown in *Figure 8.1* and *Figure 8.2*, respectively. It should be noted, however, that a wedge die for measuring the viscosity was attached to the end of the twin-screw extruder after the devolatilization. The secondary die for controlling the pressure in the wedge die was not required in this reactive system because the injected CO_2 was already removed through the devolatilization zone. It should be noted that the tandem system allows not only the preferential sorption of CO_2 but also the reaction after combining the two streams.

A metered amount of CO_2 was injected into the single-screw extruder or the twin-screw extruder using a syringe pump and dissolved into the polymer melt. The melt stream in the single-screw extruder (PE-g-MAH or PE/PE-g-MAH blend) was fed into the barrel of the twin-screw extruder through a connector. The other polymer (PE/PA6 blend) was fed into the twin-screw extruder and plasticized. The two polymer streams were blended in the twin-screw extruder. It should be noted that PE-g-MAH pellets were blended with PE pellets for diluting the MAH concentration at certain experimental conditions. An optimum screw configuration was also used for generating high pressure and high mixing performance in a section of the twin-screw extruder. Right after the high pressure section, a series of right-handed screw elements were located in order to precipitate the dissolved CO_2 from the PE/PA6/ PE-g-MAH blends. The precipitated CO_2 was vented out before the die exit as indicated in *Figure 8.1*. By attaching a wedge die, the viscosity of the blends was measured after the devolatilization. It should be noted that all samples were taken from the devolatilization section in order to prevent the further reaction without CO_2.

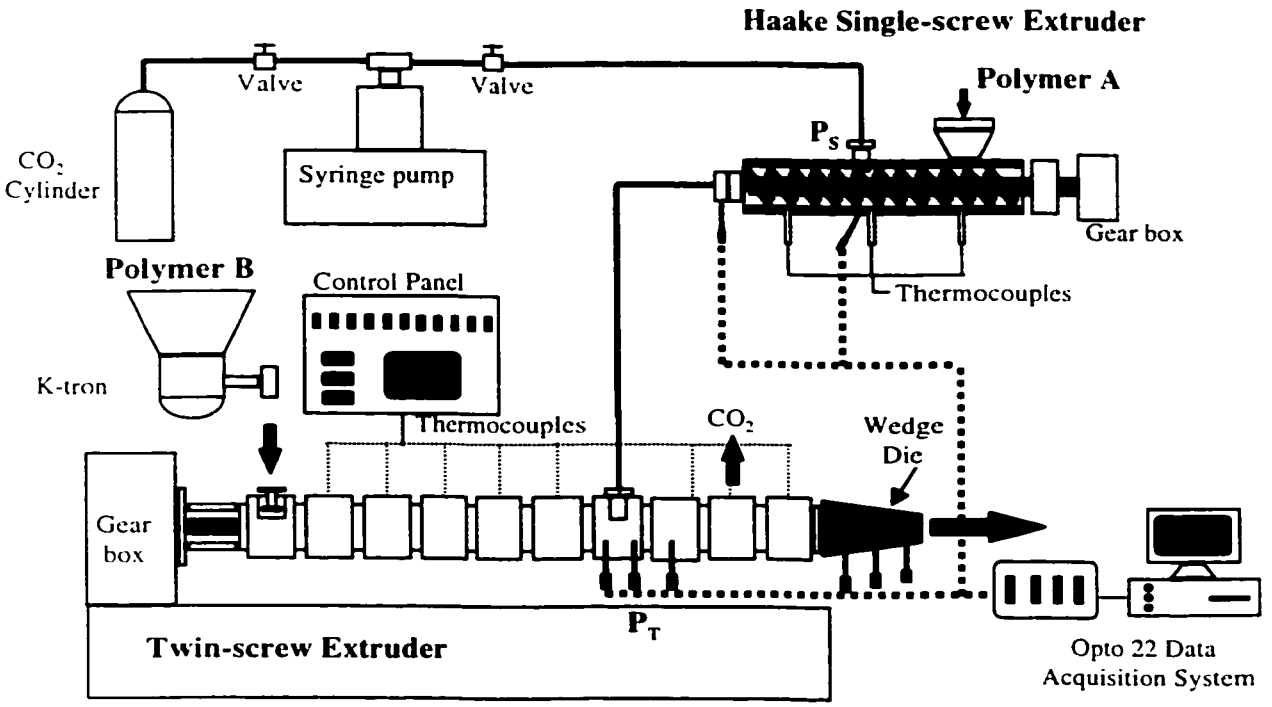

Figure 8.1. Schematic diagram of a twin/single tandem system for the reactive extrusion

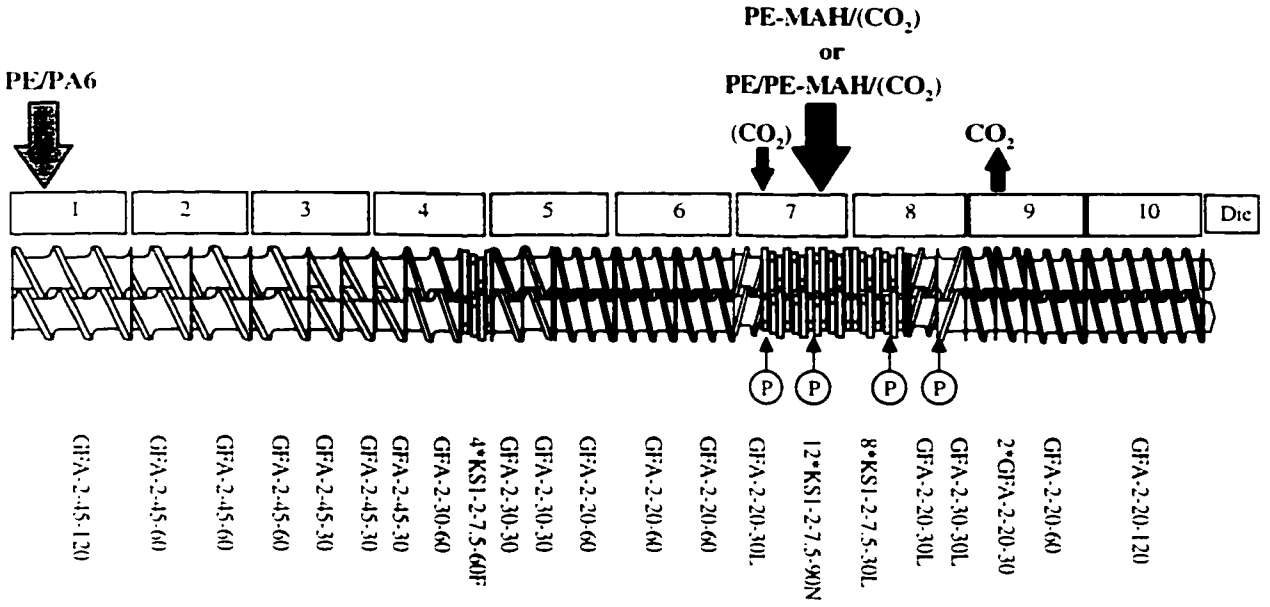

Figure 8.2. Schematic diagram of a twin-screw configuration for the reactive extrusion

8.3.3. Experimental Conditions

Various experimental conditions such as the concentrations of PE-g-MAH and CO_2, the reaction temperature, and the CO_2 injection location, were used in the experiments using the tandem extrusion system. Detailed conditions are listed in *Table 8.1*. During the extrusion, the screw speed of the twin-screw extruder was fixed at 100 rpm while the screw speed of the single-screw extruder was changed for the control of the feed rate. The pressure generation in the twin-screw extruder was difficult due to the low viscosity of PA6 when the PA6 phase was a major component. Therefore, experiments in this work were performed only at low concentration of PA6 (fixed at 20 wt%). The lower pressure leads to two-phase polymer / CO_2 mixtures in the barrel of the twin-screw extruder due to the precipitation of the injected CO_2. It should be also noted that the concentration of CO_2 was controlled based on the amount of PE-g-MAH or the total amount of resin as indicated in *Table 8.1*. Finally, two different reaction temperatures were tested.

8.3.4. Sample Analysis

After the reaction in the designated section of the twin-screw extruder, the blend samples were collected from the devolatilization zone instead of the exit of the wedge die for analyzing FTIR and electron microscopy. All samples were quenched immediately in a water bath right after the collection. Samples were analyzed using microscopy. For the SEM analysis, the collected specimens were fractured in liquid N_2 and the fractured surfaces were coated with gold. The uncompatibilized PE/PA6 blend (R-1 in *Table 8.1*) was successfully characterized using SEM. When PE-g-MAH was added, however, the interface between PE

Table 8.1. Experimental conditions in a tandem extrusion system

Number	Composition (PE/PA6/ PE-g-MAH)	CO_2 Content (wt%)	Fed Polymer		CO_2 Injection Location	Temperature Profile
			Twin (g/min)	Single (g/min)		
R-1	80/20/0	0	PE/PA6 (80/20)	PE-g-MAH (0)	-	1*
R-2	60/20/20	0	PE/PA6 (60/20)	PE-g-MAH (20)	-	1*
R-3	50/20/30	0	PE/PA6 (50/20)	PE-g-MAH (30)	-	1*
R-4	40/20/40	0	PE/PA6 (40/20)	PE-g-MAH (40)	-	1*
R-5	20/20/60	0	PE/PA6 (10/10)	PE-g-MAH (30)	-	1*
R-6	40/20/40	3*	PE/PA6 (40/20)	PE-g-MAH (40)	Single screw	1*
R-7	40/20/40	5*	PE/PA6 (40/20)	PE-g-MAH (40)	Single screw	1*
R-8	75/20/5	0	PE/PA6 (70/20)	PE/PE-g-MAH (5/5)	-	2**
R-9	75/20/5	1**	PE/PA6 (70/20)	PE/PE-g-MAH (5/5)	Twin screw	2**
R-10	75/20/5	3**	PE/PA6 (70/20)	PE/PE-g-MAH (5/5)	Twin screw	2**

* CO_2 content based on the amount of PE-g-MAH

** CO_2 content based on the amount of total resin

* Temperature Profile 1:
Twin-screw extruder: 100-200-240-240-240-240-240-240-240-240°C
Single-screw extruder: 170-240-240-240°C

** Temperature Profile 2:
Twin-screw extruder: 100-150-230-230-220-220-220-220-220-220°C
Single-screw extruder: 150-220-220-220°C

and PA6 phases was not clearly distinguished due to the induced compatibility. Therefore, TEM analysis was used for the compatibilized samples. A cryogenic microtoming technique at -120°C was used for the TEM sample preparation. Ruthenium tetroxide vapor was used for staining the dispersed PA6 phases during 1 hr at the room temperature. The stained samples were dried at room temperature during 24 hours in vacuum. Finally, TEM observation was carried using the election voltage of 100 kV at LG Chemical Research Park (Taejon, Korea).

FTIR analysis was also carried out to verify the reaction between PE-g-MAH and PA6 using a Nicolet 520 FTIR spectrometer. For the characterization of pure polymers, thin films were prepared using a hot press, and the films were put at 120°C during 3 hours in vacuum for transforming the acid group to anhydride group. It should be noted that a quantitative analysis for the reaction was performed at various concentrations of PE-g-MAH and CO_2. For the quantitative study, a solution casting method was used for preparing the FTIR samples and the residual amount of maleic anhydride was chosen instead of the imide peak. It should be noted that the ratio of the peak height is directly proportional to the ratio of the concentration in the absorbance spectrum. Therefore, the absorbance spectra were used and the height of the characteristic peaks was maintained less than unity. PE and PE-g-MAH phases were extracted from PA6 phase using a boiling toluene, and the PE/PE-g-MAH/toluene solution was cast on NaCl plates. The solution cast film was also put in a vacuum oven not only for drying out the toluene but also for the transformation of the acid group. It is assumed that the PE-PA6 copolymer generated through the reaction is soluble in the boiling toluene, and peaks of PA6 were found in the solution cast film. Before analyzing the blend samples, pure polymers were first analyzed, and the absorbance spectra are shown in *Figure 8.3*. As indicated in ***Figure 8.3***, the anhydride group shows a characteristic peak

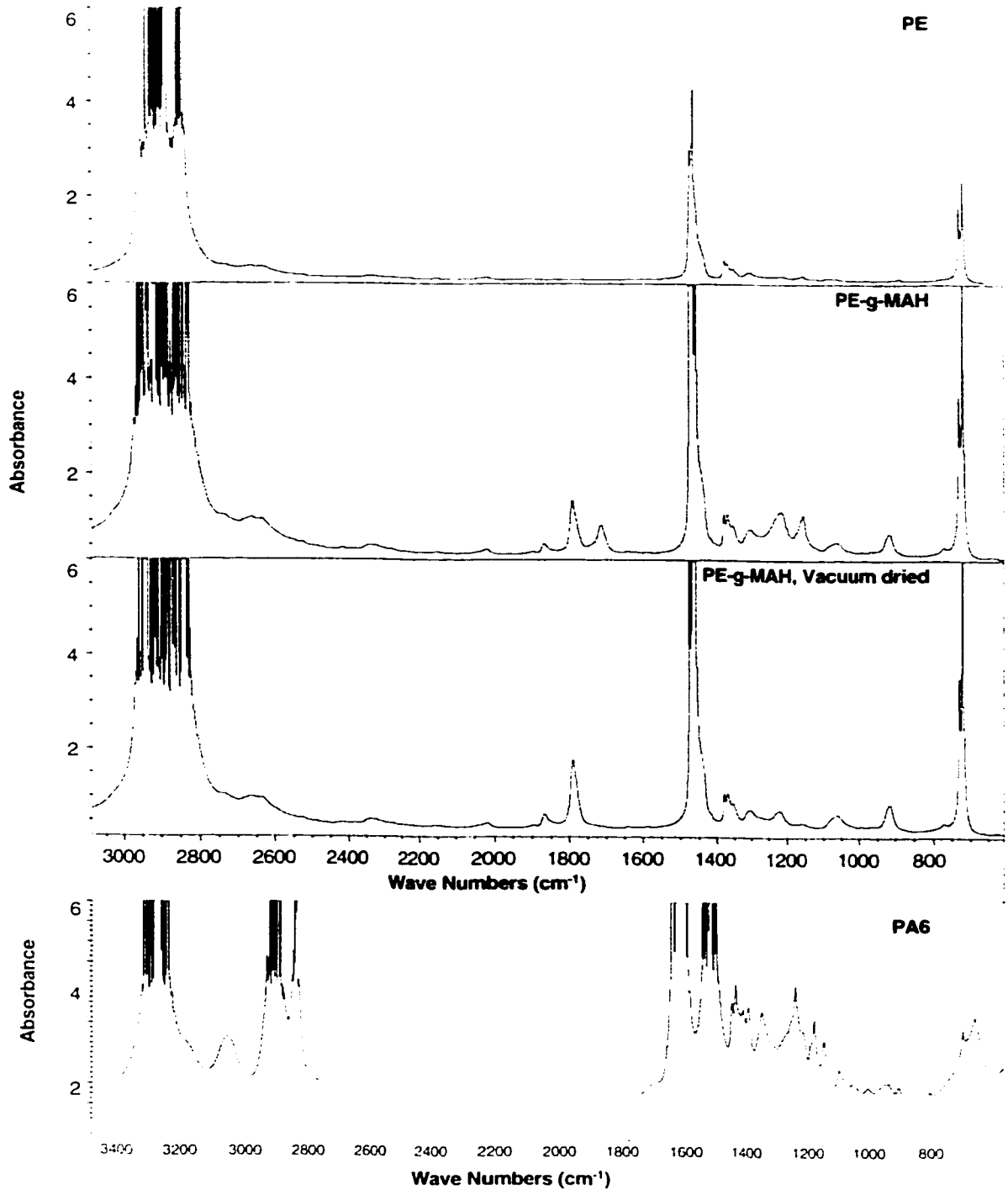

Figure 8.3. FTIR spectra of PE, PE-g-MAH and PA6

around 1792 cm^{-1}. It should be noted that the amic acid shown at 1713 cm^{-1} was transformed to the anhydride peak at 1792 cm^{-1} after the drying process at 120°C during 3 hours in a vacuum oven. A spectrum of PA6 is also included in *Figure 8.4* showing a characteristic peak for amide at 1620 cm^{-1}.

8.4. RESULTS AND DISCUSSION

8.4.1. Reaction in a Batch Mixer

Blends having the composition of PE-g-MAH/PA6=20/80 and PE/PA6=20/80 were mixed at 240°C in a batch mixer for 30 minutes and the torque behaviors are compared in *Figure 8.4*. As indicated in the figure, the torque of the reactive system is higher than that of the non-reactive system even at the early stage of mixing. It is believed that two contributions on this torque behavior might be involved. First, the viscosity difference between PE and PE-g-MAH affects the torque level. As indicated in *Figures 3.1* and *3.3*, the viscosity of PE-g-MAH is higher than that of PE at this operating temperature. Thus, a higher torque was expected when PE-g-MAH was used. However, the reactive system showed a much higher torque behavior than the pure PE-g-MAH, indicating another contribution was involved. Second, the rapid reaction between two polymers will generate high molecular weight PE-PA6 copolymer, and the copolymer results in the higher torque behavior at the early stage of mixing in *Figure 8.4*. It should be noted that an additional torque increase was observed after 7 minutes and the torque shows a maximum approximately at 12 minutes.

During the reaction, blend samples were analyzed by FTIR and a spectrum at 15 minutes, for example, is shown in *Figure 8.5*. The overall spectrum (*Figure 8.5(a)*) shows a typical anhydride peak due to carbonyl groups at 1792 cm^{-1} for a PE/PA6 blend. Thus, the

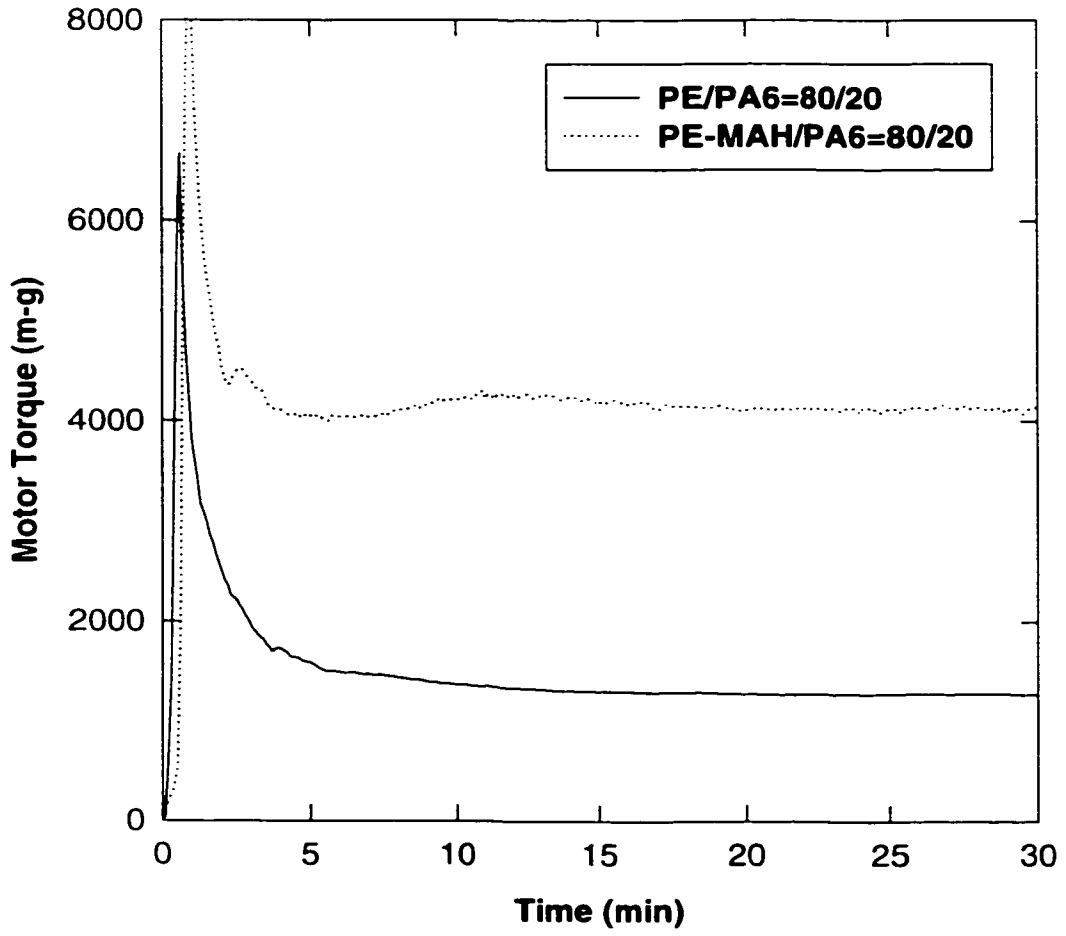

Figure 8.4. Torque behaviors of the non-reactive and reactive blends in a batch mixer

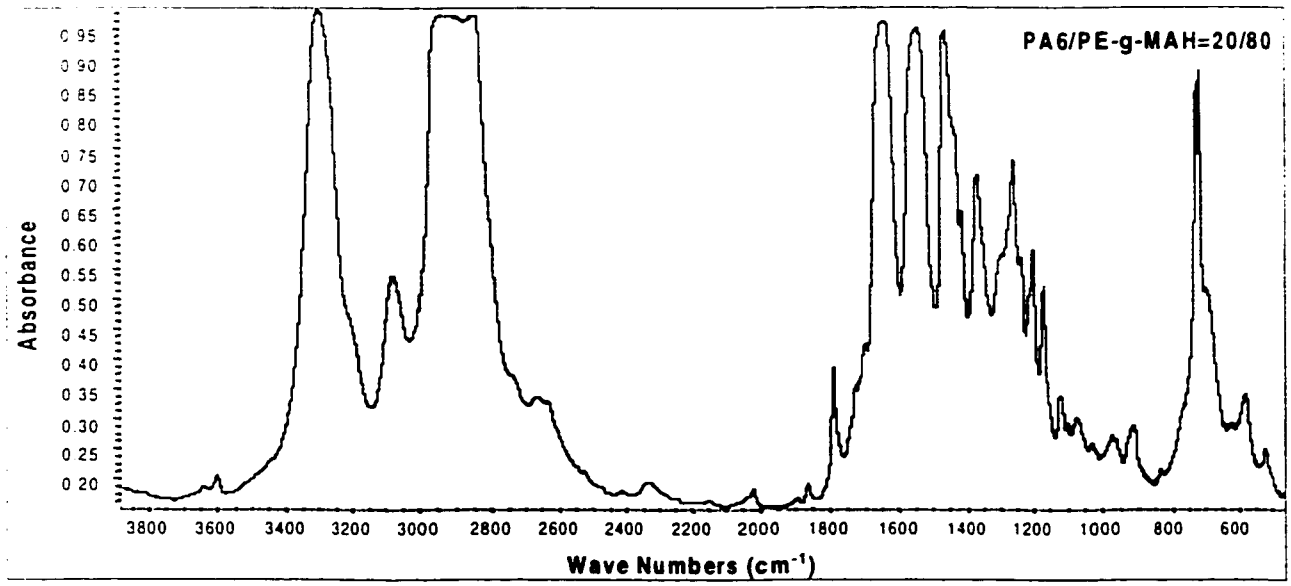

(a)

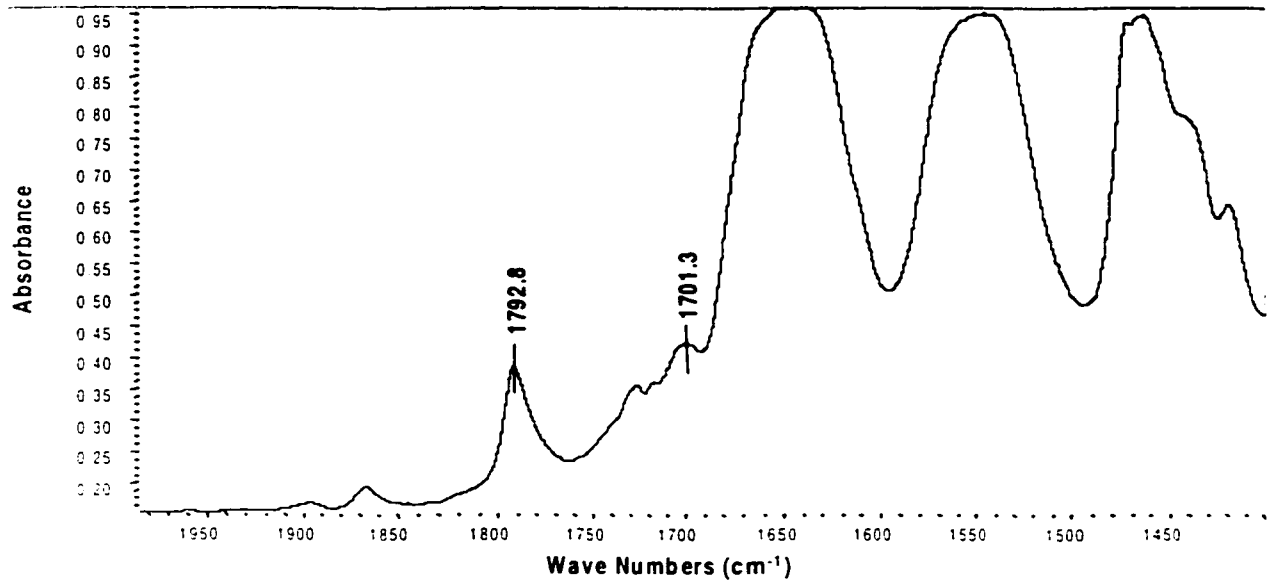

(b)

Figure 8.5. FTIR spectra of the PE-g-MAH/PA6=80/20 blend

anhydride peak indicates that a portion of the maleic anhydrides in PE-g-MAH is involved in the reaction with PA6 at these experimental conditions. As reported in the literature, an imide peak at 1701 cm^{-1} was observed.

Quantitative studies based on the FTIR spectra were carried out for estimating the reaction conversion of maleic anhydride. The residual anhydride peak was used instead of the imide peak because the imide peak interferes with the amide peak as shown in *Figure 8.5(b)*. In addition, it has been known that formation of the imide group is generated very slowly (Scott and Macosko, 1994). The residual amount of the maleic anhydride before and after the reaction was determined by taking the peak height ratio at 1792 cm^{-1} to 719 cm^{-1}. The peak at 719 cm^{-1} represents the -(CH_2)- group, and it has been used for quantifying PE in PE/PS blends (Sun and Baker, 1997). Samples were collected at various mixing times and the conversions of maleic anhydride for each sample were measured. As shown in *Figure 8.6*, most of the maleic anhydride reacts with PA6 in the early stage of mixing. Thus, 60% MAH based on the total amount of MAH in PE-g-MAH was consumed in 30 min at this experimental condition, and 80% of the consumed MAH reacts with PA6 within 3 min. It should also be noted that the maximum conversion was achieved at 12 minutes. The decrease in conversion after 12 minutes might be attributed to experimental error in the FTIR measurement.

The torque behavior in *Figure 8.4* can be explained using the reaction conversion. As mentioned, the reactive blending system shows a higher torque than the non-reactive one even at the early stage of mixing. Also, the torque of the reactive system shows its maximum at 12 minutes. As pointed out by Scott and Macosko (1994) and Marechal et al. (1995), it is believed that the amine end group reacts with MAH in the early stage of mixing due to the

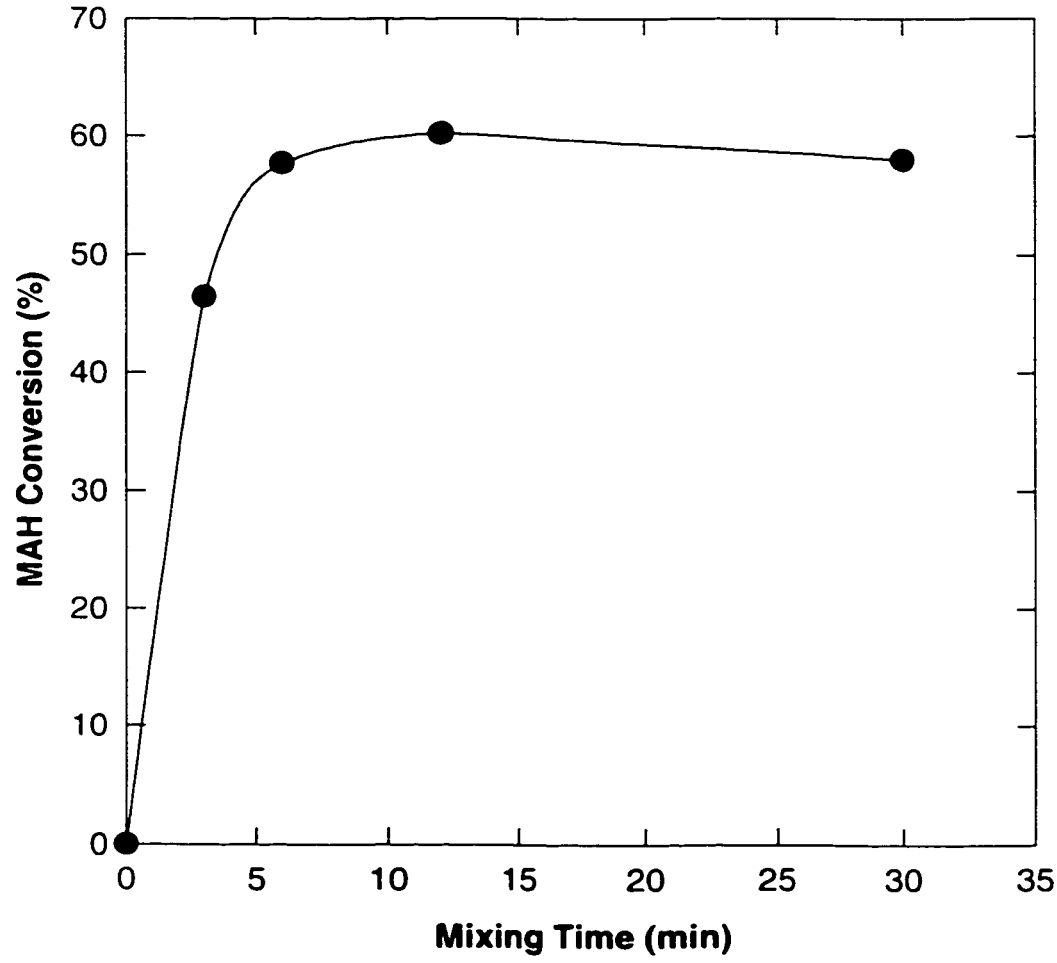

Figure 8.6. MAH conversions at various mixing time in a batch mixer

high reactivity. Further reaction associated with the amide group on the main PA6 chain, might follow in this blending experiment. The reaction between amide and MAH groups only takes place when PA6 is the minor component. Thus, after the completion of the amine end group, the amide group starts to react with MAH with a low reactivity (Marechal et al., 1995). Therefore, it is believed that the maximum torque at 12 min might result from the amide/MAH reaction.

8.4.2. Effects of PE-g-MAH on PE/PA6 Blends in a Tandem Extruder

The effects of PE-g-MAH on the PE/PA6 blends were investigated using a twin/single tandem extruder shown in *Figures 8.1* and 8.2 without dissolving CO_2. Detailed experimental conditions are listed in *Table 8.1*. The PE-g-MAH stream in a single-screw extruder was blended with the PE/PA6 melt stream at the 7th barrel section of a twin-screw extruder, and samples were taken from the 9th barrel for scanning electron microscopy. The blend viscosity at various concentrations of PE-g-MAH was measured using the wedge die, and the viscosity after the Rabinowitsch correction is shown in *Figure 8.7*. Due to the viscous heating, the actual resin temperatures through R-1 to R-5 were varied from 260 to 269°C even though the barrel setting temperatures were fixed at 240°C. Therefore, the viscosity values at each run were normalized to 270°C using a temperature shift factor (Rauwendaal, 1990). It should be pointed out that the non-reactive PE/PA6 blend (R-1) covers higher shear rates than the other reactive blends due to the low power-law index. The blend viscosity generally increases with increasing the concentration of PE-g-MAH. The first 20 wt% addition of PE-g-MAH shows a relatively higher increase in the blend viscosity if it

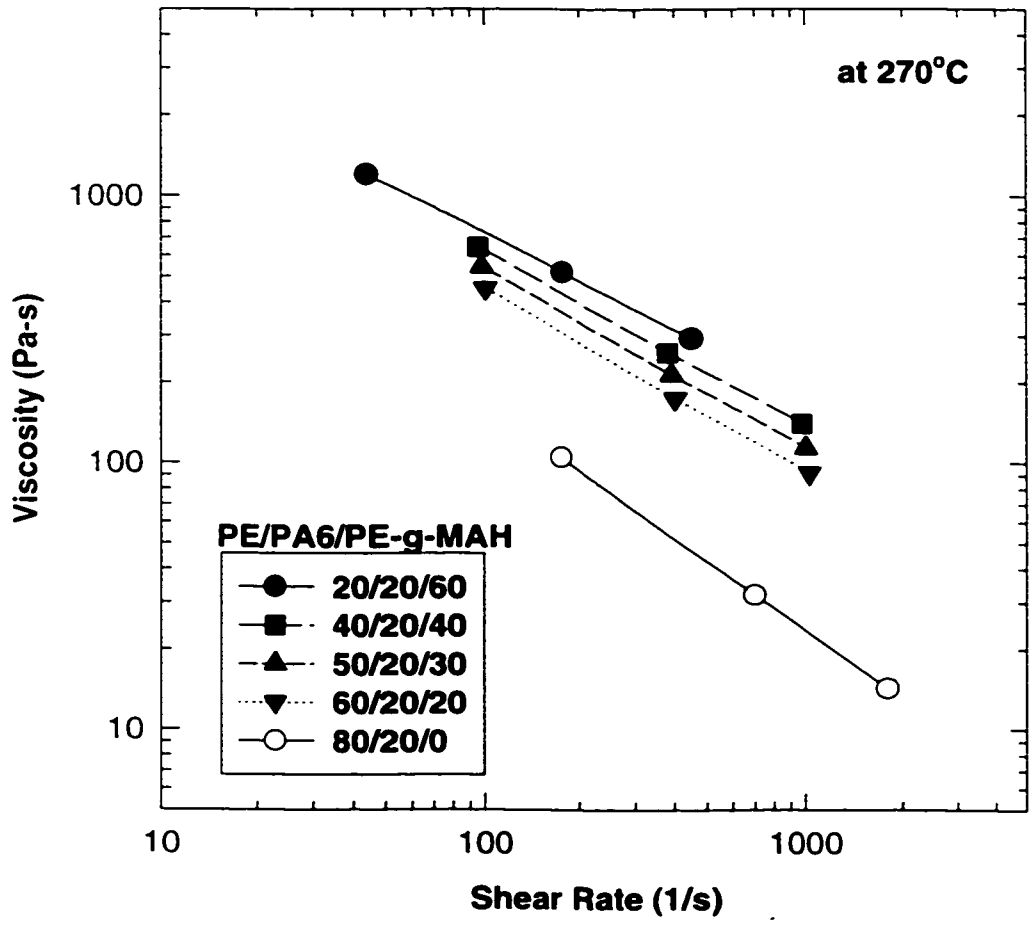

Figure 8.7. Viscosities of PE/PA6/PE-g-MAH blends at various blending compositions

is compared to the other additional increase of the PE-g-MAH concentration. It is believed that the first rapid increase in the viscosity is related to the reaction, and then the followed gradual increase in the viscosity is caused due to the inherent high viscosity of PE-g-MAH.

The morphologies of the blending samples were investigated, and SEM photographs are shown in *Figure 8.8*. The dispersed PA6 phase and the interface are clearly distinguished when PE-g-MAH is not used (R-1), as shown in *Figure 8.8(a)*. However, it was difficult to locate the dispersed particles on the fractured surfaces of the reactive systems (R-2 through R-5) due to the high interfacial strength. Even the 20 wt% of PE-g-MAH led to high interfacial strength as indicated in *Figure 8.8(c)*. When the concentration of PE-g-MAH was reduced to 5 wt% (R-8), dispersed PA6 particles could be observed in *Figure 8.8(b)*. But, the interface was still not clear. The size of the dispersed PA6 was dramatically reduced from over 10 μm to submicron order by adding 5 wt% of PE-MAH. Due to the ambiguous interface, it is recommended to use the TEM analysis technique in order to analyze the morphology of the reactive PE/PA6/PE-g-MAH blends.

TEM photographs give a quite clear view of the interface. The same trend observed in *Figure 8.8*, a decrease of the dispersed phase with increasing the concentration of PE-g-MAH, was also found in the TEM observations, and the photographs are shown in *Figure 8.9*. The diameter of the dispersed phase decreased from 0.17 to 0.1 μm by increasing the concentration of PE-g-MAH from 5 to 40 wt%.

(a)

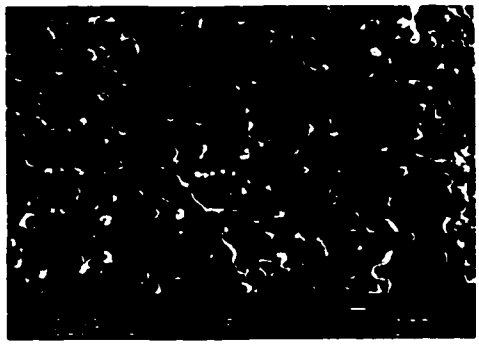

(b)

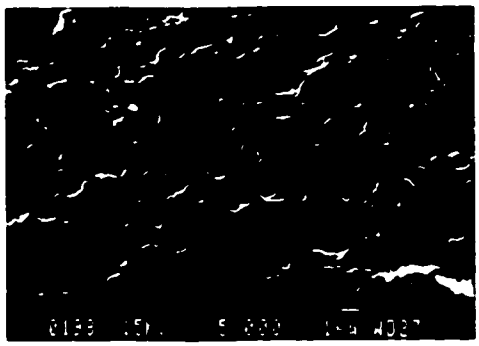

(c)

Figure 8.8. SEM photographs of PE/PA6/PE-g-MAH blends (a) PE/PA6/PE-g-MAH=80/20/0 (b) PE/PA6/PE-g-MAH=75/20/5 (c) PE/PA6/PE-g-MAH=60/20/20

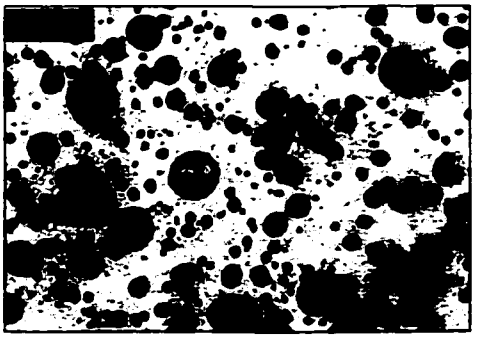

(a)

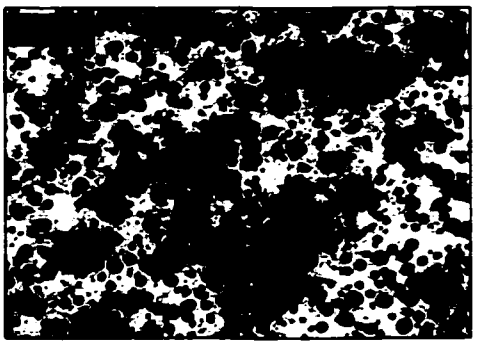

(b)

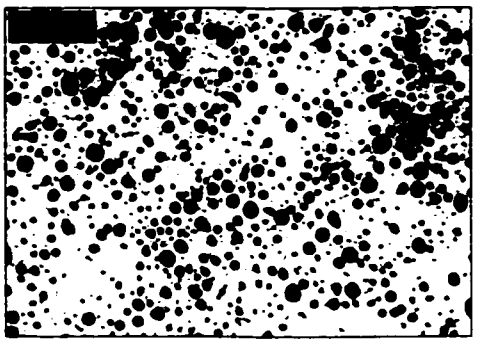

(c)

Figure 8.9. TEM photographs of PE/PA6/PE-g-MAH blends at various blending ratios (without CO_2)
(a) 75/20/5,d_{avg}=0.17 (b) 60/20/20, d_{avg}=0.12 (c) 40/20/40, d_{avg}=0.1

8.4.3. Effects of CO_2 on PE/PA6/PE-g-MAH Blends

The effects of CO_2 on the PE-MAH/PA6 blending system were investigated using a twin/single tandem extruder. The concentration of PE-MAH was varied from 5 to 40 wt% in this work as listed in *Table 8.1*. In order to investigate the effect of CO_2 on the blend viscosity after devolatilization, the viscosity was measured on-line using a wedge die attached to the twin-screw extruder. During the extrusion, it was found that the barrel pressure at the high pressure mixing section of the twin-screw extruder was significantly reduced by increasing the concentration of CO_2. For example, the barrel pressure decreased from 14.5 to 12.4 MPa by injecting 5 wt% of CO_2 at a composition of PE/PA6/PE-g-MAH=40/20/40. As indicated in *Figure 8.2*, the barrel pressure is generated by the pumping capacity of a series of the left handed screw elements and kneading discs, and the generated pressure is directly proportional to the melt viscosity. Thus, the barrel pressure drop observed reflects the viscosity reduction in the mixing section. It is expected that the viscosity reduction affect the mixing performance and the final blend viscosity. However, no CO_2 effect on the viscosity was observed after the devolatilization, as shown in *Figure 8.10*. This behavior was observed regardless of the concentration of PE-g-MAH. Therefore, it can be concluded that the mixing efficiency is high enough due to the hard screw configuration at the given composition.

The effect of CO_2 on the blending morphology was also investigated. Due to the ambiguous interface on the fractured surface, TEM analysis was performed and the results are presented in *Figure 8.11* at various concentration of CO_2. It was found that the size of the dispersed PA6 slightly decreased by dissolving CO_2 at PE/PA6/PE-g-MAH=75/20/5. The size and the distribution based on image analysis are listed in *Table 8.2*. The smaller

Table 8.2. The particle size and the deviation of the dispersed PA6 phase at various concentrations of CO_2

Sample	Injected amount of CO_2 (wt%)	Number Average Particle Diameter (μm)	Standard Deviation (μm)
R-8	0	0.17	0.14
R-9	1	0.14	0.10
R-10	3	0.14	0.10

dispersed phase indicates better mixing between PE and PA6 in the high pressure mixing section, because the coalescence of the dispersed particles was minimized in this experiment. It should be mentioned that in *Figure 8.11* the CO_2 concentration has no significant effect on the size of the dispersed phase. Other blending compositions having a higher concentration of PE-g-MAH were also tested. Size reduction by injecting CO_2 was not observed at the compositions of PE/PA6/PE-MAH=60/20/20 and PE/PA6/PE-g-MAH=40/20/40 as shown in *Figure 8.12*. This is due to the higher concentration of maleic anhydride and the resulting complete saturation and reaction at the interface with PA6.

FTIR studies were performed for quantifying the effect of CO_2 on the reaction conversion. Generally, the MAH conversion in the tandem system was about 60% regardless of the CO_2 concentration. Thus, no significant effect was observed by varying the CO_2 concentration in PE/PA6/PE-MAH=60/20/20 and PE/PA6/PE-g-MAH=40/20/40 blends. This may be explained using the same reason used in the morphological study above. The blend having PE/PA6/PE-MAH=75/20/5 was also analyzed. However, it was very difficult to detect the anhydride peak at 1792 cm^{-1} due to the low concentration of PE-g-MAH.

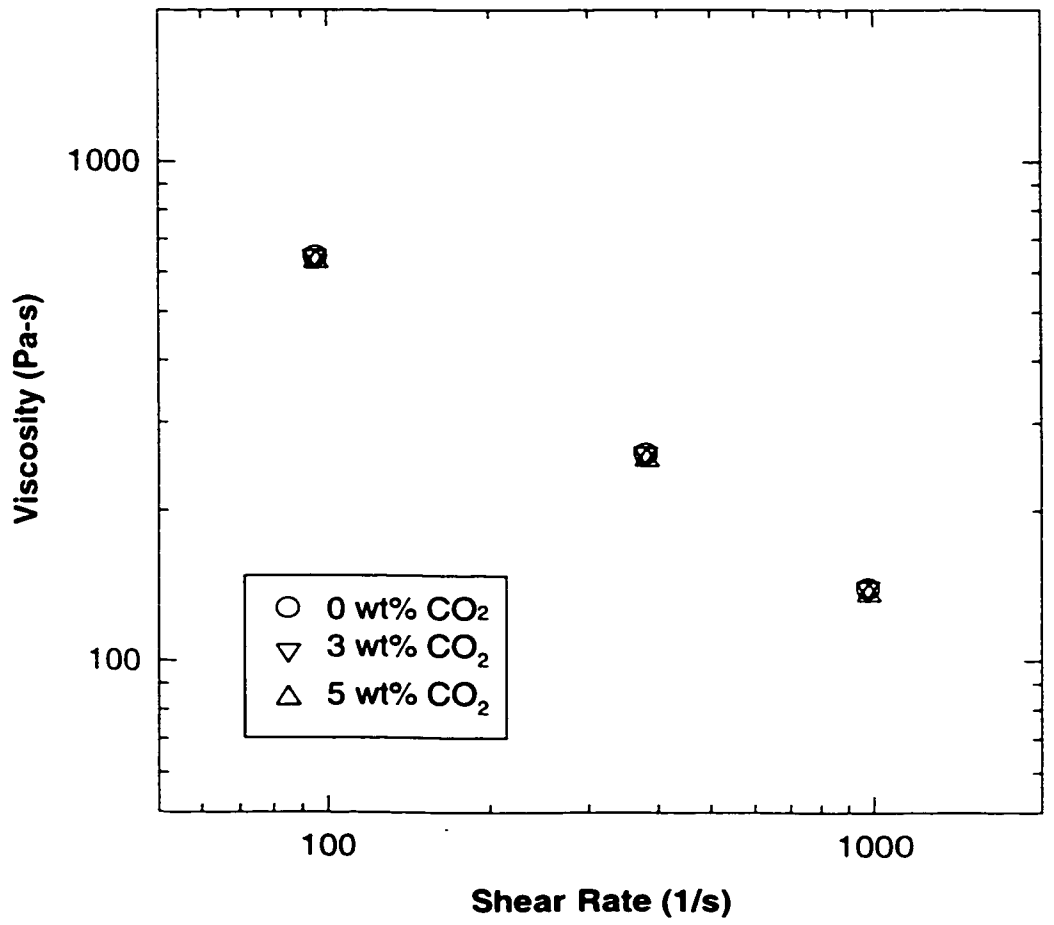

Figure 8.10. Viscosities of PE/PA6/PE-g-MAH=40/20/40 blend at various Concentrations of CO_2 (after devolatilization)

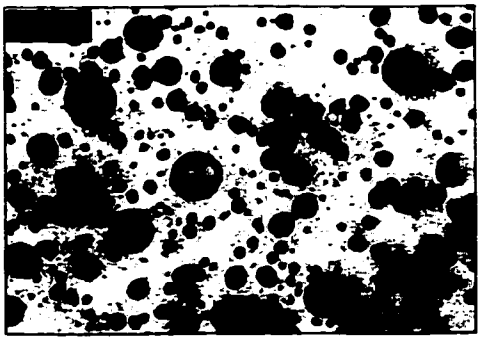

(a)

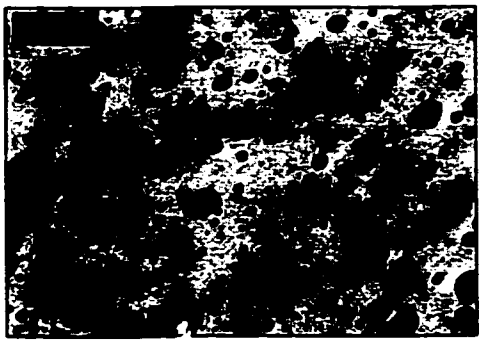

(b)

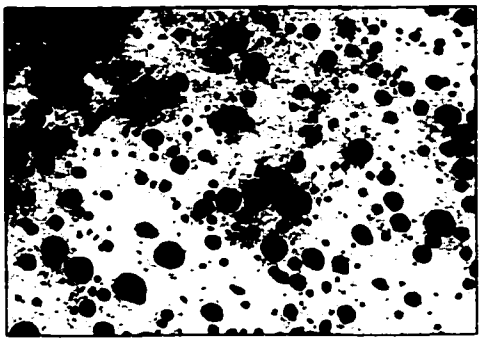

(c)

Figure 8.11. TEM photographs of PE/PA6/PE-g-MAH=75/20/5 blends at various concentrations of CO_2 (CO_2 concentration based on the amount of PE-g-MAH)
(a) 0 wt% (b) 3 wt% (c) 5 wt%

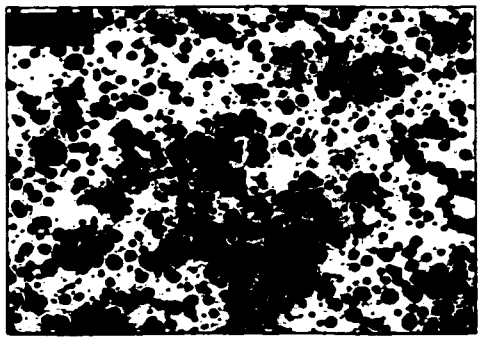

(a)

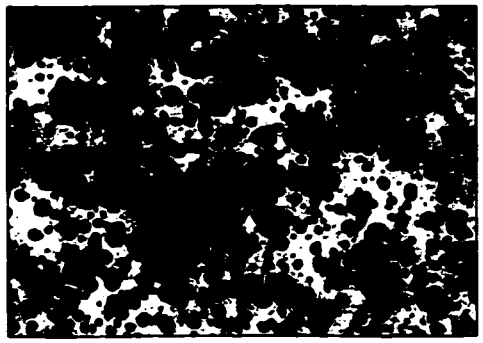

(b)

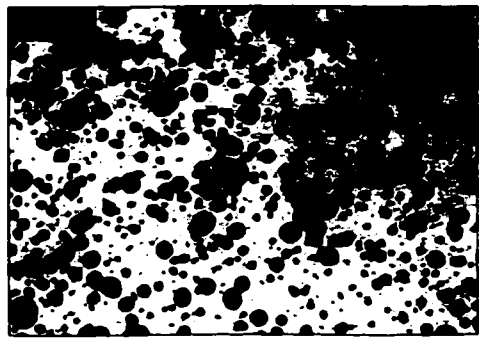

(c)

Figure 8.12. TEM photographs of PE/PA6/PE-g-MAH=60/20/20 blends at various concentrations of CO_2 (CO_2 concentration based on the amount of PE-g-MAH) (a) 0 wt% (b) 3 wt% (c) 5 wt%

8.5. CONCLUDING REMARKS

Reactive PE/PA6/PE-g-MAH blends were studied using a twin/single tandem extrusion system in the presence of supercritical carbon dioxide. From the preliminary study using a batch mixer, the reaction mechanism and the effect of PE-g-MAH on the morphology were discussed. It was found that both the MAH conversion and the motor torque were rapidly increased in the early state of mixing.

Effects of PE-g-MAH and the injected carbon dioxide on the morphology and the viscosity of the blends were investigated using a twin/single screw tandem system equipped with a devolatilization zone and a wedge die. It was found that the addition of a small amount of PE-g-MAH to PE/PA6 blends causes rapid increase of the blend viscosity, due to the reaction between PA6 and PE-g-MAH. However, an effect of the injected CO_2 on the blend viscosity after the devolatilization was not observed for all blending compositions investigated in this experiment. The size of the dispersed PA6 phase decreased by increasing the concentration of PE-g-MAH concentration. It was also found that the injected CO_2 affects the size of the dispersed phase only at low concentrations of PE-g-MAH (5 wt%).

CHAPTER 9. CONCLUSIONS AND RECOMMENDATIONS

9.1. CONCLUSIONS

This thesis has demonstrated the extrusion of PS, PE/PS blends, and PE/PA6/PE-g-MAH blends in the presence of supercritical CO_2 using various extrusion systems. The solubility of CO_2 in PS and PE was estimated using Henry's law as a first approximation. A higher solubility of CO_2 was observed in polyethylene than in polystyrene. The S-L EOS theory was also used not only for estimating the properties of pure component parameters of PS and CO_2, but also for predicting the solubility isotherm and the solution density. It should be noted that the density variation of the solution by changing the interaction parameter is small at the low concentrations of CO_2.

Based on the estimated CO_2 solubilities and the polymer / CO_2 density values, on-line measurement of the polymer / SCF solution viscosities was carried out. A theoretical model was proposed to describe the solution viscosities, specifically PS/CO_2 solution viscosities. In order to model the shear thinning behavior of the viscosity, the Cross, Carreau and generalized Cross-Carreau viscosity models were used. A generalized Arrhenius equation for describing the zero shear viscosity was proposed as a function of temperature, pressure, and CO_2 concentration. The generalized C-C model gives the best description of the viscosity behavior of PS melts and PS/CO_2 solutions. By analyzing the sensitivity of each term using the generalized Arrhenius equation, the effects of individual parameters such as temperature, pressure, concentration of CO_2 and their interactions were elucidated. The 1^{st} order terms of all parameters and the 2^{nd} order term of pressure including the interaction terms had significant effects on the zero shear viscosity under these experimental conditions.

The effects of dissolved supercritical CO_2 on the rheological and morphological properties were investigated for non-reactive PE/PS blends and for reactive PE/PA6 blends using various extrusion systems such as twin-screw and twin / single tandem extruders. In case of non-reactive PE/PS blends, a considerable reduction in the viscosity was observed when CO_2 was dissolved in the blends. The cell structure of foamed filaments was observed at various contents of CO_2 and pressures. The cell structure of the PE/PS blends showed the same behavior observed for pure polymers. Higher operating pressures and CO_2 content led to smaller cell size and it was found that CO_2 cells produced elongated cylindrical PS domains. The size and shape of the dispersed PS phase were also investigated, and while the size of these PS domains decreased by increasing the CO_2 content, it was not affected by the operating die pressure. The PE/PS blending morphology was also investigated without any foaming process using a twin / single tandem extruder having devolatilization zone. The size of the dispersed PS domain in the (PS/CO_2)/PE blending system also decreased when 5 wt% of CO_2 in PS was injected. However, no further decrease was observed by increasing the concentration of CO_2 up to 10 wt%. This behavior was discussed using a solubility limit and a viscosity ratio. The phase separation due to the skin-core effect was significant when CO_2 was used. The behaviors of the dispersed phase and the skin-core phase separation were qualitatively explained using the changed viscosity ratio of two polymers and possible effects of interfacial tension due to the dissolution of CO_2. However, there could have been a formation of a complete miscible solution due to existence of CO_2 in the blend of PE and PS. However, further studies are required. In general, the mixing between polyethylene and polystyrene was improved by dissolving CO_2.

Effects of CO_2 on the morphology and the viscosity of reactive blends were investigated using a twin / single screw tandem system equipped with a devolatilization zone and a wedge die. During the extrusion, it was found that the barrel pressure at the high pressure mixing section of the twin-screw extruder was significantly reduced by increasing the concentration of CO_2. The reduced pressure generated reflects the viscosity reduction in the mixing section. Therefore, It is expected that the viscosity reduction affects the mixing performance and the final blend viscosity. However, no CO_2 effect on the viscosity was observed after the devolatilization. The size of the dispersed PA6 phase decreased by increasing the concentration of PE-g-MAH concentration. It was also found that the injected CO_2 affects the size of the dispersed phase only at the low concentration of PE-g-MAH.

9.2. RECOMMENDATIONS

Relatively little work has been performed in the polymer processing areas using SCFs in spite of their usefulness. Many research works and industrial applications have mainly focused on the foaming process, specifically microcellular foaming process. However, the SCFs might be used for various purposes in the field of polymer processing due to their unique characteristics. Based on the knowledge obtained from experiments in this thesis, several recommendations at both academic and industrial viewpoints can be addressed.

From an academic point of view, the effects of SCFs on the surface or interfacial tension between polymer / SCF and polymer / polymer / SCF solutions might be a crucial factor. As indicated in Taylor's formula, *Eq. (2-20)*, and an equation proposed by Wu, *Eq. (2-21)*, the interfacial tension has been emphasized as one of the major factors affecting the

blending morphology. Zero surface tension of SCFs has been known. Therefore, the surface tension of a polymer should be varied by dissolving a SCF.

The phase behaviors of polymer / SCF mixtures should be an important factor in the blending process. Extensive study has been carried about the polymer / polymer phase behaviors including binary and ternary blending systems. However, the binary or ternary polymer blends dissolving a SCF, for instance, a PE/PS/CO_2 blend, have not been clearly clarified yet. The miscibility of the binary polymer blend can be affected by dissolving a SCF and the final blending morphology might be changed.

From an industrial point of view, it was found that a less motor power was required at the same polymer throughput when supercritical CO_2 was introduced. This phenomenon will be associated with the lubrication effect of CO_2 as well as the viscosity reduction investigated in this thesis. Less power consumption offers great advantages to the production scale extrusion.

The injection of SCF during the extrusion also gives color stability. Even though this phenomenon was not mentioned in this thesis, the improvement of color stability was verified for PS/CO_2 system at high temperature, 270°C. The stability might be related to the same reasons explained in the previous paragraph, the external lubricating effect of CO_2 between the extruder barrel and polymer melt and the lower viscous dissipation. The color stability can be used in the extrusion of poly(methyl methacrylate) and polycarbonate, which mainly applied for optical purpose.

For a better understanding the effects of a SCF on the blending morphology in polymer blends, several factors which would affect the dispersed phase behavior should be investigated. First, the elasticity of polymer / CO_2 is needed to be clarified. It has been

known that the elasticity of the matrix and the dispersed phase affect the drop size (Vanoene, 1972, Ghodgaonkar and Sundararaj, 1996, Levitt et al., 1996). However, the elasticity of polymer / CO_2 solutions has not been measured yet. The elasticity is related to the entrance pressure drop which can be measured through a sudden contraction in a capillary and slit dies. Second, an elongational flow of droplets during the expansion of dissolved CO_2 should be considered. Dispersed particles dissolving CO_2 experience the volume expansion during the foaming process, and the precipitation of CO_2 inside the particles leads to the volume expansion resulting in the elongational flow. Elongational rate and stress depend on the CO_2 concentration as well as the foaming rate. Therefore, studies about the foaming behaviors and the droplet deformation will provide a better explanation of the dispersed behaviors in polymer blends.

CHAPTER 10. REFERENCES

Aref-Azar, A., J. N. Hay, B. J. Marsden, and N. Walker, "Crystallization Characteristics of Polymer Blends. I. Polyethylene and Polystyrene", *J. Polym. Sci., Polym Phys.*, **18**, 637-643 (1980)

Astarita, G., M. E. Paulaitis and R. G. Wissenger, "Thermodynamics of the Glass Transition", *J. Polym. Sci. Part B*, **27**, 2105-2116 (1989)

Bae, Y. C. and E. Gulari, "Viscosity Reduction of Polymeric Liquid by Dissolved Carbon Dioxide", *J. Appl. Polym. Sci.*, **63**, 459-466 (1997)

Bagley, E. B., " End Corrections in the Capillary Flow of Polyethylene", *J. Appl. Phys.*, **28**, 624 (1957)

Baker, W. E. and M. Saleem, " Polystyrene-Polyethylene Melt Blends Obtained Through Reactive Mixing Process", *Polym. Eng. Sci.*, **27**, 1634-1641 (1987)

Baker, F. S. and M. Thomas, "The Effect of Hydrostatic Pressure on the Flow Properties of Various Polymers", *Makromol. Chem., Macromol. Symp.*, **28**, 13-24 (1993)

Baldwin, D. F., C. B. Park. and N. P. Suh, "An Extrusion System for the Processing of Microcellular Polymer Sheets: Shaping and Cell Growth Control", *Polym. Eng. Sci.*, **36**, 1425-1435 (1996a)

Baldwin, D. F., C. B. Park. and N. P. Suh, "A Microcellular Processing Study of Poly(Ethylene Terephthalate) in the Amorphous and Semicrystalline States. Part I: Microcell Nucleation", *Polym. Eng. Sci.*, **36**, 1437-1445 (1996b)

Baldwin, D. F., C. B. Park. and N. P. Suh, "A Microcellular Processing Study of Poly(Ethylene Terephthalate) in the Amorphous and Semicrystalline States. Part II: Cell Growth and Process Design", *Polym. Eng. Sci.*, **36**, 1446-1453 (1996c)

Ban, L. L. M. J. Doyle, M. M. Disko and G. R. Smith, "Morphology of Ethylene-co-Propylene Rubber-Modified Nylon 66 Blends", *Polym. Comm.*, **29**, 193-166 (1988)

Barentsen, W. M. and D. Heikens, "Mechanical Properties of Polystyrene / Low Density Polyethylene Blends", *Polymer*, **14**, 579-583 (1998)

Beckman, E. J. and R. S. Porter, *J. Polym. Sci., Part B*, **25**, 1511 (1987)

Beckman, E. J. and R. D. Smith, "Phase Behavior of Inverse Microemulsions for the Polymerization of Acrylamide in Near-Critical and Supercritical Continuous Phases", *J. Phys. Chem.*, **94**, 345-350 (1990)

Berens, A. R., G. S. Huvard, R. W. Korsmeyer and F. W. Kunig, "Application of Compressed Carbon Dioxide in the Incorporation of Additives into Polymers", ", *J. Appl. Polym. Sci.*, **46**, 231-242 (1992)

Bersted, B. H., "Refinement of the Converging Flow Method of Measuring Extensional Viscosity in Polymers", *Polym. Eng. Sci.*, **33**, 1079-1083 (1993)

Bigg, D. M., J. R. Preston and D. Brenner, "An Experimental Technique for Predicting Foam Processibility and Physical Properties", *Polym. Eng. Sci.*, **16**, 706-711 (1976)

Binding, D. M. and D. M. Jones, "On the Interpretation of Data from Converging Flow Rheometers", *Rheol. Acta*, **28**, 215-222 (1989)

Bird, R. B., R. C. Armstrong and O. Hassager, "*Dynamics of Polymeric Liquids*", *Vol. 1*, John Wiley & Sons, New York (1987)

Blanks, R. F. and J. M. Prausnitz, "Thermodynamics of Polymer Solubility in Polar and Nonpolar Systems", *Ind. Eng. Chem. Fund.*, **3**, 1 (1964)

Blyler, L. L. Jr. and T. K. Kwei, "Flow Behavior of Polyethylene Melts Containing Dissolved Gases", *J. Polym. Sci., Part C, No35*, 165-176 (1971)

Bonner, D. C. and Y-I. Cheng, "A New Method for Determination of Equilibrium Sorption of Gases by Polymers at Elevated Temperature and Pressure", *J. Polym. Sci., Polym. Lett.*, **13**, 259-264 (1975)

Bonner, D. C., "Solubility of Supercritical Gases in Polymers - A Review", *Polym. Eng. Sci.* **17**, 65-72 (1977)

Bonner, J. G. and P. S. Hope, "Compatibilization and Reactive Blending", *Polymer Blends and Alloys*, M. J. Folkes and P. S. Hope (eds.), Blackie Academic & Professional, 46-74, (1993)

Borggreve, R. J. M., R. J. Gaymans and A. R. Luttmer, "Influence of Structure on the Impact Behaviour of Nylon-Rubber Blends", *Makromol. Chem., Macromol. Symp.*, **16**, 195-207 (1988)

Bourry, D. and B. D. Favis, "Morphology Development in a Polyethylene / Polystyrene Binary Blend During Twin-screw Extrusion", *Polymer*, **39**, 1851-1856 (1998)

Carreau, P. J., PhD Thesis, University of Wisconsin (1968)

Casale, A., R. C. Penwell and R. S. Porter, "The Influence of Pressure on the Capillary Flow of Poly(methyle methacrylate)", *Rheol. Acta*, **10**, 412-417 (1971)

Chapleau, N., B. D. Favis and P. J. Carreau, "Measuring the Interfacial Tension of Polymers in the Presence of an Interfacial Modifier: Migrating the Modifier to the Interface", *J. Polym. Sci., Part B*, **36**, 1947-1958 (1998)

Chin, H. B. and C. D. Han, "Studies on Droplet Deformation and Breakup: I. Droplet Deformation in Extensional Flow", *J. Rheol.*, **23**, 557-590 (1979)

Chiou, J. S., J. W. Barlow and D. R. Paul, "Plasticization of Glassy Polymers by CO_2", *J. Appl. Polym. Sci.*, **30**, 2633-2642 (1985)

Choi, S. Y., "Determination of Melt Viscosity as a Function of Hydrostatic Pressure in an Extrusion Rheometer", *J. Polym. Sci.*, Part A-2, **6**, 2043-2049 (1968)

Clifford, A., "Reactions in Supercritical Fluids", *Supercritical Fluid: Fundamentals for Applications*, E. Kiran and J. M. H. Levelt Senger (eds.), Kluwer Academic Publishers, 449-479 (1994)

Cogswell, F. N. and J. C. McGowan, "The Effects of Pressure and Temperature upon the Viscosities of Liquids with Special Reference to Polymeric Liquids", *Br. Polym. J.*, **4**, 183-198 (1972)

Cogswell, F. N., "Converging Flow of Polymer Melts in Extrusion Dies", *Polym. Eng. Sci.*, **12**, 64-73 (1972)

Colton, J. S. and N. P. Suh, "Nucleation of Microcellular Foam: Theory and Practice", *Polym. Eng. Sci.*, **27**, 500-503 (1987)

Cox, W. P. and E. H. Merz, *J. Polym. Sci.*, **28**, 619 (1958)

Cross, M. M., "Relation between Viscoelasticity and Shear-thinning Behavior in Liquid", *Rheol. Acta*, **18**, 609-614 (1979)

Dagli, S. S., M. Xanthos and J. A. Biesenberger, "Kinetic Studies and Process Analysis of the Reactive Compatibilization of Nylon 6 / Polypropylene Blends", *Polym. Eng. Sci.*, **34**, 1720-1730 (1994)

Daneshvar, M. and E. Gulari, "Supercritical Fluid Fractionation of Poly(ethylene glycol)", *J. Supercrit. Fluids*, **5**, 143-150 (1992)

de Filippi, R. P., V. J. Krukonis, R. J. Robey and M. Modell, "Supercritical Fluid Regeneration of Activated Carbon for Adsorption of Pesticides", *Report EPA-600/2-80054*, March (1980)

Dealy, J. M. and K. F. Wissburn, "Melt Rheology and its Role in Plastics Processing", Van Nostrand Reinhold (1990)

Debenedetti, P. G., "Supercritical Fluids as Particle Formation Media", *Supercritical Fluid: Fundamentals for Applications*, E. Kiran and J. M. H. Levelt Senger (eds.), Kluwer Academic Publishers, 719-729 (1994)

Dey, S. K., C. Jacob and J. A. Biesenberger, "Effect of Physical Blowing Agents on Crystallization Temperature of Polymer Melts", *SPE ANTEC Tech. Papers*, 2197-2198 (1994)

Dey, S. K., P. Natarajan, M. Xanthos and M. D. Braathen, "Use of Inert Gases in Extruded Medium Density Polypropylene Foams", *SPE ANTEC Tech. Papers*, 1955-1958 (1996)

Doolittle, A. K., "Studies in Newtonian Flow. II. The Dependence of the Viscosity of Liquids on Free Space", *J. Appl. Phys.*, **22**, 1471-1475 (1951)

Doroudiani, S., C. B. Park, and M. T. Kortschot, "Effect of the Crystallinity and Morphology on the Microcellular Foam Structure of Semicrystalline Polymers", *Polym. Eng. Sci.*, **36**, 2645-2662 (1996)

Draper, N. R. and H. Smith, "Applied Regression Analysis", 3rd ed., John Wiley and Sons, Inc., New York (1998)

Driscoll, P. D. and D. C. Bogue, "Pressure Effect in Polymer Melt Rheology", *J. Appl. Polym. Sci.*, **39**, 1755-1768 (1990)

Durrill, P. L. and R. G. Griskey, "Diffusion and Solution of Gases in Thermally Softened or Molten Polymers: Part I. Development of Technique and Determination of Data", *AIChE J*, **12**, 1147-1151 (1966)

Durrill, P. L. and R. G. Griskey, "Diffusion and Solution of Gases in Thermally Softened or Molten Polymers: Part II. Relation of Diffusivities and Solubilities with Temperature Pressure and Structural Characteristics", *AIChE J*, **15**, 106-110 (1969)

Duvdevani, I. J. and I. Klein, "Analysis of Polymer Melt Flow in Capillaries Including Pressure Effects", *SPE Journal*, Dec., 41-45 (1967)

Elkovitch, M. D., L. J. Lee and D. L. Tomasko, "Polymer Blending with the Addition of Supercritical Carbon Dioxide", *Proc. 13th PPS Annual Meeting*, 6-F (1997)

Elkovitch, M. D., L. J. Lee and D. L. Tomasko, "Supercritical Fluid Assisted Polymer Blending", *SPE ANTEC Tech. Papers*, 2538-2541 (1998)

Elmgren, H, *J. Polym. Sci., Polym. Lett.*, **18**, 339 (1980)

Favis B. D., J. P. Chalifoux and P. van Gheluwe, "Factors Controlling the Dimension of the Phase in Polypropylene / Polycarbonate Blends", *SPE ANTEC Tech. Papers*, 1326-1333 (1987)

Favis, B. D. and J. P. Chalifoux, "The Effect of Viscosity Ratio on the Morphology of Polypropylene / Polycarbonate Blends During Processing", *Polym. Eng. Sci.*, **27**, 1591-1600 (1987)

Fleming, G. K. and W. J. Koros, "Dilatation of Polymers by Sorption of Carbon Dioxide at Elevated Pressure. 1. Silicone Rubber and Unconditioned Polycarbonate", *Macromolecules*, **19**, 2285-2291 (1986)

Flory, P. J., "Thermodynamics of High Polymer Solutions", *J. Chem. Phys.*, **10**, 51-61 (1942)

Flory, P. J., *J. Am. Chem. Soc.*, **87**, 1833 (1965)

Forsyth, T. H., "Converging Flow of Polymers", *Polym-Plast. Technol. Eng.*, **6**(1), 101-131 (1976)

Fox, T. G. and P. J. Flory, "Second-Order transition Temperatures and Related Properties of Polystyrene. I. Influence of Molecular Weight", *J. Appl. Phys.*, **21**, 581-591 (1950)

Garg, A, "Thermodynamics of Polymer Melts Swollen with Supercritical Gases", Ph. D. dissertation, Wayne State University (1993)

Garg, A., E. Gulari and C. W. Manke, "Thermodynamics of Polymer Melts Swollen with Supercritical Gases", *Macromolecules*, **27**, 5643-5653 (1994)

Gendron, R., L. E. Daigneault and L.-M. Caron, "Rheological Behavior of Polystyrene/Blowing Agent Mixtures", *SPE ANTEC Tech. Papers*, 1118-1122 (1996)

Gendron, R. and L. E. Daigneault, "Rheological Behavior of Mixtures of Various Polymer Melts with CO_2", *SPE ANTEC Tech. Papers*, 1096-1100 (1997)

Gerhardt, L. J., A. Garg, Y. C. Bae, C. W. Manke and E. Gulari, *Proceedings of the XIth International Congress on Rheology*, 348 (1992)

Gerhardt, L. J., "A Rheological Investigation of Poly(dimethylsiloxane) Swollen with Supercritical Carbon Dioxide", Ph. D. dissertation, Wayne State University (1994)

Gerhardt, L. J., A. Garg, C. W. Manke and E. Gulari, "Supercritical Fluids as Polymer Processing Aids", *Proceedings of 3rd International Symposium on Supercritical Fluids*, **3**, 265-270 (1994)

Gerhardt, L. J., C. W. Manke and E. Gulari, "Rheology of Polydimethylsiloxane Swollen with Supercritical Carbon Dioxide", *J. Polym. Sci.*, Part B, **35**, 523-534 (1997)

Ghodgaonkar, P. G. and U. Sundararaj, "Prediction of Dispersed Phase Drop Diameter in Polymer Blends: the Effect of Elasticity", *Polym. Eng. Sci.*, **36**, 1656-1665 (1996)

Goel, S. K. and E. J. Beckman, "Generation of Microcellular Polymeric Foams Using Supercritical Carbon Dioxide. I: Effect of Pressure and Temperature on Nucleation", *Polym. Eng. Sci.*, **34**, 1137-1147 (1994a)

Goel, S. K. and E. J. Beckman, "Generation of Microcellular Polymeric Foams Using Supercritical Carbon Dioxide. II: Cell Growth and Skin Formation", *Polym. Eng. Sci.*, **34**, 1148-1156 (1994b)

Goldblatt, P. H. and R. S. Porter, "A Comparison of Equations for the Effect of Pressure on the Viscosity of Amorphous Polymers", *J. Appl. Polym. Sci.*, **20**, 1199-1208 (1976)

Gonzalez-Montiel, A., H. Keskkula and D. R. Paul, "Impact-Modified Nylon 6 / Polypropylene Blends: 1. Morphology-Property Relationships", *Polymer*, **36**, 4587-4603 (1995)

Gorski, R. A., R. B. Ramsey and K. T. Dishart, "Physical Properties of Blowing Agent Polymer System - I. Solubility of Fluorocarbon Blowing Agents in Thermoplastic Resins", *Proc. SPI 29th Ann. Tech. Mark. Conf.*, 286-299 (1983)

Guzman, J. de, *An. R. Soc. Esp. Fis. Quim.*, **11**, 353 (1913)

Han, C. D. and T. C. Yu, "Rheological Properties of Molten Polymers. II. Two-Phase Systems", *J. Appl. Polym. Sci.*, **15**, 1163-1180 (1971)

Han, C. D. and Y. W. Kim, "Dispersed Two-Phase Flow of Viscoelastic Polymeric Melts in a Circular Tube", *Trans. Soc. Rheol.*, **19**:2, 245-269 (1975)

Han, C. D., "Rheology in Polymer Processing", Academic Press, New York (1976)

Han, C. D. and C. A. Villamizar, "Studies on Structural Foam Processing. I. The Rheology of Foam Extrusion", *Polym. Eng. Sci.*, **18**, 687-698 (1978)

Han, C. D., "Multiphase Flow in Polymer Processing", Academic Press, New York (1981)

Han, C. D. and C.-Y. Ma, "Rheological Properties of Mixtures of Molten Polymer and Fluorocarbon Blowing Agent. I. Mixtures of Low-Density Polyethylene and Fluorocarbon Blowing Agent", *J. Appl. Polym. Sci.*, **28**, 831-850 (1983a)

Han, C. D. and C.-Y. Ma, "Rheological Properties of Mixtures of Molten Polymer and Fluorocarbon Blowing Agent. II. Mixtures of Polystyrene and Fluorocarbon Blowing Agent", *J. Appl. Polym. Sci.*, **28**, 851-860 (1983b)

Han, C. D. and C.-Y. Ma, "Foam Extrusion Characteristics of Thermoplastic Resin with Fluorocarbon Blowing Agent. I. Low Density Polyethylene Foam Extrusion", *J. Appl. Polym. Sci.*, **28**, 2961-2982 (1983c)

Hannay, J. B. and J., Hogarth. "On the Solubility of Solids in Gases", *Proc. R. Soc. London*, **29**:324 (1879)

Hansen, C. M., *J. Paint Technol.*, **39**, 104, 505, 511 (1967)

Harrats, C., S. Blacher, R. Fayt, R. Jerome and P. Teyssie, "Molecular Design of Multicomponent Polymer System XIX: Stability of Cocontinuous Phase Morphologies in Low-Density Polyethylene-Polystyrene Blends Emulsified by Block Copolymers", *J. Polym. Sci.*, Part B, **33**, 801-811 (1995)

Heikens, D., N. Hoen, P. Barentsen, P. Piet and H. Ladan, "Mechanical Properties and Morphology of Copolymer Modified Polymer Blends", *J. Polym. Sci.,Polym. Symposium*, **62**, 309-341 (1978)

Hieber C. A. and H. H. Chiang, "Shear-Rate-Dependence Modeling of Polymer Melt Viscosity", *Polym. Eng. Sci.*, **32**, 931-938 (1992)

Hietaoja, P. T., R. M. Holsti-Miettinen, J. V. Seppala and O. T. Ikkala, "The effect of Viscosity Ratio on the Phase Inversion of Polyamide 66 / Polypropylene Blends", *J. Appl. Polym. Sci.*, **54**, 1613-1623 (1994)

High, M. S. and R. P. Danner, "A Group Contribution Equation of State for Polymer Solutions", *Fluid Phase Equil.*, **53**, 323 (1989)

High, M. S. and R. P. Danner, "Application of the Group Contribution Lattice-Fluid EOS to Polymer Solutions", *AIChE J.*, **36**, 1625 (1990)

Hildebrand, J. H. and R. L. Scott, "Regular Solutions", Prentice-Hall, Englewood Cliffs, NJ (1962)

Hobbs, S. Y., R. C. Bopp and V. H. Watkins, "Toughened Nylon Resins", *Polym. Eng. Sci.*, **23**, 380-389 (1983)

Huggins, M. L., "Thermodynamic Properties of Long Chain Compounds", *Ann. N. Y. Acad. Sci.*, **43**, 1-32 (1942)

Ide, F. and A. Hasegawa, "Studies on Polymer Blend of Nylon 6 and Polypropylene or Nylon 6 and Polystyrene Using the Reaction of Polymer", *J. Appl. Polym. Sci.*, **18**, 963-974 (1974)

Jacob, C. and S. K. Dey, "Inert Gases as Alternative Blowing Agents for Extruded Low-Density Polystyrene Foam", *SPE ANTEC Tech. Papers*, **40**, 1964-1967 (1994)

Jacob, C. and S. K. Dey, "Inert Gases as Alternative Blowing Agents for Extruded Low-Density Polystyrene Foam", *SPE ANTEC Tech. Papers*, 1964-1967 (1994); *J. Cellular. Plast.*, **31**, 38-47 (1995)

Johnston, K. P. and J. M. L. Penninger, *ACS Symposium Series 406, Supercritical Fluid Science and Technology* (1989)

Kadijk, S. E. and B. H. A. A. Van den Brule, "On the Pressure Dependency of the Viscosity of Molten Polymers", *Polym. Eng. Sci.*, **34,** 1535-1546 (1994)

Kamal, M. R. and H. Nyun, "The Effect of Pressure on the Shear Viscosity of Polymer Melt", *Trans. Soc. Rheol.*, **17:2**, 271-285 (1973)

Kamiya, Y., K. Mizoguchi, K. Terada, Y. Fujiwara and J-S. Wang, "CO_2 Sorption and Dilatation of Poly(methyl methacrylate), *Macromolecules*, **31**, 472-478 (1998)

Kato, S., Y. Tsujita, H. Yoshimizu and T. Kinoshita, "Characterization and CO_2 Sorption Behavior of Polystyrene / Polycarbonate Blend System", *Polymer*, **38**, 2807-2811 (1997)

Kelley, F. N. and F. Bueche, "Viscosity and Glass Temperature Relations for Polymer-Diluent Systems", *J. Polym. Sci.*, **50**, 549-556 (1961)

Kim, K. U. and B. C. Kim, "Rheological Measurements of Rigid Foam Extrusion", *in Two Phase Polymer Systems*, L. A. Utraki., ed. Munich, Hanser 138-163 (1991)

Kiran, E., "Polymer Formation, Modification and Processing in or with Supercritical Fluid", *Supercritical Fluid: Fundamentals for Applications*, E. Kiran and J. M. H. Levelt Senger (eds.), Kluwer Academic Publishers, 541-588 (1994)

Kiszka, M. B., M. A. Meilchen and M. A. McHugh, "Modeling High-Pressure Gas-Polymer Mixtures Using Sanchez-Lacombe Equation of State", *J. Appl. Polym. Sci.*, **36**, 583-597 (1988)

Krukonis, V. J., "Supercritical Fluid Nucleation of Difficult-to-Comminute Solids", AIChE Fall Meeting, San Fransisco, CA, paper 140f (1984)

Kumar, S. K. and U. W. Suter, "Precipitation Polymerization of Styrene in Supercritical Ethane", *ACS Polym. Preprint*, **28**, 286-287 (1987)

Kumar, V. and N. P. Suh, "A Processing for Making Microcellular Thermoplastic Parts", *Polym. Eng. Sci.*, **30**, 1323-1330 (1990)

Kumar, V. and O. S. Gebizlioglu, "Thermal and Microscopy Studies of CO_2-Induced Morphology in Crystalline PET Foams", *SPE ANTEC*, 1536-1540 (1992)

Kung, E. A. J. Lesser and T. J. McCarthy, "Mechanical Properties of Polystyrene / Polyethylene Blends Prepared Using Supercritical CO_2 Processing", *ACS Polym. Preprint*, Vol-2, 462-163 (1997)

Kwag, C., L. J. Gerhardt, V. Khan, E. Gulari and C. W. Manke, "Plasticization of Polymer Melts with Dense or Supercritical CO_2", *Meetings of the ACS, Polymeric Materials Science and Engineering Div.*, 183-185 (1996)

Kwon, T. H., S. F. Shen and K. K. Wang, "Pressure Drop of Polymeric Melts in Conical Converging Flow: Experiments and Predictions", *Polym. Eng. Sci.*, **26**, 214-224 (1986)

Lavallee C. and B. D. Favis, "Morphology of Reactive Polyamide / Polyethylene Copolymer Blends and Preparation of Composite Droplet Morphologies", *SPE ANTEC Tech. Papers*, 973-977 (1991)

Lee, B.-L. and J. L. White, "Experimental Studies of Disperse Two-Phase Flow of Molten Polymers Through Dies", *Trans. Soc. Rheol.*, **19**:3, 481-492 (1975)

Lee, J-D. S-M. Yang, "Effects of Mixing Procedures on Properties of Compatibilized Polypropylene / Nylon 6 Blends", *Polym. Eng. Sci.*, **35**, 1821-1833 (1995)

Lee, M., C. B. Park and C. Tzoganakis, "On-Line Measurement of PS/CO_2 Solution Viscosities", *SPE ANTEC Tech. Papers*, 1991-1995 (1997)

Lee, M., C. Tzoganakis and C. B. Park, "Extrusion of PE/PS Blends with Supercritical Carbon Dioxide", *Polym. Eng. Sci.*, **38**, 1112-1120 (1998)

Lee, M., C. B. Park and C. Tzoganakis, "Measurements and Modeling of PS/Supercritical CO_2 Solution Viscosities", *Polym. Eng. Sci.*, **39**, 99-109 (1999)

Lee, S-T., "Shear Effects on Thermoplastic Foam Nucleation", *Polym. Eng. Sci.*, **33**, 418-422 (1993)

Lee, S-T, "Gas Loss During Foam Sheet Formation", *SPE ANTEC Tech. Papers*, 2217-2224 (1995)

Lee, S-T., "Fundamental Study of Foaming with Physical Blowing Agent", *ACS Polym. Preprint*, **37**, 791-792 (1996)

Lenk, R. S., "Pressure Drop Through Tapered Dies", *J. Appl. Polym. Sci.*, **22**, 1775-1779 (1978)

Lenk, R. S. and G. Slater, "Pressure Drop Through a Tapered Die With Optimized Flow Characteristics", *J. Appl. Polym. Sci.*, **23**, 2793-2802 (1979)

Lenk, R. S. and R. A. Frenkel, "Pressure Drop Through Tapered Wide Slit Dies. A Revised Version", *J. Appl. Polym. Sci.*, **26**, 2801-2804 (1981)

Leonov, A. I., "Nonequilibrium Thermodynamics and Rheology of Viscoelastic Polymer Media", *Rheol. Acta*, **15**, 85-98 (1976)

Leonov, A. I., E. H. Lipkina, E. D. Paskhin, and A. N. Prokunin, "Theoretical and experimental investigation of Shearing in Elasic Polymer Liquids", *Rheol. Acta*, **15**, 411-426 (1976)

Leonov, A. I., and A. N. Prokunin, "An Improved Simple Version of a Nonlinear Theory of Elasto-viscous Polymer Media", *Rheol. Acta*, **19**, 393-403 (1980)

Levelt Sengers, J. M. H. and W. T. Chen, "Vapor Pressure, Critical Isochore and Some Metastable States of CO_2", *J. Chem. Phys.*, **56**, 595-608 (1972)

Levenberg, K., *Quart. Appl. Math.*, **2**, 164 (1944)

Levitt, L., C. W. Macosko and S. D. Pearson, "Influence of Normal Stress Difference on Polymer Drop Deformation", *Polym. Eng. Sci.*, **36**, 1647-1655 (1996)

Li, T., V. A. Topolkaraev, A. Hiltner, E. Bear, X. Z. Ji and R. P. Quirk, "block Copolymers as Compatibilizers for Blends of Linear Low Density Polyethylene and Polystyrene", *J. Polym. Sci.*, Part B, **33**, 667-683 (1995)

Lodge, A. S. and L. de Vargas, "Positive Hole Pressure and Negative Exit Pressures Generated by Molten Polyethylene Flowing Through a Slit Die", *Rheol. Acta*, **22**, 583-587 (1983)

Lundberg, J. L. and Mooney E. J., "Diffusion and Solubility of Methane in Polyisobutylene", *J. Polym. Sci, Part A-2*, **7**, 947-962 (1969)

Ma, C.-Y. and C. D. Han, "Foam Extrusion Characteristics of Thermoplastic Resin with Fluorocarbon Blowing Agent. II. Polystyrene Foam Extrusion", *J. Appl. Polym. Sci.*, **28**, 2983-2998 (1983c)

Madge, E. W., "Latex Foam Rubber", John Wiley & Sons, New York (1962)

Marechal, P, G. Coppens, R. Legras and J-M. Dekoninck, "Amine / Anhydride Reaction Versus Amide / Anhydride Reaction in Polyamide / Anhydride Carriers", *J. Polym. Sci.*, Part A, 33, 757-766 (1995)

Marquardt, D.W., *J. Soc. Indust. Appl. Math.*, **11**, 431 (1963)

Martini-Vvedensky, J. E., N. P. Suh, and F. A. Waldman, "Microcellular Closed Cell Foams and Their Method of Manufacture", USP 4473665 (1984)

Matheson, A. J., "Role of Free Volume in the Pressure Dependence of the Viscosity of Liquids", *J. Chem. Phys.*, **44**, 695-699 (1966)

Maxwell, B. and A. Jung, *Modern Plastics*, **25**, 174 (1957)

McHugh, M. A. and V. J. Krukonis, "Supercritical Fluids", *Encyclopedia of Polymer Science and Technology*, H. F. Mark, N. M. Bikales, C. G. Overberger and G. Menges (eds.) Wiley-Interscience, New York, Vol. **16**, 368-399 (1989)

McHugh, M. A. and V. J. Krukonis, "Supercritical Fluid Extraction: Principles and Practice", 2 eds., Butterworth-Heinemann, Boston (1994)

Mendelson, R. A., "A Method for Viscosity Measurements of Concentrated Polymer Solutions in Volatile Solvent at Elevated Temperatures", *J. Rheol.*, **23**, 545-556 (1979)

Mendelson, R. A., "Concentrated Solution Viscosity Behavior at Elevated Temperatures-Polystyrene in Ethylbenzene", *J. Rheol.*, **24**, 765-781 (1980)

Michels, A. and C. Michels, "Isotherms of CO_2 Between 0° and 150° and Pressures from 16 to 250 Atm (Amagat Densities 18-206)", *Proc. R. Soc, Ser. A*, **153**, 201-214 (1936)

Michels, A. and C. Michels, "Series Evaluation of the Isotherm Data of CO_2 between 0° and 150°C and up to 3000 atm", *Proc. R. Soc, Ser. A*, **160**, 348-357 (1937)

Michels, A., C. Michels and H. Wouters, "Isotherms of CO_2 Between 70 and 3000 Atmospheres (Amagat Densities between 200 and 600)", *Proc. R. Soc, Ser. A*, **153**, 214-224 (1936)

Michels, A., B. Blaisse and C. Michels, "The Isotherm of CO_2 in the Neighbourhood of the Critical Point and Round the Coexistence Line", *Proc. R. Soc, Ser. A*, **160**, 358-375 (1937)

Miller, A. A., "Analysis of the Melt Viscosity and Glass Transition of Polystyrene", *J. Polym. Sci.*, Part A-2, **6**, 1161-1175 (1968)

Miller, A. A., "Pressure Coefficients for Newtonian Viscosity of Polymeric Liquids", *Macromolecules*, **4**, 757-761 (1971)

Min, K., J. L. White and J. F. Fellers, "High Density Polyethylene/Polystyrene Blends: Phase Distribution Morphology, Rheological Measurements, Extrusion, and Melt Spinning Behavior", *J. Appl. Polym. Sci.*, **29**, 2117-2141 (1984)

Newitt, D. M. and K. E. Weale, "Solution and Diffusion of Gases in Polystyrene at High Pressures", *J. Chem. Soc. Part II*, 1541-1549 (1948)

Nguyen, T. Q. and H. H. Kausch, "Chain Extension and Degradation in Convergent Flow", *Polymer*, **36**, 1517 (1995)

Olabisi, O. and R. Simha, "Pressure-Volume-Temperature Studies of Amorphous and Crystallizable Polymers. I. Experimental", *Macromolecules*, **8**, 206-210 (1975)

Oyanagi, Y. and J. L. White, "Basic Study of Extrusion of Polyethylene and Polystyrene Foams", *J. Appl. Polym. Sci.*, **23**, 1013-1026 (1979)

Pabedinskas, A., W. R. Cluett and S. T. Balke, "Development of an In-Line Rheometer Suitable for Reactive Extrusion Processes", *Polym. Eng. Sci.*, **31**, 365-374 (1991)

Pabedinskas, A., "Wedge Rheometer Development", Ph. D. Dissertation, Chapter 3, University of Toronto (1992)

Palierne, J. F., "Linear Rheology of Viscoelastic Emulsions with Interfacial Tension", *Rheol. Acta*, **29**, 204-214 (1990)

Panayiotou, C. and J. H. Vera, "Statistical Thermodynamics of r-Mer Fluids and Their Mixtures", *Polym. J.*, **14**, 681-694 (1982)

Park, C. B. and N. P. Suh, "Extrusion of Microcellular Filament: A Case Study of Axiomatic Design", In: *Cellular Polymers*, V. Kumar and S. G. Advani, eds., ASME, MD-Vol **38**, 69-91, New York (1992)

Park, C. B. and N. P. Suh, "Extrusion of Microcellular Polymers Using a Rapid Pressure Drop Device", *SPE ANTEC Tech. Papers*, 1818-1822 (1993)

Park, C. B., D. F. Baldwin and N. P. Suh, "Formation and Application of Polymer/Gas Mixtures in Continuous Processing of Microcellular Polymers", In: *Cellular Polymers*, V. Kumar and K. A. Sealer, eds., ASME, MD-Vol **53**, 109-124, New York (1994)

Park, C. B., D. F. Baldwin and N. P. Suh, "Effect of Pressure Drop Rate on Cell Nucleation in Continuous Processing of Microcellular Polymers", *Polym. Eng. Sci.*, **35**, 432-440 (1995)

Park, C. B. and N. P. Suh, "Filamentary Extrusion of Microcellular Polymers Using a Rapid Pressure Drop Element", *Polym. Eng. Sci*, **36**, 34-48 (1996a)

Park, C. B. and N. P. Suh, "Rapid Polymer/Gas Solution Formation for Continuous Production of Microcellular Plastics", *J. Manuf. Sci. Eng.*, **118**, 639-645 (1996b)

Park, S. J., B. K. Kim and H. M. Jeong, "Morphological, Thermal and Rheological Properties of the Blends Polypropylene / Nylon-6, Polypropylene / Nylon-6 / (maleic Anhydride-g-Polypropylene) and (Maleic Anhydride-g-Polypropylene) / Nylon-6", *Eur. Polym. J.*, 26, 131-136 (1990)

Park, S. S., C. B. Park, D. Ladin, H. E. Naguib, and C. Tzoganakis, "Development of a Dilatometer for Measurement of PVT Properties of a Polymer/Gas Solution Using a Foaming Extruder and a Gear Pump", *J. Manu. Sci. Eng.*, submitted, Aug., 1999.

Paul, D. R. and S. Newman, *"Polymer Blends"*, Vol. 2, Academic Press Inc., New York (1978)

Penwell, R. C. and R. S. Porter, "Effect of Pressure in Capillary Flow of Polystyrene", *J. Polym. Sci.*, Part A-2, **9**, 463-482 (1971)

Penwell, R. C., R. S. Porter and S. Middleman, "Determination of the Pressure Coefficient and Pressure Effects in Capillary Flow", *J. Polym. Sci.*, Part A-2, **9**, 731-745 (1971)

Petersen, R. C., D. E. Matson and R. D. Smith, *Polym. Eng. Sci.*, **27**, 1693 (1987)

Poirier, M. G., A. Ahmed, J-L. Grandmaison and S. C. F. Kaliaguine, "Supercritical Gas Extraction of Wood with Methanol in a Tubular Reactor", *Ind. Eng. Chem. Res.*, **26**, 1738-1743 (1987)

Quach, A. and R. Simha, "Pressure-Volume-Temperature Properties and Transitions of Amorphous Polymers; Polystyrene and Poly(orthomethylstyrene)", *J. Appl. Phys.*, **42**, 4592-4606 (1971)

Mertsch, R. and B.A. Wolf, *Macromolecules*, **27**, 3289 (1994)

Ramesh, N. S., D. H. Rasmussen and G. A. Campbell, "The Heterogeneous Nucleation of Microcellular Foams Assisted by the Survival of Microvoids in Polymers Containing Low Glass Transition Particles. Part I: Mathematical Modeling and Numerical Simulation", *Polym. Eng. Sci.*, **34**, 1685-1697 (1994a)

Ramesh, N. S., D. H. Rasmussen and G. A. Campbell, "The Heterogeneous Nucleation of Microcellular Foams Assisted by the Survival of Microvoids in Polymers Containing Low Glass Transition Particles. Part II: Experimental Results and Discussion", *Polym. Eng. Sci.*, **34**, 1698-1706 (1994b)

Rauwendaal, C. and F. Fernandez, "Experimental Study and Analysis of a Slit Die Viscometer", *Polym. Eng. Sci.*, **25**, 765-771 (1985)

Rauwendaal, C. R., "*Polymer Extrusion*", Hanser Publishers, Munich (1990)

Rodgers, P. A. and I. C. Sanchez, "Improvement to the Lattice-Fluid Prediction of Gas Solubilities in Polymer Liquids", *J. Polym. Sci., Part B*, **31**, 273-277 (1993)

Sanchez, I. C. and R. H. Lacombe, "An Elementary Molecular Theory of Classical Fluids. Pure Fluids", *J. Phys. Chem.*, **80**, 2352-2362 (1976)

Sanchez, I. C. and R. H. Lacombe, "An Elementary Equation of State for Polymer Liquids", *Polym. Lett.*, **15**, 71-75 (1977)

Sanchez, I. C. and R. H. Lacombe, "Statistical Thermodynamics of Polymer Solutions", *Macromolecules*, **11**, 1145-1156 (1978)

Sanchez, I. C. and P. A. Rodgers, "Solubility of Gases in Polymers", *Pure & Appl. Chem.*, **62**, 2107-2114 (1990)

Sanchez-Valdes, S., I. Yanez-Flores, L. F. Ramos de Valle, O. S. Rodriguez-Fernandez, F. Orona-Villarreal and M. Lopez-Quintanilla, "Fusion Bonding of Maleated Polyethylene Blends to Polyamide 6", *Polym. Eng. Sci.*, **38**, 127-133 (1998)

Saraf, V. P. and E. Kiran, "Free Radical Polymerization of Styrene in Supercritical Fluids", *ACS Polym. Preprint*, **31**, 687-688 (1990)

Sathe, S. N., S. Devi, G. S. S. Rao and K. V. Rao, "Relationship Between Morphology and Mechanical Properties of Binary Compatibilized Ternary Blends of Polypropylene and Nylon 6", *J. Appl. Polym. Sci.*, **61**, 97-107 (1996)

Sato, Y., M. Yurugi, K. Fujiwara, S. Takishima and H. Masuoka, "Solubilities of Carbon Dioxide and Nitrogen in Polystyrene under High Temperature and Pressure", *Fluid Phase Equil.*, **125**, 129-138 (1996)

Sato, Y., K. Fujiwara, Sumarno, S. Takishima and H. Masuoka, "Solubility of Carbon Dioxide and Nitrogen in Polyolefins and Polystyrene under High Pressures and Temperatures", *Proceedings of 5th Meeting on Supercritical Fluids Materials and Natural Products Processing*, **Tome 1**:Materials, Nice France (1998)

Scholsky, K. M., "Process Polymers with Supercritical Fluids", *Chemitech*, December, 750-757 (1987)

Scott, C. and Macosko, "Model Experiments for the Interfacial Reaction Between Polymers During Reactive Polymer Blending", *J. Polym. Sci.*, Part B, **32**, 205-213 (1994)

Scott, C. E. and S. K. Joung, "Viscosity Ratio Effects in the Compounding of Low Viscosity, Immiscible Fluids into Polymeric Matrices", *Polym. Eng. Sci.*, **36**, 1666-1674 (1996)

Sen, Y. L. and E. Kiran, "A Novel Apparatus for Simultaneous Measurement of Solubility, Density, and Viscosity of Polymer Solutions at High Pressures and Temperatures", *ACS, Polym. Preprint*, **31**, (1990a)

Shafi, M. A., J. G. Lee and R. W. Flumerfelt, "Prediction of Cellular Structure in Free Expansion Polymer Foam Processing", *Polym. Eng. Sci.*, **36**, 1950-1959 (1996)

Simha, R. and T. Somcynski, "On the Statistical Thermodynamics of spherical and Chain Molecule Fluids", *Macromolecules*, **2**, 342-350 (1969)

Stern, S. A., J. T. Mullhaupt and P. J. Gareis, "The Effect of Pressure on the Permeation of Gases and Vapors through Polyethylene. Usefulness of the Corresponding States Principle", *AIChE J.*, **15**, 64-73 (1969)

Stiel, L. I. and D. F. Harnish, "Solubility of Gases and Liquids in Molten Polystyrene", *AIChE J.*, **22**, 117-122 (1976)

Sundararaj, U. and C. W. Macosko, "Drop Breakup and Coalescence in Polymer Blends: The Effects of Concentration and Compatibilization", *Macromolecules*, **28**, 2647-2657 (1995)

Sundararaj, U., Y. Dori and C. W. Macosko, "Sheet Formation in Immiscible Polymer Blends" Model Experiments on Initial Blend Morphology", *Polymer*, **36**, 1957-1968 (1995)

Tammann, G. and W. Hesse, *Z. Anorg. Allgem. Chem.*, **156** (1926)

Taylor, G. I., " The Formation of Emulsions in Definable Fields of Flow", *Proc. R. Soc. London A.*,**146**, 501-523 (1934): *A.*,**138** (1932)

Throne, J. L., "*Thermoplastic foams*", Sherwood Publishers, Hinckley Ohio (1996)

Tseng, H.-S. and D. R. Lloyd and T. C. Ward, "Correlation of Organic Solubility in Poly(vinyl acetate)", *Polym. Comm.*, **25**, 262-265 (1984)

Tseng, H.-S. and D. R. Lloyd, "Correlation of Solubility in Polydimethylsiloxane and Polyisobutylene Systems", *J. Appl. Polym. Sci.*, **30**, 307-315 (1985a)

Tseng, H.-S. and D. R. Lloyd, "Solubility of Nonpolar and Slightly Polar Organic Compounds in Low-Density Polyethylene by Inverse Gas Chromatography with Open Tubular Column", *J. Appl. Polym. Sci.*, **30**, 1815-1826 (1985b)

Tseng, H.-S., P.-C. Wong and D. R. Lloyd, "Thermodynamic Interaction in Polybutadiene/Solute Systems by Inverse Gas Chromatography", *Polym. Eng. Sci.*, **27**, 1141-1147 (1987)

Utracki, L. A., "Temperature and Pressure Dependence of Liquid Viscosity", *Can. J. Chem. Eng.*, **61**, 753-755 (1983)

Utracki, L. A., "A Method of Computation of the Pressure Effect on Melt Viscosity", *Polym. Eng. Sci.*, **25**, 655-668 (1985)

Utracki, L. A. and P. Sammut, "Rheological Evaluation of Polystyrene/Polyethylene Blends", *Polym. Eng. Sci.*, **28**, 1405-1415 (1988)

van Ballegooie, P. and A. Rudin, "Reactive Extrusion of Polystyrene/Polyethylene Blends", *Polym. Eng. Sci.*, **28**, 1434-1442 (1988)

Vanoene, H., "Modes of Dispersion of Viscoelastic Fluids in Flow", *J. Colloid and Interface Sci.*, **40**, 448-467 (1972)

Vicentini-Missoni, M., J. M. H. Levelt Sengers and M. S. Green, "Scaling Analysis of Thermodynamic Properties in the Critical Region of Fluid", *J. Res. Nat. Bur. Stand.*, **73A**, 563-583 (1969)

Vlachopoulos, J. and P. S. Scott, "Pressure Drop for Molten Polymer Flow Through Tapered Dies", *Adv. Polym. Tech.*, **5**, 81-86 (1985)

Wang, N.-H., S. Takishima and H. Masuoka, "Measurement and Correlation of Solubility of a High Pressure Gas in a Polymer by Piezoelectric Quartz Sorption - CO_2+PVAc and CO_2+PBME Systems", *Int. Chem. Eng.*, **34**, 255-262 (1994)

Watkins, J. J. and T. J. McCarthy, "Polymerization in Supercritical Fluid-Swollen Polymers: A New Route to Polymer Blends", *Macromolecules*, **27**, 4845-4847 (1994)

Wentorf, R. H., Jr., "Isotherms in the Critical Regions of Carbon Dioxide and Sulfur Hexafluoride", *J. Chem. Phys.*, **24**, 607-615 (1956)

Wessling, M., Z. Borneman, T. van den Boomgaard and C. A. Smolders, "Carbon Dioxide Foaming of Glassy Polymers", *J. Polym. Sci.*, **53**, 1497-1512 (1994)

Westover, R. F., "Effect of Hydrostatic Pressure on Polyethylene Melt Rheology", *SPE Trans.*, **1**;40, 14-20 (1961)

Williams, M. L., R. F. Landel and J. D. Ferry, "The Temperature Dependence of Relaxation Mechanisms in Amorphous Polymers and Other Glass-forming Liquids", *J. Am. Chem. Soc.*, **77**, 3701-3707 (1955)

Wissinger, R. G. and M. E. Paulaitis, "Swelling and Sorption in Polymer-CO_2 Mixtures at Elevated Pressures", *J. Polym. Sci., Part B*, **25**, 2497-2510 (1987)

Wolf, B. A., M. Klimiuk, M.J.R. Cantow, "PvT Data of Poly(perfluoro ether)s and How They Govern the Flow Behavior", *J. Phys. Chem.*, **93**, 2672-2675 (1989)

Wu, S., "Phase Structure and Adhesion in Polymer Blends: A Criterion for Rubber Toughening", *Polymer*, **26**, 1855-1863 (1985)

Wu, S., "Formation of Dispersed Phase in Incompatible Polymer Blends: Interfacial and Rheological Effects", *Polym. Eng. Sci.*, **27**, 335-343 (1987)

Yang, L.-Y., T. G. Smith and D. Bigio, "Melt Blending of Linear Low-Density Polyethylene and Polystyrene in a Haake Internal Mixer: 1. Compatibilization and Morphology Development", *J. Appl. Polym. Sci.*, **58**, 117-127 (1995a)

Yang, L.-Y., T. G. Smith and D. Bigio, "Melt Blending of Linear Low-Density Polyethylene and Polystyrene in a Haake Internal Mixer: 2. Morphology-Processing Relationships", *J. Appl. Polym. Sci.*, **58**, 129-141 (1995b)

Yasuda, K.Y., R.C. Armstrong, and R.E. Cohen, *Rheol. Acta*, **20**, 163 (1981)

Yoo, H. J. and C. D. Han, "Stress Distribution of Polymers in Extrusion through a Converging Die", *J. Rheol.*, **25**, 115-137 (1981)

Zhang, Y., K. K. Gangwani and R. M. Lemert, "Sorption and Swelling of Block Copolymer in the Presence of Supercritical Fluid Carbon Dioxide", *J. Supercrit. Fluids*, **11**, 115-134 (1997)

Zatloukal, M., C. Tzoganakis, J. Perdikoulias and P. Saha, "Viscoelastic Stress Calculation in Polymer Coextrusion Flows", Gordon Research Conference, CAE in Polymer Processing, Ventura, CA, March, 1999

Appendix I:
LABVIEW PROGRAM FOR DATA ACQUISITION

1. Flow Chart

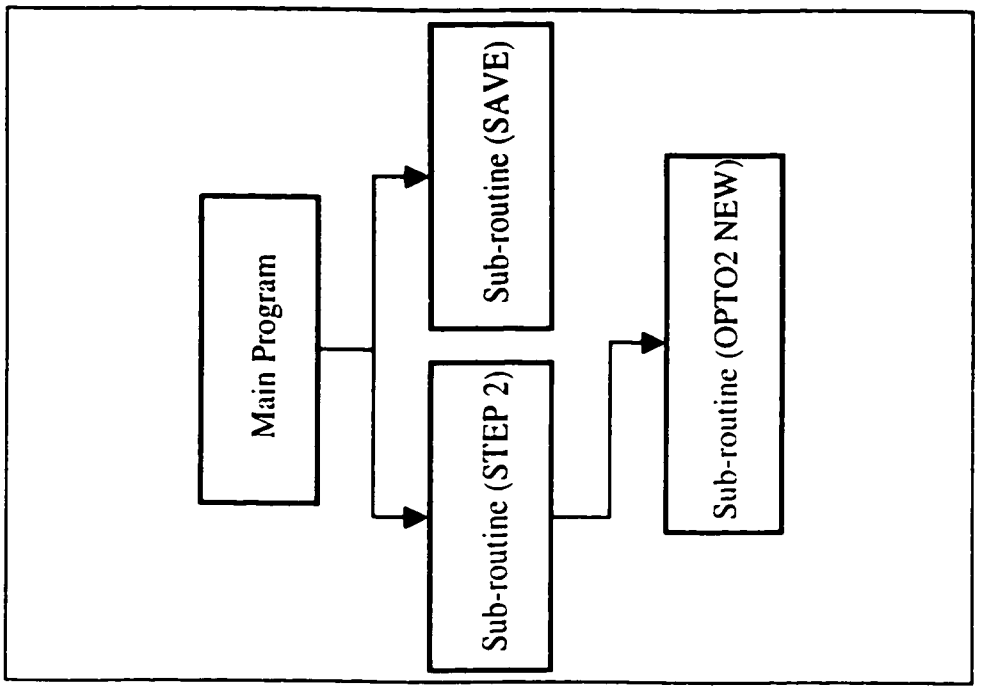

2. Main Program

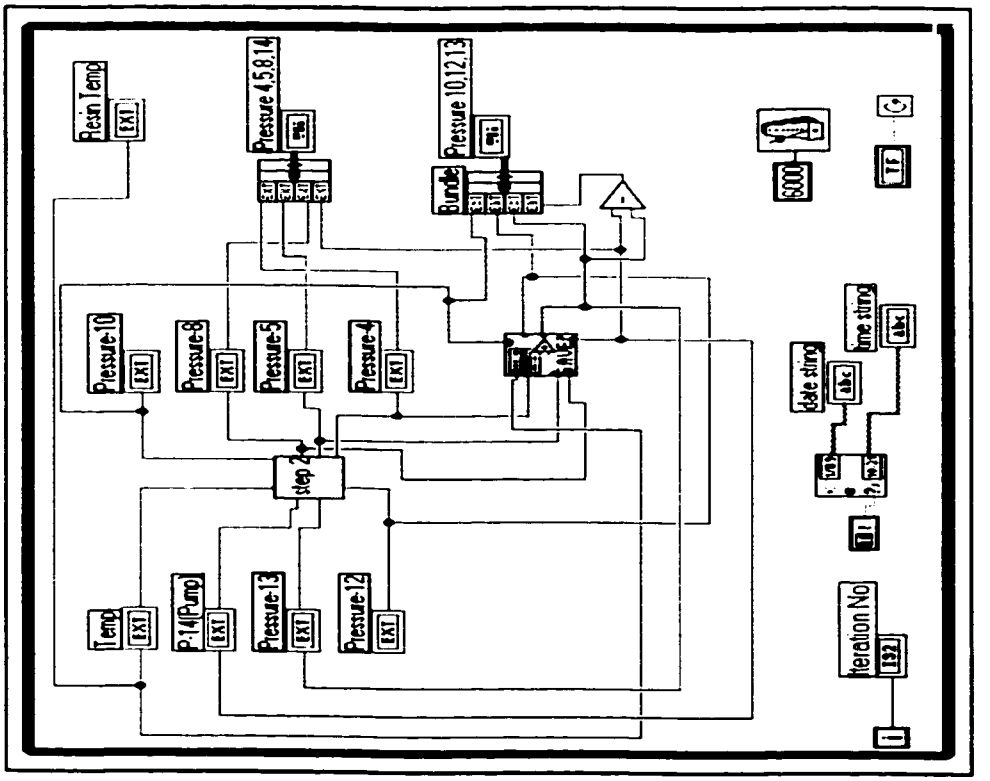

4. Sub-routine (SAVE.VI)

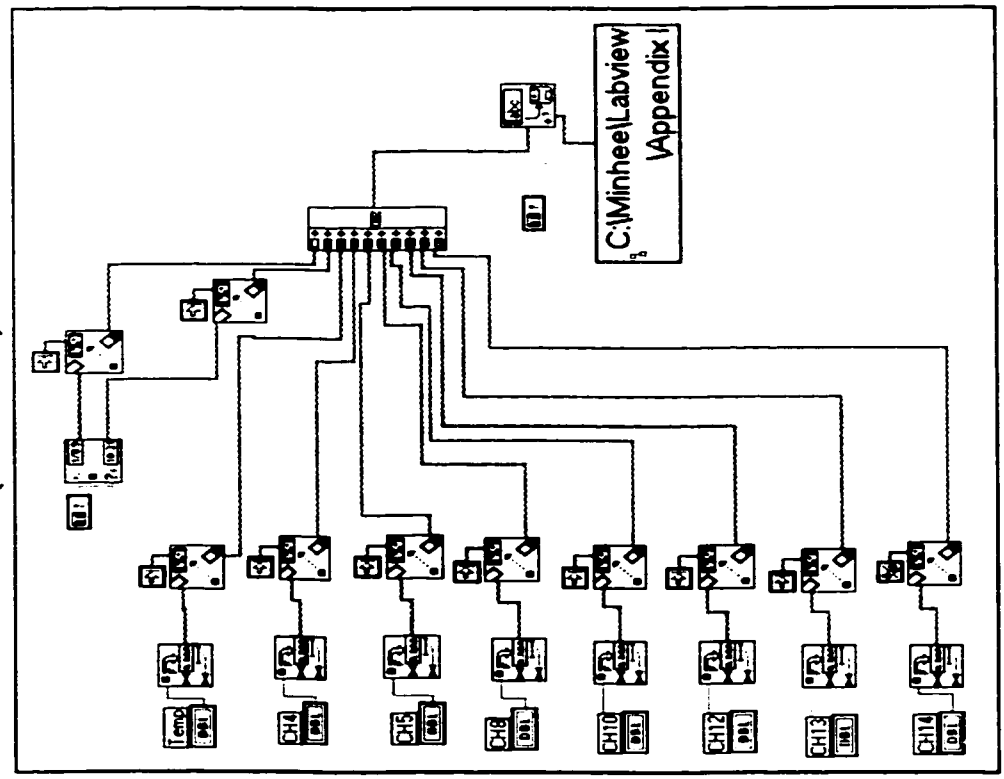

3. Sub-routine (STEP 2.VI)

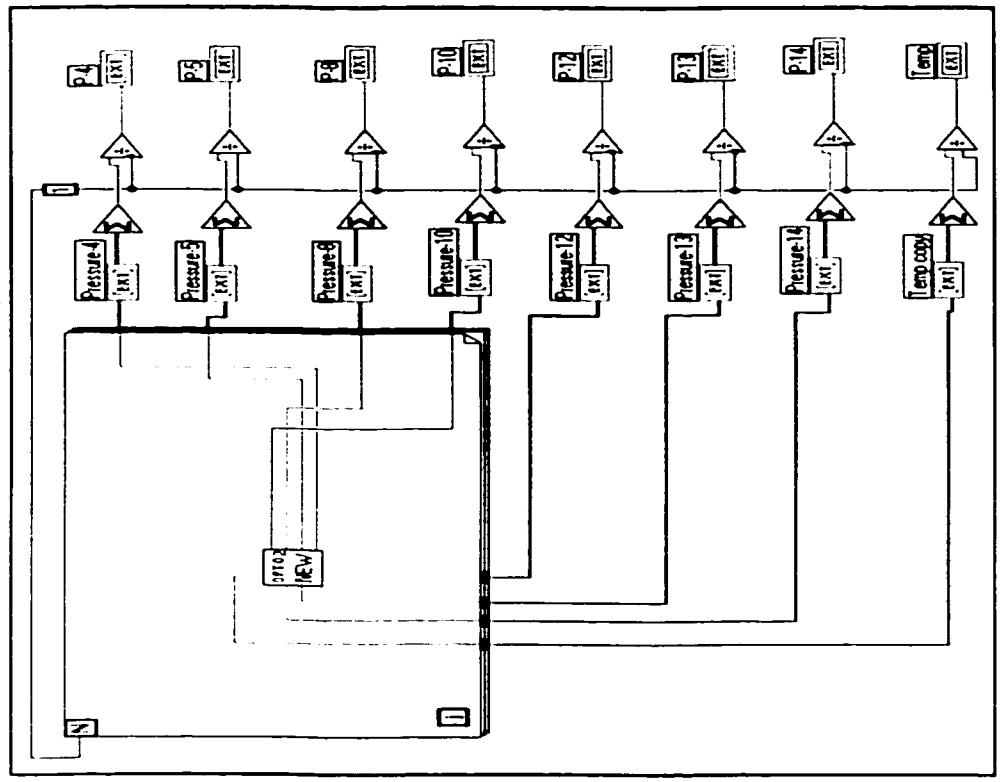

5. Sub-routine (OPTO2 NEW.VI)

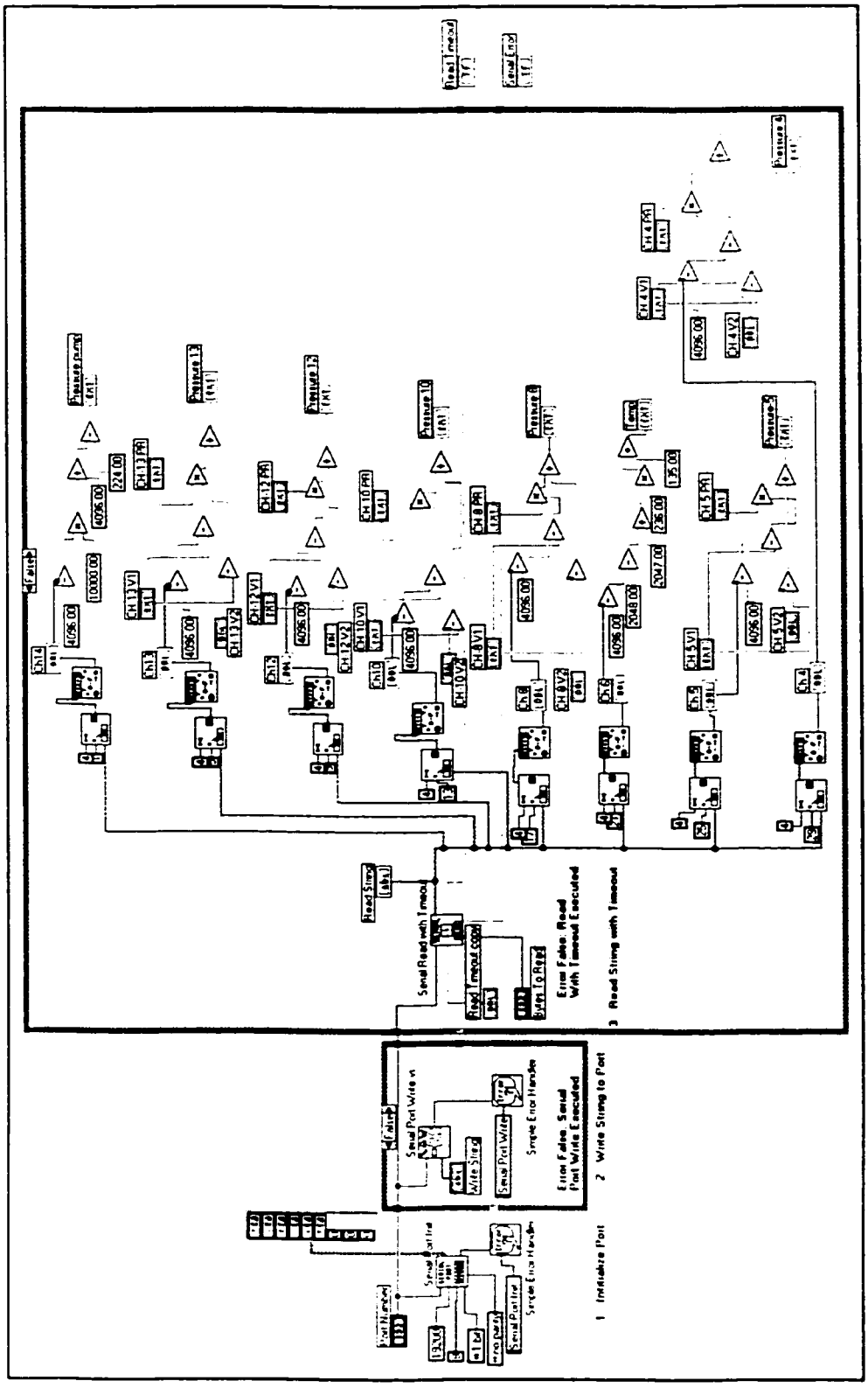

Appendix II:
FORTRAN PROGRAMS USED FOR S-L EOS

PROGRAM-1:
DETERMINATION OF CHARACTERISTIC PARAMETERS OF PURE COMPONENTS AND POLYMER / CO_2 SOLUTIONS

```
IMPLICIT REAL*8 (A-H, O-Z)
    DOUBLE PRECISION T,P,P1S,P2S,RH1S,RH2S,T1S,T2S,PS,RHS,TS,
   #    R1,R2,R,PI1Z,PI2Z,PI1,PI2,V1S,V2S,VS,X1,X2,GS,R1Z,R2Z,
   #    AM1,AM2,AMW1,AMW2,DEL,J
    DOUBLE PRECISION EPS, ETA, X
    DOUBLE PRECISION F,G
    EXTERNAL F,G
    EXTERNAL C05AJF
    COMMON T,P,P1S,P2S,RH1S,RH2S,T1S,T2S,PS,RHS,TS,
   #    R1,R2,R,PI1Z,PI2Z,PI1,PI2,V1S,V2S,VS,X1,X2,GS,R1Z,R2Z,
   #    AM1,AM2,AMW1,AMW2,DEL,J
    OPEN(UNIT=5, FILE='rh.dat', STATUS='old')
    OPEN(UNIT=6, FILE='rh.out', STATUS='new')
    READ(5,*) P1S, P2S, T1S, T2S, RH1S, RH2S, AMW1, AMW2
    T=423.
    DEL=0.1
    NP=100000
    WRITE(6,30)P1S,P2S,T1S,T2S,RH1S,RH2S,AMW1,AMW2,DEL,NP
  30 FORMAT(F8.2,1X,F8.2,1X,F7.2,1X,F7.2,1X,F6.4,1X,F6.4,1X,F4.1,1X,
   #    F10.2,1X,F6.4,1X,I6)
    DO 50 P=10,1000,10
    DO 20 PI1Z=0.01,0.5,0.001
    GS=82.05
    R1Z=P1S*AMW1/(GS*T1S*RH1S)
C
    CALL CO2(X)
C    ---------- Calculation of variables ----------
    GS=82.05
    R1Z=P1S*AMW1/(GS*T1S*RH1S)
    R2Z=P2S*AMW2/(GS*T2S*RH2S)
    V1S=AMW1/(R1Z*RH1S)
    V2S=AMW2/(R2Z*RH2S)
    PI2Z=1.-PI1Z
    VS=PI1Z*V1S+PI2Z*V2S
    PI1=PI1Z*V1S/(PI1Z*V1S+PI2Z*V2S)
    PI2=1.-PI1
    R1=R1Z*V1S/VS
    R2=R2Z*V2S/VS
    X1=PI1Z*R2Z/(PI1Z*R2Z+PI2Z*R1Z)
    X2=1.-X1
    R=X1*R1+X2*R2
    AM1=X1*AMW1/(X1*AMW1+X2*AMW2)
    AM2=1.-AM1
    RHS=1./(AM1/RH1S+AM2/RH2S)
```

```
PS=PI1**2*P1S+PI2**2*P2S+2*PI1*PI2*SQRT(P1S*P2S)*(1-DEL)
   TS=PS*VS/GS
   RHS=1/(AM1/RH1S+AM2/RH2S)
c
   CALL SOLU(Y)
   WRITE(6,100)T,P,R1,R2,PI1Z,PI1,AM1,VS,PS,RHS,X,Y
 100 FORMAT(F6.1,1X,F6.1,1X,F5.2,1X,F7.1,1X,F6.4,1X,F6.4,1X,F6.4,
  #     1X,F5.2,1X,F7.1,1X,F6.4,1X,F8.4,1X,F8.4)
  20 CONTINUE
  50 CONTINUE
   WRITE(6,200)
 200 FORMAT('0.')
   STOP
   END   c%%%%%%%%%%%%%%%%%%%%%%%%%%%%%%%%%%%%%%%%%%%%%%
   SUBROUTINE  CO2(X)
   IMPLICIT REAL*8 (A-H, O-Z)
   DOUBLE PRECISION T,P,P1S,P2S,RH1S,RH2S,T1S,T2S,PS,RHS,TS,
  #    R1,R2,R,PI1Z,PI2Z,PI1,PI2,V1S,V2S,VS,X1,X2,GS,R1Z,R2Z,
  #    AM1,AM2,AMW1,AMW2,DEL,J
   DOUBLE PRECISION EPS, ETA, X
   DOUBLE PRECISION G
   EXTERNAL G
   EXTERNAL C05AJF
   COMMON T,P,P1S,P2S,RH1S,RH2S,T1S,T2S,PS,RHS,TS,
  #    R1,R2,R,PI1Z,PI2Z,PI1,PI2,V1S,V2S,VS,X1,X2,GS,R1Z,R2Z,
  #    AM1,AM2,AMW1,AMW2,DEL,J
   EPS=.0001
   X=1.0
   ETA=0.0
   NFMAX=10000
   IFAIL=1
   CALL C05AJF(X, EPS, ETA, G, NFMAX, IFAIL)
     IF(IFAIL.EQ.0) THEN
     ELSE
       IF (IFAIL.EQ.3 .OR.IFAIL.EQ.4) THEN
       END IF
     END IF
  55 FORMAT(2F8.2, 'IFAIL=', I3)
   RETURN
   END
c
   DOUBLE PRECISION FUNCTION G(X)
   DOUBLE PRECISION X
   IMPLICIT REAL*8 (A-H, O-Z)
   COMMON T,P,P1S,P2S,RH1S,RH2S,T1S,T2S,PS,RHS,TS,
  #    R1,R2,R,PI1Z,PI2Z,PI1,PI2,V1S,V2S,VS,X1,X2,GS,R1Z,R2Z,
  #    AM1,AM2,AMW1,AMW2,DEL,J
     G=P/P1S+X**2/RH1S**2+T/T1S*(log(1.-X/RH1S)+(1.-1./R1z)
  #    *X/RH1S)
   RETURN
   END   c%%%%%%%%%%%%%%%%%%%%%%%%%%%%%%%%%%%%%%%%%%%%%%
   SUBROUTINE SOLU(Y)
   IMPLICIT REAL*8 (A-H, O-Z)
   DOUBLE PRECISION T,P,P1S,P2S,RH1S,RH2S,T1S,T2S,PS,RHS,TS,
  #    R1,R2,R,PI1Z,PI2Z,PI1,PI2,V1S,V2S,VS,X1,X2,GS,R1Z,R2Z,
  #    AM1,AM2,AMW1,AMW2,DEL,J
```

```
      DOUBLE PRECISION EPS, ETA, X
      DOUBLE PRECISION F
      EXTERNAL F
      EXTERNAL C05AJF
      COMMON T,P,P1S,P2S,RH1S,RH2S,T1S,T2S,PS,RHS,TS,
     #    R1,R2,R,PI1Z,PI2Z,PI1,PI2,V1S,V2S,VS,X1,X2,GS,R1Z,R2Z,
     #    AM1,AM2,AMW1,AMW2,DEL,J
      EPS=.0001
      X=1.0
      ETA=0.0
      NFMAX=10000
      IFAIL=1
      CALL C05AJF(X, EPS, ETA, F, NFMAX, IFAIL)
      IF(IFAIL.EQ.0) THEN
         Y=X
      ELSE
        IF (IFAIL.EQ.3 .OR.IFAIL.EQ.4) THEN
        END IF
      END IF
      RETURN
      END
C
      DOUBLE PRECISION FUNCTION F(X)
      DOUBLE PRECISION X
      IMPLICIT REAL*8 (A-H, O-Z)
      COMMON T,P,P1S,P2S,RH1S,RH2S,T1S,T2S,PS,RHS,TS,
     #    R1,R2,R,PI1Z,PI2Z,PI1,PI2,V1S,V2S,VS,X1,X2,GS,R1Z,R2Z,
     #    AM1,AM2,AMW1,AMW2,DEL,J
        F=P/PS+X**2/RHS**2+T/TS*(LOG(1.-X/RHS)+(1.-1./R)
     #    *X/RHS)
      RETURN
      END
```

PROGRAM-2:
ESTIMATION OF THE DENSITY OF PURE COMPONENTS

```
      IMPLICIT REAL*8 (A-H, O-Z)
      DOUBLE PRECISION P, T
      DOUBLE PRECISION P1S,P2S,RH1S,RH2S,T1S,T2S,PS,RHS,TS,
     *  R1,R2,R,PI1Z,PI2Z,PI1,PI2,V1S,V2S,X1,X2,GS,R1Z,R2Z,AM1,AM2,AMW1,AMW2,DEL
      DOUBLE PRECISION EPS, ETA, X, Y
      DOUBLE PRECISION F
      DOUBLE PRECISION G
      EXTERNAL F,G
      EXTERNAL C05AJF
      COMMON  T,P, P1S,P2S,RH1S,RH2S,T1S,T2S,PS,RHS,TS,
     *  R1,R2,R,PI1Z,PI2Z,PI1,PI2,V1S,V2S,X1,X2,GS,R1Z,R2Z,AM1,AM2,AMW1,AMW2,DEL,J
      OPEN(UNIT=5, FILE='pure.dat', STATUS='old')
      OPEN(UNIT=6, FILE='pure.out', STATUS='new')
      READ(5,*) P1S, P2S, T1S, T2S, RH1S, RH2S, AMW1, AMW2
      T=372.9
      DO 50 P=1,500,10
      GS=82.05
      R1Z=P1S*AMW1/(GS*T1S*RH1S)
      R2Z=P2S*AMW2/(GS*T2S*RH2S)
      CALL CO2(X)
      CALL POLY(Y)
      WRITE(6,45) T, P, X, Y
   45 FORMAT('Temp(K)=', F8.2,3x,'Press(atm)=',F8.2, 3x, 'rh1(g/cm3) =',F8.5, 3x, 'rh2=',F8.5)
   50 CONTINUE
      STOP
      END
%%%%%%%%%%%%%%%%%%%%%%%%%%%%%%%%%%%%%%%%%%%%%%%%%%%%%%%%%%%%
      SUBROUTINE  CO2(X)
      IMPLICIT REAL*8 (A-H, O-Z)
      DOUBLE PRECISION P, T
      DOUBLE PRECISION P1S,P2S,RH1S,RH2S,T1S,T2S,PS,RHS,TS,
     *  R1,R2,R,PI1Z,PI2Z,PI1,PI2,V1S,V2S,X1,X2,GS,R1Z,R2Z,AM1,AM2,AMW1,AMW2,DEL
      DOUBLE PRECISION EPS, ETA, X
      DOUBLE PRECISION G
      EXTERNAL G
      EXTERNAL C05AJF
      COMMON  T,P, P1S,P2S,RH1S,RH2S,T1S,T2S,PS,RHS,TS,
     *  R1,R2,R,PI1Z,PI2Z,PI1,PI2,V1S,V2S,X1,X2,GS,R1Z,R2Z,AM1,AM2,AMW1,AMW2,DEL,J
      EPS=.0001
      X=1.0
      ETA=0.0
      NFMAX=10000
      IFAIL=1
      CALL C05AJF(X, EPS, ETA, G, NFMAX, IFAIL)
      IF(IFAIL.EQ.0) THEN
      ELSE
        IF (IFAIL.EQ.3 .OR.IFAIL.EQ.4) THEN
         WRITE(6,55) T, P, IFAIL
        END IF
   55 FORMAT(2F8.2, 'IFAIL=', I3)
      END IF
      RETURN
```

```
      END
      DOUBLE PRECISION FUNCTION G(X)
      DOUBLE PRECISION X
      IMPLICIT REAL*8 (A-H, O-Z)
      COMMON  T,P, P1S,P2S,RH1S,RH2S,T1S,T2S,PS,RHS,TS,
     *    R1,R2,R,PI1Z,PI2Z,PI1,PI2,V1S,V2S,X1,X2,GS,R1Z,R2Z,AM1,AM2,AMW1,AMW2,DEL,J
       G = P/P1S+X**2/RH1S**2+T/T1S*(LOG(1.-X/RH1S)+(1.-1./R1z)
     #*X/RH1S)
      RETURN
      END
%%%%%%%%%%%%%%%%%%%%%%%%%%%%%%%%%%%%%%%%%%%%%%%%%%%%%%%%%%%
      SUBROUTINE POLY(Y)
      IMPLICIT REAL*8 (A-H, O-Z)
      DOUBLE PRECISION P, T
      DOUBLE PRECISION P1S,P2S,RH1S,RH2S,T1S,T2S,PS,RHS,TS,
     *    R1,R2,R,PI1Z,PI2Z,PI1,PI2,V1S,V2S,X1,X2,GS,R1Z,R2Z,AM1,AM2,AMW1,AMW2,DEL
      DOUBLE PRECISION EPS, ETA, X,Y
      DOUBLE PRECISION F
      EXTERNAL F
      EXTERNAL C05AJF
      COMMON T,P, P1S,P2S,RH1S,RH2S,T1S,T2S,PS,RHS,TS,
     *    R1,R2,R,PI1Z,PI2Z,PI1,PI2,V1S,V2S,X1,X2,GS,R1Z,R2Z,AM1,AM2,AMW1,AMW2,DEL,J
      EPS=.0001
      X=1.0
      ETA=0.0
      NFMAX=10000
      IFAIL=1
      CALL C05AJF(X, EPS, ETA, F, NFMAX, IFAIL)
      IF(IFAIL.EQ.0) THEN
         Y=X
      ELSE
        IF (IFAIL.EQ.3 .OR.IFAIL.EQ.4) THEN
         WRITE(6,55) T, P, IFAIL
        END IF
   55 FORMAT(2F8.2, 'IFAIL=', I3)
      END IF
      RETURN
      END
      DOUBLE PRECISION FUNCTION F(X)
      DOUBLE PRECISION X,Y
      IMPLICIT REAL*8 (A-H, O-Z)
      COMMON T,P, P1S,P2S,RH1S,RH2S,T1S,T2S,PS,RHS,TS,
     *    R1,R2,R,PI1Z,PI2Z,PI1,PI2,V1S,V2S,X1,X2,GS,R1Z,R2Z,AM1,AM2,AMW1,AMW2,DEL,J
       F = P/P2S+X**2/RH2S**2+T/T2S*(LOG(1.-X/RH2S)+(1.-1./R2Z)
     #*X/RH2S)
      RETURN
      END
```

PROGRAM-3:
SOLUBILITY ISOTHERMS OF POLYMER / CO_2 SOLUTIONS

```
c    INPUT DATA(iso.dat) IS THE RESULTS OF THE PROGRAM 2(rh.out)
c    "DEL" WAS ASSUMED AS A CONSTANT IN THE PROGRAM 2
c    ------------------------------------------------------------------------------------------
     IMPLICIT REAL*8 (A-H, O-Z)
     DOUBLE PRECISION P,T,P1S,P2S,RH1S,RH2S,T1S,T2S,PS,RHS,TS,
    #    R1,R2,R,PI1Z,PI2Z,PI1,PI2, V1S,V2S,VS,X1,X2,GS,R1Z,R2Z,
    #    AM1,AM2,AMW1,AMW2,DEL,RH1,RH,P2,SMALL,DIFF,PM,PI1M,AM1M,
    #    XM,RHM
     DOUBLE PRECISION EPS, ETA, X
     DOUBLE PRECISION F
     EXTERNAL F
     EXTERNAL C05AJF
     COMMON T,P,P1S,P2S,RH1S,RH2S,T1S,T2S,PS,RHS,TS,
    #    R1,R2,R,PI1Z,PI2Z,PI1,PI2, V1S,V2S,VS,X1,X2,GS,R1Z,R2Z,
    #    AM1,AM2,AMW1,AMW2,DEL,RH1,RH,P2,SMALL,DIFF,PM,PI1M,AM1M,
    #    XM,RHM
     OPEN(UNIT=5, FILE='iso.dat', STATUS='old')
     OPEN(UNIT=6, FILE='iso.out', STATUS='new')
     WRITE(6,50)
  50 FORMAT("%%%%%%%%%%%%%%%%%%%% Result of Program 2 %%%%%%%%",
    # "%%%%%%%%%%%%%%%%%%%%%%%%%%%%%%%%%%%%%%%%%%%%%%%%%%%%%%%")
     WRITE(6,100)
 100 FORMAT('TEMP',5X,'PRESS',4X,'PI1',
    #    3X,'wt.frac',3X,'EQU.PI1',2X,
    #    'SOLUTION-DENSITY',2X,'CO2-DENSITY',3X,'SMALL')
     SMALL=1000.
     P2=10.
     READ(5,200) P1S, P2S,T1S,T2S,RH1S,RH2S,AMW1,AMW2,DEL,NP
 200 FORMAT(F8.2,1X,F8.2,1X,F7.2,1X,F7.2,1X,F6.4,1X,F6.4,1X,F4.1,1X,
    #    F10.2,1X,F6.4,1X,I6)
     DO 10 j=1,NP
     READ(5,300) T,P,R1,R2,PI1Z,PI1,AM1,VS,PS,RHS,RH1,RH
 300 FORMAT(F6.1,1X,F6.1,1X,F5.2,1X,F7.1,1X,F6.4,1X,F6.4,1X,F6.4,
    #    1X,F5.2,1X,F7.1,1X,F6.4,1X,F8.4,1X,F8.4)
     IF(T.EQ.0.) GOTO 400
     IF(P.NE.P2) GOTO 10
c%%%%%%%%%%%%%%%%%%%%%%%%%%%%%%%%%%%%%%%%%%%%%%%%%%%%%%%%%%%%%%%%%%%%%%%%%%%%%%%%%%%%%%%%%%%%
     GS=82.05
     R1Z=P1S*AMW1/(GS*T1S*RH1S)
     V1S=AMW1/(R1Z*RH1S)
c&&&&&&&&&&&&&&&&&&&&&&&&&&&&&&&&&&&&&&&&&&&&&&&&&&&&&&&&&&&&&&&&&&&&&&&&&&&&&&&&&&&&&&&&&&&&
c                EQUILIBIUM CO2 CONTENT
c&&&&&&&&&&&&&&&&&&&&&&&&&&&&&&&&&&&&&&&&&&&&&&&&&&&&&&&&&&&&&&&&&&&&&&&&&&&&&&&&&&&&&&&&&&&&
     EPS=.0001
     X=0.01
     ETA=0.0
     NFMAX=10000
     IFAIL=1
     CALL C05AJF(X, EPS, ETA, F, NFMAX, IFAIL)
     IF(X.LT.0) GOTO 10
     DIFF=ABS(PI1-X)
     IF(IFAIL.EQ.0) THEN
```

```
      IF(DIFF.LE.SMALL) THEN
        SMALL=DIFF
        PM=P
        PI1M=PI1
        AM1M=AM1
        XM=X
        RHM=RH
      ELSE
       WRITE(6,500) T,PM,PI1M,AM1M,XM,RHM,RH1,SMALL
500     FORMAT(F5.1,3X,F5.1,3X,F6.4,3X,F6.4,3X,F6.4,8X,
     #    F7.4,6X,F7.4,5X,F8.5)
       p2=p+10
       SMALL=1000.0
      END IF
    ELSE
     IF(IFAIL.EQ.3 .OR.IFAIL.EQ.4) THEN
       WRITE(6,600)T,P,IFAIL
     END IF
    END IF
   10 CONTINUE
  400 WRITE(6,700)
  600 FORMAT(2F8.2,'IFAIL=',I3)
  700 FORMAT("%%%%%%%%%%%%%%%%%%%% END OF CALCULATION %%%%%%%%",
     # "%%%%%%%%%%%%%%%%%%%%%%%%%%%%%%%%%%%%%%%%%%%%%%%%%%%%%%%")
      STOP
      END  %%%%%%%%%%%%%%%%%%%%%%%%%%%%%%%%%%%%%%%%%%%%%%%%%%%%%%%%
      DOUBLE PRECISION FUNCTION F(X)
      DOUBLE PRECISION X
      DOUBLE PRECISION P,T,P1S,P2S,RH1S,RH2S,T1S,T2S,PS,RHS,TS,
     #    R1,R2,R,PI1Z,PI2Z,PI1,PI2, V1S,V2S,VS,X1,X2,GS,R1Z,R2Z,
     #    AM1,AM2,AMW1,AMW2,DEL,RH1,RH,P2,SMALL,DIFF,PM,PI1M,AM1M,
     #    XM,RHM
      IMPLICIT REAL*8 (A-H, O-Z)
      COMMON T,P,P1S,P2S,RH1S,RH2S,T1S,T2S,PS,RHS,TS,
     #    R1,R2,R,PI1Z,PI2Z,PI1,PI2, V1S,V2S,VS,X1,X2,GS,R1Z,R2Z,
     #    AM1,AM2,AMW1,AMW2,DEL,RH1,RH,P2,SMALL,DIFF,PM,PI1M,AM1M,
     #    XM,RHM
      INTRINSIC SQRT
       F = LOG(X) + (1.-(R1/R2))*(1.-X) + R1Z*(RH/RHS)*
     #    (P1S+P2S-2.*SQRT(P1S*P2S)*(1.-DEL))*(V1S/(GS*T))*
     #    (1.-X)**2 + LOG(RH/RHS) - LOG(RH1/RH1S)+ R1Z*
     #    ((-1.)*((RH/RHS)-(RH1/RH1S))/(T/T1S)+(P/P1S)*
     #    ((RHS/RH)-(RH1S/RH1))/(T/T1S)+(RHS/RH)*(1.-(RH/RHS))*
     #    LOG(1.-(RH/RHS))-(RH1S/RH1)*(1.-(RH1/RH1S))*
     #    LOG(1.-(RH1/RH1S)))
      RETURN
      END
```

Appendix III:
CALCULATIONS IN A WEDGE DIE

A. DERIVATION OF THE PRESSURE DROP FOR A CARREAU FLUID

For flow in a slit die having the constant width, w, height, h, and the length, L, expressions for the shear stress and the shear rate at the wall are given by

$$\tau_w = \left(-\frac{\partial P}{\partial z}\right)\frac{1}{2}\left(\frac{wh}{w+h}\right) \tag{A-1}$$

$$\dot{\gamma}_w = \left(\frac{2n+1}{3n}\right)\left(\frac{6Q}{wh^2}\right) \tag{A-2}$$

For Carreau fluid, the shear stress is shown by

$$\tau_w = \eta\dot{\gamma}_w \tag{A-3}$$

where $\eta = \eta_0\left[1+(\lambda\dot{\gamma}_w)^2\right]^{\frac{n-1}{2}}$

From *Eq. (A-1)* to *Eq. (A-3)*

$$\left(-\frac{\partial P}{\partial z}\right) = 2\eta_0\left(\frac{w+h}{wh}\right)\left(\frac{2n+1}{3n}\right)\left[1+\left(\frac{2n+1}{3n}\right)^2\left(\frac{6\lambda Q}{wh^2}\right)^2\right]^{\frac{n-1}{2}}\left(\frac{6Q}{wh^2}\right) \tag{A-4}$$

By integration, *Eq. (A-4)* reduces

$$-\Delta P = P_0 - P_1 = 2\eta_0 L\left(\frac{w+h}{wh}\right)\left(\frac{2n+1}{3n}\right)\left[1+\left(\frac{2n+1}{3n}\right)^2\left(\frac{6\lambda Q}{wh^2}\right)^2\right]^{\frac{n-1}{2}}\left(\frac{6Q}{wh^2}\right) \tag{A-5}$$

A slit die having infinite small length, dl, is assumed. Then, *Eq. (A-5)* can be expressed as

$$-dP = 2\eta_0\left(\frac{w+h}{wh}\right)\left(\frac{2n+1}{3n}\right)\left[1+\left(\frac{2n+1}{3n}\right)^2\left(\frac{6\lambda Q}{wh^2}\right)^2\right]^{\frac{n-1}{2}}\left(\frac{6Q}{wh^2}\right)dl \tag{A-6}$$

In the wedge die, dl is given by

$$dl = -\frac{dh}{2\tan\theta} \tag{A-7}$$

Therefore, *Eq. (A-6)* yields

$$-\Delta P = -\frac{6\eta_0 Q}{\tan\theta}\left(\frac{2n+1}{3n}\right)\int_{h_0}^{h_1}\left(\frac{w+h}{wh}\right)\left(\frac{1}{wh^2}\right)\left[1+\left(\frac{2n+1}{3n}\right)^2\left(\frac{6\lambda Q}{wh^2}\right)^2\right]^{\frac{n-1}{2}} dh \tag{A-8}$$

In order to integrate *Eq. (A-8)*, the form having $(1+x)^{-p}$ should be expanded to two cases expressed by the binomial series function:

First, when $x<1$,

$$(1+x)^{-p} = 1 - px + \frac{p(p+1)}{2!}x^2 - \frac{p(p+1)(p+2)}{3!}x^3\cdots \tag{A-9}$$

Second, when $x>1$,

$$(1+x)^{-p} = x^{-p} - px^{-p-1} + \frac{-p(-p-1)}{2!}x^{-p-2} + \frac{-p(-p-1)(-p-2)}{3!}x^{-p-3}\cdots \tag{A-10}$$

In case of $\left(\frac{2n+1}{3n}\right)\left(\frac{6\lambda Q}{wh^2}\right) < 1$, therefore, *Eq. (A-8)* yields

$$-\Delta P = -\frac{6\eta_0 Q}{\tan\theta}\left(\frac{2n+1}{3n}\right)$$
$$\int_{h_0}^{h_1}\left(\frac{1}{w^2h^2}+\frac{1}{wh^3}\right)\left[1+\frac{1-n}{2}\left(\frac{2n+1}{3n}\right)^2\left(\frac{6\lambda Q}{wh^2}\right)^2+\frac{1}{2!}\left(\frac{1-n}{2}\right)\left(\frac{3-n}{2}\right)\left(\frac{2n+1}{3n}\right)^4\left(\frac{6\lambda Q}{wh^2}\right)^4\cdots\right]dh \tag{A-11}$$

After the integration and generalization, *Eq. (A-11)* reduces

$$-\Delta P=\frac{6\eta_0 Q}{\tan\theta}\left(\frac{2n+1}{3n}\right)\left[\frac{1}{w^2}\left(\frac{1}{h_1}-\frac{1}{h_0}\right)+\frac{1}{2w}\left(\frac{1}{h_1^2}-\frac{1}{h_0^2}\right)\right]+\frac{6\eta_0 Q}{\tan\theta}\left(\frac{2n+1}{3n}\right)$$
$$\left\{\sum_{k=1}^{\infty}\left(\prod_{s=1}^{k}\frac{2s-1-n}{2}\right)\frac{(-1)^k}{k!}\left(\frac{6Q\lambda}{w}\right)^{2k}\left(\frac{2n+1}{3n}\right)^{2k}\right. \tag{A-12}$$
$$\left.\left[\frac{1}{w^2}\left(\frac{1}{4k+1}\right)\left(\frac{1}{h_1^{4k+1}}-\frac{1}{h_0^{4k+1}}\right)+\frac{1}{2w}\left(\frac{1}{4k+2}\right)\left(\frac{1}{h_1^{4k+2}}-\frac{1}{h_0^{4k+2}}\right)\right]\right\}$$

Also, in case of $\left(\frac{6Q\lambda}{wh_1^2}\right)\left(\frac{2n+1}{3n}\right)>1$, *Eq. (A-8)* yields

$$-\Delta P=\frac{6\eta_0 Q}{\tan\theta}\left(\frac{2n+1}{3n}\right)^n\left(\frac{6Q\lambda}{w}\right)^{n-1}\left[\frac{1}{w^2}\left(\frac{1}{2n-1}\right)\left(\frac{1}{h_1^{2n-1}}-\frac{1}{h_0^{2n-1}}\right)+\frac{1}{w}\left(\frac{1}{2n}\right)\left(\frac{1}{h_1^{2n}}-\frac{1}{h_0^{2n}}\right)\right]$$
$$+\frac{6\eta_0 Q}{\tan\theta}\left(\frac{2n+1}{3n}\right)\left\{\sum_{k=1}^{\infty}\left(\prod_{s=1}^{k}\frac{n-2s+1}{2}\right)\frac{1}{k!}\left(\frac{6Q\lambda}{w}\right)^{n-2k-1}\left(\frac{2n+1}{3n}\right)^{n-2k-1}\right. \tag{A-13}$$
$$\left.\left[\frac{1}{w^2}\left(\frac{1}{2n-4k-1}\right)\left(\frac{1}{h_1^{2n-4k+1}}-\frac{1}{h_0^{2n-4k+1}}\right)+\frac{1}{w}\left(\frac{1}{2n-4k}\right)\left(\frac{1}{h_1^{2n-4k}}-\frac{1}{h_0^{2n-4k}}\right)\right]\right\}$$

B. TEMPERATURE INCREASE OF THE POWER-LAW FLUID IN A WEDGE DIE

For flow in a slit die having the constant width, w, height, h, and the length, L, the heat balance is given by

$$\rho c_p v_x \frac{\partial T}{\partial x} = -\tau_{yx}\left(\frac{\partial v_x}{\partial y}\right) \tag{B-1}$$

The shear stress for power-law fluids is also given by

$$\tau_{yx} = \eta\left(-\frac{\partial v_x}{\partial y}\right) = K\left(-\frac{\partial v_x}{\partial y}\right)^{n-1}\left(-\frac{\partial v_x}{\partial y}\right) = K\left(-\frac{\partial v_x}{\partial y}\right)^{n} \tag{B-2}$$

From *Eq. (B-1)* and *Eq. (B-2)*,

$$\rho c_p v_x \frac{\partial T}{\partial x} = K\left(-\frac{\partial v_x}{\partial y}\right)^{n+1} \tag{B-3}$$

The momentum balance of the slit die is given by

$$\frac{\partial \tau_{yx}}{\partial y} = -\frac{\partial P}{\partial x} \tag{B-4}$$

From Eq (B-4), the velocity profile is obtained as the following equation. Zero shear stress at the center of the slit die is used as a boundary condition.

$$v_x = v_{\max}\left[1-\left(\frac{y}{h/2}\right)^{\frac{n+1}{n}}\right] \tag{B-5}$$

where $v_{\max} = \frac{n}{n+1}\left(\frac{1}{K}\right)^{\frac{1}{n}}\left(-\frac{\partial P}{\partial x}\right)^{\frac{1}{n}}\left(\frac{h}{2}\right)^{\frac{n+1}{n}}$

The average velocity in the slit die is defined by

$$\bar{v}_x = \frac{2}{wh}\int_0^{h/2} w v_x\, dy = v_{\max}\left(\frac{n+1}{2n+1}\right) \tag{B-6}$$

From *Eq. (B-5)* and *Eq. (B-6)*, the relationship between v_x and $\bar{v}_x$ is

$$v_x = \bar{v}_x \left(\frac{n+1}{2n+1} \right) \left[1 - \left(\frac{y}{h/2} \right)^{\frac{n+1}{n}} \right] \tag{B-7}$$

Therefore, *Eq. (B-3)* yields

$$\rho c_p v_x \frac{\partial T}{\partial x} = K \left(\bar{v}_x \left(\frac{2n+1}{n} \right) \left(\frac{1}{h/2} \right)^{\frac{n+1}{n}} \right)^{n+1} y^{\frac{n+1}{n}} \tag{B-8}$$

Right side of *Eq. (B-8)* is independent upon x. Thus, *Eq. (B-8)* reduces

$$\Delta T = \frac{K}{\rho c_p} \frac{1}{v_x} y^{\frac{n+1}{n}} \left(\bar{v}_x \left(\frac{2n+1}{n} \right) \left(\frac{1}{h/2} \right)^{\frac{n+1}{n}} \right)^{n+1} x \tag{B-9}$$

The flow average temperature increase, $(\Delta T)_{bulk}$ is defined as follows

$$(\Delta T)_{bulk} = \frac{(v_x \Delta T)_{avg}}{(v_x)_{avg}} = \frac{2w \int_0^{h/2} v_x dy}{2w \int_0^{h/2} v_x \Delta T dy} \tag{B-10}$$

By substituting *Eq. (B-7)* and *Eq. (B-9)* into *Eq. (B-10)*, the temperature increase in a slit die is given

$$(\Delta T)_{bulk} = \frac{K}{\rho c_p} \left(\frac{2n+1}{n} \right)^n \bar{v}_x^{\,n} \left(\frac{h}{2} \right)^{-n-1} x \tag{B-11}$$

In order to derive an equation for the wedge, a slit die having infinite small length, dx, is assumed. By definition, the average velocity has a relation to the volumetric flow rate, Q, as follows $\bar{v}_x = \frac{Q}{wh}$

And dx is defined as

$$dx = -\frac{dh}{2\tan\theta} \tag{B-12}$$

From *Eq. (B-11)* and *Eq. (B-12)*,

$$(dT)_{bulk} = -\frac{K}{\rho c_p}\frac{1}{2\tan\theta}\left(\frac{2n+1}{n}\right)^n\left(\frac{Q}{w}\right)^n h^{-n}\left(\frac{h}{2}\right)^{-n-1} dh \tag{B-13}$$

Finally, the temperature increase in a wedge die is

$$(\Delta T)_{bulk} = \frac{1}{2n\tan\theta}\left(\frac{1}{3^n}\right)\left(\frac{K}{\rho c_p}\right)\left(\frac{2n+1}{n}\right)^n\left(\frac{6Q}{wh_1^2}\right)^n\left[1-\left(\frac{h_1}{h_0}\right)^{2n}\right] \tag{B-14}$$

Appendix IV:
VISCOSITY DATA OF PS AND PS/CO_2 SOLUTIONS

#	CO_2 (wt%)	Temper-ature (°C)	Press-ure (MPa)	Shear Rate (1/s)	Viscosity (Pa-s)
1	0	200.00	3.50	4.19	10293.08
2	0	200.00	3.91	6.28	7677.34
3	0	200.00	4.26	7.68	6862.61
4	0	200.00	6.59	30.02	2722.53
5	0	220.00	1.78	4.19	5169.70
6	0	220.00	2.06	6.28	3996.17
7	0	220.00	2.32	7.68	3699.14
8	0	220.00	4.26	30.02	1752.97
9	0	240.00	0.81	4.19	2260.59
10	0	240.00	0.99	6.28	1865.29
11	0	240.00	1.15	7.68	1783.87
12	0	240.00	2.52	30.02	1029.03
13	0	200.00	7.93	93.17	1058.05
14	0	200.00	8.84	124.59	881.89
15	0	200.00	9.27	180.03	640.47
16	0	200.00	10.95	350.47	388.78
17	0	200.00	13.07	699.23	232.89
18	0	200.00	14.39	1085.14	165.27
19	0	200.00	15.38	1432.18	133.89
20	0	200.00	16.27	1777.36	114.11
21	0	200.00	19.22	3555.94	67.43
22	0	220.00	5.61	90.33	769.04
23	0	220.00	6.33	120.79	649.65
24	0	220.00	6.61	169.36	484.21
25	0	220.00	8.00	333.64	298.01
26	0	220.00	9.61	694.74	172.05
27	0	220.00	10.54	1105.27	118.68
28	0	220.00	11.25	1484.37	94.36
29	0	220.00	11.82	1850.20	79.58
30	0	220.00	13.84	3701.67	46.58
31	0	240.00	4.05	82.38	607.71
32	0	240.00	4.68	110.16	525.27
33	0	240.00	4.95	156.55	391.20
34	0	240.00	6.15	314.69	242.21
35	0	240.00	7.50	662.65	140.67
36	0	240.00	8.29	1051.42	98.00
37	0	240.00	8.91	1428.16	77.58
38	0	240.00	9.37	1830.60	63.66
39	0	240.00	11.00	3662.46	37.38
40	0	260.00	3.00	74.27	495.91
41	0	260.00	3.61	99.31	448.62
42	0	260.00	3.86	144.08	330.52

#	CO_2 (wt%)	Temper-ature (°C)	Press-ure (MPa)	Shear Rate (1/s)	Viscosity (Pa-s)
43	0	260.00	4.98	291.29	211.70
44	0	260.00	6.26	619.95	125.33
45	0	260.00	6.99	1015.36	85.42
46	0	260.00	7.51	1348.31	69.23
47	0	260.00	8.00	1719.63	57.84
48	0	260.00	9.52	3440.45	34.42
49	0	200.00	6.45	48.23	1659.17
50	0	200.00	8.32	112.17	921.73
51	0	200.00	9.11	174.15	650.51
52	0	200.00	11.99	532.38	280.37
53	0	200.00	14.62	1248.05	146.00
54	0	200.00	16.05	1745.64	114.63
55	0	200.00	19.03	3492.49	67.95
56	0	220.00	4.25	43.99	1193.73
57	0	220.00	5.80	102.30	702.61
58	0	220.00	6.40	159.52	498.02
59	0	220.00	8.87	503.27	219.24
60	0	220.00	10.77	1273.33	105.24
61	0	220.00	11.76	1804.07	81.14
62	0	220.00	13.80	3609.38	47.65
63	0	240.00	2.97	39.89	914.57
64	0	240.00	4.35	92.77	579.86
65	0	240.00	4.92	152.33	399.49
66	0	240.00	6.95	479.20	180.04
67	0	240.00	8.68	1195.30	90.32
68	0	240.00	9.49	1835.77	64.29
69	0	240.00	11.06	3672.80	37.48
70	0	260.00	3.13	85.05	453.13
71	0	260.00	3.63	139.51	320.76
72	0	260.00	5.48	443.54	153.12
73	0	260.00	7.01	1140.16	76.38
74	0	260.00	7.68	1692.97	56.37
75	0	260.00	9.24	3387.11	33.94
76	0	220.00	0.10	0.54	8269.52
77	0	220.00	0.10	0.41	8689.62
78	0	220.00	0.10	0.31	9281.29
79	0	220.00	0.10	0.23	9812.58
80	0	220.00	0.10	0.18	10155.70
81	0	220.00	0.10	0.14	10481.40
82	0	220.00	0.10	0.11	10712.30
83	0	220.00	0.10	0.08	10855.40
84	0	220.00	0.10	0.07	10942.70

#	CO_2 (wt%)	Temper-ature (°C)	Press-ure (MPa)	Shear Rate (1/s)	Viscosity (Pa-s)
85	0	220.00	0.10	0.05	11204.40
86	0	220.00	0.10	0.04	11240.60
87	0	220.00	0.10	0.03	11708.50
88	0	220.00	0.10	0.02	11587.60
89	0	220.00	0.10	0.02	11602.90
90	0	220.00	0.10	0.01	12142.60
91	0	220.00	0.10	0.01	11966.80
92	0	220.00	0.10	0.01	11711.60
93	0	220.00	0.10	0.01	12021.40
94	0	220.00	0.10	0.00	12140.40
95	0	220.00	0.10	0.00	11725.20
96	0	240.00	0.10	1.12	2526.45
97	0	240.00	0.10	0.83	2719.39
98	0	240.00	0.10	0.63	2832.63
99	0	240.00	0.10	0.49	2906.07
100	0	240.00	0.10	0.38	2954.95
101	0	240.00	0.10	0.30	2989.76
102	0	240.00	0.10	0.24	3015.51
103	0	240.00	0.10	0.19	3044.29
104	0	240.00	0.10	0.15	3071.25
105	0	240.00	0.10	0.12	3094.61
106	0	240.00	0.10	0.09	3107.95
107	0	240.00	0.10	0.07	3105.90
108	0	240.00	0.10	0.06	3144.72
109	0	240.00	0.10	0.05	3149.22
110	0	240.00	0.10	0.04	3207.27
111	0	240.00	0.10	0.03	3175.51
112	0	240.00	0.10	0.02	3201.13
113	0	240.00	0.10	0.02	3183.98
114	0	240.00	0.10	0.01	3299.04
115	0	240.00	0.10	0.01	3179.11
116	0	240.00	0.10	0.01	3644.56
117	0	240.00	0.10	0.01	3600.33
118	0	240.00	0.10	0.00	3661.14
119	0	240.00	0.10	0.00	3560.97
120	0	240.00	0.10	0.00	3355.23
121	0	240.00	0.10	0.00	3636.51
122	0	240.00	0.10	0.00	3177.56
123	0	260.00	0.10	2.12	1065.00
124	0	260.00	0.10	1.69	1058.78
125	0	260.00	0.10	1.34	1063.71
126	0	260.00	0.10	1.04	1086.13
127	0	260.00	0.10	0.82	1094.19
128	0	260.00	0.10	0.65	1089.10
129	0	260.00	0.10	0.52	1088.83
130	0	260.00	0.10	0.41	1087.38
131	0	260.00	0.10	0.33	1087.64
132	0	260.00	0.10	0.26	1085.08
133	0	260.00	0.10	0.21	1082.69

#	CO_2 (wt%)	Temper-ature (°C)	Press-ure (MPa)	Shear Rate (1/s)	Viscosity (Pa-s)
134	0	260.00	0.10	0.17	1080.90
135	0	260.00	0.10	0.13	1088.47
136	0	260.00	0.10	0.10	1083.94
137	0	260.00	0.10	0.08	1086.85
138	0	260.00	0.10	0.07	1083.94
139	0	260.00	0.10	0.05	1088.30
140	0	260.00	0.10	0.04	1090.13
141	0	260.00	0.10	0.03	1075.31
142	0	260.00	0.10	0.03	1087.15
143	0	260.00	0.10	0.02	1068.57
144	0	260.00	0.10	0.02	1101.33
145	0	260.00	0.10	0.01	1116.82
146	0	260.00	0.10	0.01	1088.57
147	0	260.00	0.10	0.01	1076.41
148	0	203.29	26.30	51.60	1831.86
149	0	203.70	23.20	51.53	1813.88
150	0	204.29	20.76	51.33	1796.08
151	0	204.34	16.72	49.57	1771.58
152	0	205.87	18.58	49.96	1760.00
153	0	206.69	25.07	95.65	1142.00
154	0	207.32	21.08	94.15	1089.32
155	0	207.63	23.04	93.53	1101.81
156	0	207.67	18.30	93.11	1081.20
157	0	209.45	19.12	136.13	804.26
158	0	209.52	21.14	138.09	798.48
159	0	209.56	25.04	138.50	842.12
160	0	209.57	23.16	138.45	812.69
161	0	211.28	20.94	210.24	573.58
162	0	211.80	25.06	213.62	588.07
163	0	211.86	22.92	211.78	570.92
164	0	224.54	12.33	47.24	1317.37
165	0	224.66	14.38	48.32	1326.79
166	0	225.19	20.54	50.00	1352.81
167	0	225.38	16.56	48.66	1320.10
168	0	225.44	16.90	90.97	852.23
169	0	225.55	25.09	51.69	1390.72
170	0	225.65	18.68	49.68	1342.09
171	0	225.76	22.51	50.69	1368.46
172	0	226.30	14.53	89.23	843.85
173	0	227.48	25.04	98.98	853.38
174	0	227.57	18.59	92.24	843.31
175	0	227.75	20.73	94.47	844.64
176	0	228.21	14.82	138.49	604.10
177	0	228.60	22.81	95.88	842.20
178	0	230.29	21.00	147.02	593.59
179	0	230.59	16.50	140.13	586.91
180	0	231.51	18.88	142.44	588.58
181	0	231.79	23.19	148.22	593.35
182	0	232.62	16.77	221.58	409.10

#	CO_2 (wt%)	Temper-ature (ºC)	Press-ure (MPa)	Shear Rate (1/s)	Viscosity (Pa-s)
183	0	232.75	24.79	149.82	584.36
184	0	232.89	14.70	217.31	407.52
185	0	233.16	20.59	226.86	411.51
186	0	233.30	22.69	230.74	412.40
187	0	233.65	18.38	303.96	320.58
188	0	233.69	16.64	302.74	319.58
189	0	233.85	24.98	233.00	415.30
190	0	234.27	18.65	221.79	408.21
191	0	234.54	20.70	307.15	323.56
192	0	234.79	22.84	312.90	321.65
193	0	235.33	25.18	316.50	322.35
194	0	247.02	20.65	91.21	651.06
195	0	247.61	10.36	45.48	902.70
196	0	247.79	12.23	45.76	914.62
197	0	247.90	14.44	87.73	616.35
198	0	248.13	14.61	130.27	473.60
199	0	248.14	12.57	86.64	601.81
200	0	248.24	12.57	129.36	460.64
201	0	248.25	10.08	85.24	589.84
202	0	248.26	10.38	127.24	460.92
203	0	248.54	24.79	94.26	649.50
204	0	248.55	22.81	137.14	489.20
205	0	248.63	16.51	131.40	474.60
206	0	248.74	20.61	135.37	486.57
207	0	248.78	8.17	44.24	857.68
208	0	249.01	22.60	91.76	641.95
209	0	249.08	18.84	88.20	616.74
210	0	249.25	14.33	45.57	910.09
211	0	249.49	18.88	132.41	479.50
212	0	249.52	22.70	48.11	986.94
213	0	249.73	25.34	137.05	487.02
214	0	249.81	20.30	47.23	961.59
215	0	250.02	24.44	48.57	998.34
216	0	250.95	16.35	45.77	902.81
217	0	250.98	12.54	201.24	339.50
218	0	251.22	18.21	46.23	925.81
219	0	251.24	14.65	203.32	338.46
220	0	251.36	18.80	286.50	273.90
221	0	251.94	19.08	207.63	348.24
222	0	252.00	25.30	216.06	353.21
223	0	252.02	21.02	211.96	346.02
224	0	252.10	16.73	205.39	341.79
225	0	252.20	22.87	213.57	349.47
226	0	252.35	22.88	291.93	273.80
227	0	252.40	20.94	288.53	272.17
228	0	252.60	16.97	282.78	269.12
229	0	252.68	12.57	274.85	265.19
230	0	252.96	25.24	293.98	273.35
231	0	253.17	14.58	276.27	267.96

#	CO_2 (wt%)	Temper-ature (ºC)	Press-ure (MPa)	Shear Rate (1/s)	Viscosity (Pa-s)
232	0	266.24	10.45	120.96	372.62
233	0	266.54	12.29	80.27	498.07
234	0	266.58	12.36	43.72	682.95
235	0	266.84	12.42	122.39	371.41
236	0	266.90	18.51	128.49	382.20
237	0	267.21	8.10	77.15	478.93
238	0	267.27	14.35	81.23	509.54
239	0	267.39	12.26	190.27	283.62
240	0	267.54	24.73	136.28	384.76
241	0	267.59	10.10	78.76	488.26
242	0	267.72	8.20	117.53	362.24
243	0	267.74	24.77	87.52	524.56
244	0	267.77	14.28	123.82	373.56
245	0	268.04	18.63	45.52	710.16
246	0	268.11	24.60	48.03	764.42
247	0	268.18	20.71	130.45	377.85
248	0	268.39	23.06	41.65	614.53
249	0	268.59	14.58	193.72	281.87
250	0	268.66	16.45	81.51	490.90
251	0	268.78	20.93	45.45	659.75
252	0	268.79	10.02	188.00	274.65
253	0	268.85	16.43	125.64	371.65
254	0	268.91	14.24	43.64	652.80
255	0	269.00	16.50	194.93	283.91
256	0	269.18	10.47	257.71	225.44
257	0	269.31	20.83	84.76	511.95
258	0	269.42	22.98	85.43	513.98
259	0	269.53	16.31	44.53	679.52
260	0	269.82	18.52	83.02	505.78
261	0	269.92	12.37	259.53	225.72
262	0	270.06	18.63	198.73	282.41
263	0	270.15	22.93	46.09	700.80
264	0	270.27	24.62	289.38	228.66
265	0	270.46	20.49	200.58	284.95
266	0	270.78	23.09	204.54	284.63
267	0	270.79	24.84	209.64	282.52
268	0	271.11	16.67	267.28	225.50
269	0	271.16	18.70	272.82	226.33
270	0	271.20	14.56	262.57	225.15
271	0	271.27	22.85	281.97	226.78
272	0	271.36	20.82	277.78	226.52
273	1	226.92	22.97	221.88	386.40
274	1	227.69	24.16	220.31	401.63
275	1	228.48	25.16	220.28	399.46
276	1	230.07	26.37	218.48	405.45
277	1	242.42	25.36	140.91	454.09
278	1	242.68	16.55	145.98	381.93
279	1	242.92	18.54	145.31	392.30
280	1	243.39	24.35	144.30	436.08

#	CO_2 (wt%)	Temper-ature (ºC)	Press-ure (MPa)	Shear Rate (1/s)	Viscosity (Pa-s)
281	1	243.49	27.02	141.75	462.28
282	1	243.53	22.90	143.50	427.45
283	1	243.83	20.60	143.93	406.38
284	1	244.95	26.18	220.76	309.80
285	1	244.95	21.08	217.71	331.90
286	1	245.47	22.93	217.58	318.07
287	1	245.95	25.03	218.04	327.70
288	1	246.65	24.32	216.85	311.35
289	1	246.75	24.82	296.32	260.62
290	1	246.84	20.84	304.72	239.85
291	1	247.12	26.65	297.35	264.72
292	1	247.49	23.25	300.99	250.42
293	1	248.76	24.43	298.48	248.99
294	1	261.69	25.20	127.35	380.84
295	1	261.94	26.81	126.20	390.23
296	1	262.21	22.80	127.92	369.12
297	1	262.50	27.33	201.08	289.20
298	1	262.57	24.76	203.35	277.13
299	1	262.73	24.63	201.52	282.14
300	1	262.75	20.50	128.82	354.24
301	1	263.58	18.35	211.40	242.99
302	1	264.04	24.69	277.98	230.73
303	1	264.12	22.70	201.07	269.69
304	1	264.22	21.39	208.33	255.69
305	1	264.50	24.61	125.52	366.33
306	1	267.11	20.02	280.99	205.10
307	1	267.24	22.54	277.55	213.95
308	1	267.37	24.94	278.24	219.28
309	1	267.45	26.57	273.29	225.68
310	1	267.47	18.90	281.55	200.79
311	2	208.61	26.96	147.98	615.29
312	2	209.33	25.24	152.04	599.88
313	2	209.76	23.01	53.49	1221.85
314	2	209.83	23.30	153.58	588.72
315	2	224.64	24.76	134.70	526.94
316	2	225.43	23.35	136.79	523.16
317	2	225.48	27.32	133.60	547.12
318	2	225.51	22.89	89.59	687.93
319	2	225.85	25.13	89.09	702.07
320	2	226.19	25.47	215.91	369.30
321	2	226.48	20.81	137.11	499.26
322	2	226.64	25.24	217.30	372.62
323	2	226.66	27.42	88.40	716.44
324	2	226.98	21.01	219.53	345.23
325	2	227.12	24.72	211.39	369.10
326	2	227.14	27.16	213.13	381.20
327	2	227.21	22.75	213.56	357.78
328	2	242.07	27.04	91.69	562.27
329	2	242.39	25.22	91.50	529.23

#	CO_2 (wt%)	Temper-ature (ºC)	Press-ure (MPa)	Shear Rate (1/s)	Viscosity (Pa-s)
330	2	242.44	20.99	139.88	383.41
331	2	242.91	27.41	138.90	418.61
332	2	243.04	23.00	136.29	394.70
333	2	243.17	22.33	91.02	504.62
334	2	243.23	24.79	138.39	400.93
335	2	243.43	26.06	91.35	536.43
336	2	244.58	25.03	214.25	303.62
337	2	244.67	24.90	139.48	398.56
338	2	244.71	20.83	216.67	284.51
339	2	245.09	22.40	212.48	292.72
340	2	245.13	26.43	209.38	319.04
341	2	245.62	24.53	209.32	309.67
342	2	245.81	24.28	289.23	232.46
343	2	246.17	26.12	289.94	243.47
344	2	246.78	22.66	296.03	231.55
345	2	247.42	20.91	300.15	222.45
346	2	247.98	24.57	295.44	236.28
347	2	260.10	27.03	77.17	480.47
348	2	260.28	25.06	77.97	459.34
349	2	260.31	24.57	77.60	476.45
350	2	260.76	24.79	129.54	340.51
351	2	261.07	24.95	130.42	342.22
352	2	261.25	22.99	128.60	324.02
353	2	261.36	27.09	127.45	352.48
354	2	261.37	20.60	129.67	302.41
355	2	262.08	20.41	201.53	249.96
356	2	262.29	22.59	198.45	253.08
357	2	262.67	22.06	77.78	428.46
358	2	264.20	20.80	261.94	214.74
359	2	264.24	22.57	258.39	220.25
360	2	264.79	27.02	255.22	228.58
361	2	264.90	24.74	257.41	220.57
362	2	265.17	24.39	257.22	222.95
363	3	204.51	26.99	95.63	793.23
364	3	205.17	25.50	99.12	731.34
365	3	206.29	26.73	53.82	1288.19
366	3	206.38	26.74	97.53	743.69
367	3	207.36	27.09	143.38	592.91
368	3	207.71	25.03	145.84	584.15
369	3	207.94	25.07	145.57	579.69
370	3	208.50	22.83	145.39	572.91
371	3	208.82	27.09	140.31	595.46
372	3	209.14	27.06	142.36	582.03
373	3	209.16	25.21	144.38	582.55
374	3	222.12	22.89	49.26	1011.24
375	3	222.86	26.40	48.22	1047.13
376	3	223.37	24.80	86.97	666.80
377	3	224.10	22.88	48.40	971.11
378	3	224.18	27.00	132.13	509.12

#	CO_2 (wt%)	Temper -ature (ºC)	Press- ure (MPa)	Shear Rate (1/s)	Viscosity (Pa-s)
379	3	224.54	25.08	47.96	988.18
380	3	224.55	24.90	47.96	957.09
381	3	224.93	25.25	132.97	499.37
382	3	225.43	27.17	85.67	661.13
383	3	226.21	27.13	213.73	355.51
384	3	226.41	24.40	209.94	348.45
385	3	226.97	25.10	212.35	340.63
386	3	228.05	26.41	293.10	267.30
387	3	228.68	25.03	294.81	264.47
388	3	229.11	24.40	297.80	260.37
389	3	241.63	24.67	135.32	379.30
390	3	242.55	25.01	88.68	489.06
391	3	242.67	25.04	136.56	377.36
392	3	242.85	25.15	211.07	288.73
393	3	243.28	24.29	212.29	279.13
394	3	243.30	27.12	135.33	388.53
395	3	243.38	22.81	136.68	366.05
396	3	243.43	22.54	89.08	478.29
397	3	243.54	22.64	213.61	276.66
398	3	243.63	26.46	208.79	289.83
399	3	243.97	26.62	87.66	496.82
400	3	244.92	24.81	289.06	224.69
401	3	245.11	25.00	291.87	221.92
402	3	245.77	27.11	286.72	227.72
403	3	246.61	22.63	291.01	218.31
404	3	260.21	27.13	74.77	426.47
405	3	260.37	24.29	76.17	400.32
406	3	260.66	24.40	40.31	532.48
407	3	261.13	26.40	123.78	312.28
408	3	261.92	26.47	40.03	534.17
409	3	263.14	25.45	123.91	299.01
410	3	263.25	22.35	125.28	286.31
411	4	205.05	22.88	96.68	692.91
412	4	205.72	29.06	141.63	549.34
413	4	205.82	26.79	145.07	535.35
414	4	206.29	26.73	94.43	734.24
415	4	206.35	27.12	99.09	717.25
416	4	206.94	25.34	93.87	697.16
417	4	207.20	25.47	142.70	521.35
418	4	208.56	24.99	50.01	985.98
419	4	209.42	23.07	49.23	938.60